A Comparison of the Physicochemical Characterisation of Powders using a selection of current methods

Submitted June 1998

The School of Pharmacy

University of London

Jason Willoughby Dove

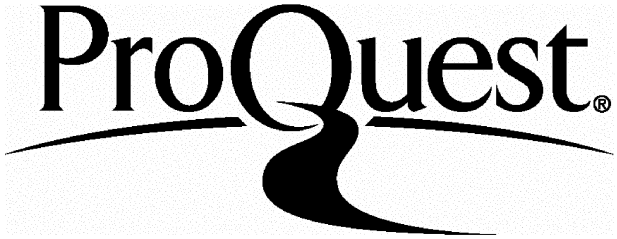

I would like to thank my supervisor, Dr. Graham Buckton, for his assistance and encouragement throughout my period as a postgraduate.

Roche Products for their financial support, especially Dr. Chris Doherty for his guidance and advice in the continual development of my Ph.D.

The technical staff, especially Brian who were always able to find the correct and fully functioning apparatus when required.

My friends and colleagues, who have all made my time spent at the School of Pharmacy an enjoyable one, in particular Jon and Sam, without whose help I would not be able to accredit my abysmal golf handicap.

Alka for much needed thesis writing advice, as well as being a great friend and companion.

Finally, my parents and little sister for their never ending support.

The surface characterisation of six powders (Caffeine, Ethacrynic acid, Ibuprofen, Salicylic acid, Saquinavir and Theophylline) was compared using a selection of traditional and novel methods; one liquid penetration and two Wilhelmy plate methods utilising contact angles, inverse gas chromatography (IGC), isothermal microcalorimetry (IM) and dynamic vapour sorption (DVS).

All the techniques distinguished between the chemically different powders, although only IGC, IM and DVS were sensitive enough to detect batch to batch variation of the Saquinavir after it had been wetted and dried under different conditions.

Of the three methods using contact angle analysis, the powder coated Wilhelmy plate method was the most versatile and accurate, as reproducible contact angles were consistently obtained with all powder and probe liquid combinations. Surface energy data were calculated using two theories, one producing a more complete analysis, with non-polar, polar, and acid-base values.

IGC, DVS and IM discovered small variations with Saquinavir between batches, IM being the most sensitive. IGC produced non-polar surface energies that were directly comparable to the contact angle analysis, whilst it only gave a qualitative indication of acid-base nature. DVS and IM measured water vapour adsorption, useful in their own right, which were combined to achieve a detailed thermodynamic analysis of the adsorption process with changing relative humidity.

In conclusion, the ideal surface characterisation method depends on many factors, for example, sensitivity required, powder quantity available and whether the surface energy is being evaluated or compared for batch to batch variation. It is evident that batch to batch variation is not readily detectable with contact angle techniques, which should therefore be reserved for a quick indication of the magnitude of a powder's surface energy. Whereas DVS, IM and IGC provide straightforward and highly sensitive methods of analysing surface properties and the degree of variation between batches of the same drug.

Acknowledgements 2

Abstract 3

Table of Contents 4

List of Tables 12

List of Figures 15

List of Symbols 21

1 INTRODUCTION 24

1.1 Surface Energy 26

1.2 Wetting process 29

1.2.1 Adhesion 30

1.2.2 Immersion 31

1.2.3 Spreading 31

1.3 Critical Surface Tension (γc) 32

1.4 Deriving contact angles experimentally 33

1.4.1 Liquid with unknown surface energy 33

1.4.2 Solid with unknown surface energy 33

1.4.2.1 Liquid penetration 33

1.4.2.2 Powder compacts 34

1.5 Surface energy determination using contact angle data 34

1.5.1 Van Oss theory 34

1.5.1.1 Van der Waals interactions (γ_S^{LW}) 35

1.5.1.2 Lewis Acid-Base interactions (γ_S^{AB}) 35
1.5.1.3 Possible interactions 36
1.5.1.4 Van Oss equation derivation 37
1.5.1.5 Polarity ratios 37
1.5.1.6 Two possible methods using the Van Oss theory 39
1.5.2 Wu's theory 40

1.6 Potential use of surface energy data 41

1.7 Alternative methods of surface analysis 42
1.7.1 Adsorption 42
1.7.2 Inverse gas chromatography 43
1.7.2.1 History of IGC development 43
1.7.2.2 Theory 44
1.7.3 Isothermal microcalorimetry 45
1.7.3.1 Introduction 45
1.7.3.2 Enthalpy of adsorption 46
1.7.4 Dynamic vapour sorption 47
1.7.4.1 Theory 47
1.7.4.2 Gibb's function 48
1.7.5 Combining dynamic vapour sorption and microcalorimetry data 49
1.7.5.1 Entropy of adsorption 49

2 MATERIALS 52

2.1 Model powders 52

2.2 Test powder 55
2.2.1 Preparation of batches of Saquinavir 55

2.3 Raw material suppliers 56

3 WILHELMY PLATE 59

3.1 Introduction 59

3.1.1 Compressed powder plate 59

3.1.2 Powder covered glass slide 60

3.2 Method 60

3.2.1 Powder compact manufacture 60

3.2.2 Powder covered glass slide 61

3.2.2.1 The influence of coverage of the slide by the powder on the measured contact angle 62

3.2.3 Cahn Dynamic Contact Angle Analyser (312) 63

3.2.3.1 Calibration of Cahn 64

3.2.4 Choice of test liquids 64

3.2.5 Analysis 65

3.2.6 Errors associated with quoting contact angles 67

3.3 Results and discussion 69

3.3.1 Wilhelmy plate analysis of test powders using a powder compact 69

3.3.1.1 Van Oss theory 69

3.3.1.2 Wu theory 70

3.3.2 Wilhelmy plate analysis of test powders using a powder covered glass slide 75

3.3.3 Wilhelmy plate analysis of Saquinavir batches using a powder compact 81

3.3.4 Wilhelmy plate analysis of Saquinavir batches using a powder covered glass slide 87

3.3.4.1 Summary of results 93

3.3.5 Negative polarity values 94

3.3.6 Test liquid choice 95

3.3.7 Comparison between two Wilhelmy plate methods 99

3.3.8 Compression effect 102

3.4 Conclusions 103

4 LIQUID PENETRATION 105

4.1 Introduction 105

4.2 Method 106

4.3 Contact angle calculation 108

4.4 Results and discussion 108

4.4.1 Comparison between liquid penetration and glass slide Wilhelmy plate methods 111

4.4 Conclusions 112

5 INVERSE GAS CHROMATOGRAPHY 115

5.1 Introduction 115

5.1.1 Possible probe interactions 116

5.1.2 Calculation 117

5.1.3 Acid and base behaviour 122

5.2 Method 125

5.2.1 Silanisation method 125

5.2.2 Packing of glass loop 125

5.2.3 Powder analysis protocol 126

5.3 Results and discussion 127

5.3.1 Caffeine, Theophylline, Salicylic acid, Ethacrynic acid and Ibuprofen 127

5.3.1.1 Effect of temperature 127

5.3.1.2 Analysis using $a(\gamma_L^D)^{0.5}$ 128

5.3.1.3 Using delta Heat of vaporisation (ΔH_d^{vap}) 132

5.3.1.4 Using boiling points 135

5.3.1.5 Summary of three methods of analyses 138

5.3.2 Saquinavir 139

5.3.2.1 Surface energy analysis using $a(\gamma_L^D)^{0.5}$ 144

5.3.2.1.1 Non-polar surface energy component using $a(\gamma_L^D)^{0.5}$ 144

5.3.2.1.2 Acid-base characterisation using $a(\gamma_L^D)^{0.5}$ 146

5.3.2.2 Acid-base characterisation using enthalpy of vaporisation 148

5.3.2.3 Acid-base characterisation using boiling points 152

5.3.2.4 Overall conclusions with the batches of Saquinavir from the IGC results 154

5.4 Conclusions 155

5.4.1 High non-polar surface energy values 155

5.4.2 Acid-base analysis 156

5.4.3 Accuracy 157

5.4.3.1 Y-axis errors 157

5.4.3.2 X-axis errors 157

5.4.4 Advantages of IGC 158

5.4.5 Disadvantages of IGC 158

6 ISOTHERMAL MICROCALORIMETRY 161

6.1 Introduction 161

6.2 Method 162

6.2.1 Calibration 163
6.2.2 Surface area analysis 165
6.2.2.1 Method 165

6.3 Results and discussion 166
6.3.1 Cumulative adsorption isotherms of the five model powders 166
6.3.2 Cumulative adsorption isotherms of the Saquinavir batches 167
6.3.3 Non-cumulative adsorption isotherms of Saquinavir 169
6.3.4 Summary of isotherm data 172
6.3.5 Alterations in adsorption isotherms of Saquinavir with repeating cycle 174
6.3.5.1 Reproducibility 177

6.4 Conclusions 178

7 DYNAMIC VAPOUR SORPTION 181

7.1 Introduction 181

7.2 Method 183
7.2.1 Validation of relative humidity 183
7.2.2 Calibration 183
7.2.3 Cleaning 184
7.2.4 Static 184
7.2.5 Loading sample 184

7.3 Results and discussion 185
7.3.1 Humidity validation 185
7.3.2 Adsorption isotherms of five model powders 186
7.3.3 Adsorption isotherms of Saquinavir batches 189
7.3.4 Hysteresis measurements 195

7.4 Conclusions 198

7.5 Combining DVS and Microcalorimetry data 200

7.5.1 Thermodynamic consideration of three model powders 200

7.5.2 Thermodynamic consideration of the Saquinavir batches 202

7.5.3 The monolayer capacity of the powder samples 205

7.5.4 Discussion 206

7.5.5 Thermodynamic changes on repeated cycling of Saquinavir batches 210

7.5.6 Conclusions 216

8 FURTHER ANALYSIS 218

8.1 Mixer Torque Rheometer 218

8.1.1 Investigation of the granulation process 219

8.2 Methods 220

8.3 Results 220

8.4 Microscopy 222

8.5 Thermogravimetric analysis (TGA) and differential scanning calorimetry (DSC) 224

8.6 Conclusions 224

9 DISCUSSION 227

9.1 Comparison of techniques 227

9.1.1 Contact Angle methods 227

9.1.1.1 Compressed powder Wilhelmy plate 227

9.1.1.2 Powder covered glass slide 227

9.1.1.3 Liquid penetration 228
9.1.1.4 Procedure for contact angle measurement 228
9.1.2 Inverse Gas Chromatography 229
9.1.3 Flow cell Microcalorimetry 229
9.1.4 Dynamic Vapour Sorption 230
9.1.5 Differences between methods 230
9.1.6 Combining DVS with Microcalorimetry 230

9.2 Effect of processing Saquinavir 231

9.3 Conclusions 232

9.4 Future Work 234

References 237

Table 1.1 Advantages and disadvantages of contact angle measurement methods. 34
Table 1.2 Selection of polar probe liquids and their corresponding equation. 39
Table 2.1 Raw material suppliers. 56
Table 2.2 Liquids used as gaseous probes for inverse gas chromatography. 57
Table 3.1 Test probe liquid surface energy component values ($mJ.m^{-2}$). 65
Table 3.2 Contact angles of five model powders with a selection of test liquids. 69
Table 3.3 Surface energy values of Theophylline using a powder compact. 70
Table 3.4 Surface energy values of Caffeine using a powder compact. 70
Table 3.5 Surface energy values of Ethacrynic acid using a powder compact. 71
Table 3.6 Surface energy values of Salicyclic acid using a powder compact. 71
Table 3.7 Surface energy values of Ibuprofen using a powder compact. 72
Table 3.8 Contact angles of five model powders with a selection of test liquids. 75
Table 3.9 Surface energy values of Theophylline using a powder covered glass slide.76
Table 3.10 Surface energy values of Caffeine using a powder covered glass slide. 76
Table 3.11 Surface energy values of Ethacrynic acid using a powder covered glass slide. 77
Table 3.12 Surface energy values of Salicylic acid using a powder covered glass slide. 78
Table 3.13 Surface energy values of Ibuprofen using a powder covered glass slide. 78
Table 3.14 Contact angles of Saquinavir batches with a selection of test liquids. 81
Table 3.15 Surface energy values of original Saquinavir using a powder compact. 82
Table 3.16 Surface energy values of tray dried Saquinavir (b001) using a powder compact. 82
Table 3.17 Surface energy values of spin dried Saquinavir (b002) using a powder compact. 83
Table 3.18 Surface energy values of tray dried Saquinavir (b010) using a powder compact. 84
Table 3.19 Surface energy values of Vacuum dried Saquinavir (b020) using a powder compact. 84
Table 3.20 Surface energy values of heated Saquinavir (b030) using a powder compact. 85
Table 3.21 Contact angles of Saquinavir batches with a selection of test liquids. 87

Table 3.22 Surface energy values of original Saquinavir using a powder covered glass slide. 88

Table 3.23 Surface energy values of tray dried Saquinavir (b001) using a powder covered glass slide. 89

Table 3.24 Surface energy values of spin dried Saquinavir (b002) using a powder covered glass slide. 89

Table 3.25 Surface energy values of tray dried Saquinavir (b010) using a powder covered glass slide. 90

Table 3.26 Surface energy values of vacuum dried Saquinavir (b020) using a powder covered glass slide. 91

Table 3.27 Surface energy values of heated Saquinavir (b030) using a powder covered glass slide. 91

Table 3.28 Process of error determination. 98

Table 4.1 Contact angles of model powders. 109

Table 4.2 Surface energetics of Theophylline. 110

Table 4.3 Surface energetics of Caffeine. 110

Table 4.4 Surface energetics of Ethacrynic acid. 110

Table 4.5 Surface energetics of Ibuprofen. 111

Table 5.1 Probe liquid physical data table required for IGC analysis. 124

Table 5.2 Non-polar surface energy of Caffeine over a range of temperatures. 128

Table 5.3 Acid / base character for the model powders using $a(\gamma_L^D)^{0.5}$. 129

Table 5.4 Non-polar component of surface energy for the model powders using $a(\gamma_L^D)^{0.5}$. 131

Table 5.5 Statistical differences between the non-polar component of surface energy for the model powders. 132

Table 5.6 Acid / base character for the model powders using ΔH_d^{vap}. 134

Table 5.7 Acid / base character for the model powders using boiling point data. 137

Table 5.8 Non-polar component of surface energy for all Saquinavir batches using $a(\gamma_L^D)^{0.5}$. 144

Table 5.9 Statistical differences between the non-polar component of surface energy for the Saquinavir batches. 145

Table 5.10 Acid / base character for all Saquinavir batches using $a(\gamma_L^D)^{0.5}$. 147

Table 5.11 Acid / base character for the Saquinavir batches using ΔH_d^{vap}. 150

Table 5.12 Acid / base character for the Saquinavir batches using boiling point data. 153

Table 5.13 Acid character of all six powders using three methods of analysis. 156

Table 5.14 Base character of all six powders using three methods of analysis. 156

Table 6.1 Surface areas of five model powders using BET analysis (Section 6.2.2). 167

Table 6.2 Surface areas of Saquinavir batches using BET analysis (Section 6.2.2). 168

Table 7.1 Deliquescent relative humidities of a range of crystalline salts. 185

Table 7.2 Relative humidities required for monolayer formation in the DVS. 206

Table 7.3 Thermodynamic analysis of Caffeine, Theophylline, Ethacrynic Acid and Saquinavir batches. 207

Table 7.4 Thermodynamic analysis of Saquinavir batches between 60% and 90% RH. 209

Table 8.1 Tabulated results from DSC and TGA analysis of Saquinavir batches. 224

Table 9.1 Checklist for choosing surface characterisation technique. 233

Table 9.2 Overview of powder surface characteristics. 234

Figure 1.1 Diagrammatic representation of a surface and a bulk molecule within a powder solid. 26
Figure 1.2 Surface tension effect. 27
Figure 1.3 Possible interactions of a droplet on a powder surface. 28
Figure 1.4 Importance of wetting phenomena. 30
Figure 1.5 Theory behind wetting (steps 1-4). 31
Figure 1.6 Graphs of water sorption onto a model powder over an increasing relative humidity range. 46
Figure 2.1 Salicylic acid structure. 52
Figure 2.2 Caffeine structure. 53
Figure 2.3 Theophylline structure. 53
Figure 2.4 Ibuprofen structure. 54
Figure 2.5 Ethacrynic acid structure. 54
Figure 2.6 Saquinavir structure. 55
Figure 3.1 Steel die used in compact manufacture. 61
Figure 3.2 Graph showing the change in contact angle with percentage coverage of caffeine over a glass slide previously coated with adhesive. 62
Figure 3.3 Cahn apparatus. 63
Figure 3.4 Microbalance apparatus. 64
Figure 3.5 Force / depth isotherm used in calculation of contact angle. 66
Figure 3.6 Graph showing region used for calculation. 67
Figure 3.7 The cosine curve. 68
Figure 3.8 Assessment of non-polar surface energies of the five test powders using the Van Oss theory (powder compacts used). 73
Figure 3.9 Assessment of non-polar surface energies of the five test powders using the Wu theory (powder compacts used). 74
Figure 3.10 Assessment of non-polar surface energies of the five test powders using the Van Oss theory (powder covered glass slides used). 79
Figure 3.11 Assessment of non-polar surface energies of the five test powders using the Wu theory (powder covered glass slides used). 80
Figure 3.12 Assessment of non-polar surface energies of the Saquinavir batches using the Van Oss theory (powder compact used). 86
Figure 3.13 Assessment of non-polar surface energies of the Saquinavir batches using the Wu theory (powder compact used). 86

Figure 3.14 Assessment of non-polar surface energies of the Saquinavir batches using the Van Oss theory (powder covered glass slide used). 92

Figure 3.15 Assessment of non-polar surface energies of the Saquinavir batches using the Wu theory (powder covered glass slide used). 93

Figure 3.16 Assessment of non-polar surface energies of all powders using diiodomethane. 99

Figure 3.17 Assessment of non-polar surface energies of all powders using polar liquids with Wu theory. 100

Figure 3.18 Assessment of non-polar surface energies of all powders using polar liquids on powder covered glass slides with Wu theory. 101

Figure 3.19 Assessment of non-polar surface energies of all powders using polar liquids on powder compacts with Wu theory. 101

Figure 4.1 Typical graph showing straight line gradient. 106

Figure 4.2 Liquid penetration apparatus. 107

Figure 4.3 Liquid penetration of water into an ibuprofen powder bed. 108

Figure 4.4 Comparison between liquid penetration and a Wilhelmy plate method. 111

Figure 5.1 Schematic diagram of IGC apparatus:- Model F33 system. 115

Figure 5.2 Graph showing calculation of the interaction forces at a powder surface. 121

Figure 5.3 Example of straight line plot used to calculate acid-base characteristics. 123

Figure 5.4 Passage of n-alkane probes through a caffeine powder column at four elevated temperatures. 127

Figure 5.5 Acid / base plot for acidic model powders using $a(\gamma_L^D)^{0.5}$. 128

Figure 5.6 Acid character for the model powders using $a(\gamma_L^D)^{0.5}$. 129

Figure 5.7 Basic character for the model powders using $a(\gamma_L^D)^{0.5}$. 129

Figure 5.8 Acid / base plot for basic model powders using $a(\gamma_L^D)^{0.5}$. 130

Figure 5.9 Comparison between IGC and glass slide Wilhelmy plate using $a(\gamma_L^D)^{0.5}$ for the model powders. 132

Figure 5.10 Acid / base plot for model acidic powders using ΔH_d^{vap}. 133

Figure 5.11 Acid / base plot for basic model powders using ΔH_d^{vap}. 133

Figure 5.12 Acid character for the model powders using ΔH_d^{vap}. 134

Figure 5.13 Basic character for the model powders using ΔH_d^{vap}. 135

Figure 5.14 Acid / base plot for acidic model powders using boiling point data. 136

Figure 5.15 Acid / base plot for basic model powders using boiling point data. 136

Figure 5.16 Acid character for the model powders using boiling point data. 137

Figure 5.17 Base character for the model powders using boiling point data. 138

Figure 5.18 Raw data graph of Saquinavir (Ro8959-003) original sample using $a(\gamma_L^D)^{0.5}$. 140

Figure 5.19 Raw data graph of Saquinavir (Ro8959-003) original sample using ΔH_d^{vap}. 140

Figure 5.20 Raw data graph of Saquinavir (Ro8959-003) original sample using boiling point data. 141

Figure 5.21 Raw data graph of tray dried Saquinavir (batch 001) using $a(\gamma_L^D)^{0.5}$. 142

Figure 5.22 Raw data graph of spin dried Saquinavir (batch 002) using $a(\gamma_L^D)^{0.5}$. 142

Figure 5.23 Raw data graph of tray dried Saquinavir (batch 010) using $a(\gamma_L^D)^{0.5}$. 143

Figure 5.24 Raw data graph of vacuum dried Saquinavir (batch 020) using $a(\gamma_L^D)^{0.5}$. 143

Figure 5.25 Raw data graph of heated Saquinavir (batch 030) using $a(\gamma_L^D)^{0.5}$. 144

Figure 5.26 Acid / base plot for original, b001, b002 Saquinavir batches using $a(\gamma_L^D)^{0.5}$. 146

Figure 5.27 Acid / base plot for original, b010, b020 and b030 Saquinavir batches using $a(\gamma_L^D)^{0.5}$. 146

Figure 5.28 Acid character for all Saquinavir batches using $a(\gamma_L^D)^{0.5}$. 147

Figure 5.29 Base character for all Saquinavir batches using $a(\gamma_L^D)^{0.5}$. 148

Figure 5.30 Acid / base plot for original, b001, b002 Saquinavir batches using ΔH_d^{vap}. 149

Figure 5.31 Acid / base plot for original, b010, b020 and b030 Saquinavir batches using ΔH_d^{vap}. 149

Figure 5.32 Acid character for the Saquinavir batches using ΔH_d^{vap}. 151

Figure 5.33 Base character for the Saquinavir batches using ΔH_d^{vap}. 151

Figure 5.34 Acid / base plot for original, b001 and b002 Saquinavir batches using boiling point data. 152

Figure 5.35 Acid / base plot for original, b010, b020 and b030 Saquinavir batches using boiling point data. 153

Figure 5.36 Acid character for Saquinavir batches using boiling point data. 154

Figure 5.37 Base character for Saquinavir batches using boiling point data. 154

Figure 6.1 Type II adsorption isotherm 161

Figure 6.2 Schematic diagram of a single microcalorimetric unit of the TAM. 162

Figure 6.3 Schematic diagram of a single flow cell. 164

Figure 6.4 Cumulative adsorption isotherms of model powders with corrected surface areas. 167

Figure 6.5 Cumulative adsorption isotherm of Saquinavir batches. 168
Figure 6.6 Cumulative adsorption of all Saquinavir batches (corrected for surface area variation). 169
Figure 6.7 Adsorption isotherm of tray dried batches (b0-10,11,12) compared to the original Saquinavir. 170
Figure 6.8 Adsorption isotherm of vacuum dried batches (b0-20,21,22) compared to the original Saquinavir. 170
Figure 6.9 Adsorption isotherm of heated batches (b0-30,31,32) compared to the original Saquinavir. 171
Figure 6.10 Adsorption isotherm of original, tray dried (b001) and spin dried (b002) Saquinavir batches. 172
Figure 6.11 Mean adsorption isotherm of Saquinavir batches. 173
Figure 6.12 Mean adsorption of Saquinavir batches (corrected for surface areas variation). 173
Figure 6.13 Individual adsorption isotherm of original Saquinavir. 175
Figure 6.14 Individual adsorption isotherm of tray dried Saquinavir (b010). 175
Figure 6.15 Individual adsorption isotherm of vacuum dried Saquinavir (b020). 176
Figure 6.16 Individual adsorption isotherm of heated Saquinavir (b030). 177
Figure 7.1 Schematic diagram of the DVS apparatus. 182
Figure 7.2 Diagrammatic representation of DVS setup. 183
Figure 7.3 Graphical representation of experimental protocol. 185
Figure 7.4 Adsorption isotherm of Caffeine. 186
Figure 7.5 Adsorption isotherm of Theophylline. 187
Figure 7.6 Adsorption isotherm of Ethacrynic acid. 187
Figure 7.7 Adsorption isotherm of Ibuprofen. 188
Figure 7.8 Adsorption isotherms of model powders (corrected for surface area variation). 189
Figure 7.9 Adsorption isotherm of Saquinavir (original sample). 190
Figure 7.10 Adsorption isotherm of tray dried Saquinavir (b010). 190
Figure 7.11 Adsorption isotherm of vacuum dried Saquinavir (b020). 191
Figure 7.12 Adsorption isotherm of heated Saquinavir (b030). 192
Figure 7.13 Adsorption isotherm of tray dried Saquinavir (b001). 192
Figure 7.14 Adsorption isotherm of spin dried Saquinavir (b002). 193

Figure 7.15 Adsorption isotherm of Saquinavir batches (corrected for surface area variation). 194
Figure 7.16 Desorption isotherm of Saquinavir batches (corrected for surface area variation). 194
Figure 7.17 Sorption hysteresis of original Saquinavir. 195
Figure 7.18 Sorption hysteresis of tray dried Saquinavir (b010). 196
Figure 7.19 Sorption hysteresis of vacuum dried Saquinavir (b020). 196
Figure 7.20 Sorption hysteresis of heated Saquinavir (b030). 197
Figure 7.21 Sorption hysteresis of spin dried Saquinavir (b002). 197
Figure 7.22 Sorption hysteresis of tray dried Saquinavir (b001). 198
Figure 7.23 Gibbs free energy of adsorption for three model powders. 200
Figure 7.24 Ethalpy of adsorption for three model powders. 201
Figure 7.25 Entropy of adsorption for three model powders. 202
Figure 7.26 The Gibbs free energy of sorption for Saquinavir batches. 203
Figure 7.27 Enthalpy of sorption for Saquinavir batches. 203
Figure 7.28 Entropy of sorption for Saquinavir batches. 204
Figure 7.29 Two possible methods of adsorption. 208
Figure 7.30 The Gibbs free energy of sorption for the original Saquinavir over 3 cycles. 210
Figure 7.31 The Gibbs free energy of sorption for the tray dried Saquinavir over 3 cycles. 210
Figure 7.32 The Gibbs free energy of sorption for the vacuum dried Saquinavir over 3 cycles. 211
Figure 7.33 The Gibbs free energy of sorption for the heated only Saquinavir over 3 cycles. 211
Figure 7.34 Change in ΔG between 60% and 90%RH with repeated cycling. 212
Figure 7.35 Enthalpy of sorption for the original Saquinavir over 3 cycles. 212
Figure 7.36 Enthalpy of sorption for the tray dried Saquinavir over 3 cycles. 213
Figure 7.37 Enthalpy of sorption for the vacuum dried Saquinavir over 3 cycles. 213
Figure 7.38 Enthalpy of sorption for the heated only Saquinavir over 3 cycles. 213
Figure 7.39 Change in ΔH between 60% and 90%RH with repeated cycling. 214
Figure 7.40 Entropy of sorption for the original Saquinavir over 3 cycles. 214
Figure 7.41 Entropyy of sorption for the tray dried Saquinavir over 3 cycles. 215
Figure 7.42 Entropyy of sorption for the vacuum dried Saquinavir over 3 cycles. 215

Figure 7.43 Entropyy of sorption for the heated only Saquinavir over 3 cycles. 215

Figure 7.44 Change in ΔS between 60% and 90%RH with repeated cycling. 216

Figure 8.1 Diagrammatic representation of the dynamometer output. 218

Figure 8.2 Wetting process. 219

Figure 8.3 Rheometer analysis of granulation properties of Saquinavir batches by sequential addition of liquid binder. 221

Figure 8.4 Rheometer analysis of granulation properties of Saquinavir batches over time (with addition of liquid binder at time zero). 221

Figure 8.5 Caffeine. 222

Figure 8.6 Theophylline. 222

Figure 8.7 Salicylic acid. 222

Figure 8.8 Ibuprofen. 222

Figure 8.9 Ethacrynic acid. 222

Figure 8.10 Original Saquinavir. 223

Figure 8.11 Tray dried Saquinavir (b010). 223

Figure 8.12 Tray dried Saquinavir (b001). 223

Figure 8.13 Vacuum dried Saquinavir (b020). 223

Figure 8.14 Heated only Saquinavir (b030). 223

Figure 8.15 Spin dried Saquinavir (b002). 223

Figure 9.1 Ideal technique for contact angle measurement. 228

Symbols

γ_{SL}	Interfacial tension between solid and liquid phases
γ_{SV}	Solid surface free energy
γ_{LV}	Liquid surface tension
γ^{LW}	Non-polar component of surface energy (Lifshitz van der Waals)
γ^{P}	Polar component of surface energy
γ^{d}	Non-polar (dispersive) component of surface energy
γ^{+}	Electron accepting character
γ^{-}	Electron donating character
K_A	Acidic behaviour
K_B	Basic behaviour
Wi	Work of immersion
Wa	Work of adhesion
Ws	Work of spreading
W_c	Work of cohesion
λ	Spreading coefficient.
p	Compact perimeter
θ	Contact angle
η	Viscosity
F	Carrier gas flow rate (ml/min)
J	Correction factor due to pressure differences
t_r	Retention time of the probe
t_0	Retention of the non-interacting standard
$\Delta G_{cal}°$	Gibbs free energy of adsorption.
$\Delta H_{cal}°$	Enthalpy of adsorption.
$\Delta S_{cal}°$	Entropy of adsorption.
b	No. of water molecules sorbed per gram
P_0	Saturated water vapour pressure at 25°C
ΔH^{d}_{vap}	The dispersive component of the heat of vaporisation of probes
P_0	Saturated vapour pressure

A_i	Total surface area of stationary phase
V_i	Total surface volume of stationary phase
K_S	Surface partition coefficient
K_l	Bulk partition coefficient
w	weight of adsorbent in column (g)
S_a	Specific surface area of adsorbent
Γ	Surface concentration of adsorbate
C	Adsorbate concentration in gas phase
H	Height liquid has risen in time t.
R	Effective interstitial pore radius between packed particles
$P_{s.s}$	Adsorbate vapour pressure in equilibrium with standard adsorption state
$P_{s.g}$	Adsorbate vapour pressure in the gaseous standard state
T	Temperature of column (K)
R	Gas constant
P_i	Pressure at the inlet of the column ($kN.m^{-2}$)
P_o	Atmospheric pressure ($kN.m^{-2}$)
η	Viscosity of the liquid.($N.s.m^{-2}$)
ρ	Density of the liquid (g/cm^3)
σ	Surface tension of the liquid ($mJ.m^{-2}$)
c	Unknown geometric environment
m	Mass gain (mg)
t	Time (seconds)
DN	Defined by the reaction enthalpy of the probe liquid with a reference acceptor, $SbCl_5$
AN	Defined as the NMR chemical shift of ^{31}P contained in $(C_2H_5)_3PO$ when reacting with the probe liquid

Chapter 1

Introduction

1 Introduction

The properties of all adhesives, coatings and composites are dependent on interaction phenomena. With adhesion, wicking, catalysis, composite formation and many other related phenomena, the intermolecular interactions across the interface decide the success or failure of a process. The presence and nature of these intermolecular interactions, which include Lifshitz van der Waals (non-polar) and acid-base (polar) interactions, each govern different behaviour. For a complete understanding of surface and interface phenomena, including adhesion, cohesion and wetting, one must be able to comprehensively characterise the powder surface. There are a variety of methods available for surface characterisation, all with their own individual advantages and disadvantages.

Wetting is a macroscopic manifestation of molecular interactions across the interface separating different liquids and solids. The wetting process is an important factor in the preparation, storage and use of all pharmaceuticals, for example:-

a) Dispersion of powders to form suspensions.
b) Addition of binders during wet granulation.
c) Adhesion of polymer films to tablets.
d) Dissolution rate of solid dosage forms in the gastrointestinal tract.

To ensure that the best formulation is chosen for mass production the accurate physical characterisation of all pharmaceutical ingredients is crucial. With new chemical entities, where only a few grams of drug are available, experiments would ideally require only minute quantities so that any difficult powder is effectively discarded or placed on a more suitable development strategy before too much time and expense have been wasted. As yet this is not the case, as it may take several grams before a useful, wide ranging examination of the surface properties can be made, leaving this section of research well up the ladder of a product's development. By investigating a range of common and novel analytical techniques, the surface characterisation may become an integral part of a new compound's screening.

Pharmaceutical powders are usually prepared in batches, whereby a specific quantity of formulation are mixed together under specific conditions which remain constant for the production of further batches. Unfortunately, having only minor differences in the batch process, or for that matter the raw materials used, may give rise to subtle variations between batches. If the drug is a sensitive one, the resulting batch may have to be rejected (Ticehurst et al., 1996). In the past, changes in batches have been assigned to variations in the raw materials from suppliers (Landin et al., 1993 and Phadke et al., 1994), but variations in the surface character may also play a major part. Changes in the crystalline nature of a solid (e.g. polymorphic form, crystal habit and crystal lattice imperfections) result in different surface properties (Buckton and Beezer, 1991). These changes can alter the processability (flow, compression) and wetting (dissolution) behaviour and thus the bioavailability of the product.

Drugs used in production of solid dosage forms are often assumed to be crystalline in nature, even though they may have been through varied production processes, for example freeze drying, spray drying and comminution (Hutteurauch, 1988, Hersey and Krycer, 1980), which have led to the formation of amorphous structures with higher energy than their counterparts. It has been shown that these 'hot spots' of higher energy may cause the powder to behave in a totally different manner than to other totally crystalline batches. Examples include:- A decrease in stabilty (Otsuka and Kaneniwa, 1990) and increased dissolution rates (Chiou and Kyle, 1979, Hendriksen, 1990). In addition, drying along with milling and compression (Hutteurauch, 1988) can influence the prevalence of lattice imperfections.

Even if only the top surface layers are affected, this may still cause the physicochemical properties to change drastically. It is therefore very important to be able to measure and, if possible, control amorphous content in pharmaceutical drug formulations. Techniques that analyse the bulk (e.g. X-ray analysis, infra-red spectroscopy and solid-state NMR spectrometry) are not necessarily sensitive enough to detect surface modifications, therefore other more selective surface analysis techniques are required (e.g. inverse gas chromatography, dynamic vapour sorption).

In this thesis, a selection of surface analytical methods have been studied, with the aim of interrelating and comparing their individual results and so putting together a step by step guide to the most useful determination of the surface properties of an unknown powder. Six powders have been studied, all with different surface characteristics, so that each method can be assessed on its ability to distinguish between very different powder samples. In addition, one of the powders has been subjected to a range of drying conditions, to test whether a particular method is sensitive enough to pinpoint any batch to batch variation, if present.

1.1 Surface Energy

The surface free energy of a solid powder (γ_{SV}) refers to the intermolecular forces between the solid and vapour molecules at the surface in addition to a force of attraction between the surface solid molecules themselves which hold the lattice together. This leaves an excess of energy per unit area, γ_{SV}.

Figure 1.1 Diagrammatic representation of a surface and a bulk molecule within a powder solid.

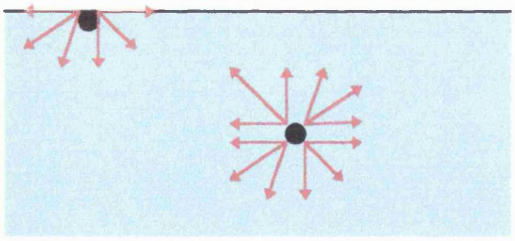

Therefore it is possible that atoms and molecules at powder surfaces and interfaces can have energies that are significantly altered to those inside the bulk phase. The molecules at the surface are influenced by unbalanced molecular forces and therefore possess additional energy in excess of the bulk materials (Figure 1.1) (Van Krevelen, 1976). In a solid, these molecules are held relatively firmly in place, the 'free' energy cannot be directly measured and therefore indirect techniques have to be used. The surface is usually a region between a liquid or solid and a gas or vacuum, whilst the interface is usually a region between a liquid or solid and another liquid or solid.

All reactions, chemical or physical, occur at an interface between two different solids, liquids or gases. If the surface energy or tension of a surface is known, one can predict the outcome of the physical reaction. At a liquid surface, the intermolecular forces of attraction are greater than the liquid-gas interaction, which results in a net inward force, known as the surface tension. This unbalanced interaction at the surface interface results in a tendency for the liquid to minimise its surface area, causing a small drop of liquid to form a spherical shape. To demonstrate the surface tension of a liquid, as a vertical capillary tube (Figure 1.2) is lowered into a liquid, the liquid rises up the capillary above the height of the reservoir. This can also be used to measure the upward force being the liquid surface tension.

Figure 1.2 Surface tension effect.

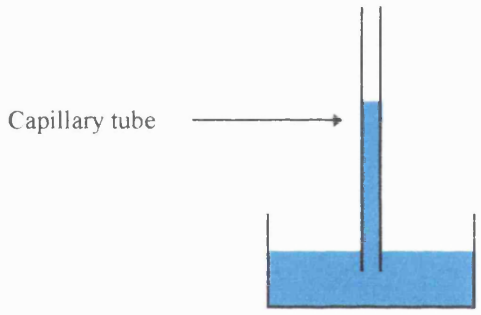

The force acting downwards, is the gravitational pull of the liquid, whilst this is counterbalanced with the upward force caused by the liquid's surface tension, which is able to maintain a column of liquid above the main reservoir.

The same is true for the surface energy of a powder, except that the intermolecular forces are large enough to prevent molecules from moving around freely. When a small volume of liquid comes into contact with a solid surface, a droplet forms, its dimensions determined by a combination of the surface energy of the solid, the surface tension of the liquid and the solid \ liquid interfacial energy as in Figure 1.3.

Figure 1.3 Possible interactions of a droplet on a powder surface.

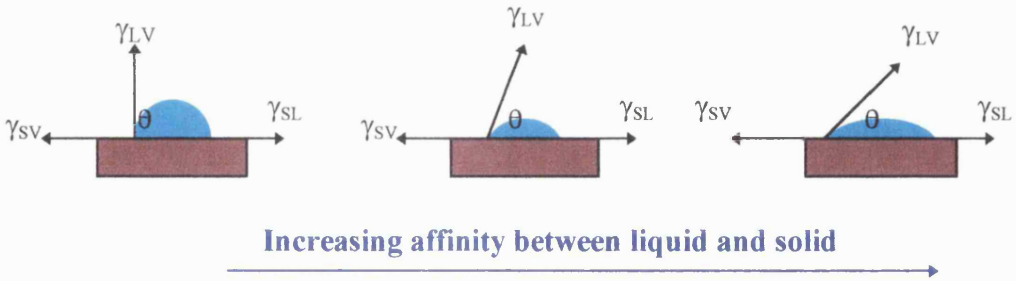

The surface energy of a solid is affected by any vapour in contact with the surface, therefore the real value is given by:-

$$\Pi_e = \gamma_S - \gamma_{SV} \qquad \text{Equation 1.1}$$

γ_S	-Powder surface energy in a vacuum.
γ_{SV}	-Powder surface energy
Π_e	-Equilibrium spreading pressure
θ	-Contact angle of a liquid with a powder
γ_{SL}	-Powder / liquid interfacial energy
γ_{LV}	-Liquid surface tension

The contact angle is the angle that is formed between a liquid coming into contact with a solid, and it represents an equilibrium of three interfacial force, first described by Young in Equation 1.2.

$$\gamma_{SV} = \gamma_{SL} + \gamma_{LV}(\cos\theta) + \Pi_e \quad \text{(Young, 1805)} \qquad \text{Equation 1.2}$$

The equilibrium spreading pressure, Π_e, is assumed to be negligible for non-volatile liquids and can be ignored. Therefore if the surface energy of the solid is known, the solid's behaviour with any known test liquid can, in theory, be predicted. To derive

Equation 1.2, Young assumed that the solid is an ideal one; one that is chemically homogenous, rigid and completely flat at an atomic level on the surface. In addition, the solid does not chemically react with or absorb into the bulk any other molecules, be they gaseous or liquid. The affect of gaseous absorption into a solid is therefore assumed to be negligible. With all these assumptions in mind, one can predict a single contact angle for the solid as a whole. Since the contact angle represents an equilibrium of the energies at a three phase interface, it provides information about surface energetics, surface roughness and surface heterogeneity (Johnson and Dettre, 1969).

Certain techniques, discussed later, are able to provide two types of contact angles, those being advancing and receding contact data. In theory, they should be equal although in practise the surface roughness of the powder being presented to the liquid results in differing advancing and receding contact angles. Commonly, the receding angle is close to zero and therefore the advancing angle is mainly used to calculate surface energy data (Good, 1953). The difference between the two angles is called hysteresis, and it is given the simple mathematical form:-

$$\text{Hysteresis} = \theta_a - \theta_r \qquad \text{Equation 1.3}$$

Other factors such as powder heterogeneity and bulk penetration of a liquid will often result in contact angle hysteresis (Anhang and Gray, 1982), and even the environment and preparation of the powder surface may also affect the contact angle. Therefore the thermodynamic significance of the contact angle measurement is often questionable.

1.2 Wetting process

Wetting occurs when one fluid or vapour is displaced by another at a surface. In most pharmaceutical situations, air is displaced by a liquid.

Figure 1.4 Importance of wetting phenomena.

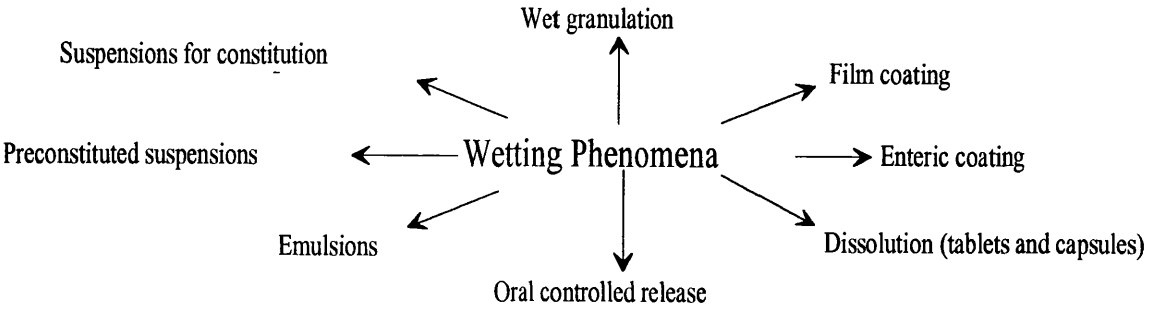

(Shanker, 1994)

The thermodynamics of a powder being wetted by a liquid are comprised of three distinct steps as shown in Figure 1.5.

1.2.1 Adhesion

Adhesion can occur when one side of the model solid cube has exchanged contact with vapour for contact with the liquid phase. The energy required for this step is termed the 'work of adhesion', Wa, whereby:-

$$Wa = \gamma_{SL} - (\gamma_{SV} + \gamma_{LV}) \qquad \text{Equation 1.4}$$

One solid/liquid interfacial energy is gained while both one solid surface energy and one liquid surface energy are lost.

When Equation 1.4 is combined with the Young's Equation 1.2, the Young-Dupre equation is formed:-

$$Wa = -\gamma_{LV} (Cos\theta+1) \qquad \text{Equation 1.5}$$

Figure 1.5 Theory behind wetting (steps 1-4).

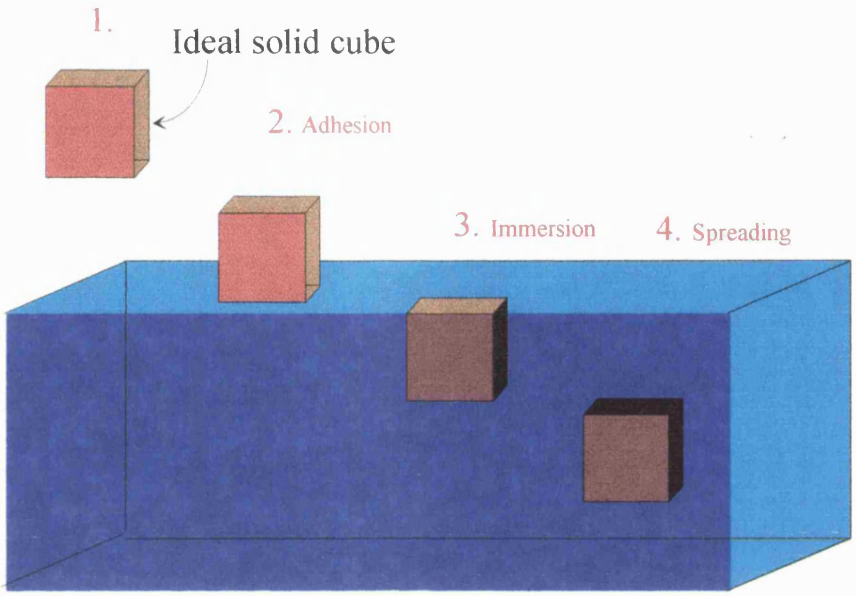

(Parfitt, 1969)

1.2.2 Immersion

The liquid spreads over more of the powder surface, so reducing the interaction between powder and vapour. The 'work of immersion', Wi, is the energy process involved, whereby four faces of the cube which were in contact with vapour are now immersed in liquid:-

$$Wi = 4\gamma_{SL} - 4\gamma_{SV} \qquad \text{Equation 1.6}$$

Combining Young's Equation 1.2 with Equation 1.6:-

$$Wi = -4\gamma_{LV}(Cos\theta) \qquad \text{Equation 1.7}$$

1.2.3 Spreading

The 'work of spreading', Ws, or the spreading coefficient, s, causes one surface/liquid energy and one liquid vapour to be gained whilst losing one solid vapour energy. This is described as:-

$Ws = \gamma_{SL} + \gamma_{LV} - \gamma_{SV}$ Equation 1.8

Combining Young's Equation 1.2 with Equation 1.8:-

$Ws = -\gamma_{LV} (Cos\theta-1)$ Equation 1.9

From Equations 1.5, 1.7 and 1.9, the wettability of a powder with several different liquids can be predicted.

For spontaneous wetting to occur, all Wa, Wi and Ws must be positive in nature:-

a) Adhesion...	$\gamma_{LV} (1+Cos\theta)>0$	$\therefore Cos\theta > -1$ and $\theta < 180°$
b) Immersion...	$\gamma_{LV} (Cos\theta)\geq 0$	$\therefore Cos\theta > 0$ and $\theta < 90°$
c) Spreading...	$\gamma_{LV} (Cos\theta-1)\leq 0$	$\therefore Cos\theta \leq +1$ and $\theta \leq 0°$

Therefore, the greater the affinity between powder surface and liquid, the more the liquid spreads and therefore the smaller the contact angle. A point is reached when the contact angle becomes zero, the liquid perfectly wets the powder surface and spreading occurs. Therefore the contact angle is able to indicate the degree of wettability of a particular solid with a known liquid.

1.3 Critical Surface Tension (γc)

γ_c is the critical surface tension of a solid and is defined as the surface tension of a wetting liquid, above which spontaneous wetting does not occur. It is derived by finding the contact angles of a solid with various liquids of differing surface tension and extrapolating them back to $Cos\theta=1$ (Fox and Zisman, 1950). In practice this is inaccurate, due to increases in error by extrapolation, and that certain liquid combinations produce unsuitable data (discussed in detail in Chapter 3). Therefore the critical surface tension should only be used for non-polar solids tested with non-polar liquids (Good, 1973).

1.4 Deriving contact angles experimentally

1.4.1 Liquid with unknown surface energy

There are several methods of surface tension analysis available:-

a) Capillary rise - extent of ascension of liquid through a powder bed.
b) Drop volume/weight - drops of liquid are formed at the end of a capillary tube, and by measuring their volume and weight, the surface tension can be calculated.
c) Du Nouy ring tensionmeter - measures the force of interaction between the solid ring and the liquid with unknown surface tension.
d) Wilhelmy plate - uses the same theory as the Du Nouy ring, except that the ring is substituted with a solid plate of known perimeter.

Both parts c) and d) involve the interaction of a characterised solid (e.g. glass slide) which is brought into contact with the liquid in question.

1.4.2 Solid with unknown surface energy

Contact angle measurement can either be achieved by liquid penetration into the solid powder bed, a sessile drop placed onto a powder plate or the interaction between a powder plate that is slowly brought into and out of a test liquid reservoir.

1.4.2.1 Liquid penetration

Liquid penetration involves the passage of a test liquid into a powder bed. By measuring the rate of liquid uptake, one can calculate a contact angle with the knowledge of the liquid's viscosity, density and surface tension. It is discussed in more detail in Chapter 4.

1.4.2.2 Powder compacts

All techniques that involve the compaction of powders may be of questionable use since alterations in surface energy may occur with sensitive powders under compression. The advantages and disadvantages of these methods are given in the table below. The Wilhelmy plate technique is discussed more fully in Chapter 3, since it has been used in my research.

Table 1.1 Advantages and disadvantages of contact angle measurement methods.

	Advantages	Disadvantages
Capillary rise at a vertical plate.	Simple to use	No receding and advancing angles
Tilting plate method	Simple to use	operator dependent
Sessile drops onto a compact	Measures advancing and receding angles	operator dependent
Adhering gas bubbles.		Difficult to differentiate between advancing and receding angles
Liquid penetration	Powder is unaltered in preparation	Careful selection of test liquids required. No receding data.
Wilhelmy plate technique	Automated to reduce operator dependence Advancing and receding angles	Compaction of plate may alter powder properties

1.5 Surface energy determination using contact angle data

Several different theoretical methods have been utilised over the 20th Century, although only two of the most recent theories have been utilised in this thesis.

1.5.1 Van Oss theory

Surface energy (γ_{SV}) can be subdivided into polar and non-polar (dispersive) components, the sum of the components being equal to the total surface energy (Van Oss et al., 1987).

$$\gamma_{SV} = \gamma_S^{LW} + \gamma_S^{AB}$$ Equation 1.10

LW - Lifshitz Van der Waals interactions (non-polar) combining all the electromagnetic interactions, temporary oscillating dipoles, permanent dipoles and the induced dipole-induced dipole forces. (Section 1.5.1.1)

AB - Lewis acid-base interactions (polar) involve electrostatic interactions. (Section 1.5.1.2)

The two components are additive since there is no physical interaction between LW and AB forces.

1.5.1.1 Van der Waals interactions (γ_S^{LW})

Intermolecular interactions in liquids always involve van der Waals interactions especially between the nearest and next nearest neighbouring molecules. Van der Waals interactions also occur in gases, when a gas molecule has a near collision with another gas molecule. As the two molecules approach one another, dipoles become orientated to maximise their attractive forces. The Lifshitz mathematical theory of the attraction between macroscopic bodies is used to estimate the free energy values. Three kinds of attractive forces can occur, all of which contribute to the van der Waals interactions.

a) London dispersion forces which are proportional to the square of the molecular polarizability.
b) Keesom dipole - dipole interactions which can occur only if dipoles are already present.
c) Debye interactions of dipoles with dipoles which are induced in adjacent molecules. In each case the attractive energy is proportional to the inverse sixth power of the intermolecular distance between the two molecules.

1.5.1.2 Lewis Acid-Base interactions (γ_S^{AB})

The polar component, (γ_S^{AB}), is an important force of attraction involved in adhesive bonds of coatings, laminates and in stabilised particulate suspensions. It is comprised of two parameters which describe the electron acceptor (γ_S^+) and donor (γ_S^-) affects, whereby:-

$$\gamma_S^{AB} = 2(\gamma_S^+.\gamma_S^-)^{0.5} \qquad \text{Equation 1.11}$$

The two values that give γ_S^{AB} are not additive. Since absolute values of γ_S^+ and γ_S^- cannot be measured, all values are compared to water. γ_W^{AB} = 51 mJ.m^{-2} , whereby both γ_S^+ and γ_S^- have been ascribed the value 25.5 mJ.m^{-2}.

These polar interactions involve hydrogen bonding which contributes to the surface energy. These commonly consist of a hard subset of the Lewis acid/base (HSAB) interactions. Hard acid/base interactions are dominated by electrostatic interactions, which occur to a great extent with hydrogen bonds between protons (H^+) and electron donors. It has been proved that the energy of hydrogen bonds is entirely independent of dipole moments and depends only on the acidity of the hydrogen donor and the basicity of the hydrogen acceptor (Pimental and McClellan, 1960). Acid/base interactions (such as hydrogen bonding) provide a considerable interaction making up the cohesive energy in polar liquids. For this to occur, the polar liquid requires both acidic (electron accepting) and basic (electron donating) sites. Therefore it follows that acidic liquids with negligible basicity and basic liquids with negligible acidity have no specific self association, resulting in that their cohesive energy and surface tension being only due to their non-polar (dispersion) force interactions (Fowkes, 1964).

1.5.1.3 Possible interactions

From Equations 1.10 and 1.11 it can be seen that materials can be either non-polar, bipolar or monopolar, where any purely non-polar material has no acid-base interaction capacity. There are seven possible interactions that can occur between two molecules (Van Oss et al., 1988):-

1). Non-polar / Non-polar
2). Non-polar / monopolar (+ve)
3). Non-polar / monopolar (-ve)
4). Monopolar / monopolar (both the same sign)
5). Monopolar/monopolar (different signs)
6). Monopolar / bipolar
7). Bipolar / bipolar

1.5.1.4 Van Oss equation derivation

Equation 1.11 can be expanded to describe the polar interaction between a liquid and a solid to give:-

$$\gamma_{SL}^{AB} = 2\{(\gamma_S^+.\gamma_S^-)^{0.5} + (\gamma_L^+.\gamma_L^-)^{0.5} - (\gamma_S^+.\gamma_L^-)^{0.5} - (\gamma_S^-.\gamma_L^+)^{0.5}\} \qquad \text{Equation 1.12}$$

Fowkes (1964) showed that for a totally non-polar liquid the non-polar interaction with a solid is described as:-

$$\gamma_{SL}^{LW} = \gamma_S^{LW} + \gamma_L^{LW} - 2(\gamma_S^{LW}.\gamma_S^{LW})^{0.5} \qquad \text{Equation 1.13}$$

The sum of Equations 1.12 and 1.13 is equivalent to the polar and non-polar interactions:-

$$\gamma_{SL}^{TOT} = \{(\gamma_S^{LW})^{0.5} + (\gamma_L^{LW})^{0.5}\}^2 + 2\{(\gamma_S^+.\gamma_S^-)^{0.5} + (\gamma_L^+.\gamma_L^-)^{0.5} - (\gamma_S^+.\gamma_L^-)^{0.5} - (\gamma_S^-.\gamma_L^+)^{0.5}\}$$

Equation 1.14

It is now possible to rewrite Young's equation in terms of LW and AB interactions:-

$$\gamma_{LV}^{TOT}(1+\cos\theta) = 2\{(\gamma_S^{LW}.\gamma_L^{LW})^{0.5} + (\gamma_S^+.\gamma_L^-)^{0.5} + (\gamma_S^-.\gamma_L^+)^{0.5}\} \qquad \text{Equation 1.15}$$

1.5.1.5 Polarity ratios

Equation 1.15 is theoretically solvable, but the square roots make it difficult to handle. To simplify matters, one can remove both the polar factors (γ_S^+ and γ_S^-) and replace them with a polarity ratio which describes the unknown terms in relation to water (Buckton, 1995). The derivation is shown below:-

In this example, the test liquid is formamide (F) with an unknown solid (S).

$$\gamma_F^{TOT}(1+\cos\theta_{SF}) = 2\{(\gamma_S^{LW}.\gamma_F^{LW})^{0.5} + (\gamma_S^+.\gamma_F^-)^{0.5} + (\gamma_S^-.\gamma_F^+)^{0.5}\} \qquad \text{Equation 1.16}$$

Equation 1.11 can be converted for formamide, giving:-

$$\gamma_F^{AB} = 2\,(\gamma_F^{+}.\gamma_F^{-})^{0.5} \qquad \text{Equation 1.17}$$

$$\therefore\ (\gamma_F^{+})^{0.5} = \frac{\gamma_F^{AB}}{2(\gamma_F^{-})^{0.5}} \qquad \text{Equation 1.18}$$

$$\gamma_F^{AB} = 19\text{mJ.m}^{-2}$$

Combining Equations 1.16 and 1.18:-

$$\gamma_F^{TOT}(1+\cos\theta_{SF}) = 2((\gamma_S^{LW}.\gamma_F^{LW})^{0.5} + 9.5\left(\frac{\gamma_S^{+}}{\gamma_F^{+}}\right)^{0.5} + 9.5\left(\frac{\gamma_S^{-}}{\gamma_F^{-}}\right)^{0.5}) \qquad \text{Equation 1.19}$$

$$\therefore \gamma_F^{TOT}(1+\cos\theta_{SF}) = 2(\gamma_S^{LW}.\gamma_F^{LW})^{0.5} + 19\left(\frac{\gamma_S^{+}}{\gamma_F^{+}}\right)^{0.5} + 19\left(\frac{\gamma_S^{-}}{\gamma_F^{-}}\right)^{0.5} \qquad \text{Equation 1.20}$$

The polarity ratio for formamide in respect of water (w) is defined as:-

$$\delta_{FW}^{+} = \left(\frac{\gamma_F^{+}}{\gamma_W^{+}}\right)^{0.5} \qquad \text{Equation 1.21}$$

$$\therefore (\gamma_F^{+})^{0.5} = \delta_{FW}^{+}.(\gamma_W^{+})^{0.5} \qquad \text{Equation 1.22}$$

Combining Equations 1.20 and 1.22:-

$$\gamma_F^{TOT}(1+\cos\theta_{SF}) = 2(\gamma_S^{LW}.\gamma_F^{LW})^{0.5} + 19\left[\frac{(\gamma_S^{+})^{0.5}}{\delta_{FW}^{+}.(\gamma_W^{+})^{0.5}}\right] + 19\left[\frac{(\gamma_S^{-})^{0.5}}{\delta_{FW}^{-}.(\gamma_W^{-})^{0.5}}\right]$$

Equation 1.23

Using Equation 1.21 for water and the unknown solid, δ_{SW} values can be substituted:-

$$\gamma_F^{TOT}(1+\cos\theta_{SF}) = 2(\gamma_S^{LW}.\gamma_F^{LW})^{0.5} + 19\left(\frac{\delta_{SW}^{+}}{\delta_{FW}^{+}}\right) + 19\left(\frac{\delta_{SW}^{-}}{\delta_{FW}^{-}}\right) \qquad \text{Equation 1.24}$$

Since δ_{FW}^{+} and δ_{FW}^{-} can be given true values using Equation 1.21, the final equation

becomes:-

$$\gamma_F^{TOT}(1+\cos\theta_{SF}) = 2(\gamma_S^{LW}.\gamma_F^{LW})^{0.5} + 63.55\delta_{SW}^{+} + 15.25\delta_{SW}^{-} \quad \text{Equation 1.25}$$

Equation 1.25 can be derived in the same manner for any of the test probe liquids, as long as all the liquid's surface energy parameters are known, including γ^+ and γ^- values.

Table 1.2 Selection of polar probe liquids and their corresponding equation.

Test probe liquid	Equation
Water (W)	$\gamma_W^{TOT}(1+\cos\theta_{SW}) = 2(\gamma_S^{LW}.\gamma_W^{LW})^{0.5} + 51\delta_{SW}^{+} + 51\delta_{SW}^{-}$
Formamide (F)	$\gamma_F^{TOT}(1+\cos\theta_{SF}) = 2(\gamma_S^{LW}.\gamma_F^{LW})^{0.5} + 63.55\delta_{SW}^{+} + 15.25\delta_{SW}^{-}$
Ethylene Glycol (E)	$\gamma_E^{TOT}(1+\cos\theta_{SE}) = 2(\gamma_S^{LW}.\gamma_E^{LW})^{0.5} + 69.24\delta_{SW}^{+} + 13.995\delta_{SW}^{-}$

This enables all acid-base and non-polar interactions to be found with contact angles for the test material using only three probe liquids.

1.5.1.6 Two possible methods using the Van Oss theory

a) Using one non-polar liquid and two polar liquids.

The totally non-polar liquid has no polar properties, therefore γ_S^{AB} is equal to zero and can be ignored from Equation 1.15, leaving:

$$\gamma_{LV}^{TOT}(1+\cos\theta) = 2(\gamma_S^{LW}.\gamma_L^{LW})^{0.5} \quad \text{Equation 1.26}$$

Since only the non-polar component (γ_S^{LW}) of the powder is unknown, this contact angle alone can be used to calculate the non-polar component of surface energy for the powder. Subsequently, the two polar liquids yield powder contact angles that can be placed into Equation 1.15 to form two separate equations. These are solved simultaneously to determine the electron acceptor (γ_S^+) and donor (γ_S^-) values.

b) Using three polar liquids.

This is only necessary if the non-polar liquid is unable to produce a contact angle with the test material due to immediate spreading on contact ($\cos\theta \geq 1$). By using three polar liquids, three equations can be formed all having three unknowns. Solving two equations at a time to eliminate the dispersive component (γ_S^{LW}) will produce two hybrid equations each having only two unknowns. They are solved simultaneously giving the electron acceptor (γ_S^+) and donor (γ_S^-) which can then be used to back calculate the non-polar component of surface energy (γ_S^{LW}).

1.5.2 Wu's theory

A harmonic mean approach was developed by Wu (1971), which was able to obtain a greater correlation between experimental and theoretical calculations than previously for low energy systems, such as organic liquids.

$$\gamma_{12} = \gamma_1 + \gamma_2 - 4\left(\frac{\gamma_1^d \cdot \gamma_2^d}{\gamma_1^d + \gamma_2^d}\right) - 4\left(\frac{\gamma_1^p \cdot \gamma_2^p}{\gamma_1^p + \gamma_2^p}\right) \qquad \text{Equation 1.27}$$

γ^p - Polar component

γ^d - Non-polar (dispersive) component

For higher energy systems (e.g. mercury or glass) Wu was able to simplify the above equation to:-

$$\gamma_1(1 + \cos\theta) = 2\{(\gamma_1^d \cdot \gamma_2^d)^{0.5} + (\gamma_1^p \cdot \gamma_2^p)^{0.5}\} \qquad \text{Equation 1.28}$$

The two Equations 1.27 and 1.28 can be combined with Young's equation to give Equations 1.29 and 1.30.

$$\gamma_{12} = \gamma_1 + \gamma_2 - 2\left(\gamma_1^d . \gamma_2^d\right)^{0.5} - 4\left(\frac{\gamma_1^p \cdot \gamma_2^p}{\gamma_1^p + \gamma_2^p}\right) \qquad \text{Equation 1.29}$$

and

$$\gamma_1(1 + \cos\theta) = 4\left(\frac{\gamma_1^d \cdot \gamma_2^d}{\gamma_1^d + \gamma_2^d} + \frac{\gamma_1^p \cdot \gamma_2^p}{\gamma_1^p + \gamma_2^p}\right) \qquad \text{Equation 1.30}$$

Equations 1.29 and 1.30 each contain two unknown terms, those being the solid's non-polar (dispersive) and polar components of surface energy. Contact angle data from only two liquids can produce a pair of simultaneous equations that can be solved to give values for the two unknowns. Alternatively, an iterative computer program is able to do this upon entering the contact angle data.

1.6 Potential use of surface energy data

Surface energies are more useful than contact angles since they describe the general characteristics of a powder surface which can then be related to any liquid. Whereas a single contact angle only describes how one particular liquid interacts with that powder surface. Surface energy can be used to give values for work of adhesion, W_a, work of cohesion, W_c and the spreading coefficient, λ.

$$W_a = 4\left\{\left(\frac{\gamma_1^p \cdot \gamma_2^p}{\gamma_1^p + \gamma_2^p}\right) + \left(\frac{\gamma_1^d \cdot \gamma_2^d}{\gamma_1^d + \gamma_2^d}\right)\right\} \qquad \text{Equation 1.31}$$

Where:-

$$W_{c1} = 2\gamma_1 \qquad \text{Equation 1.32}$$

$$\lambda_{12} = W_{a12} - W_{c1} \qquad \text{Equation 1.33}$$

$$\lambda_{21} = W_{a21} - W_{c2} \qquad \text{Equation 1.34}$$

$$\therefore \lambda_{12} = 4\left\{\left(\frac{\gamma_1^p \cdot \gamma_2^p}{\gamma_1^p + \gamma_2^p}\right) + \left(\frac{\gamma_1^d \cdot \gamma_2^d}{\gamma_1^d + \gamma_2^d}\right) - \left(\frac{\gamma_1}{2}\right)\right\} \qquad \text{Equation 1.35}$$

The spreading coefficient is the difference between W_a and W_c, where Equation 1.35 describes the spreading of phase 1 over phase 2 and vice versa. If λ_{12} is positive, phase 1 will spread easily over phase 2 while if negative spreading of phase 1 over phase 2 will not be favourable. These values have been used to predict the physical stability in non-polar, non-aqueous suspensions (Parsons et al., 1992).

1.7 Alternative methods of surface analysis

Other techniques and theories have been developed that do not use contact angle data and being able to interrelate all of them would be prove useful.

1.7.1 Adsorption

Adsorption can be defined as the presence of a greater concentration of foreign molecules at the surface than in the bulk of the material and it can occur at any type of interface. There are two kinds of adsorption, chemical and physical.

a) Chemisorption - usually an irreversible process where strong bonds are able to form a monolayer coverage.
b) Physisorption - a reversible process whereby a monolayer or multilayer of foreign molecules completely cover the solid surface, but are only held there with weak bonds (e.g. hydrogen bonds).

In pharmaceutical research, physisorption is interesting due to its reversible nature. Within a crystalline solid, although the majority of its atoms or molecules will be arranged in a ordered, repeatable pattern, there will often exist defects, imperfections and regions of amorphous structure. These alterations are referred to as 'hot spots' consisting of molecules in an activated state in comparison with the crystalline

majority. They have a greater molecular mobility and often expose more reactive chemical groups of their molecule to the environment, allowing them to react differently with gaseous vapours. These factors affect the overall characteristics of the crystalline solid.

The following techniques of surface analysis all involve adsorption of gaseous molecules to a powder surface, showing that the nature of sorption can give information on the actual characteristics of a particular powder surface.

1.7.2 Inverse gas chromatography

Gas chromatography involves the separation process of a mobile phase (gaseous molecules) over a solid phase (powder column). With inverse gas chromatography (IGC), the solid phase is the powder of unknown character while the mobile phase consists of a number of well characterised low molecular weight probe molecules.

1.7.2.1 History of IGC development

The original definition of acidity and basicity was described by Lewis (1923), stating:-

"An acid molecule or ion whose incomplete electronic arrangement allows it to bind to another species by accepting an electron pair from that species, whereas a base is a molecule or ion capable of donating an electron pair to a Lewis acid, resulting in the formation of a co-ordinate covalent bond."

It is limited in that it excludes reactions such as single electron transfer reactions (redox), free radical combination reactions and the like. Several years later, Sedgwich (1927) used the terms electron donor or donor for a Lewis base, and electron acceptor or acceptor for a Lewis acid. The same concept was introduced by Ingold (1933) but it used the new terms 'electrophile' for a Lewis acid which accepts electrons from carbon and 'nucleophile' for a Lewis base which donates electrons to a carbon atom.

Attention was then focused on the quantum mechanical calculations involving changes

in electron density distribution (Coulson and Longuet-Higgins, 1947) resulting in the molecular orbital theories favoured by Pauling and others. The first monograph on the quantum mechanical approach to calculations was published by Briegleb in 1961. Using this, a quantitative scale for Lewis' acid base concept was needed. Three approaches were developed:-

a) The hard-soft acid-base principle of Pearson, 1963.
b) Equations by Drago and Wayland, 1965.
c) Donor-acceptor approach of Gutmann et al., 1966.

The principle of IGC is based on the characteristic equilibrium partitioning of the vapour molecules (adsorbate) between the mobile and the solid stationary phases (adsorbent). Difference in behaviour is due to the presence and nature of intermolecular interactions, including Lifshitz van der Waals forces (non-polar - primarily London dispersion forces but can include a small contribution from Keesom and Debye forces) and possible acid-base interactions (due to a sharing of a proton or an electron pair between neighbouring molecules or functional groups).

1.7.2.2 Theory

The following experimental techniques that currently utilise acid-base surface chemistry theory are:- Inverse gas chromatography, microcalorimetry, contact angle measurements, ellipsometry, Fourier transform infrared spectroscopy, nuclear magnetic resonance and x-ray photoelectron spectroscopy. IGC is becoming more popular and widely used since it has both operational flexibility and it allows data to be rapidly generated over a broad range of solid surface chemistries through a range of temperatures that can traverse processing and use conditions.

IGC has been applied in general research for many years, being a standard technique for the characterisation of polymers and carbon fibres (Bonifaci and Ravinetti, 1993). In pharmaceutical research, IGC has only begun to be used widely over the last couple of years. The first pharmaceutical use of IGC studied the interaction of water with cyclosporin A (Djordjevic et al, 1992). More recently, this analytical technique was

able to distinguish between different batches of α-lactose monohydrate (Ticehurst et al., 1996) all obtained from the same supplier which therefore should have been both chemically and physically equivalent but this was found not to be the case. Various other analytical techniques were tried (FT - laser Raman spectroscopy, Differential Scanning Calorimetry, Thermogravimetric analysis, quantitative X-ray powder diffraction), but only IGC was sensitive enough to discover significant differences between the batches acid-base natures. This was thought to have been caused either by changes in the batch process leading to slight changes in the surface crystallinity or variable amounts of impurities within each batch. IGC is a sensitive and powerful tool which, used in conjunction with other more mainstream techniques, will only improve the surface energy analysis of pharmaceutical powders. IGC is able to measure the surface adsorption below monolayer coverage, which is very useful in anticipating surface wetting properties, with further multilayer coverage being controlled by condensation interactions (Braunauer et al., 1938). IGC has several advantages over other surface chemistry analytical techniques:-

a) Sample does not require evacuation.
b) Temperature effects can be easily investigated.
c) Measurements are rapid and easy to obtain.
d) Accurate measurements at low surface concentrations.
e) Ability to study both chemical and physical sorption.
f) Measurements can be made using conventional gas chromatography apparatus with the minimum of alterations.

1.7.3 Isothermal microcalorimetry

1.7.3.1 Introduction

The wetting of powders was first studied using the microcalorimeter by Buckton and Beezer (1988) who investigated the adsorption characteristics of a series of barbiturates, showing the advantages of microcalorimeter experiments to detect changes that other methods would readily detect.

Two processes are involved, firstly the desorption of the air molecules and secondly the adsorption of the water molecules. It is the initial adsorption of water molecules onto the powder surface that is most indicative of the interaction between a powder and a liquid. With further adsorption, after the initial adsorption of a few molecule layers, the interaction tends to be equivalent to condensation and immersion of the powder surface and will result in a reordering of the molecules of the condensed liquid, usually water, to be accommodated into the bulk liquid.

1.7.3.2 Enthalpy of adsorption

As the relative humidity within the stainless steel test cell is altered, the heat flow with time is measured, resulting in a series of peaks equivalent to each relative humidity step (Figure 1.6). Calculating the area under each peak yields the energy output in Joules. The energy values are then standardised to Joules per mole of adsorbed water onto that weight of powder, so that any surface area variations between samples are removed from the calculation. This value is the heat of adsorption, ΔH_{cal}, which is finally converted to the standard heat of adsorption, $\Delta H_{cal}°$ ($kJ.mol^{-1}$).

Figure 1.6 Graphs of water sorption onto a model powder over an increasing relative humidity range.

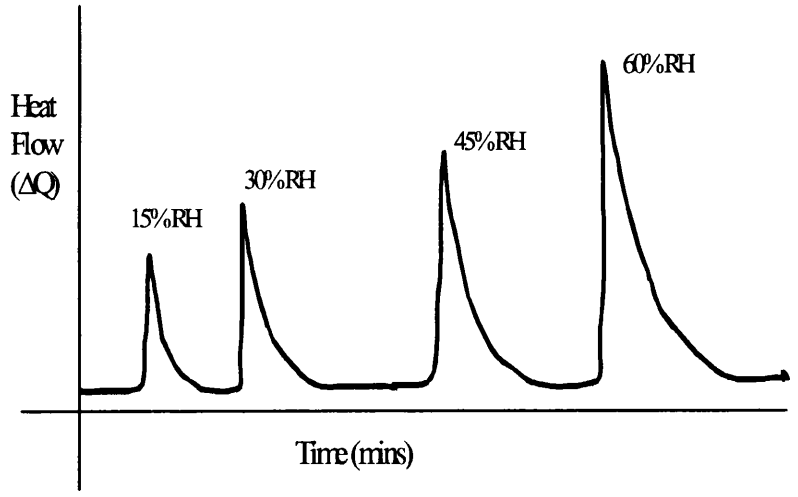

$$\Delta_{imm}H_{(x-0)} - \Delta_{imm}H_{(x-n)} = n\,(\Delta_{ads}H_{(x-n)} - \Delta_{cond}H_{L}) \qquad \text{Equation 1.36}$$

The amount adsorbed (x) varies from zero to n ($mol.m^{-2}$), and $\Delta_{cond}H_L$ is the enthalpy of condensation of the liquid.

And if $\Delta_{imm}G_{(x-n)} = -\gamma_{LV}Cos\theta$ Equation 1.37

$\Delta_{imm}G_{(x-n)} = T\Delta_{imm}S_{(x-n)} - \gamma_{LV}Cos\theta$ Equation 1.38

Since

$\Delta G_{cal}^{\circ} = \Delta H_{cal}^{\circ} - T\,\Delta S_{cal}^{\circ}$ Equation 1.39

ΔG_{cal}° - Gibbs free energy of adsorption

ΔH_{cal}° - Enthalpy of adsorption

ΔS_{cal}° - Entropy of adsorption

Every reaction causes a change in heat, either taken in or given out. Isothermal microcalorimetry is able to measure this change in heat extremely accurately, allowing detailed analysis of a reaction profile. For pharmaceutical powders where only a minute alteration at the surface may affect the powder 'performance', this microcalorimetric technique has been able to show batch to batch variation between three lactose samples, whilst they appeared identical in nature using traditional contact angle methods of analysis (Sheridan et al., 1993).

1.7.4 Dynamic vapour sorption

1.7.4.1 Theory

The interaction between water and pharmaceutical excipients or drug substances is of essential importance for the chemical, physical and microbiological stability of the product (Ahlneck and Zografi, 1990). Water can affect rates of chemical degradation, crystal growth and dissolution, dispersibility and wetting, powder flow, lubricity, powder compactibility and compact hardness. Water can either adsorb to the surface and/or absorb into the powder bulk. The wetting process is controlled by the relative gas, liquid and solid surface energy values. Water can interact with a solid in three

different ways:-

a) Adsorption of water vapour to the solid - air interface.
b) Crystal hydrate formation, whereby water molecules enter into the crystal lattice.
c) Deliquescence which allows water to enter the bulk powder, and once there, it is able to dissolve any water soluble molecules that it comes into contact with.

Adsorption onto a surface is thought to exist, primarily, as a monolayer of water molecules which are hydrogen bonded to that surface, with possibly two or three more layers of water molecules on top only if the relative humidity is high enough to encourage the build up. These water layers can be quickly removed with only a slight humidity decrease or temperature increase, since they are only weakly bonded.

The dynamic vapour sorption (DVS) allows powders to be examined over a range of humidities for any length of time. When water vapour is placed in contact with a solid surface it can be absorbed into the bulk of the material or adsorbed just onto the surface. Both processes will cause an increase in mass. The powder is suspended on a microbalance which is able to detect minute changes in mass due to water sorption and desorption. The DVS apparatus is able to measure this mass change with varying relative humidities passing over the sample.

Adsorption isotherms can then give vital information about the amount of water attaching itself to the powder, from which surface area, porosity, enthalpies of adsorption and activation energies of adsorption can be determined.

1.7.4.2 Gibb's function

The DVS apparatus allows the water sorption (absorption, adsorption and desorption) process to be studied in detail producing sorption isotherms over a range of relative humidities. Gibb's function can be calculated using Equation 1.40.

$$K_{ad} = \frac{b}{P_o}$$ Equation 1.40

b - No. of water molecules adsorbed per gram of powder

P_0 - Saturated water vapour pressure at 25°C

The free energy of adsorption, ΔG_{dvs}, of water vapour to a solid powder can be derived from Equation 1.41 below:-

$$\Delta G_{dvs} = -RT.\ln(K_{ad})$$ Equation 1.41

1.7.5 Combining dynamic vapour sorption and microcalorimetry data

Sections 1.7.3 and 1.7.4 have shown how the DVS and microcalorimetry are able to derive the free energy of adsorption, ΔG_{dvs}, and the heat of adsorption, ΔH_{cal}, and by using the two thermodynamic data sets it is possible to further calculate the entropy of adsorption, ΔS_{cal} (Equation 1.42).

$$\Delta G = \Delta H - T\Delta S$$ Equation 1.42

ΔG - A positive change in this value indicates a process that is not favoured in addition to how far the reaction has gone.

ΔH - A positive change again indicates a process that is not favoured in addition to the amount of heat required for it to occur.

ΔS - A positive change indicates a process that is increasingly favourable in addition to the degree of disorder in the reaction.

1.7.5.1 Entropy of adsorption

The second law of thermodynamics states that, 'The entropy of an isolated system increases in an irreversible process and remains unchanged in a reversible process. It can never decrease'.

Third law of thermodynamics states that, 'Every substance has a finite positive entropy, but at the absolute zero of temperature the entropy may become zero, and does so become in the case of a perfectly crystalline solid'.

Gibbs free energy is useful in that both enthalpy and entropy factors can be considered in a reaction, in this case as water vapour is adsorbed onto a powder surface. The adsorption process can be quantified and explained, providing a method by which small changes in powder surfaces can be examined without the traditional contact angle measurements.

Chapter 2

Materials

2 Materials

2.1 Model powders

Five model powders were chosen due to their different chemical characteristics.

a) Salicylic acid (2-hydroxybenzoic acid), ($C_7H_6O_3$).

A white crystalline powder and a readily soluble acid which is a major metabolite of aspirin, methyl salicylate and salsalate. It occurs naturally in the form of esters in several plants, most notably in wintergreen leaves and the bark of sweet birch. It is used as a preservative of food products, although not allowed in most countries. It is usually converted to more useful salicylates (e.g. acetylsalicylic acid).

Figure 2.1 Salicylic acid structure.

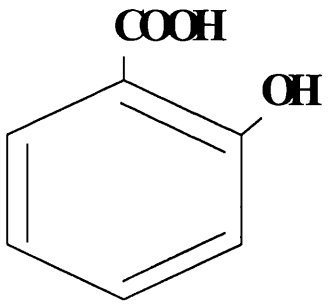

b) Caffeine (3,7-diydro-1,3,7-trimethylpurine-2,6(H)-dione), ($C_8H_{10}N_4O_2$).

A white crystalline powder and a soluble base which is found in several plant species, most notably, tea, coffee and cola plant species. It is also widely used in pharmaceutical preparations, mainly having a stimulatory affect on the central nervous system.

Figure 2.2 Caffeine structure.

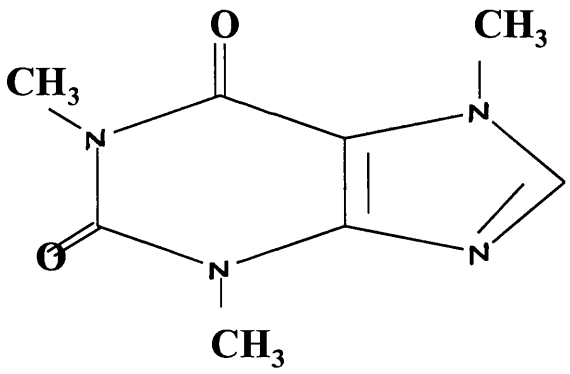

c) Theophylline (3,7-dihydro-1,3-dimethylpurine -2,6(1H)-dione), ($C_7H_8N_4O_2$).

It is a xanthine derivative diuretic, cardiac stimulant and smooth muscle relaxant properties. Theophylline has the main action of bronchodilation within the lungs and therefore is a major drug used in the treatment of asthma. It is a white crystalline powder and also a weak base although not as soluble in water as Caffeine.

Figure 2.3 Theophylline structure.

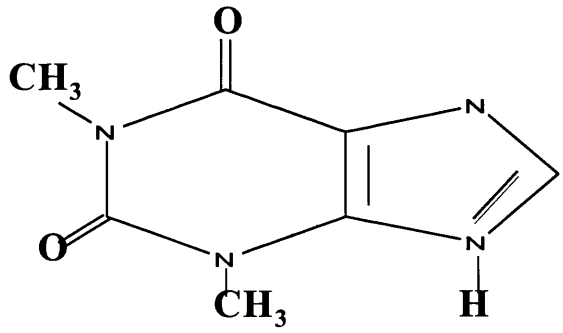

d) Ibuprofen (α-Methyl-4-(2-methylpropyl)benzeneacetic acid), ($C_{13}H_{18}O_2$).

Ibuprofen is a white crystalline solid that is relatively insoluble in water. It is used as an analgesic anti-inflammatory agent (non-steroidal).

Figure 2.4 Ibuprofen structure.

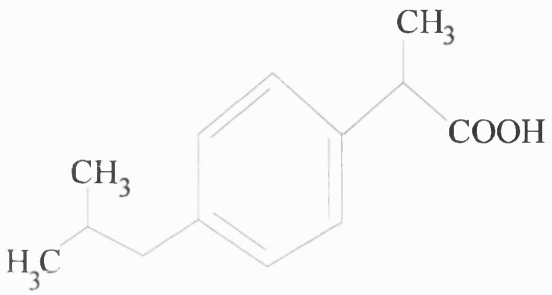

e) Ethacrynic acid {[2,3-Dichloro-4-(2-methylene-1-oxybutyl)phenoxy]acetic acid}, ($C_{13}H_{12}Cl_2O_4$).

Ethacrynic acid is a white crystalline solid that is sparingly soluble in water; it is used as a diuretic.

Figure 2.5 Ethacrynic acid structure.

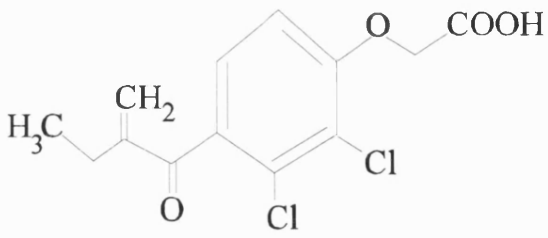

2.2 Test powder

Saquinavir mesylate (Ro8959-003): The monomethanesulphonate salt - anti-viral ($C_{38}H_{50}N_6O_5.CH_4O_3S$).

It is a selective HIV-1 and HIV-2 protease inhibitor developed by Roche (Invirase) normally used in combination with anti-viral in the treatment of HIV and AIDS. It is a white crystalline powder that is poorly soluble in water (0.22g / 100ml).

Figure 2.6 Saquinavir structure.

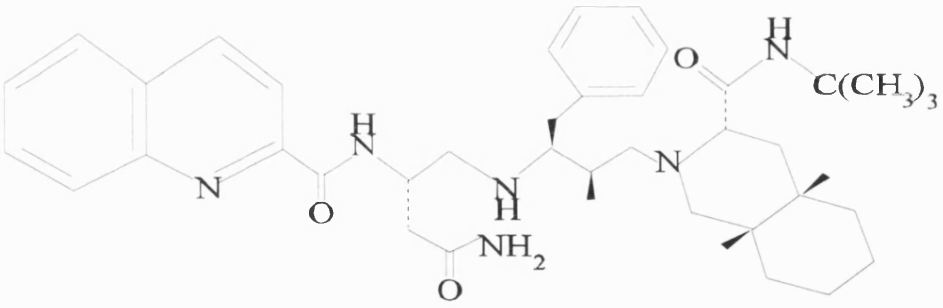

2.2.1 Preparation of batches of Saquinavir

Saquinavir was subjected to three different drying processes:-

1) A dry batch heated to 160°C in a tray oven for 2 hours.
2) Wetted thoroughly and dried in a tray oven at 160°C for 2 hours.
3) Wetted thoroughly and dried in a vacuum oven at 80°C at 200mBar for 4 hours.

Three separate 30g batches were prepared for each of the three drying methods. Wetting was achieved using 90mls of distilled water.

In addition, two preliminary batches were prepared, a tray dried sample prepared in the same manner as part 2) and a spin dried sample that was wetted and then placed in a slowly rotating beaker with a 100 watt bulb as a heat source.

2.3 Raw material suppliers

Table 2.1 Raw material suppliers.

Material	Supplier	Batch Number
Salicylic acid	Sigma	LOT 72H-3495
Caffeine	Sigma	LOT 43H-0392
Theophylline	Sigma	LOT 102H-0521
Ethacrynic acid	MSD	LOT 6178/161293
Ibuprofen	Sigma	LOT 439952
Glycerol	Sigma	LOT 54H0645
Diiodomethane	Sigma	LOT 45H3475
Bromonapthalene	Aldrich	LOT 03702-094
Sucrose 55%$^{w}/_{w}$ (aq.)	Aldrich	LOT 06228DG
Formamide	Sigma	LOT 124H0580
Ethylene glycol	Aldrich	LOT 04551MN
Octane	Sigma	LOT 54H3485
Potassium chloride	Sigma	LOT 15H0530
NaCl (98%+ pure)	Aldrich	LOT 4041440408011
Potassium sulphate	Aldrich	LOT TF04209PF
Potassium carbonate	Aldrich	LOT JG01522DG
Lithium chloride	Aldrich	LOT HG07315HG
Potassium hydroxide	Aldrich	LOT PZ02823DZ
Magnesium chloride	Aldrich	LOT 939091

Liquids used for contact angle determination with the Cahn.

Salts used in the Dynamic Vapour Sorption.

Table 2.2 Liquids used as gaseous probes for inverse gas chromatography.

Liquid	Acid/base character	Supplier	Liquid	Acid/base character	Supplier
Acetone	Amphoteric	Aldrich	Benzene	Acidic	Aldrich
Ethyl acetate	Amphoteric	Aldrich	n-Hexane	Apolar	Sigma
Diethyl ether	Basic	Aldrich	n-Heptane	Apolar	Sigma
Tetrahydrofuran	Basic	Aldrich	n-Octane	Apolar	Sigma
Chloroform	Acidic	Aldrich	n-Nonane	Apolar	Sigma
Carbon tetrachloride	Acidic	Aldrich	n-Decane	Apolar	Sigma

Chapter 3

Wilhelmy Plate

3 Wilhelmy Plate

3.1 Introduction

The Wilhelmy plate technique measures the force pulled on a plate suspended from a microbalance when brought into contact with a test liquid. This force is a function of the surface tension of the liquid (known), the perimeter of the compact (known) and the nature of the solid expressed as a contact angle. Therefore the contact angle can be swiftly calculated.

There are three different ways of using the Wilhelmy plate listed as follows:-

a) *Equilibrium* - uses the force reading when the plate just comes in contact with the liquid.
b) *Detachment* - After the plate has made contact with the liquid, it is slowly raised from the liquid and the force reading is taken just before the plate detaches from the liquid surface.
c) *Dynamic* - The plate enters the liquid and emerges from it at a set rate all the while collecting force data. This results in a complete force analysis giving more accurate contact angle data.

The dynamic method has been chosen as the preferable method since it is the most commonly practised and also the measurement and calculation have been incorporated into a computerised set-up thus reducing any operator error to a minimum.

3.1.1 Compressed powder plate

A compressed powder plate is suspended from a microbalance above a test liquid. The plate is brought into contact with the liquid which results in a downward force on the plate. This force, measured by the microbalance, is a function of:-

a) The surface tension of the liquid (known).

b) The nature of the solid (unknown).

c) The total perimeter of the compact, measured with a micrometer.

The Cahn is able to plot a graph of force versus stage position, which is used to calculate the contact angle of the unknown powder with a particular test liquid. By using several test liquids, the surface energy of the powder can be calculated. Automation allows more reproducible work since operator dependency is greatly reduced.

3.1.2 Powder covered glass slide

This alternative Wilhelmy plate method (Shanker, 1994) is identical to the compressed powder Wilhelmy plate technique (Section 3.1.1) in theory, except that instead of a compressed powder plate, a glass slide coated with the test powder is used as the Wilhelmy plate. The glass slide is firstly coated with spray adhesive and then the powder is gently brushed on. This method has been chosen for investigation since it has an advantage in that the test powder is not compressed during the manufacture of the plate.

3.2 Method

Each powder was stored in a desiccator containing silica gel maintaining the relative humidity close to 0% RH and at controlled temperature of 18 °C whilst not being used. The Cahn Dynamic Contact Angle Analyser is encased in a draught proof cabinet with sliding glass door to allow access.

3.2.1 Powder compact manufacture

300mg of test powder was spread evenly, to ensure an even porosity, into the polished rectangular die and compressed using the Specac press for 2 minutes with a force of 3 $*10^{-3}$kN. The compact was carefully removed by dismantling the die as shown in Figure 3.1 to prevent any damage to the compact. The compacts produced were all of

similar dimensions, since three main factors remained constant, those being the amount of powder compressed, the length in time of compression and the pressure involved. They were also sufficiently compacted so as not to break up too easily and were not over compacted which would have resulted in flaking at the compact surface.

Figure 3.1 Steel die used in compact manufacture.

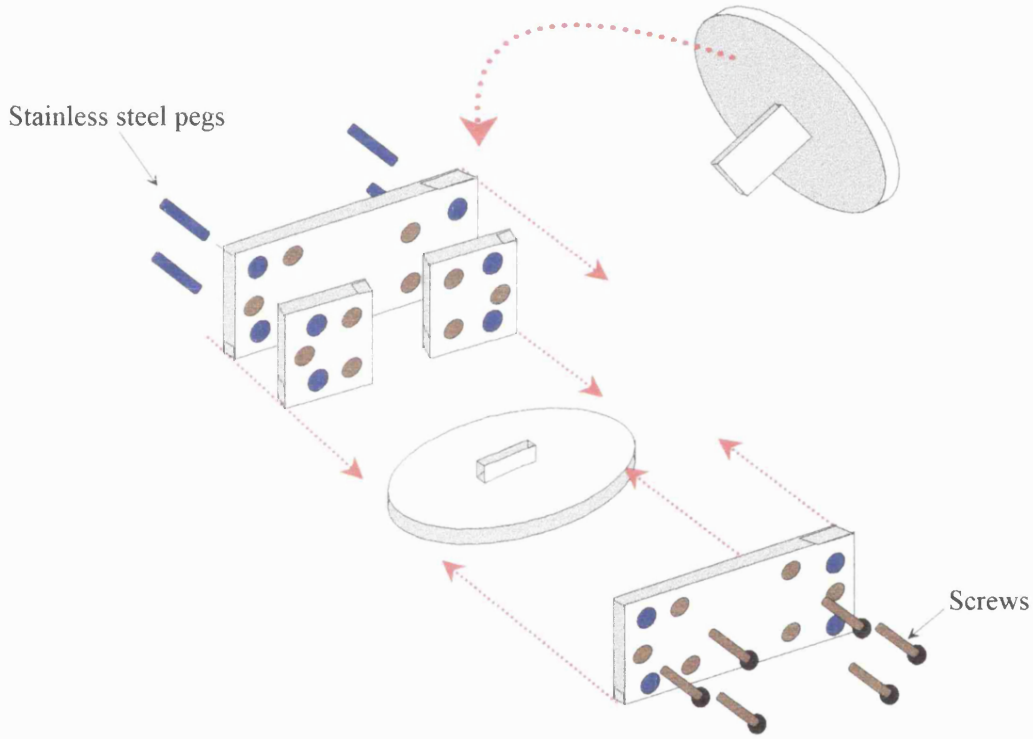

It must be noted that the parameters required for compacting a powder into a plate are unique for each powder used, depending on the powder's molecules ability to adhere to one another.

3.2.2 Powder covered glass slide

Glass slides were sprayed on both slides with an adhesive (3M Spray Mount Adhesive), and left for one minute, after which the test powder was liberally brushed onto the glass slide and any excess powder lightly brushed off (Shanker, 1994). For each powder, the coated glass slide (five for each liquid), after having its perimeter measured, was suspended in the Cahn above the test liquid maintained at 25°C. The

contact angle of each coated slide can then be determined using the identical methodology and apparatus required when using the Wilhelmy plate technique (Section 3.2.3). Control runs were also made with glass slides with adhesive only, to ensure that the adhesive had no similarity with the contact angles of the powdered slides.

3.2.2.1 The influence of coverage of the slide by the powder on the measured contact angle

One concern over the use of the approach of coating the glass slide with powder is the influence on the contact angle of any adhesive that is not covered with powder. In an attempt to assess the influence of this, plates were prepared such that varying amounts of their surface were covered with powder (Caffeine). This was achieved by covering one region totally, whilst leaving another region with just adhesive. The contact angle data are shown in Figure 3.2 for different extents of powder contact.

Figure 3.2 Graph showing the change in contact angle with percentage coverage of Caffeine over a glass slide previously coated with adhesive.

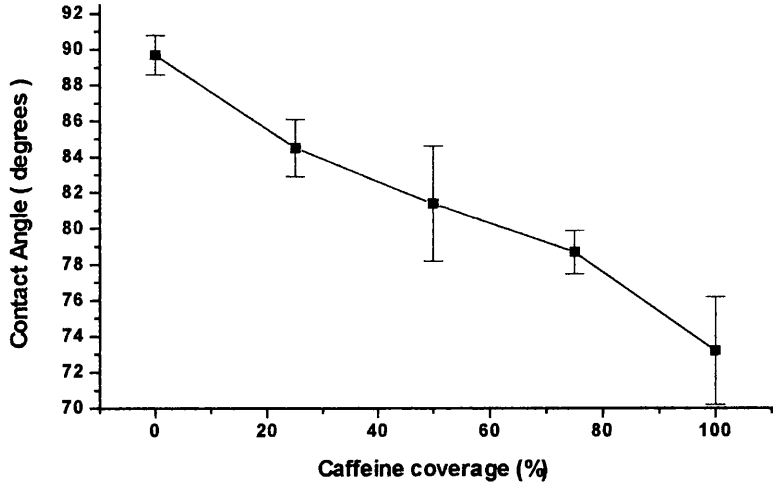

It can be seen that as the percentage of Caffeine coverage decreases to zero (only

adhesive present), the contact angle increases in a linear fashion. This is in keeping with the Cassie equation, in that the observed contact angle is a weighted mean of the contact angles for both adhesive and powder. This does not prove that the area where powder is coated on the glass is a total coverage, but shows it to be a consistent value which is distinctly different from the contact angle obtained for the adhesive only. It is therefore reasonable to assume that this is a fair reflection of the surface properties of non-compacted powder.

3.2.3 Cahn Dynamic Contact Angle Analyser (312)

Once made, the Wilhelmy plate's perimeter was measured using a micrometer held steady on a stand. The Wilhelmy plate was subsequently attached to a crocodile clip and placed onto the balance loop of the microbalance inside the cahn. The probe liquid was placed in a clean glass beaker (50ml) into the water bath underneath the compact. The water bath was maintained at 25 °C.

Figure 3.3 Cahn apparatus.

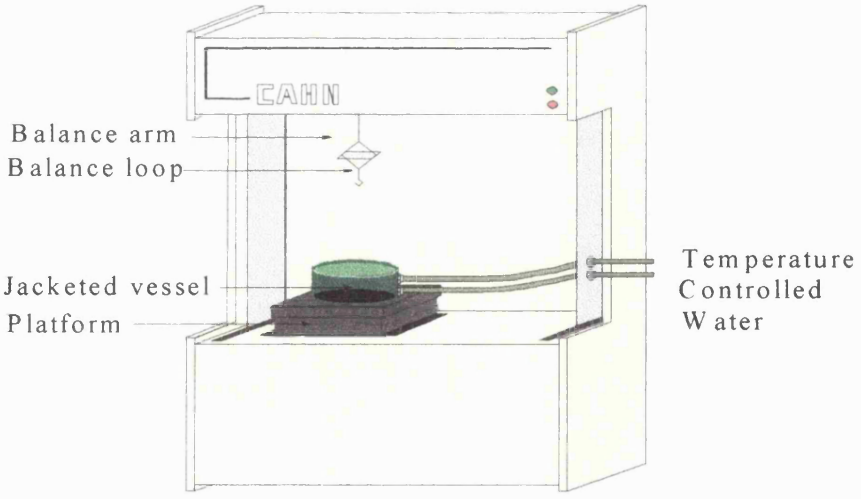

Figure 3.4 Microbalance apparatus.

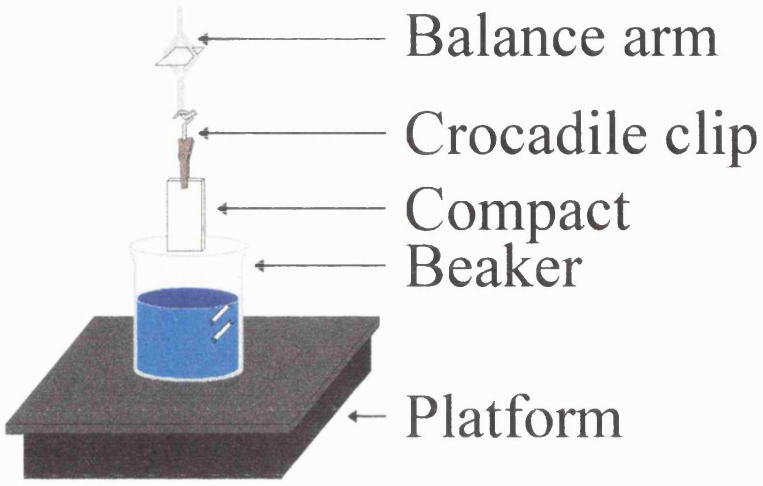

(Carthew, 1996)

3.2.3.1 Calibration of Cahn

The microbalance of the Cahn was calibrated daily with a 500mg weight before use to ensure accurate mass recording. The test liquids also had to be checked against any decomposition by both visual and surface tension analysis using a clean, dry glass slide to ensure that they have correct surface tension values.

3.2.4 Choice of test liquids

Ideally, it is necessary to obtain three different contact angles using three different test liquids, with one of those being a totally non-polar liquid (i.e. Diiodomethane or 1-bromonapthalene). Without the contact angle data from a totally non-polar liquid, which can happen if the liquid spreads immediately on contact with the powder surface (Cosine θ greater than 1), three polar liquids will be adequate although the resulting surface energy data may not be as accurate (Section 3.3.6).

Table 3.1 Test probe liquid surface energy component values ($mJ.m^{-2}$).

Material	γ^{TOT}	γ^{LW}	γ^{+}	γ^{-}	Material	γ^{TOT}	γ^{LW}	γ^{+}	γ^{-}
Hexane	18.4	18.4	0	0	Diiodomethane	50.8	50.8	0	0
Octane	21.6	21.6	0	0	1-Bromonapthalene	44.4	44.4	0	0
Decane	23.8	23.8	0	0	Ethylene glycol	48.0	29.0	1.92	47.0
Glycerol	64.0	34.0	3.92	57.4	$55\%^{w}/_{w}$ Sucrose	75.7	28.8	24.6	22.3
Water	72.8	21.8	25.5	25.5	Formamide	58.0	39.0	2.28	39.6

Sources: 1) Van Oss et al., 1992a.

1*) Van Oss et al., 1992a, corrected for misprint.

2) Van Oss et al., 1992b.

3.2.5 Analysis

The computer was programmed to raise and lower the platform a distance of approximately 10mm at a constant speed of $151.7\mu m.s^{-1}$, so that the compact would enter the liquid to at least 5mm of its length. During this experiment, force data were collected by the interfaced computer at regular intervals as a function of platform height. Five compacts for each powder with each liquid were used to reduce errors.

Since the surface tension of the liquid is known and the perimeter of the compact easily measured, a simple equation can be used in conjunction with a plot to determine the advancing and receding contact angle of the powder with that specific liquid.

$$\cos\theta = \frac{mg}{p\gamma_{LV}}$$ Equation 3.1

$mg = F_{(Z.D.O.I.)}$

$F_{(Z.D.O.I.)}$ -Force at zero depth of immersion

m - mass (mg)

g - acceleration due to gravity ($g.m^{-2}$)

p - perimeter of the solid compact (mm)

γ_{LV} - surface tension of liquid ($mJ.m^{-2}$)

Figure 3.5 Force / depth isotherm used in calculation of contact angle.

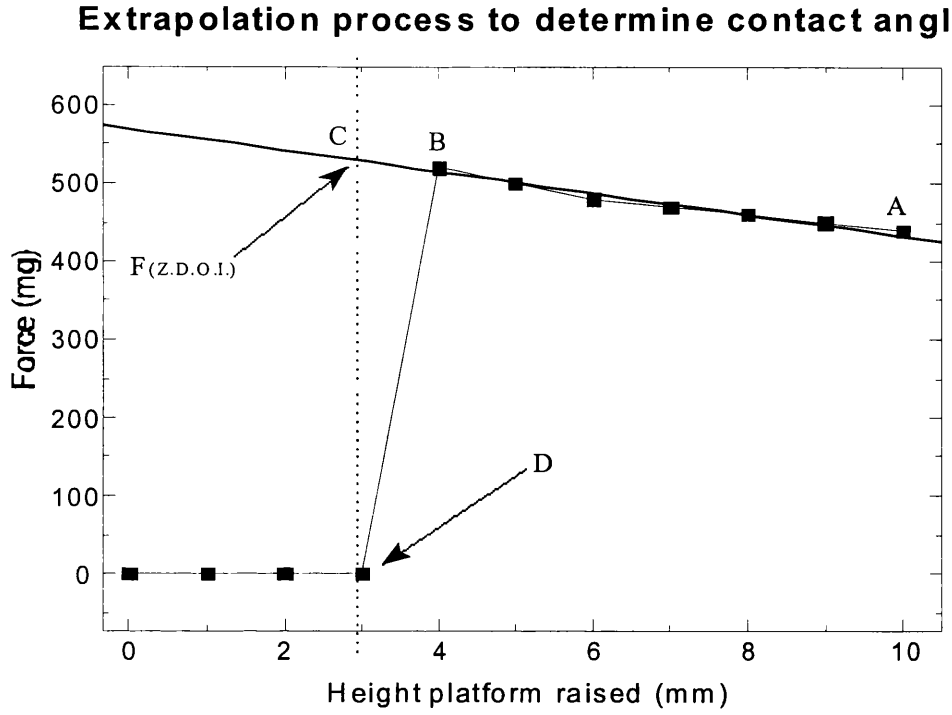

The computer is manually shown point D, which is the first contact point of the compact with the liquid. The computer extrapolates the straight line AB back to C at the intersect with the vertical line CD. The Y co-ordinate at C is equal to the force at zero depth of immersion, $F_{(Z.D.O.I.)}$, equivalent to the force required in Equation 3.1.

Since this method is mainly automated, there is less room for operator error, and advancing and receding angles are quickly and easily obtained. Contact angle hysteresis can also be studied.

The first 1.5 mm of the downward slope was analysed (Figure 3.6) to ensure that every contact angle was calculated from exactly the same part of the slope.

Figure 3.6 Graph showing region used for calculation.

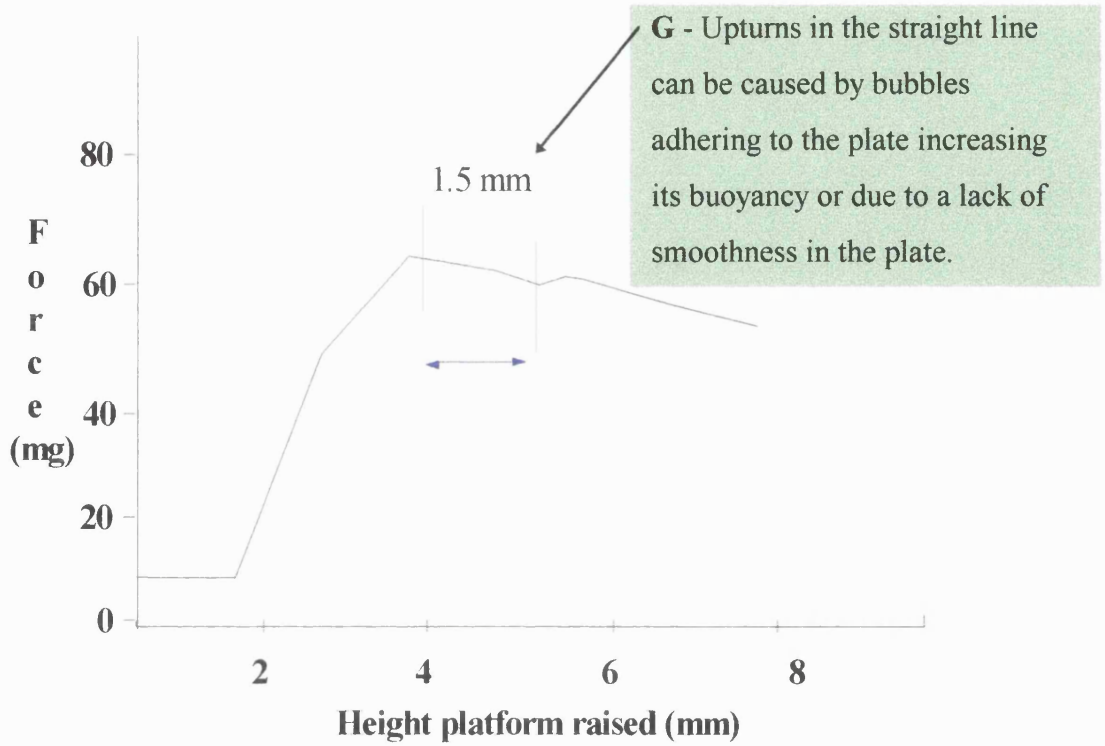

The contact angles were then calculated using linear regression analysis as described earlier in this section. For each liquid used to characterise a powder, five compacts were used and the average contact angle taken.

3.2.6 Errors associated with quoting contact angles

Previous studies with contact angle determination using liquid penetration (Parsons and Buckton, 1992) have shown that it is more accurate to express the contact angle in its cosine form. The error in a contact angle can be heavily dependant on the magnitude of that angle, which will mask the true accuracy of the experiment. The theory used in contact angle determination results in a value for cosine θ, which is then converted to an angle θ. The cosine curve (Figure 3.7) clearly shows how this conversion is achieved.

Figure 3.7 The cosine curve.

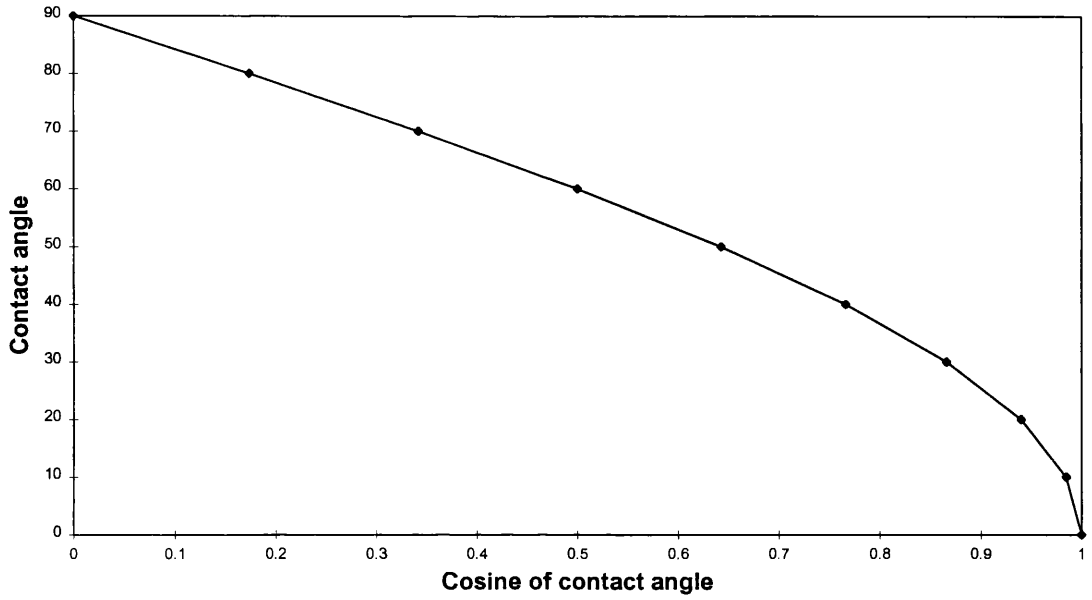

For example, if two cosine values with equal error are converted to angles, the error is altered to a significant degree depending on which part of the curve is used.

a) A Cosine value of 0.9, with an error of ± 0.1 results in an angle of 25.8°, with an error between 0° and 36.9°, a range of 36.9°.
b) A Cosine value of 0.1, with an error of ± 0.1 results in an angle of 84.3°, with an error between 78.5° and 90°, a range of 11.5°.

It is evident that as the contact angle falls, so the error increases since the cosine curve becomes steeper and any error is greatly magnified. Thus a true representative of the experimental error can only be expressed in the cosine form.

3.3 Results and discussion

3.3.1 Wilhelmy plate analysis of test powders using a powder compact

3.3.1.1 Van Oss theory

Diiodomethane, a non-polar liquid, immediately spreads over the Theophylline, Salicylic acid and Caffeine powder compacts on contact resulting in contact angles of below zero. For these powders the theory by Van Oss could only be used by incorporating the values from three polar liquids, thus allowing the surface energies of the three powders to be calculated without contact angle data from a non-polar liquid.

Table 3.2 Contact angles of five model powders with a selection of test liquids.

Sample	Water			Formamide		
	θ°	Cosine θ	SD_{n-1}	θ°	Cosine θ	SD_{n-1}
Theophylline	47.6	0.673	0.0382	27.9	0.883	0.0214
Caffeine	29.1	0.873	0.0204	22.8	0.921	0.0169
Ethacrynic acid	77.3	0.220	0.0541	65.8	0.409	0.0611
Salicylic acid	78.3	0.203	0.0546	39.7	0.769	0.0158
Ibuprofen	65.8	0.407	0.1100	56.8	0.546	0.0540
	Ethylene glycol			Diiodomethane		
Theophylline	16.0	0.960	0.0142	<0		
Caffeine	17.9	0.952	0.0081	<0		
Ethacrynic acid	38.4	0.782	0.0445	54.4	0.582	0.0288
Salicylic acid	31.2	0.854	0.0237	<0		
Ibuprofen	48.9	0.656	0.0362	56.3	0.555	0.0255

<0 - Less than zero

3.3.1.2 Wu theory

This theory was chosen as a comparison to surface energy data obtained from the Van Oss theory. It was able to calculate surface energy values using all the pair combinations of the test liquids, with or without one of each pair being totally non-polar (diiodomethane).

Table 3.3 Surface energy values of Theophylline using a powder compact.

Theophylline	γ_{sv}^{TOT} mJ.m^{-2}	γ_s^{LW} mJ.m^{-2}	γ_s^{AB} mJ.m^{-2}	γ_s^{+} mJ.m^{-2}	γ_s^{-} mJ.m^{-2}
Van Oss - 3 polar	61.3	61.3(∓12.4)	0	0	26.6
Wu		γ_s^{D}	γ_s^{AB}		
Water + Formamide	55.6	26.7(∓2.1)	29.0		
Water + Ethylene glycol	52.7	18.6(∓1.6)	34.1		
Ethylene glycol + Formamide	60.2	54.0(∓8.9)	6.2		

Table 3.4 Surface energy values of Caffeine using a powder compact.

Caffeine	γ_{sv}^{TOT} mJ.m^{-2}	γ_s^{LW} mJ.m^{-2}	γ_s^{AB} mJ.m^{-2}	γ_s^{+} mJ.m^{-2}	γ_s^{-} mJ.m^{-2}
Van Oss - 3 polar	72.8	72.8(∓9.6)	0	0	47.4
Wu		γ_s^{D}	γ_s^{AB}		
Water + Formamide	64.9	24.1(∓1.2)	40.7		
Water + Ethylene glycol	65.2	14.3(∓0.6)	50.9		
Ethylene glycol + Formamide	71.7	68.0(∓7.2)	3.7		

Table 3.5 Surface energy values of Ethacrynic acid using a powder compact.

Ethacrynic acid	γ_{sv}^{TOT} mJ.m^{-2}	γ_s^{LW} mJ.m^{-2}	γ_s^{AB} mJ.m^{-2}	γ_s^{+} mJ.m^{-2}	γ_s^{-} mJ.m^{-2}
Van Oss - 3 polar	31.9	0.4 (∓4.4)	31.5	26.0	9.5
Van Oss - 2polar + 1non polar (diiodomethane)					
D. + Water + Formamide	31.8	31.8 (∓1.2)	0	0	12.4
D. + Ethylene glycol + Formamide	31.8	31.8 (∓1.2)	0	44.8	0
D. + Ethylene glycol + Water	37.9	31.8 (∓1.2)	6.1	1.9	4.9
Wu		γ_s^{D}	γ_s^{AB}		
Water + Formamide	33.4	16.0 (∓4.1)	17.4		
Water + Ethylene glycol	38.9	25.9 (∓7.0)	13.0		
Ethylene glycol + Formamide	N/A	N/A	N/A		
Diiodomethane + Water	44.2	33.2 (∓1.0)	11.0		
Diiodomethane + Formamide	36.1	33.2 (∓1.0)	2.9		
Diiodomethane + Ethylene glycol	41.8	33.2 (∓1.0)	8.6		

Table 3.6 Surface energy values of Salicyclic acid using a powder compact.

Salicylic acid	γ_{sv}^{TOT} mJ.m^{-2}	γ_s^{LW} mJ.m^{-2}	γ_s^{AB} mJ.m^{-2}	γ_s^{+} mJ.m^{-2}	γ_s^{-} mJ.m^{-2}
Van Oss - 3 polar	63.4	63.4(∓12.4)	0	0	1.9
Wu		γ_s^{D}	γ_s^{AB}		
Water + Formamide	47.8	38.3 (∓5.0)	9.5		
Water + Ethylene glycol	43.8	33.3 (∓7.5)	10.5		
Ethylene glycol + Formamide	52.8	47.2 (∓8.7)	5.6		

Table 3.7 Surface energy values of Ibuprofen using a powder compact.

Ibuprofen	γ_{sv}^{TOT} mJ.m^{-2}	γ_s^{LW} mJ.m^{-2}	γ_s^{AB} mJ.m^{-2}	γ_s^{+} mJ.m^{-2}	γ_s^{-} mJ.m^{-2}
Van Oss - 3 polar	35.8	31.3(∓34.6)	4.5	0.3	20.1
Van Oss - 2polar + 1non polar (diiodomethane)					
D. + Water + Formamide	35.6	30.7 (∓1.0)	4.9	0.3	20.1
D.+ Ethylene glycol + Formamide	35.0	30.7 (∓1.0)	4.3	0.2	23.5
D. + Ethylene glycol + Water	35.6	30.7 (∓1.0)	4.9	0.3	20.3
Wu		γ_s^{D}	γ_s^{AB}		
Water + Formamide	41	17(∓4.9)	23		
Water + Ethylene glycol	40	12(∓3.9)	27		
Ethylene glycol + Formamide	39.7	34(∓17.2)	5		
Diiodomethane + Water	49.1	32.3 (∓0.9)	16.8		
Diiodomethane + Formamide	38.7	32.3 (∓0.9)	6.3		
Diiodomethane + Ethylene glycol	38.4	32.3 (∓0.9)	6.1		

With the Van Oss theory, the powder compacts of Theophylline, Caffeine and Salicylic acid have an unusually large non-polar (dispersive) component, which is greater than that of diiodomethane (50.8 mJ.m^{-2}). This would explain why diiodomethane spreads over the compact immediately on contact. It follows that the apparent high value for the non-polar (dispersive) nature of the surface, which has been obtained using the contact angle data for the polar liquids on the solids, is in keeping with the zero contact angle for the non-polar liquid on the surface. The internal consistency of these independent data sets is encouraging, but cannot be taken to imply that the data are a true reflection of the nature of the material (i.e. the material in a non-compacted form). It has been shown previously (Buckton et al, 1995) that the Wilhelmy plate compact approach gives different contact angle data for a gold coated compact of powder than it does for a gold coated glass plate. As the surface energy of the two gold coated surfaces was assumed to be the same, it was argued that the error

was due to the geometry of the powder compact, and perhaps associated with a serious error in the true perimeter of the plate due to substantial penetration into the compact by the liquid. Such an error in effective perimeter may explain the consistent observation in these data that the solid has a very high non-polar surface energy (which, given the nature of the solids, seems unrealistic).

Figure 3.8 Assessment of non-polar surface energies of the five test powders using the Van Oss theory (powder compacts used).

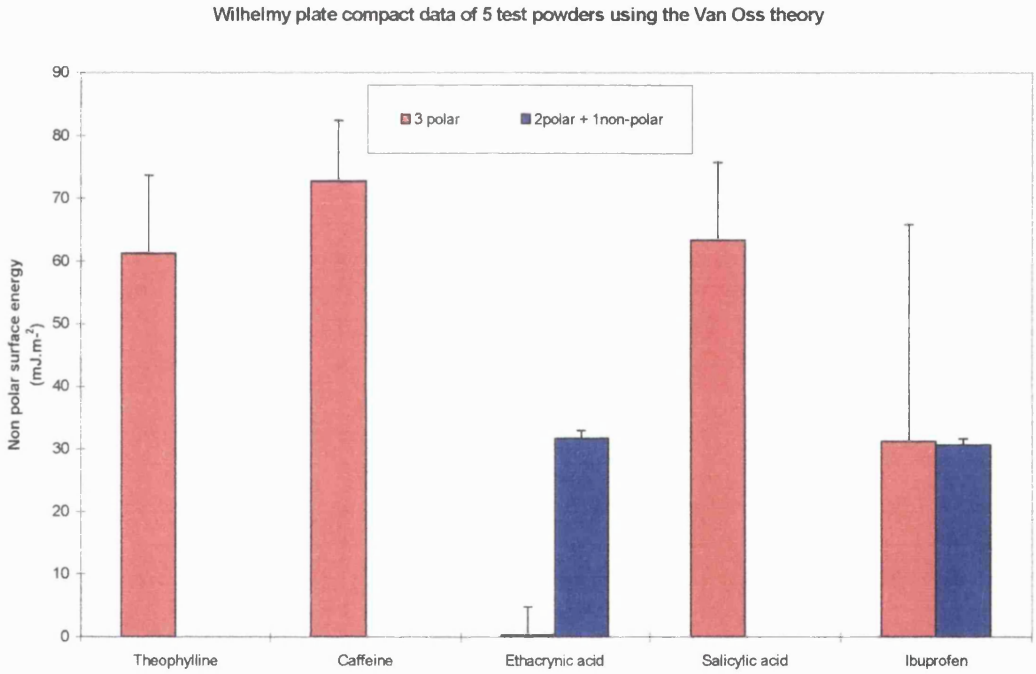

There is a large 'in built' error with the non-polar surface energy values where three polar liquids are used with the Van Oss theory (Figure 3.8). The value is dependent on three contact angles of three liquids each having their own corresponding error value which magnifies the total error by such a degree that the overall accuracy is brought into question. The second method using two polar liquids and one non-polar liquid for Ibuprofen and Ethacrynic acid has a reduced error margin, due to the calculation of non-polar surface energy being solely reliant on the non-polar liquid contact angle. The reason for this is discussed further in Section 3.3.6.

Figure 3.9 Assessment of non-polar surface energies of the five test powders using the Wu theory (powder compacts used).

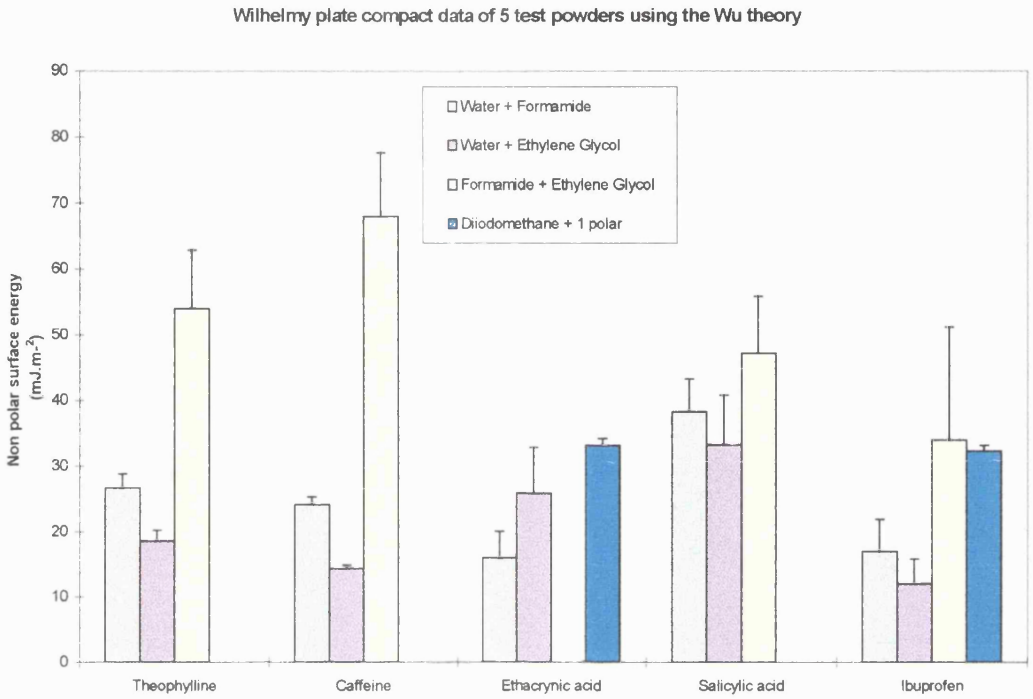

Using Wu's theory, it is clear that the combination of test liquids used in the calculation does have a marked effect on the resulting non-polar surface energies and their error margins (Figure 3.9). Similar to the Van Oss theory, when a non-polar liquid is used with any polar liquid, the resulting non-polar surface energy is solely due to the non-polar contact angle, therefore the error margin is very small. When using two polar liquids where one is water, again the error margins are relatively small, whilst it is only when formamide and ethylene glycol are used in combination with each other that the resultant non-polar surface energy value and error margin are both greatly magnified. This is explained in detail in Section 3.3.6.

3.3.2 Wilhelmy plate analysis of test powders using a powder covered glass slide

In contrast to the compressed plate of powder, diiodomethane (a totally non-polar liquid) did give a contact angle (of greater than zero) with all the five model powders, suggesting that the non-polar component of the powders were all below 50.8 $mJ.m^{-2}$ (the surface energy of diiodomethane).

Table 3.8 Contact angles of five model powders with a selection of test liquids.

Sample	Water			Formamide		
	θ°	Cosine θ	SD_{n-1}	θ°	Cosine θ	SD_{n-1}
Theophylline	77.0	0.225	0.0522	54.0	0.586	0.0507
Caffeine	73.2	0.288	0.0492	44.4	0.713	0.0330
Ethacrynic acid	91.1	-0.0197	0.0227	81.8	0.163	0.0828
Salicylic acid	89.7	0.005	0.0183	62.8	0.457	0.0187
Ibuprofen	91.7	-0.029	0.0274	66.3	0.401	0.0559
	Ethylene glycol			Diiodomethane		
Theophylline	47.9	0.670	0.0324	42.6	0.734	0.0514
Caffeine	33.3	0.836	0.0166	65.5	0.414	0.0834
Ethacrynic acid	79.7	0.178	0.0296	75.3	0.253	0.0505
Salicylic acid	63.1	0.452	0.0373	59.7	0.504	0.0552
Ibuprofen	73.4	0.285	0.0226	68.7	0.363	0.0494

Table 3.9 Surface energy values of Theophylline using a powder covered glass slide.

Theophylline	$\gamma_{\zeta v}^{TOT}$ mJ.m^{-2}	γ_S^{LW} mJ.m^{-2}	γ_S^{AB} mJ.m^{-2}	γ_S^{+} mJ.m^{-2}	γ_S^{-} mJ.m^{-2}
Van Oss - 3 polar	44.4	43.8 (∓23.2)	0.7	0.0	6.7
Van Oss - 2polar + 1non polar (diiodomethane)					
D. + Water + Formamide	41.1	38.3 (∓1.5)	2.8	0.3	6.5
D. + Ethylene glycol + Formamide	38.3	38.3 (∓1.5)	0	0	25.0
D. + Ethylene glycol + Water	40.7	38.3 (∓1.5)	2.4	0.2	7.1
Wu		γ_S^{D}	γ_S^{AB}		
Water + Formamide	38.2	24.6 (∓4.9)	13.6		
Water + Ethylene glycol	34.7	18.6 (∓3.9)	16.2		
Ethylene glycol + Formamide	44.3	40.5 (∓17.0)	3.8		
Diiodomethane + Water	48.9	39.0 (∓2.1)	9.9		
Diiodomethane + Formamide	43.3	39.0 (∓2.1)	4.3		
Diiodomethane + Ethylene glycol	43.1	39.0 (∓2.1)	4.2		

Table 3.10 Surface energy values of Caffeine using a powder covered glass slide.

Caffeine	$\gamma_{\zeta v}^{TOT}$ mJ.m^{-2}	γ_S^{LW} mJ.m^{-2}	γ_S^{AB} mJ.m^{-2}	γ_S^{+} mJ.m^{-2}	γ_S^{-} mJ.m^{-2}
Van Oss - 3 polar	47.9	44.5 (∓15.2)	3.4	0.5	5.9
Van Oss - 2polar + 1non polar (diiodomethane)					
D. + Water + Formamide	36.1	25.4 (∓3.0)	10.7	5.5	5.2
D. + Ethylene glycol + Formamide	25.4	25.4 (∓3.0)	0	0	129.9
D. + Ethylene glycol + Water	35.8	25.4 (∓3.0)	10.4	3.7	7.3

Wu's		γ_S^D	γ_S^{AB}
Water + Formamide	43.5	29.7 (∓4.4)	13.8
Water + Ethylene glycol	40.8	25.6 (∓4.0)	15.1
Ethylene glycol + Formamide	46.1	38.4 (∓10.1)	7.8
Diiodomethane + Water	42.2	27.8 (∓2.6)	14.4
Diiodomethane + Formamide	43.6	27.8 (∓2.6)	15.8
Diiodomethane + Ethylene glycol	41.1	27.8 (∓2.6)	13.3

Table 3.11 Surface energy values of Ethacrynic acid using a powder covered glass slide.

Ethacrynic acid	$\gamma_{\zeta V}^{TOT}$ mJ.m^{-2}	γ_S^{LW} mJ.m^{-2}	γ_S^{AB} mJ.m^{-2}	γ_S^+ mJ.m^{-2}	γ_S^- mJ.m^{-2}
Van Oss - 3 polar	25.0	25.0 (∓24.6)	0	0	7.95
Van Oss - 2polar + 1non polar (diiodomethane)					
D. + Water + Formamide	20.0	20.0 (∓1.6)	0	0	7.7
D. + Ethylene glycol + Formamide	20.0	20.0 (∓1.6)	0	0	32.0
D. + Ethylene glycol + Water	20.0	20.0 (∓1.6)	0	0	8.5
Wu		γ_S^D	γ_S^{AB}		
Water + Formamide	24.4	11.5 (∓4.3)	13		
Water + Ethylene glycol	23.7	6.0 (∓3.0)	17.7		
Ethylene glycol + Formamide	31.7	32.9 (∓27.6)	-1.2		
Diiodomethane + Water	30.8	23.2 (∓1.4)	7.6		
Diiodomethane + Formamide	25.5	23.2 (∓1.4)	2.3		
Diiodomethane + Ethylene glycol	24.5	23.2 (∓1.4)	1.3		

Table 3.12 Surface energy values of Salicylic acid using a powder covered glass slide.

Salicylic acid	$\gamma_{\zeta v}^{TOT}$ mJ.m^{-2}	γ_S^{LW} mJ.m^{-2}	γ_S^{AB} mJ.m^{-2}	γ_S^{+} mJ.m^{-2}	γ_S^{-} mJ.m^{-2}
Van Oss - 3 polar	58.1	58.1(∓16.6)	0	0	1.9
Van Oss - 2polar + 1non polar (diiodomethane)					
D. + Water + Formamide	31.4	28.8 (∓2.1)	2.6	1.2	1.4
D. + Ethylene glycol + Formamide	28.8	28.8 (∓2.1)	0	0	189.5
D. + Ethylene glycol + Water	30.7	28.8 (∓2.1)	1.9	0.3	3.1
Wu		γ_S^{D}	γ_S^{AB}		
Water + Formamide	34.0	27 (∓2.4)	7		
Water + Ethylene glycol	27.4	16.7 (∓3.1)	10.7		
Ethylene glycol + Formamide	51.3	52.5 (∓13.3)	-1.2		
Diiodomethane + Water	36.9	30.7 (∓1.9)	6.2		
Diiodomethane + Formamide	35.7	30.7 (∓1.9)	5		
Diiodomethane + Ethylene glycol	33.6	30.7 (∓1.9)	2.9		

Table 3.13 Surface energy values of Ibuprofen using a powder covered glass slide.

Ibuprofen	$\gamma_{\zeta v}^{TOT}$ mJ.m^{-2}	γ_S^{LW} mJ.m^{-2}	γ_S^{AB} mJ.m^{-2}	γ_S^{+} mJ.m^{-2}	γ_S^{-} mJ.m^{-2}
Van Oss - 3 polar	86.6	86.6 (∓32.8)	0	0	2.4
Van Oss - 2polar + 1non polar (diiodomethane)					
D. + Water + Formamide	26.7	23.6 (∓2.5)	3.1	1.9	1.3
D. + Ethylene glycol + Formamide	23.6	23.6 (∓2.5)	0	0	636.5
D. + Ethylene glycol + Water	25.0	23.6 (∓2.5)	1.4	0.1	5.2

Wu		γ_S^D	γ_S^{AB}
Water + Formamide	32	25.3 (∓5.4)	6.7
Water + Ethylene glycol	23.7	10.0 (∓1.9)	13.9
Ethylene glycol + Formamide	74.5	78.9 (∓15.7)	-4.4
Diiodomethane + Water	32.8	26.3 (∓1.5)	6.5
Diiodomethane + Formamide	32.4	26.3 (∓1.5)	6.1
Diiodomethane + Ethylene glycol	28.1	26.3 (∓1.5)	1.8

Figure 3.10 Assessment of non-polar surface energies of the five test powders using the Van Oss theory (powder covered glass slides used).

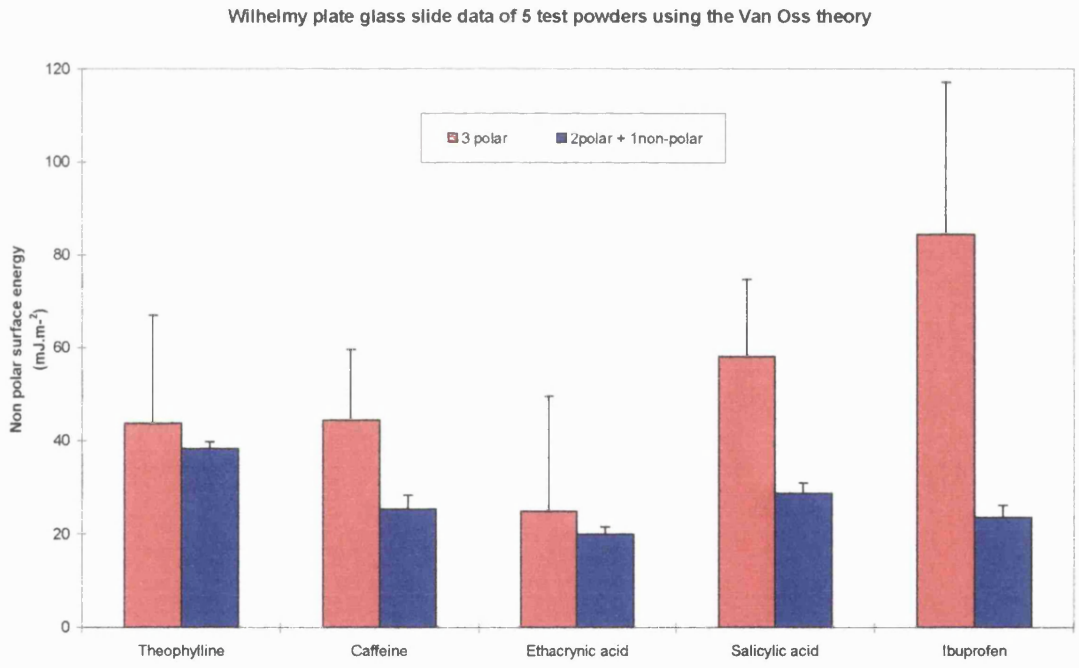

As with data from compressed powder plates, Figure 3.10 shows that the calculation using three polar liquids gave non-polar surface energies and error margins that were too large to be acceptable. The second method involving one non-polar and two polar liquids is more suitable as it consistently provides low error margins and realistic surface energy values, although these values are solely dependent on the non-polar liquid being used.

Figure 3.11 Assessment of non-polar surface energies of the five test powders using the Wu theory (powder covered glass slides used).

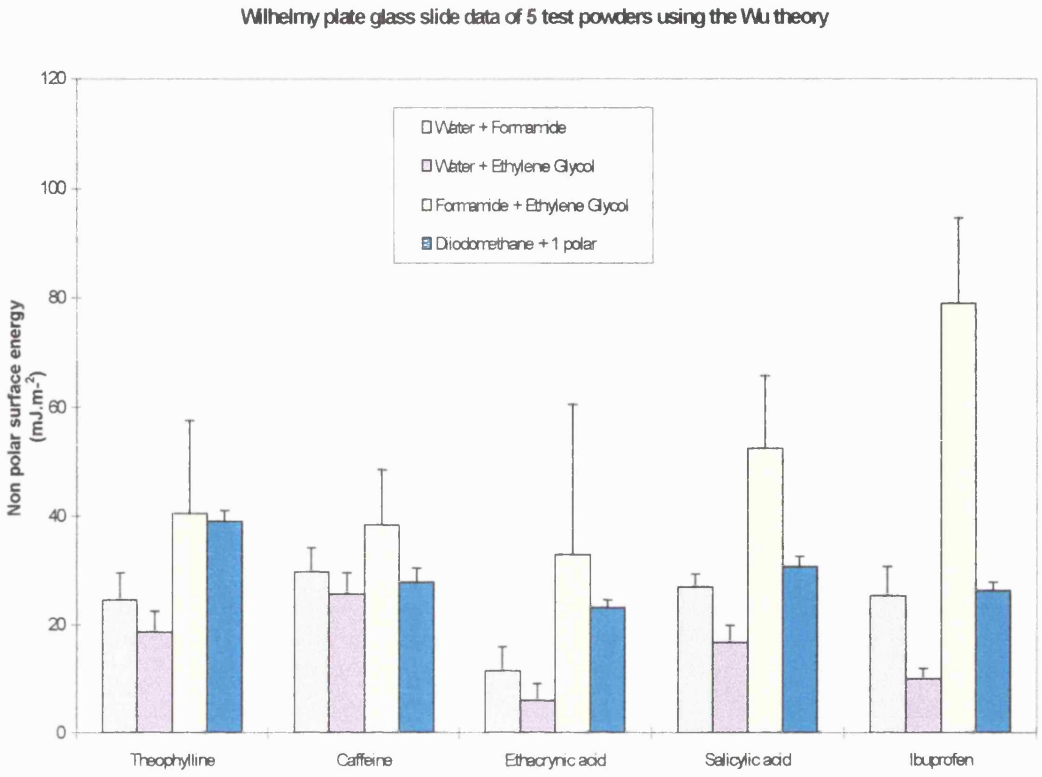

The powdered glass slide Wilhelmy plate method (Figure 3.11) has the same problems with the magnitude of error margins when using the liquid combination of formamide and ethylene glycol as the Wilhelmy plate compressed powder method had. Any of the combinations using diiodomethane (non-polar) as one of the liquids, has a corresponding low error margin, since it is solely dependent on the diiodomethane value, irrespective of any polar liquid used in conjunction with it.

3.3.3 Wilhelmy plate analysis of Saquinavir batches using a powder compact

The table of contact angles for all the Saquinavir batches do not vary significantly with each liquid used, suggesting that no differences were found, although surface energy calculations were performed in order to prove this hypothesis.

Table 3.14 Contact angles of Saquinavir batches with a selection of test liquids.

Sample	Water			Formamide		
	θ°	Cosine θ	SD_{n-1}	θ°	Cosine θ	SD_{n-1}
Ro8959-003	62.3	0.465	0.0252	41.5	0.748	0.0359
Batch 001-tray dried	62.7	0.459	0.0284	38.1	0.787	0.0092
Batch 002-spin dried	64.0	0.439	0.0333	41.8	0.745	0.0281
Batch 010-tray dried	63.7	0.442	0.0708	32.5	0.843	0.0237
Batch 020-vacuum dried	69.2	0.356	0.0357	40.1	0.765	0.0115
Batch 030-heated only	63.3	0.448	0.0491	37.7	0.791	0.0268
	Ethylene glycol			Diiodomethane		
Ro8959-003	39.6	0.770	0.0273	33.3	0.832	0.0642
Batch 001-tray dried	41.9	0.743	0.0360	44.3	0.715	0.0323
Batch 002-spin dried	40.1	0.765	0.0266	41.4	0.749	0.0348
Batch 010-tray dried	40.2	0.763	0.0188	32.4	0.842	0.0477
Batch 020-vacuum dried	43.7	0.721	0.0608	31.2	0.854	0.0293
Batch 030-heated only	33.6	0.831	0.0382	37.1	0.796	0.0444

Table 3.15 Surface energy values of original Saquinavir using a powder compact.

Ro8959-003	$\gamma_{\zeta v}^{TOT}$ mJ.m^{-2}	γ_S^{LW} mJ.m^{-2}	γ_S^{AB} mJ.m^{-2}	γ_S^+ mJ.m^{-2}	γ_S^- mJ.m^{-2}
Van Oss - 3 polar	68.1	68.1 (∓20.1)	0	0	16.3
Van Oss - 2polar + 1non polar (diiodomethane)					
D. + Water + Formamide	47.7	42.8 (∓2.8)	4.9	0.4	15.0
D. + Ethylene glycol + Formamide	42.8	42.8 (∓2.8)	0	0	180.4
D. + Ethylene glycol + Water	42.8	42.8 (∓2.8)	0	0	18.7
Wu		γ_S^D	γ_S^{AB}		
Water + Formamide	46.5	25.3 (∓2.7)	21.2		
Water + Ethylene glycol	42.4	15.5 (∓1.6)	26.9		
Ethylene glycol + Formamide	62.3	60.5 (∓16.9)	1.8		
Diiodomethane + Water	59.1	43.1 (∓2.8)	16.0		
Diiodomethane + Formamide	50.0	43.1 (∓2.8)	6.6		
Diiodomethane + Ethylene glycol	48.0	43.1 (∓2.8)	4.9		

Table 3.16 Surface energy values of tray dried Saquinavir (b001) using a powder compact.

Batch 001 (tray dried)	$\gamma_{\zeta v}^{TOT}$ mJ.m^{-2}	γ_S^{LW} mJ.m^{-2}	γ_S^{AB} mJ.m^{-2}	γ_S^+ mJ.m^{-2}	γ_S^- mJ.m^{-2}
Van Oss - 3 polar	91.8	91.8 (∓14.9)	0	0	14.9
Van Oss - 2polar + 1non polar (diiodomethane)					
D. + Water + Formamide	46.7	37.4 (∓1.4)	9.3	1.7	12.6
D. + Ethylene glycol + Formamide	37.4	37.4 (∓1.4)	0	0	520.7
D. + Ethylene glycol + Water	41.4	37.4 (∓1.4)	4.0	0.2	19.9

Wu		γ_S^D	γ_S^{AB}
Water + Formamide	47.6	27.6 (∓1.5)	20.0
Water + Ethylene glycol	42.0	14.6 (∓2.1)	27.4
Ethylene glycol + Formamide	80.9	81.4 (∓16.0)	-0.4
Diiodomethane + Water	55.0	38.2 (∓1.3)	16.9
Diiodomethane + Formamide	48.3	38.2 (∓1.3)	10.2
Diiodomethane + Ethylene glycol	44.0	38.2 (∓1.3)	5.8

Table 3.17 Surface energy values of spin dried Saquinavir (b002) using a powder compact.

Batch 002 (spin dried)	γ_{Sv}^{TOT} mJ.m^{-2}	γ_S^{LW} mJ.m^{-2}	γ_S^{AB} mJ.m^{-2}	γ_S^+ mJ.m^{-2}	γ_S^- mJ.m^{-2}
Van Oss - 3 polar	69.2	69.2 (∓16.9)	0	0	14.5
Van Oss - 2polar + 1non polar (diiodomethane)					
D. + Water + Formamide	46.1	38.9 (∓1.6)	7.2	1.0	13.1
D. + Ethylene glycol + Formamide	93.3	38.9 (∓1.6)	54.4	3.2	230.8
D. + Ethylene glycol + Water	42.6	38.9 (∓1.6)	3.7	0.2	17.3
Wu		γ_S^D	γ_S^{AB}		
Water + Formamide	45.9	25.9 (∓2.6)	20.0		
Water + Ethylene glycol	41.4	16.0 (∓2.1)	25.4		
Ethylene glycol + Formamide	62.6	60.9 (∓15.2)	1.7		
Diiodomethane + Water	55.5	39.5 (∓1.4)	15.9		
Diiodomethane + Formamide	47.6	39.5 (∓1.4)	8.1		
Diiodomethane + Ethylene glycol	45.3	39.5 (∓1.4)	5.8		

Table 3.18 Surface energy values of tray dried Saquinavir (b010) using a powder compact.

Batch 010 (tray dried)	$\gamma_{\zeta v}^{TOT}$ mJ.m^{-2}	γ_S^{LW} mJ.m^{-2}	γ_S^{AB} mJ.m^{-2}	γ_S^{+} mJ.m^{-2}	γ_S^{-} mJ.m^{-2}
Van Oss - 3 polar	112	112 (∓21.1)	0	0	12.0
Van Oss - 2polar + 1non polar (diiodomethane)					
D. + Water + Formamide	50.8	43.2 (∓2.2)	7.6	1.5	9.6
D. + Ethylene glycol + Formamide	43.2	43.2 (∓2.2)	0	0	644.4
D. + Ethylene glycol + Water	43.2	43.2 (∓2.2)	0	0	17.2
Wu		γ_S^{D}	γ_S^{AB}		
Water + Formamide	49.7	31.6 (∓4.4)	18.1		
Water + Ethylene glycol	41.5	15.8 (∓2.7)	25.7		
Ethylene glycol + Formamide	99.7	99.7 (∓21.6)	0		
Diiodomethane + Water	58.7	43.5 (∓2.1)	15.3		
Diiodomethane + Formamide	52.6	43.5 (∓2.1)	9.1		
Diiodomethane + Ethylene glycol	48.2	43.5 (∓2.1)	4.7		

Table 3.19 Surface energy values of Vacuum dried Saquinavir (b020) using a powder compact.

Batch 020 (vacuum dried)	$\gamma_{\zeta v}^{TOT}$ mJ.m^{-2}	γ_S^{LW} mJ.m^{-2}	γ_S^{AB} mJ.m^{-2}	γ_S^{+} mJ.m^{-2}	γ_S^{-} mJ.m^{-2}
Van Oss - 3 polar	92.3	92.3 (∓25.5)	0	0	9.1
Van Oss - 2polar + 1non polar (diiodomethane)					
D. + Water + Formamide	48.6	43.7 (∓1.4)	4.9	0.8	7.5
D. + Ethylene glycol + Formamide	43.7	43.7 (∓1.4)	0	0	376.0
D. + Ethylene glycol + Water	43.7	43.7 (∓1.4)	0	0	12.5

Wu		γ_S^D	γ_S^{AB}
Water + Formamide	45.8	30.1 (∓2.2)	15.8
Water + Ethylene glycol	38.3	16.5 (∓3.9)	21.8
Ethylene glycol + Formamide	79.6	79.6 (∓25.3)	0
Diiodomethane + Water	56.6	44.0 (∓1.3)	12.6
Diiodomethane + Formamide	50.6	44.0 (∓1.3)	6.7
Diiodomethane + Ethylene glycol	47.8	44.0 (∓1.3)	3.9

Table 3.20 Surface energy values of heated Saquinavir (b030) using a powder compact.

Batch 030 (heated only)	$\gamma_{\zeta v}^{TOT}$ mJ.m^{-2}	γ_S^{LW} mJ.m^{-2}	γ_S^{AB} mJ.m^{-2}	γ_S^+ mJ.m^{-2}	γ_S^- mJ.m^{-2}
Van Oss - 3 polar	67.6	67.6 (∓22.8)	0	0	13.1
Van Oss - 2polar + 1non polar (diiodomethane)					
D. + Water + Formamide	49.3	41.1 (∓2.0)	8.2	1.4	11.9
D. + Ethylene glycol + Formamide	41.1	41.1 (∓2.0)	0	0	183.6
D. + Ethylene glycol + Water	45.4	41.1 (∓2.0)	4.3	0.3	15.5
Wu		γ_S^D	γ_S^{AB}		
Water + Formamide	47.6	28.2 (∓3.3)	19.4		
Water + Ethylene glycol	42.7	18.8 (∓3.4)	23.9		
Ethylene glycol + Formamide	61.0	57.9 (∓17.2)	3.1		
Diiodomethane + Water	57.3	41.5 (∓1.9)	15.8		
Diiodomethane + Formamide	50.0	41.5 (∓1.9)	8.5		
Diiodomethane + Ethylene glycol	48.1	41.5 (∓1.9)	6.6		

Figure 3.12 Assessment of non-polar surface energies of the Saquinavir batches using the Van Oss theory (powder compact used).

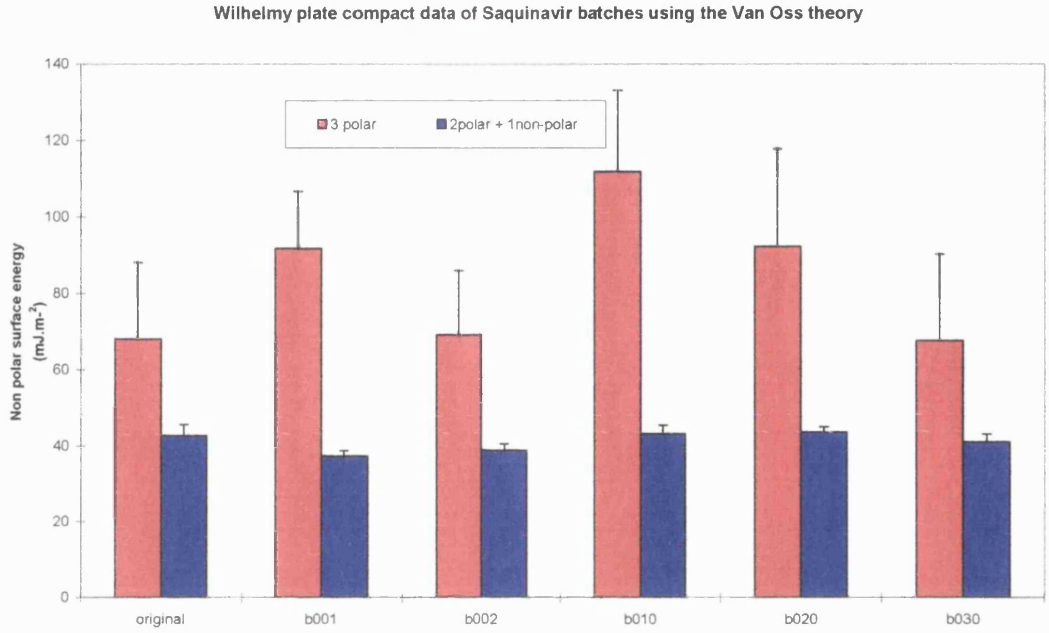

Figure 3.13 Assessment of non-polar surface energies of the Saquinavir batches using the Wu theory (powder compact used)

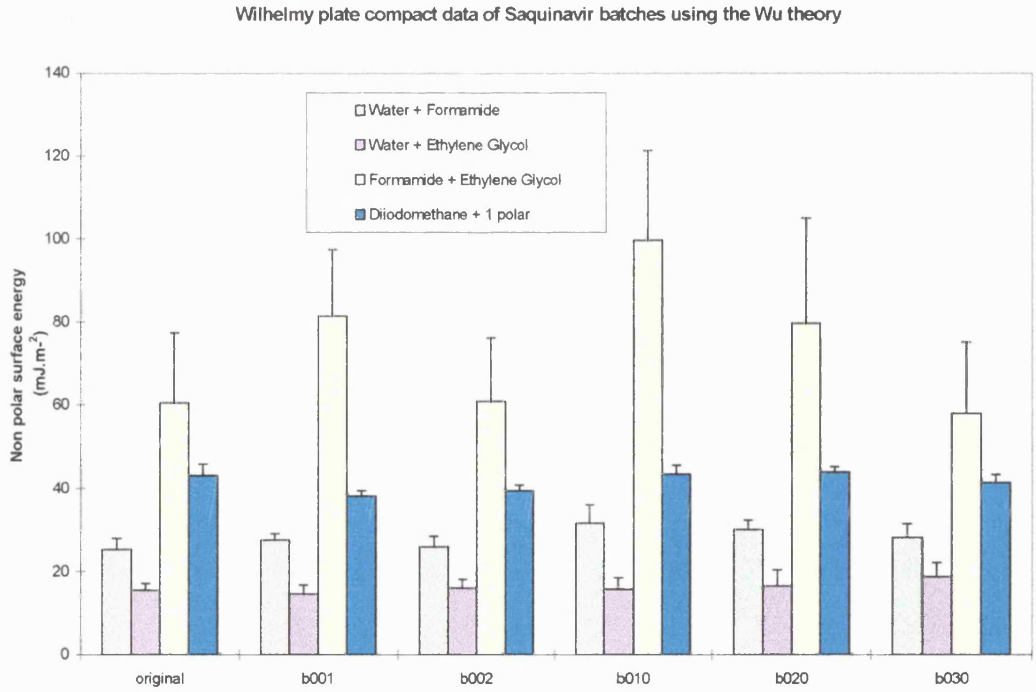

The Saquinavir batches all have very similar non-polar surface energies according to the Van Oss method using one non-polar and two polar liquids with suitably low margins of error as was the previous five model powders (Figure 3.12). The method using three polar liquids produced highly variable values with correspondingly large margins of error. Figure 3.12 highlights the necessity of the use of a non-polar liquid to achieve realistic surface energy data. Using Wu theory in comparison, the combination of ethylene glycol and formamide has again resulted in greatly magnified and variable non-polar surface energy values with large error margins (Figure 3.13). The other three methods of calculation have produced far more precise values that are very similar in magnitude depending on which combination of liquids are used.

3.3.4 Wilhelmy plate analysis of Saquinavir batches using a powder covered glass slide

The contact angles of all the Saquinavir batches do not appear to vary significantly from one another with each test liquid used (Table 3.21). Although this suggests that all the batches have very similar surface properties, these were still calculated using both Wu and Van Oss theory.

Table 3.21 Contact angles of Saquinavir batches with a selection of test liquids.

Sample	Water			Formamide		
	θ°	Cosine θ	SD_{n-1}	θ°	Cosine θ	SD_{n-1}
Ro8959-003	92.7	-0.047	0.0474	77.7	0.214	0.0447
Batch 001-tray dried	91.5	-0.026	0.0272	83.3	0.116	0.0384
Batch 002-spin dried	91.4	-0.025	0.0187	81.9	0.142	0.0270
Batch 010-tray dried	92.5	-0.044	0.0246	83.0	0.122	0.0402
Batch 020-vacuum dried	90.8	-0.014	0.0249	82.2	0.136	0.0278
Batch 030-heated only	91.6	-0.028	0.0215	82.5	0.130	0.0654

	Ethylene glycol			Diiodomethane		
Ro8959-003	70.0	0.341	0.0390	67.5	0.381	0.0604
Batch 001-tray dried	74.6	0.266	0.0623	71.5	0.317	0.0648
Batch 002-spin dried	75.8	0.245	0.0435	70.8	0.328	0.0684
Batch 010-tray dried	73.5	0.284	0.0536	67.9	0.376	0.0649
Batch 020-vacuum dried	74.1	0.273	0.0411	64.5	0.431	0.0411
Batch 030-heated only	73.5	0.283	0.0413	64.2	0.434	0.0344

Table 3.22 Surface energy values of original Saquinavir using a powder covered glass slide.

Ro8959-003	$\gamma_{\varsigma v}^{TOT}$ mJ.m^{-2}	γ_S^{LW} mJ.m^{-2}	γ_S^{AB} mJ.m^{-2}	γ_S^{+} mJ.m^{-2}	γ_S^{-} mJ.m^{-2}
Van Oss - 3 polar	20.6	15.8 (∓13.9)	4.8	1.4	4.1
Van Oss - 2polar + 1non polar (diiodomethane)					
D. + Water + Formamide	24.3	24.3 (∓2.1)	0	0	4.5
D. + Ethylene glycol + Formamide	24.3	24.3 (∓2.1)	0	2.3	0
D. + Ethylene glycol + Water	26.0	24.3 (∓2.1)	1.7	0.2	3.5
Wu		γ_S^{D}	γ_S^{AB}		
Water + Formamide	25.4	15.5 (∓4.0)	9.9		
Water + Ethylene glycol	24.33	13.2 (∓4.2)	11.1		
Ethylene glycol + Formamide	26.13	21.4 (∓13.6)	4.7		
Diiodomethane + Water	32.8	26.8 (∓1.8)	5.9		
Diiodomethane + Formamide	28.7	26.8 (∓1.8)	1.9		
Diiodomethane + Ethylene glycol	29.3	26.8 (∓1.8)	2.4		

Table 3.23 Surface energy values of tray dried Saquinavir (b001) using a powder covered glass slide.

Batch 001 (tray dried)	$\gamma_{\zeta v}^{TOT}$ mJ.m^{-2}	γ_S^{LW} mJ.m^{-2}	γ_S^{AB} mJ.m^{-2}	γ_S^{+} mJ.m^{-2}	γ_S^{-} mJ.m^{-2}
Van Oss - 3 polar	17.4	8.7 (∓11.7)	8.7	2.5	7.5
Van Oss - 2polar + 1non polar (diiodomethane)					
D. + Water + Formamide	22.1	22.1 (∓2.2)	0	0	8.3
D. + Ethylene glycol + Formamide	22.1	22.1 (∓2.2)	0	4.4	0
D. + Ethylene glycol + Water	23.6	22.1 (∓2.2)	1.5	0.1	5.9
Wu		γ_S^{D}	γ_S^{AB}		
Water + Formamide	24.0	10.6 (∓2.3)	13.3		
Water + Ethylene glycol	23.6	9.2 (∓3.3)	14.4		
Ethylene glycol + Formamide	22.5	15.5 (∓16.0)	6.9		
Diiodomethane + Water	31.9	25.0 (∓1.8)	6.9		
Diiodomethane + Formamide	26.0	25.0 (∓1.8)	1.0		
Diiodomethane + Ethylene glycol	26.9	25.0 (∓1.8)	2.0		

Table 3.24 Surface energy values of spin dried Saquinavir (b002) using a powder covered glass slide.

B002 (spin dried)	$\gamma_{\zeta v}^{TOT}$ mJ.m^{-2}	γ_S^{LW} mJ.m^{-2}	γ_S^{AB} mJ.m^{-2}	γ_S^{+} mJ.m^{-2}	γ_S^{-} mJ.m^{-2}
Van Oss - 3 polar	19.1	15.0 (∓10.8)	4.1	0.6	7.1
Van Oss - 2polar + 1non polar (diiodomethane)					
D. + Water + Formamide	22.4	22.4 (∓2.3)	0	0	7.6
D. + Ethylene glycol + Formamide	22.4	22.4 (∓2.3)	0	1.2	0
D. + Ethylene glycol + Water	22.4	22.4 (∓2.3)	0	0	6.4

Wu		γ_S^D	γ_S^{AB}
Water + Formamide	24.3	11.6 (∓1.7)	12.7
Water + Ethylene glycol	23.5	8.4 (∓2.2)	15.2
Ethylene glycol + Formamide	25.2	22.7 (∓11.1)	2.5
Diiodomethane + Water	32.1	25.3 (∓2.0)	6.8
Diiodomethane + Formamide	26.6	25.3 (∓2.0)	1.3
Diiodomethane + Ethylene glycol	26.8	25.3 (∓2.0)	1.6

Table 3.25 Surface energy values of tray dried Saquinavir (b010) using a powder covered glass slide.

Batch 010 (tray dried)	$\gamma_{\zeta v}^{TOT}$ mJ.m^{-2}	γ_S^{LW} mJ.m^{-2}	γ_S^{AB} mJ.m^{-2}	γ_S^+ mJ.m^{-2}	γ_S^- mJ.m^{-2}
Van Oss - 3 polar	16.9	7.9 (∓10.4)	9.0	3.2	6.4
Van Oss - 2polar + 1non polar (diiodomethane)					
D. + Water + Formamide	24.1	24.1 (∓2.3)	0	0	7.3
D. + Ethylene glycol + Formamide	24.1	24.1 (∓2.3)	0	6.0	0
D. + Ethylene glycol + Water	24.1	24.1 (∓2.3)	0	0	4.6
Wu		γ_S^D	γ_S^{AB}		
Water + Formamide	23.7	11.3 (∓2.4)	12.4		
Water + Ethylene glycol	23.4	10.5 (∓3.2)	12.9		
Ethylene glycol + Formamide	22.7	14.0 (∓14.2)	8.7		
Diiodomethane + Water	32.7	26.7 (∓1.9)	6.1		
Diiodomethane + Formamide	27.1	26.7 (∓1.9)	0.4		
Diiodomethane + Ethylene glycol	28.3	26.7 (∓1.9)	1.7		

Table 3.26 Surface energy values of vacuum dried Saquinavir (b020) using a powder covered glass slide.

Batch 020 (vacuum dried)	$\gamma_{\zeta v}^{TOT}$ mJ.m^{-2}	γ_S^{LW} mJ.m^{-2}	γ_S^{AB} mJ.m^{-2}	γ_S^{+} mJ.m^{-2}	γ_S^{-} mJ.m^{-2}
Van Oss - 3 polar	18.0	10.6 (∓8.9)	7.4	1.8	7.6
Van Oss - 2polar + 1non polar (diiodomethane)					
D. + Water + Formamide	26.0	26.0 (∓1.5)	0	0	8.5
D. + Ethylene glycol + Formamide	26.0	26.0 (∓1.5)	0	3.8	0
D. + Ethylene glycol + Water	26.0	26.0 (∓1.5)	0	0	5.9
Wu		γ_S^{D}	γ_S^{AB}		
Water + Formamide	24.3	10.7 (∓1.8)	13.7		
Water + Ethylene glycol	24.0	9.1 (∓2.3)	14.9		
Ethylene glycol + Formamide	23.3	17.8 (∓10.7)	5.5		
Diiodomethane + Water	34.6	28.3 (∓1.3)	6.3		
Diiodomethane + Formamide	28.4	28.3 (∓1.3)	0.1		
Diiodomethane + Ethylene glycol	29.3	28.3 (∓1.3)	1.0		

Table 3.27 Surface energy values of heated Saquinavir (b030) using a powder covered glass slide.

Batch 030 (heated only)	$\gamma_{\zeta v}^{TOT}$ mJ.m^{-2}	γ_S^{LW} mJ.m^{-2}	γ_S^{AB} mJ.m^{-2}	γ_S^{+} mJ.m^{-2}	γ_S^{-} mJ.m^{-2}
Van Oss - 3 polar	17.4	8.8 (∓13.4)	8.6	2.6	6.9
Van Oss - 2polar + 1non polar (diiodomethane)					
D. + Water + Formamide	26.1	26.1 (∓1.3)	0	0	8.0
D. + Ethylene glycol + Formamide	26.1	26.1 (∓1.3)	0	5.3	0
D. + Ethylene glycol + Water	26.1	26.1 (∓1.3)	0	0	5.1

Wu		γ_S^D	γ_S^{AB}
Water + Formamide	24.1	11.2 (∓3.3)	12.9
Water + Ethylene glycol	23.7	10.0 (∓2.4)	13.8
Ethylene glycol + Formamide	22.8	7.4 (∓16.5)	15.4
Diiodomethane + Water	34.4	28.4 (∓1.1)	6.0
Diiodomethane + Formamide	28.4	28.4 (∓1.1)	0
Diiodomethane + Ethylene glycol	29.5	28.4 (∓1.1)	1.1

Figure 3.14 Assessment of non-polar surface energies of the Saquinavir batches using the Van Oss theory (powder covered glass slide used).

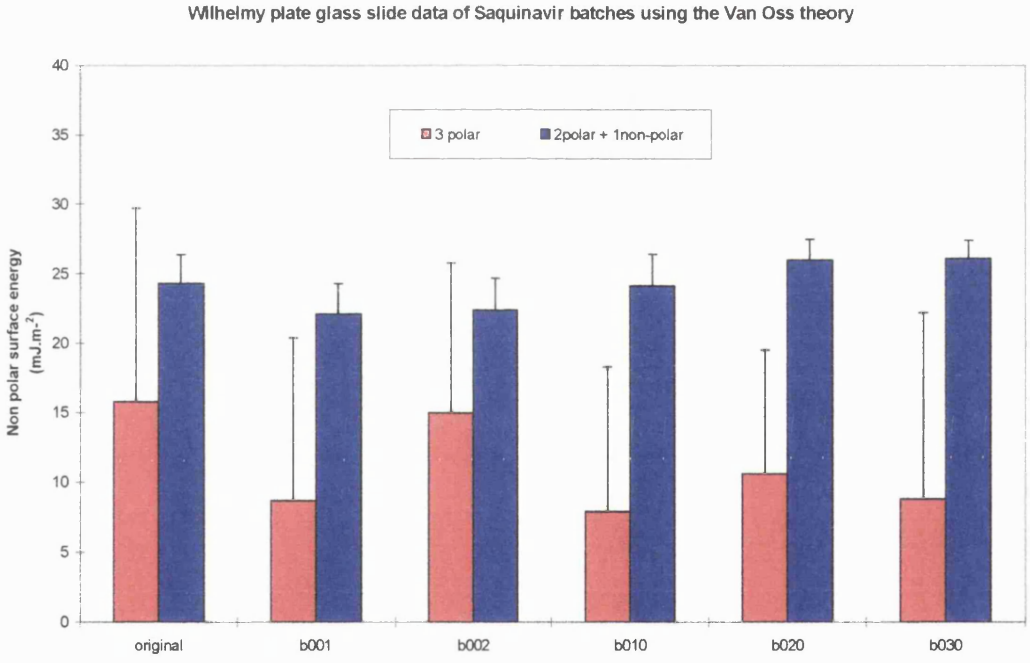

The powdered covered glass slide method again proves the unsuitability of the combination of three polar liquids (unacceptable error) to predict surface energy values (Figure 3.14). The method using the non-polar liquid shows that each Saquinavir batch has a very similar non-polar surface energy value.

Figure 3.15 Assessment of non-polar surface energies of the Saquinavir batches using the Wu theory (powder covered glass slide used).

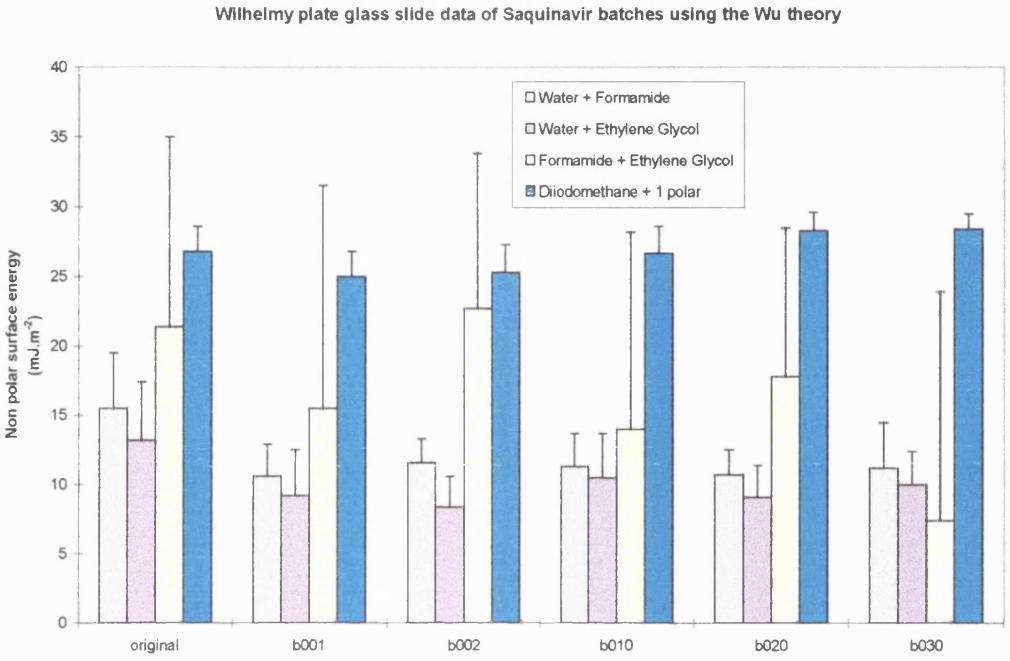

Due to the small scale on the y-axis (Figure 3.15), the combination using diiodomethane appears to be far larger than the other two liquid combinations, although all three give precise data. This is not the case, their respective values are in the same order of magnitude difference as all the other figures shown previously in this chapter. Again the ethylene glycol and formamide combination has proved unreliable due to its large error margins. Depending on which precise method of calculation is chosen, the Saquinavir batches all appear to be unchanged in non-polar surface energy when compared to the original sample.

3.3.4.1 Summary of results

- The Van Oss equation utilising three polar liquids at once, gave unreliable surface energy data due to the large errors that were incurred (Section 3.3.6).

- Equations using both formamide and ethylene glycol together gave large errors for two reasons.

a) Both formamide and ethylene glycol contact angles each yielded errors that were far greater than with water.
b) The calculation introduces a magnification effect on the true experimental error, since the two liquids are extremely similar in surface energy values. (Section 3.3.6)

- Equations using water with either formamide or ethylene glycol gave a much smaller error margin. Water gives slightly more consistent contact angles and has very different surface energy values to formamide and ethylene glycol, ensuring that no magnification error occurs in the calculation process.

- Equations using a non-polar liquid (diiodomethane) have a very small error, since the non-polar surface energy is totally dependent on diiodomethane irrespective of the other liquids used. The only drawback is that many powders, especially those presented in the compacted form, do not yield contact angles with totally non-polar liquids such as diiodomethane. This method alone cannot be depended upon for reliable surface energy data.

3.3.5 Negative polarity values

One must remember that the square of a negative number is a positive. The rarity of negative $(\gamma_S^-)^{0.5}$ values suggests that these may just be a result of experimental error (Good, 1993). Unfortunately, negative $(\gamma_S^+)^{0.5}$ values are far more common. It is possible that these negative values could be a true indication of the surface energy composition.

$$\gamma_S^{AB} = 2\{(\gamma_S^-)^{0.5}.(\gamma_S^+)^{0.5}\} \qquad \text{Equation 3.2}$$

This could be explained by an array of surface dipoles which had more positive ends sticking out on the surface than negative. Good suggests that small values (<0.05) can be taken as zero, since this problem has not been fully looked into, as yet.

3.3.6 Test liquid choice

The choice and combination of the liquid probes used in the surface energy calculation have been found to greatly affect the accuracy. Glycerol, although useful, does not produce reproducible contact angles, probably due to a lag time in the liquid front reaching its final resting place on the Wilhelmy plate as it is a highly viscous liquid. In addition, glycerol is quite deliquescent in nature and will absorb water vapour over time, changing the water content of the liquid. The accuracy level between test liquid combinations can be quantified (Good, 1992).

Main Van Oss equation:-

$$\gamma_{LV}^{TOT}(1+\cos\theta) = 2\{(\gamma_S^{LW}.\gamma_L^{LW})^{0.5} + (\gamma_S^{+}.\gamma_L^{-})^{0.5} + (\gamma_S^{-}.\gamma_L^{+})^{0.5}\} \qquad \text{Equation 3.3}$$

Formamide	Ethylene glycol
Let $A = \gamma_F^{TOT}(1+\cos\theta) - 2(\gamma_S^{LW}.\gamma_F^{LW})^{0.5}$	$B = \gamma_{EG}^{TOT}(1+\cos\theta) - 2(\gamma_S^{LW}.\gamma_{EG}^{LW})^{0.5}$
$C = 2(\gamma_F^{-})^{0.5}$	$E = 2(\gamma_{EG}^{-})^{0.5}$
$D = 2(\gamma_F^{+})^{0.5}$	$F = 2(\gamma_{EG}^{+})^{0.5}$

Since values for A,B,C,D,E and F can be easily obtained from literature, they do not vary throughout the equation and so are given letters to simplify matters. This leaves a pair of simultaneous equations:-

(formamide) $$A = C\,(\gamma_S^{+})^{0.5} + D\,(\gamma_S^{-})^{0.5} \qquad \text{Equation 3.4}$$

(ethylene glycol) $$B = E\,(\gamma_S^{+})^{0.5} + F\,(\gamma_S^{-})^{0.5} \qquad \text{Equation 3.5}$$

By multiplying Equation 3.4 by $\frac{E}{C}$:

(formamide) $$\frac{AE}{C} = \frac{CE}{C}(\gamma_S^{+})^{0.5} + \frac{DE}{C}(\gamma_S^{-})^{0.5} \qquad \text{Equation 3.6}$$

Solving Equations 3.5 and 3.6 simultaneously gives:-

$$B - \frac{AE}{C} = F\,(\gamma_S^{-})^{0.5} - \frac{DE}{C}(\gamma_S^{-})^{0.5} \qquad \text{Equation 3.7}$$

$$\therefore (\gamma_S^-)^{0.5} \left(F - \frac{DE}{C}\right) = B - \frac{AE}{C} \qquad \text{Equation 3.8}$$

$$\therefore (\gamma_S^-)^{0.5} (CF - DE) = (BC - AE) \qquad \text{Equation 3.9}$$

$$\therefore (\gamma_S^-)^{0.5} = \frac{BC - AE}{CF - DE} \qquad \text{Equation 3.10}$$

and by the same method, by multiplying Equation 3.5 by $\frac{D}{F}$:

$$\text{(ethylene glycol)} \qquad \frac{BD}{F} = \frac{DE}{F} (\gamma_S^+)^{0.5} + \frac{DF}{F} (\gamma_S^-)^{0.5} \qquad \text{Equation 3.11}$$

Solving Equations 3.4 and 3.11 simultaneously gives:-

$$A - \frac{BD}{F} = C (\gamma_S^+)^{0.5} - \frac{DE}{F} (\gamma_S^+)^{0.5} \qquad \text{Equation 3.12}$$

$$\therefore (\gamma_S^+)^{0.5} (CF - DE) = (AF - BD) \qquad \text{Equation 3.13}$$

$$\therefore (\gamma_S^+)^{0.5} = \frac{AF - BD}{CF - DE} \qquad \text{Equation 3.14}$$

It can be shown that with Equation 3.14, when a combination of ethylene glycol and formamide are chosen, the values for γ_S^+ and γ_S^- are considerably more variable than if water were one of the liquids chosen with either of the other two liquids. To prove this mathematically, one must study the denominator of equations 3.10 and 3.14. In both cases they involve CF - DE; for formamide with ethylene glycol this denominator has a value of 6.65, since the two liquids have very similar polar surface energy values. The combination of water and ethylene glycol gives a much greater value of 110.5, since water has very different polar surface energy values to ethylene glycol and formamide. Therefore any error involved in the experiments that make up the numerators may be similar for all liquids employed but if the denominator is smaller there will be a greater magnification of error. The magnification of experimental error is actually 16.6 times greater if water is not included as one of the two polar liquids.

With Wu's theory, if the polar component of the solid is higher than the polar component of either liquid, the polar surface energy will be biased towards the polar surface tension of the liquids and is therefore lowered below its true value. Therefore the mean polar surface energy of the powder is biased towards the lowest polar value

and this method must only be used with test liquids that have a relatively high surface tension.

The error can also be defined for the non-polar component of surface energy with Van Oss theory, whereby the following simplifications have been derived from Equation 3.3.

$$\gamma_{Di}^{TOT}(1+\cos\theta) = 2\{(\gamma_S^{LW}.\gamma_{Di}^{LW})^{0.5} \qquad \text{Equation 3.15}$$

Di - diiodomethane

Since diiodomethane is totally non-polar, this allows Equation 3.15 to be solved using only diiodomethane contact angle data. Any error is only dependent on the diiodomethane, and therefore is wholly representative of any experimental error with no artificial magnification. This applies to both the Van Oss and Wu theories when using a totally non-polar liquid. When the non-polar data is not available, three polar liquids can be used alone, but in practise this method again leads to larger error margins. It is possible, although more complicated, to quantify this error as follows:-

$$(\gamma_S^{+})^{0.5} = \frac{(AE-BD)(FG-DI)-(AF-CD)(EG-DH)}{(EJ-DK)(FG-DI)-(FJ-DL)(EG-DH)} \qquad \text{Equation 3.16}$$

$$(\gamma_S^{-})^{0.5} = \frac{(AE-BD)(FJ-DL)-(AF-CD)(EJ-DK)}{(EG-DH)(FJ-DL)-(FG-DI)(EJ-DK)} \qquad \text{Equation 3.17}$$

$$(\gamma_S^{LW})^{0.5} = \frac{(AH-BG)(IJ-GL)-(AI-CG)(JH-GK)}{(DH-EG)(IJ-GL)-(DI-FG)(JH-GK)} \qquad \text{Equation 3.18}$$

where

$A = \gamma_W^{TOT}(1+\cos\theta)$ $\quad$ $G = 2(\gamma_W^{+})^{0.5}$

$B = \gamma_F^{TOT}(1+\cos\theta)$ $\quad$ $H = 2(\gamma_F^{+})^{0.5}$

$C = \gamma_{EG}^{TOT}(1+\cos\theta)$ $\quad$ $I = 2(\gamma_{EG}^{+})^{0.5}$

$D = 2(\gamma_W^{LW})^{0.5}$ $\quad$ $J = 2(\gamma_W^{-})^{0.5}$

$E = 2(\gamma_F^{LW})^{0.5}$ $\quad$ $K = 2(\gamma_F^{-})^{0.5}$

$F = 2(\gamma_{EG}^{LW})^{0.5}$ $\quad$ $L = 2(\gamma_{EG}^{-})^{0.5}$

Since the denominator values correspond to a combination of the surface properties of the liquids used, which are very similar for ethylene glycol and formamide, it will be very small in comparison to the nominator, in Equations 3.16-3.18. Thus the experimental errors in the three contact angles for each polar liquid present in the nominator will be greatly magnified by their division with a smaller value and the product then being squared. Table 3.28 highlights the error magnification of the non-polar surface energy data for all powders using the powder covered glass slide Wilhelmy plate method (Section 3.3.2 and 3.2.4). The cosine error for each test liquid (formamide, water and ethylene glycol) was assumed to be the same (± 0.02) to simplify matters.

Table 3.28 Process of error determination.

Sample	Denominator value	Nominator value	Final error (mJm^{-2})
Saquinavir	2813	11853	± 3.57
Ethacrynic acid	2813	14034	± 8.25
Theophylline	2813	18650	± 10.96
Caffeine	2813	18795	± 11.03
Salicylic acid	2813	21456	± 12.62
Ibuprofen	2813	25863	± 15.21

It is evident that as the nominator value increases, the final error increases significantly even though the individual contact angle errors remain constant. The nominator value is largest when (AH-BG) is far greater than (AI-CG). Since A involves the contact angle of water, being in both of the components, it has no affect on the error margin, along with H, G and I which are constants. Therefore variations in values for B (involving formamide) and C (involving ethylene glycol) will affect the overall nominator value, whereby the greater the difference between B and C, the greater the nominator value, and consequently the greater the magnification of error. Although it may appear from Table 3.28, that Saquinavir has an acceptably low error margin (±3.57 $mJ.m^{-2}$) compared to the other powders, the true experimental error values for each liquid were approximately double the constant values used in Table 3.28, still resulting in an unacceptably large error (±13.9 $mJ.m^{-2}$).

The Van Oss theory is able to calculate surface energy data with three polar liquids although the choice of those three liquids is vital to ensure that the experimental error is not magnified too greatly. A choice involving water, formamide and a third liquid, with totally different surface energy values to the other liquids would be a more acceptable situation.

3.3.7 Comparison between two Wilhelmy plate methods

The liquid combinations that yielded unacceptably large error margins have not been included in this section.

Figure 3.16 Assessment of non-polar surface energies of all powders using diiodomethane.

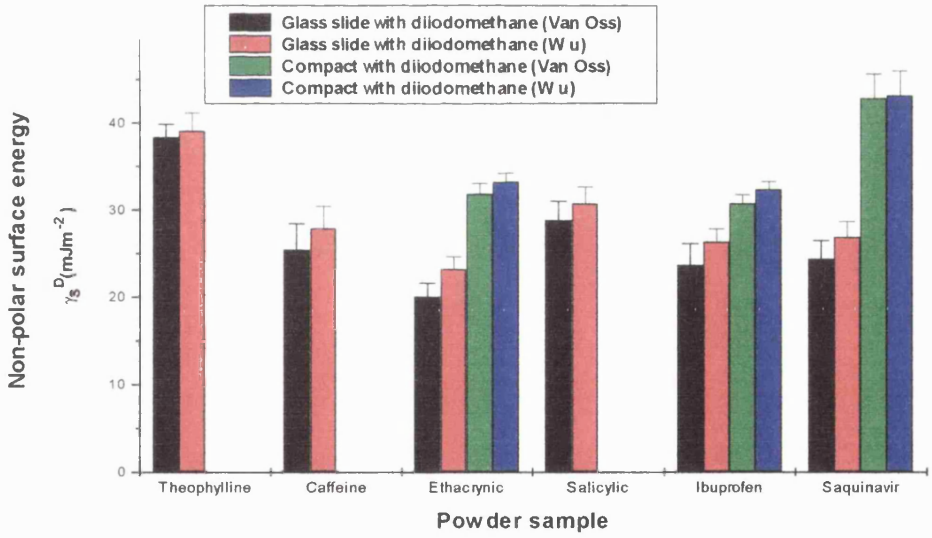

Figure 3.16 shows that the non-polar surface energy value using diiodomethane is dependant on which Wilhelmy plate method is chosen, with the compacted powder plate consistently producing higher values than the powder covered glass slide.

Figure 3.17 Assessment of non-polar surface energies of all powders using polar liquids with Wu theory.

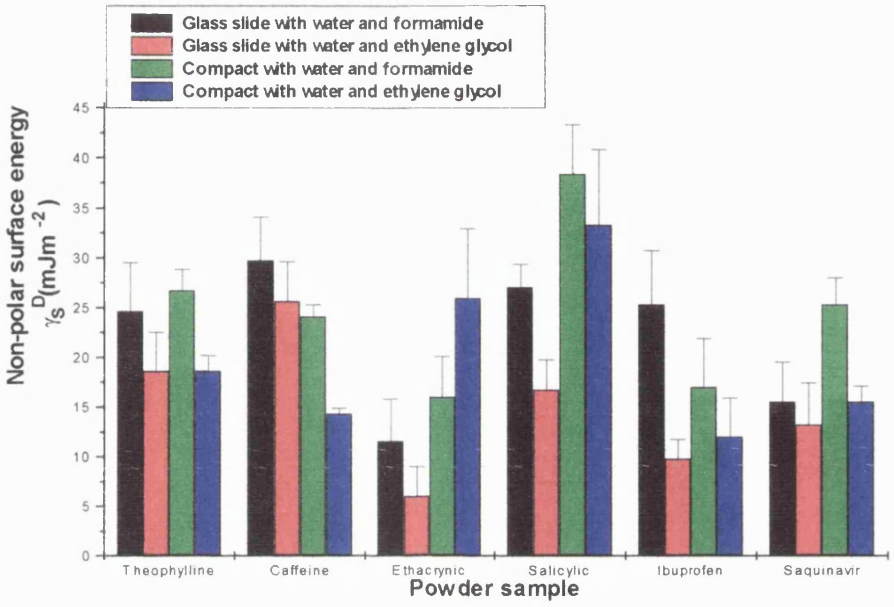

Figure 3.17 graphically represents the two most precise combinations of polar liquids that produce non-polar surface energy data. Unfortunately, any trends are difficult to differentiate, although it is clear that the choice of liquid used may rank the six powders in differing orders of magnitude. Figure 3.18 enables a trend to be seen within the powder covered glass slide Wilhelmy plate method, even if the powders are not quite ranked in the same order for both liquid combinations.

Figure 3.18 Assessment of non-polar surface energies of all powders using polar liquids on powder covered glass slides with Wu theory.

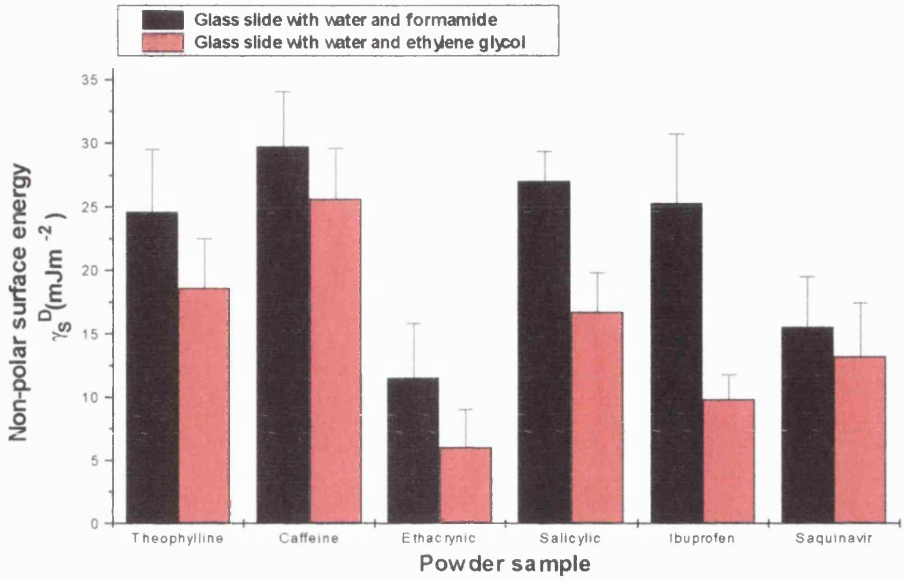

Figure 3.19 Assessment of non-polar surface energies of all powders using polar liquids on powder compacts with Wu theory.

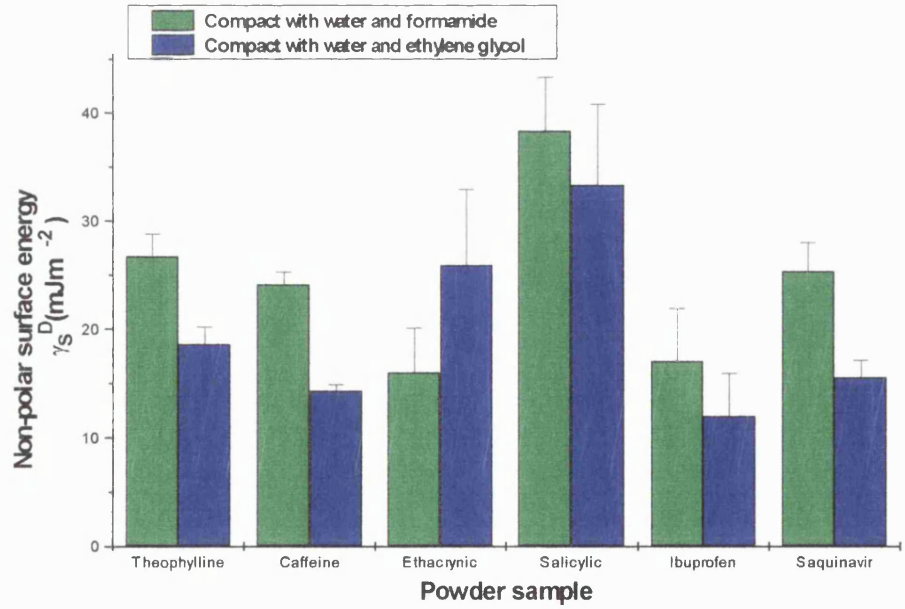

The same is true for Figure 3.19 which enables a trend to be seen within the powder compact Wilhelmy plate method, even if each powder is not quite ranked in the same order.

Since all the combinations and methods described in this section give precise, reproducible data, possibly more than one of these may give an accurate surface energy value depending on which binding sites on the powder surface are accessed. For instance, diiodomethane interacts only with non-polar sites whilst a combination of two polar liquids interact with both polar and non-polar sites. The evidence suggests that for a reasonable comparison to be made, the method of contact angle derivation must be kept constant along with the theory used to analyse that data and, if possible, the same carefully chosen probe liquids.

3.3.8 Compression effect

There is an inverse relationship between the compression force used and the contact angle obtained (Buckton and Newton, 1986), showing that as the compression force was increased the contact angles obtained fell, until a minimum angle was reached. Electron microscopy discovered this was due to plastic deformation at the powder surface. The length of time of compaction has also been found to affect the powder contact angle (Sheridan, 1994), which can be explained by several hypotheses:-

a) Plastic deformation. Electron microscopy has shown this to occur on compaction.
b) True perimeter. Changes in the true perimeter on compaction, if not accounted for will produce inaccurate contact angles.
c) Proportion of surface roughness changing with compaction.
d) Crystal alignment (Fukuoka et al., 1987; Kiesvaara and Yliruusi, 1991). Changes in the polar and non polar components of surface energy are altered differently on compaction, resulting in new contact angles.

Unfortunately, due to the high compacting forces, the original surface of the six powders may have been altered. As the force increases the contact angle falls until

plastic deformation occurs. This explains why the compacts gave smaller contact angles than with the powder covered glass slide method where the powder is not compressed.

3.4 Conclusions

The analysis of contact angle data can be made using either the Van Oss or the Wu theory, although the former does have the major advantage of calculating the two components of the polar surface energy, γ^+ and γ^- in addition to the non-polar and polar surface energies. The choice of liquids used for both theories is an important factor in minimising the errors involved.

The approach based on sticking powder to a glass plate seems to be of value despite initial reservations about the extent of coverage and risks of the adhesive spreading over the powder (Section 3.2.2.1). There are many advantages to adhering the powder to a glass slide i.e. the experiment can be done with small quantities of powder, the material is not altered in form (as would happen with compaction or precipitation of the material) and the approach is rapid and simple to perform.

Chapter 4

Liquid Penetration

4 Liquid penetration

Liquid penetration is a simple contact angle method whereby the different rates that test liquids move into a powder bed can be used to analyse the surface character of that powder.

4.1 Introduction

The basic theory of liquid penetration into a powder bed was pioneered by Washburn (1921). He combined the capillary driving force for a capillary tube with the Poiseuille equation for viscous drag in conditions of steady flow. The powder is packed into a column that can be placed horizontally (Kiesvaara et al., 1993) or vertically (Lechner et al., 1995), but all use variations of Washburn's equation:-

$$h^2 = \frac{t.R.\gamma_L.Cos\theta}{2\eta}$$ Equation 4.1

h - height liquid has risen in time t

R - effective interstitial pore radius between packed particles

For this experiment, two test liquids are required, one polar and the other totally non-polar in nature. The totally non-polar liquid chosen must instantaneously perfectly wet the solid on contact with the powder bed such that Cosine θ will become 1. To achieve this, the non-polar liquids of choice have low surface tension values, well below the surface energy of each test powder. Only in these cases can Equation 4.2 below be simplified.

$$Cos\theta = \frac{m^2.\eta}{t.\rho.\gamma_{LV}.c}$$ Equation 4.2

η - viscosity of the liquid ($N.s.m^{-2}$)

ρ - density of the liquid ($g.cm^{-3}$)

γ_{LV} - surface tension of the liquid ($mN.m^{-1}$)

c - unknown geometric environment.

m - mass gain (mg)

t - time (seconds)

(Lechner et al., 1995)

With two liquids, one being non-polar with a low surface tension, the contact angle of the polar liquid with the powder can now be calculated using Equation 4.3.

$$\text{Cos}\theta = \frac{\gamma_{LV2} \cdot \eta_2 \cdot gradient_2}{\gamma_{LV1} \cdot \eta_1 \cdot gradient_1} \qquad \text{Equation 4.3}$$

By plotting a graph of mass gain^2 versus time, the gradient of the straight section of the curve (Figure 4.1) can be used in Equation 4.3. It is assumed that the non-polar liquid is perfectly wetting, therefore cosθ will equal 1, giving a value for c, thus allowing the contact angle with the polar liquid to be determined.

Figure 4.1 Typical graph showing straight line gradient.

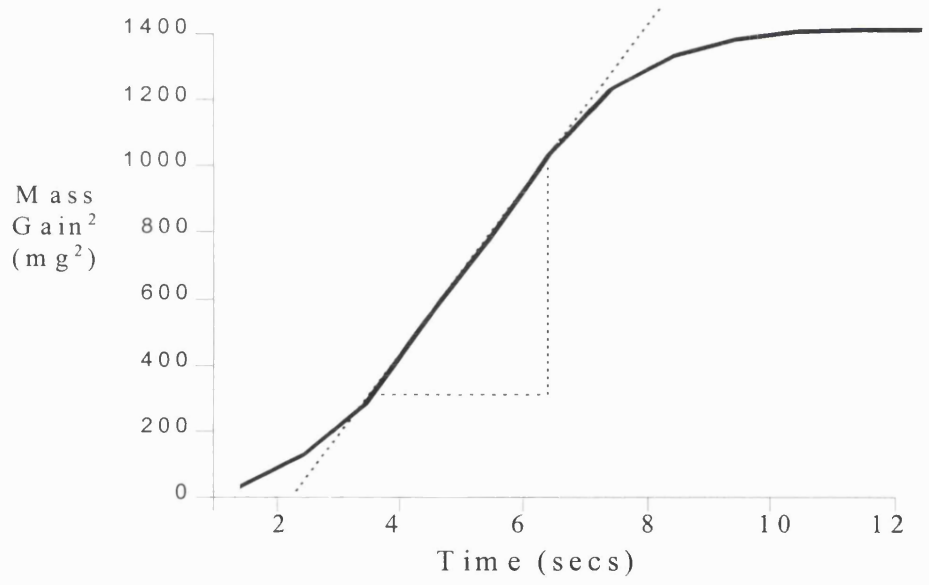

4.1 Method

The glass cylinder was originally made hydrophobic by silanisation (Section 5.2.1) so as to prevent the glass from interacting with any polar liquid used. Prior to experimentation, the glass cylinder was cleaned with ethanol, rinsed with water and dried. The test liquid was placed in a jacketed vessel maintained at 25°C inside the cahn.

Figure 4.2 Liquid penetration apparatus.

a) Compaction of powder bed.

b) Liquid penetration into powder bed.

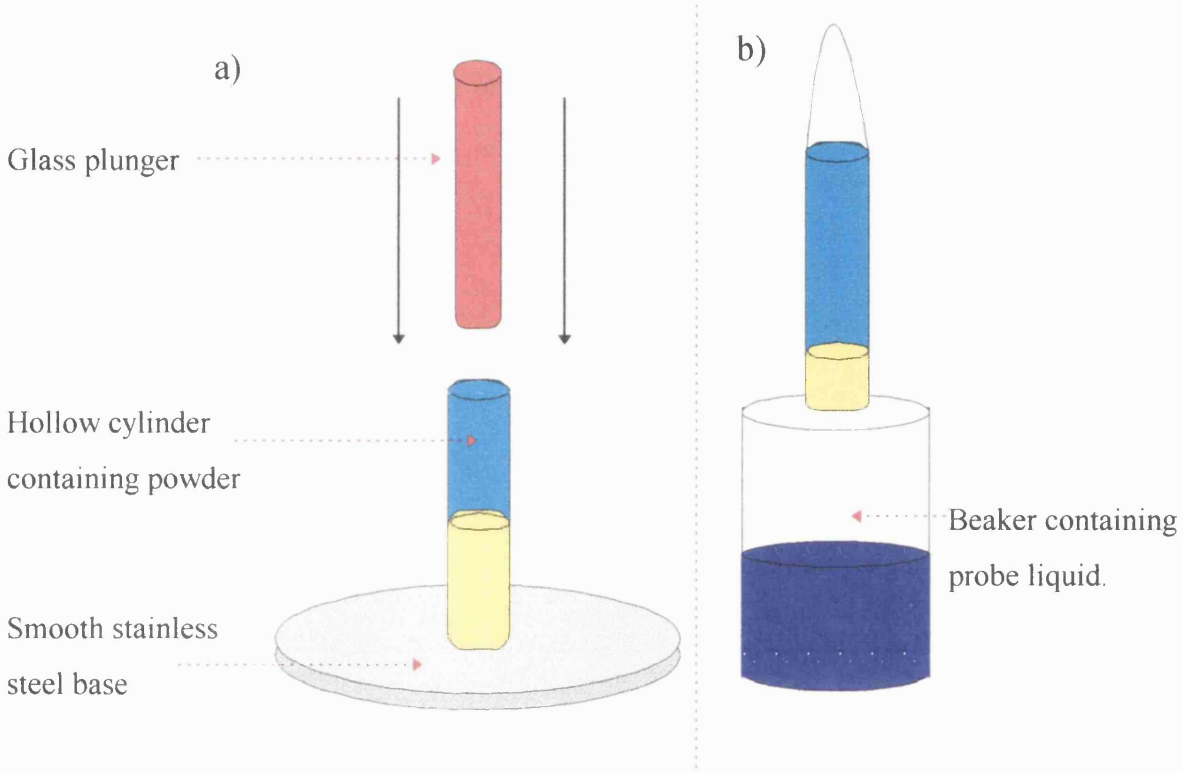

The cylinder was placed on a smooth and clean stainless steel surface and filled with 250mg of the test powder. A glass rod was manually used to compress the powder down to a marked depth of the cylinder (1.3 cm in total length). The cylinder was positioned inside the cahn above the test liquid and the platform raised manually just until the cylinder and powder base had come into contact with the liquid and then held at that position for 1 minute.

The mass gain as the liquid enters into the powder inside the glass cylinder was recorded by the computer as a function of time. The process was repeated five times for each liquid.

4.3 Contact angle calculation

The calculation of the contact angle of a powder with water is achieved as follows:-

$$Cos\theta_W = [(18.4 * 0.8904 * 0.66) / (72.8 * 0.294 * 1)] * \mathbf{(W / D)} \quad \text{Equation 4.4}$$

W = gradient of penetration with water.

D = gradient of penetration with hexane.

Where density = 1(water), 0.66 (hexane)

surface tension = 72.8 (water), 18.4 (hexane)

viscosity = 0.8904 (water), 0.294 (hexane)

Hexane is assumed to be a perfectly wetting non-polar liquid. The calculation was then repeated using ethylene glycol and formamide instead of water.

4.4 Results and discussion

Figure 4.3 Liquid penetration of water into an Ibuprofen powder bed.

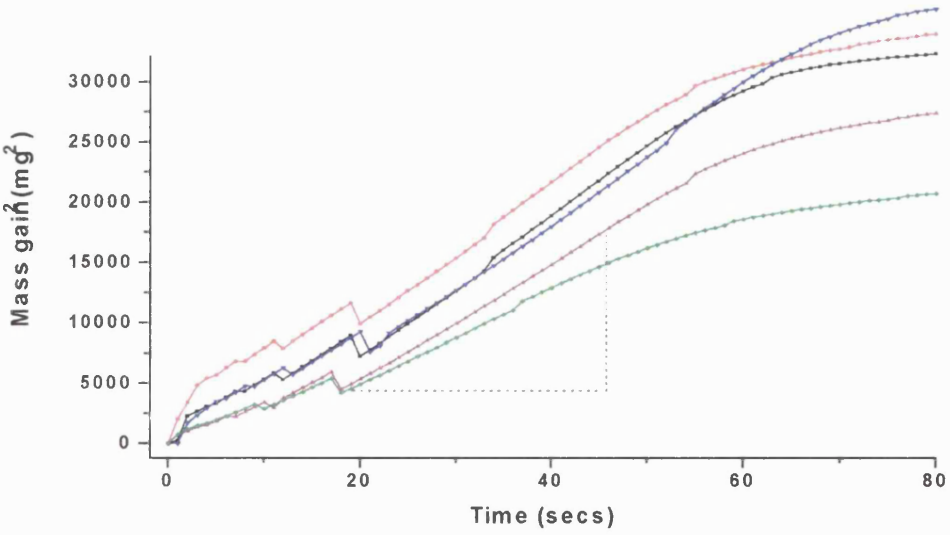

Although Figure 4.3 shows that water moves into the Ibuprofen powder bed at a steady rate over a long period of time, in other cases the liquid uptake was far more

rapid (i.e. less than ten seconds) which resulted in a greater margin of error. In such situations, the powder column length could be increased so that the linear part of the curve could be extended.

Table 4.1 Contact angles of model powders.

	Water	Formamide	Ethylene glycol	Diiodomethane
Theophylline	61.2°	75.2°	25.3°	
Caffeine	58.7°	35.3°	Less than zero	
Salicylic acid				53.4°
Ethacrynic acid		15.5°	Less than zero	87.0°
Ibuprofen	88.7°	85.4°		83.5°

Not all liquids were able to give contact angles for all the powders tested, so only a selection of different methods of calculating the surface energies could be used. Salicylic acid and Ethacrynic acid were hydrophobic in nature and did not allow water to penetrate into the powder bed at all. Salicylic acid did yield a contact angle with diiodomethane, allowing a non-polar value of 32.4 $mJ.m^{-2}$ to be calculated using Van Oss theory. The contact angles for water, formamide and diiodomethane, when available, are similar to those obtained with the powdered slide Wilhelmy plate method, although angles using ethylene glycol were significantly lower. Ethylene glycol is a more viscous liquid, which may have hindered the rate of uptake into the powder bed. The surface energies for the five test powders were calculated with all the contact angle data available:-

Table 4.2 Surface energetics of Theophylline.

Theophylline	$\gamma_{\zeta V}^{TOT}$ mJ.m^{-2}	γ_S^{LW} mJ.m^{-2}	γ_S^{AB} mJ.m^{-2}	γ_S^{+} mJ.m^{-2}	γ_S^{-} mJ.m^{-2}
Van Oss - 3 polar	143.5	28.4	115.1	93.0	35.6
Wu's		γ_S^{D}	γ_S^{P}		
Water + Formamide	45.2	6.3	38.9		
Water + Ethylene glycol	45.0	21.4	23.7		

Table 4.3 Surface energetics of Caffeine.

Caffeine	$\gamma_{\zeta V}^{TOT}$ mJ.m^{-2}	γ_S^{LW} mJ.m^{-2}	γ_S^{AB} mJ.m^{-2}	γ_S^{+} mJ.m^{-2}	γ_S^{-} mJ.m^{-2}
Van Oss - 2p 1np polar	47.1	34.7	12.4	2.5	15.4
Wu's		γ_S^{D}	γ_S^{P}		
Water + Formamide	49.7	27.3	22.3		
Water + Ethylene glycol	49.6	27.2	22.4		
Ethylene glycol + Formamide	49.5	27.5	22.0		

Table 4.4 Surface energetics of Ethacrynic acid.

Ethacrynic acid	$\gamma_{\zeta V}^{TOT}$ mJ.m^{-2}	γ_S^{D} mJ.m^{-2}	γ_S^{P} mJ.m^{-2}
Wu's			
Formamide + Diiodomethane	123.3	18.1	105.2

Table 4.5 Surface energetics of Ibuprofen.

Ibuprofen	γ_S^{TOT} mJ.m^{-2}	γ_S^{LW} mJ.m^{-2}	γ_S^{AB} mJ.m^{-2}	γ_S^{+} mJ.m^{-2}	γ_S^{-} mJ.m^{-2}
Van Oss - 2p 1np polar	17.1	15.7	1.4	0.04	12.3
Wu's		γ_S^{D}	γ_S^{P}		
Water + Formamide	25.0	8.1	16.9		
Water + diiodomethane	29.5	19.6	9.9		
Formamide + diiodomethane	22.6	19.6	3.0		

4.4.1 Comparison between liquid penetration and glass slide Wilhelmy plate methods

Although the surface analysis using liquid penetration was incomplete due to liquids being unable to penetrate the powder beds of certain powders, the values obtained were compared with the glass slide Wilhelmy plate method (Figure 4.4).

Figure 4.4 Comparison between liquid penetration and a Wilhelmy plate method

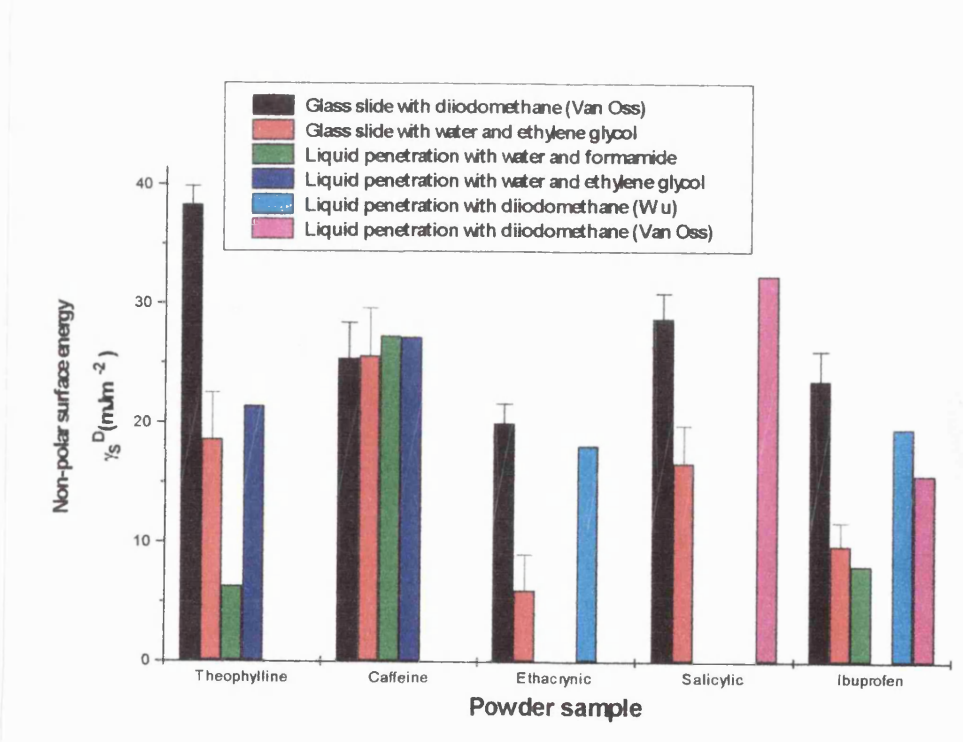

It is evident that liquid penetration is able to give non-polar surface energy values in keeping with the Wilhelmy plate method. A detailed comparison between powders cannot be made because different combinations of probe liquids were able to penetrate each powder, therefore there is no one consistent method of analysis used for all the five powders.

4.5 Conclusions

Unfortunately, due to the difficulty in achieving measurable contact angles with all test liquids, it was not carried out with the Saquinavir batches. The main draw backs with liquid penetration are listed below:-

a) One must ensure the correct portion of the graph is measured otherwise small errors in gradients may result in significant surface energy changes.

b) If a particularly hydrophobic powder is used, certain polar liquids (e.g. water) are unable to penetrate the powder, as is the case with Salicylic acid. To overcome this there have been studies using ethanol/water mixtures incorporated into the experiment with the hope of extrapolating back to zero percent ethanol. However, Buckton and Newton, (1986) have shown that a vapour containing a higher percentage of ethanol than the liquid precedes the liquid front and may help to facilitate the liquid penetration thus building an error into the calculation.

c) Test powders can be soluble in certain probe liquids and highly viscous liquids (e.g. glycerol) take too long a time to penetrate the powder bed. Both these factors ensure that very careful selection of probe liquids must be made for each individual powder.

d) The main problem with all methods incorporating a hybrid of the Washburn equation is that a major assumption has been made whereby the powder bed is perceived to be a large bundle of capillaries, all lying in the same direction, which is, of course, not strictly true. The liquid passes through a range of pore diameters and pressure differences with these pores give rise to an uneven liquid flow. The equation only applies fully in an 'ideal' situation, and a powder bed is not one of those.

e) Lastly, there is no way of measuring the receding contact angle for liquid penetration methods unless the liquid penetration is controlled using gas pressure.

Due to the multitude of disadvantages that liquid penetration provides the user, it should only be used as a rough guide to a powder's surface characteristics.

Chapter 5

Inverse Gas Chromatography

5 Inverse Gas Chromatography

' Inverse gas chromatography represents a dynamic technique that can be used to determine the amount of adsorbate on the adsorbent surface, provided that there is negligible competitive adsorption of the carrier gas. The stationary phase (adsorbent) is characterised with a selection of known volatile probes (adsorbate)' (Djordjevic et al., 1992).

5.1 Introduction

This dynamic technique requires the packing of a glass tube with the unknown test powder, injecting minute concentrations of volatile probe vapours and measuring their respective retention times against a non-interacting standard.

Figure 5.1 Schematic diagram of IGC apparatus:- Model F33 system.

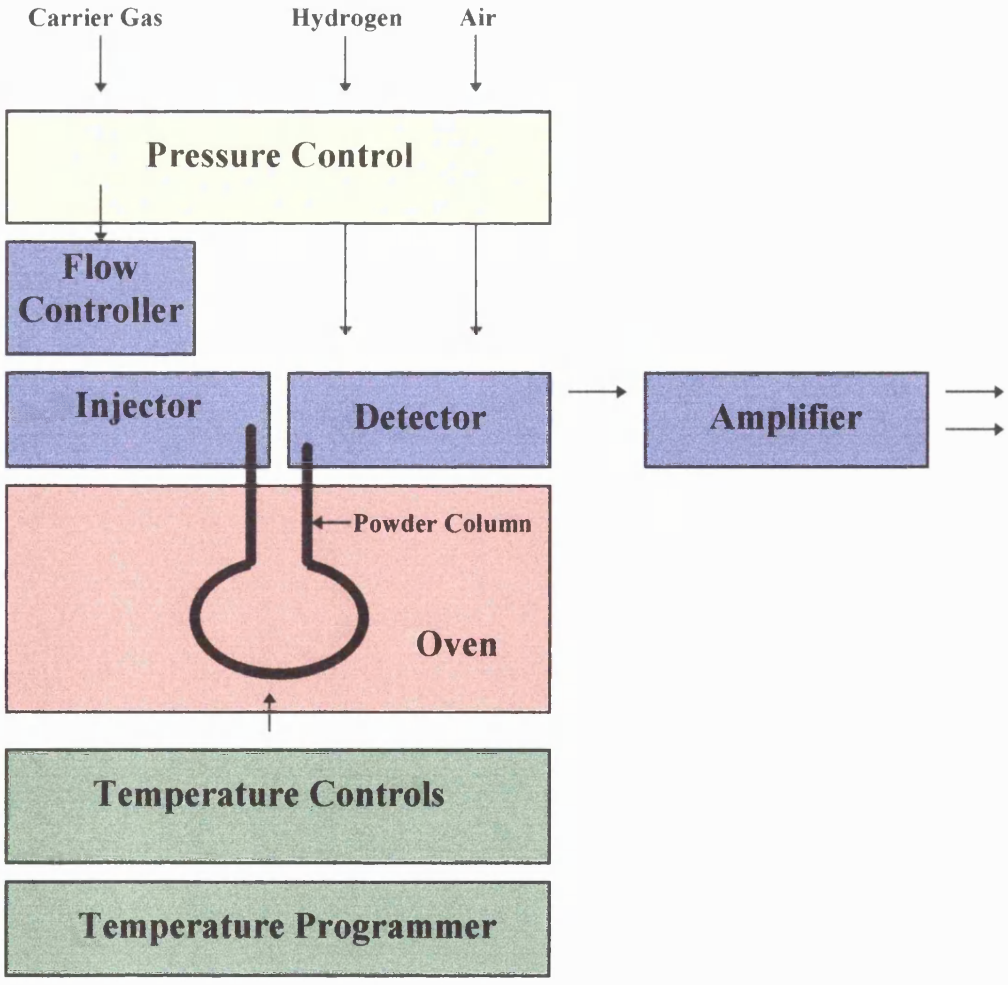

5.1.1 Possible probe interactions

There are four possible interactions that can occur between the powder and the injected probes:-

a) probe / solid bulk binding
b) probe / solid surface binding
c) probe / probe binding
d) probe / solid chemically binding

The important assumption is that the gas probes are at infinite dilution or near zero surface coverage over the powder column since if they are too concentrated their retention times would be altered significantly. This is due to the theory that at infinite dilution the main retention process is that of adsorption onto the powder surface and the other three possible interactions can be considered negligible. Adsorption occurs within the region where Henry's law holds and under these conditions it is not influenced by adsorbate - adsorbate interactions. Thus retention is due mainly to adsorbate - adsorbent interactions (Anhang and Gray, 1982). Strong interactions can only occur between an acid and a base, thus if two acids or two bases come together, even if they have high surface polarities, they will still have a negligible surface interaction (Schultz et al., 1987).

When semi-crystalline or amorphous polymers are characterised at temperatures above their glass transition temperatures (T_g), both surface adsorption and bulk sorption contribute to the retention times of the probes (Exteberria et al., 1992). With IGC at temperatures below the glass transition values, the retention times are due mainly to the adsorption onto the surface, whilst bulk sorption can be assumed to be negligible since the process has been greatly slowed down (Conder and Young, 1979). IGC allows measurement of the dispersive component of adhesion and of surface energy with non-polar probes, whilst acid and base probes are able to quantify the specific polar component due to hydrogen bonds and dipole moments. The enthalpy, the entropy and free energy of adsorption between the probe and the surface can also be measured (Dorris and Gray, 1979).

5.1.2 Calculation

The thermodynamic relationship between IGC and the concept of Fowkes on adhesion were developed between hydrocarbons and a solid phase (Dorris and Gray, 1979; Schultz et al., 1987). The non-polar component of the surface energy is determined from the retention volume of a series of n-alkanes by IGC at a constant temperature. The mathematical treatment by Schultz and Lavielle was further extended to quantify acid/base interactions. From this, one is able to relate surface properties with adhesion phenomena. Adsorbate - adsorbent interactions are a leading cause of adsorption effects. When no chemical bonds are involved, a thermodynamic function such as the work of adhesion (W_A) between the components of a multiphase system only comes from physical interactions. W_A may be attributed to dispersive and electron acceptor/donor (Lewis acid/base) interactions, whereby:-

$$W_A = W_A^{D} + W_A^{AB} + W_A^{Dipole} \qquad \text{Equation 5.1}$$

The net retention volume V_N (the amount of carrier gas required to elute the injected volume of probe molecules from the column) is determined as follows:-

$$V_N = JF\,(t_r - t_0) \qquad \text{Equation 5.2}$$

F - carrier gas flow rate (ml/min)
J - correction factor due to pressure differences
t_r - retention time of the probe
t_0 - retention of the non-interacting standard

where:-

$$J = \frac{3}{2}\cdot\left[\frac{\left(\frac{P_i}{P_0}\right)^2 - 1}{\left(\frac{P_i}{P_0}\right)^3 - 1}\right] \qquad \text{Equation 5.3}$$

P_i - pressure at the inlet of the column ($kN.m^2$)
P_o - atmospheric pressure ($kN.m^2$)

Retention volume caused by bulk and surface sorption processes occur independently of each other (Martin et al., 1961), whereby:-

$$V_N = K_S.A_i + K_1.V_i \qquad \text{Equation 5.4}$$

A_i - Total surface area of stationary phase
V_i - Total surface volume of stationary phase
K_S - Surface partition coefficient
K_1 - Bulk partition coefficient

With a relatively non-porous solid, bulk absorption is assumed to be negligible thus reducing Equation 5.4 to:-

$$V_N = K_S.A_i \qquad \text{Equation 5.5}$$

$$\therefore V_N = K_S.w.S_a \qquad \text{Equation 5.6}$$

w - Weight of adsorbent in column
S_a - Specific surface area of adsorbent

DeBoer (1953) states that the free energy of adsorption (ΔG_a°) for a molecule of gaseous probe to adsorb to one mole of powder is described as:-

$$\Delta G_a^\circ = -RT\ln\left(\frac{P_{s.g.}}{P_{s.s.}}\right) \qquad \text{Equation 5.7}$$

$P_{s.s}$ -Adsorbate vapour pressure in equilibrium with standard adsorption state
$P_{s.g}$ -Adsorbate vapour pressure in the gaseous standard state
T - Temperature of column (K)
R - Gas constant

By defining K_S:-

$$K_S = \frac{\Gamma}{C}$$ Equation 5.8

Γ - Surface concentration of adsorbate

C - Adsorbate concentration in gas phase

Assuming ideal conditions, where:-

$$C = \frac{P}{RT}$$ Equation 5.9

P - Partial pressure of the adsorbate

Combining Equation 5.8 with 5.9:-

$$K_S = \frac{\Gamma RT}{P}$$ Equation 5.10

The Gibbs equation (Aveyard et al., 1993) describes the relationship of surface concentration, Γ, with surface pressure, π:-

$$\Gamma = (1 / RT).\left(\frac{\delta\pi}{\delta \ln P}\right) = \left(\frac{P}{RT}\right).\left(\frac{\delta\pi}{\delta P}\right)$$ Equation 5.11

Since Henry's law states that in the region of infinite dilution of adsorbate:-

$$\left(\frac{\delta\pi}{\delta P}\right) \longrightarrow \left(\frac{\pi}{P}\right)$$ Equation 5.12

$$\therefore \frac{\Gamma RT}{P} = \left(\frac{\pi}{P}\right) = K_S$$ Equation 5.13

In the standard adsorption state:-

$$P_{s.s} = \left(\frac{\pi}{K_S}\right)$$ Equation 5.14

Substituting Equation 5.14 into 5.7, gives:-

$$\Delta G_a^\circ = -RT\ln\left(\frac{K_S.P_{s.g.}}{\pi}\right)$$ Equation 5.15

Rearranging Equation 5.6:-

$$K_S = \frac{V_N}{w.S_a}$$ Equation 5.16

Combining Equation 5.15 with 5.16 gives:-

$$\Delta G_a^\circ = -RT\ln\left(\frac{V_N.P_{s.g.}}{\pi.w.S_a}\right)$$ Equation 5.17

$P_{s.g} = 1.013 * 10^5$ Pa

$\pi = 3.38 * 10^{-4}$ Nm^{-1}

Since w, S_a, $P_{s.g}$ and π are all constants, Equation 5.17 can be reduced to:-

$$\Delta G_a^\circ = -RT\ln V_N + K$$ Equation 5.18

K - a constant

Since $\Delta G_a^\circ = \Delta H_a^\circ - T\Delta S_a^\circ$ Equation 5.19

A straight line plot of ΔG_a° against T(K) will enable all variables to be deduced. The work of adhesion, W_a, per surface area between an adsorbate and an adsorbent is related to ΔG_a° by:-

$$\Delta G_a^\circ = -Na_i.W_a$$ Equation 5.20

a_i - Area of one adsorbed molecule

N - Avogado's number

Placing into:-

$$W_a = 2(\gamma_1^D.\gamma_2^D)^{0.5}$$ Equation 5.21

$$RT\ln V_N = 2N(\gamma_{SV}^{D})^{0.5} \cdot a_i (\gamma_{LV}^{D})^{0.5} + K \qquad \text{Equation 5.22}$$

Thus the gradient of the slope determines the non-polar (dispersive) interaction force of the test powder as shown in Figure 5.2. The polar probes are most often plotted above the non-polar alkane line, where the vertical distance between the probe and the straight line is equivalent to the specific acid/base free energy of adsorption, $\Delta G_{a\text{-}sp}^{\circ}$, for that individual probe on the powder surface.

$$\Delta G_{a\text{-}sp}^{\circ} = -RT\ln\left(\frac{V_N}{V_n^{ref}}\right) \qquad \text{Equation 5.23}$$

The total free energy of adsorption, ΔG_a°, of the individual probe is the sum of the acid/base and the non-polar free energies of adsorption.

$$\Delta G_a^{\circ} = \Delta G_{a\text{-}sp}^{\circ} + \Delta G_{a\text{-}np}^{\circ} \qquad \text{Equation 5.24}$$

Figure 5.2 Graph showing calculation of the interaction forces at a powder surface.

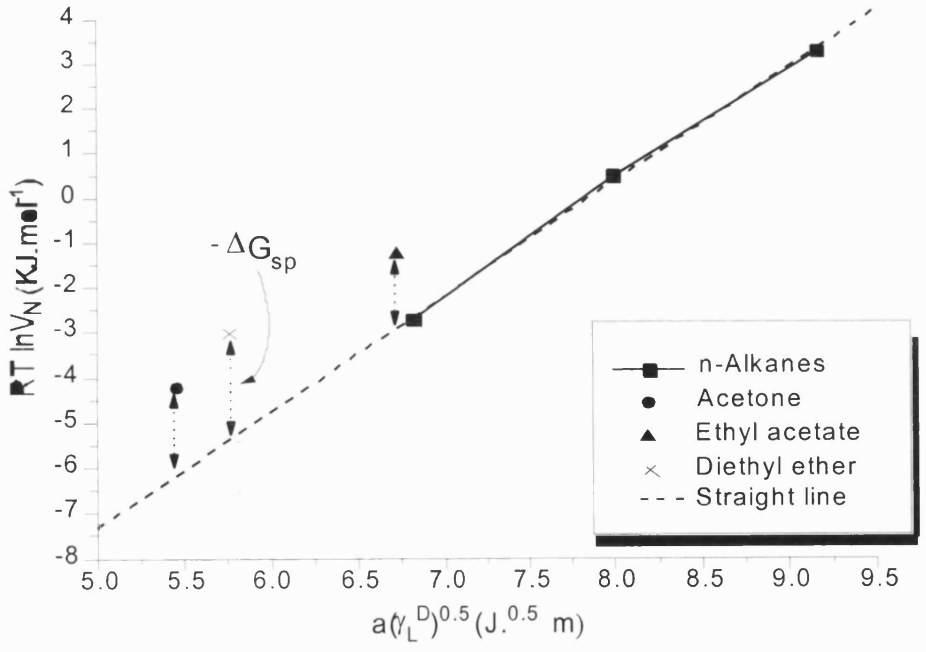

A selection of different physical criteria can be plotted against $RT\ln V_N$ indicated below, all of which are able to determine free energy of adsorption values:-

a) The dispersive component of the heat of vaporisation of probes, ΔH^d_{vap} (Chehimi and Pigois-Landureau, 1994).
b) The logarithm of the saturation vapour pressure of the solutes, $\log P_0$ (Nardin and Papirer, 1990).
c) The boiling temperatures (°C) of the probes (Sawyer and Brookman, 1968).

5.1.3 Acid and base behaviour

The evaluation of the free energy of adsorption values for each probe has only been developed recently. Gutmann (1978) originally theorised that the polar interaction could be expressed in terms of acid-base properties. Each probe could be given two values (Gutmann numbers) which were equivalent to the probe's electron donating (base), DN, and the electron accepting (acid), AN, properties.

DN - defined by the reaction enthalpy of the probe liquid with a reference acceptor, $SbCl_5$
AN - defined as the NMR chemical shift of ^{31}P contained in $(C_2H_5)_3PO$ when reacting with the probe liquid

Riddle and Fowkes (1990) determined that part of the electron acceptor value, AN, was due to dispersive forces, therefore AN* was developed, being solely due to polar interaction forces.

Neglecting any entropic effects, the specific free energy of adsorption, $\Delta G_{a\text{-}sp}°$, can be used to calculate acid-base parameters according to:-

$$-\Delta G_{a\text{-}sp}° = K_A \,.\, DN + K_D \,.\, AN^* \qquad \text{Equation 5.25}$$

Rearranging allows a suitable plot of $-\Delta G_{a\text{-}sp}° / AN^*$ against DN / AN^* to determine the acid (K_A) and base (K_B) parameters of the test powder.

$$\therefore \frac{-\Delta G^{o}_{a-sp}}{AN^{*}} = K_A \cdot \left(\frac{DN}{AN^{*}}\right) + K_B \qquad \text{Equation 5.26}$$

Figure 5.3 Example of straight line plot used to calculate acid-base characteristics.

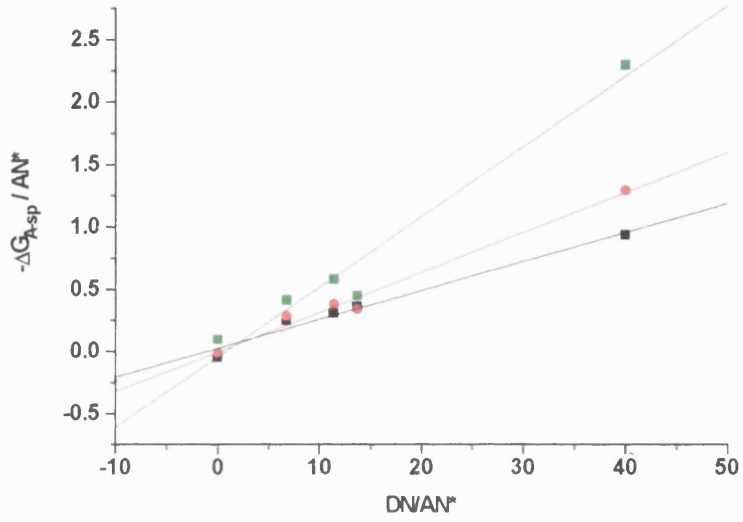

Both axes have no units as all the components are in Joules per mole. This graphical representation can clearly distinguish between different acid-base properties between different materials,but there has always been a need to be able to relate the acid-base data quantitatively with other, more traditional surface characterisation methods (Mukhopadhyay and Schreiber, 1995). An empirical approach has been attempted to remedy this by creating a specific interaction parameter, three variations of which are described below:-

a) Schultz et al., 1987 linked acid-base data to the performance of carbon fibre reinforced composites.

$$I_{sp} = (K_a)_1 \cdot (K_b)_2 + (K_a)_2 \cdot (K_b)_1 \qquad \text{Equation 5.27}$$

b) Lara and Schreiber, 1991 showed that acid-base data was an important factor in the adsorption of car primer resins (polyesters) onto various pigments.

$$I_{sp} = \{(K_a)_1 \cdot (K_b)_2\}^{0.5} + \{(K_a)_2 \cdot (K_b)_1\}^{0.5} \quad \text{Equation 5.28}$$

c) Kloubek and Schreiber, 1993 provide a third equation. All three equations are unable to provide a quantitative value of acid-base character that is comparable to other surface analytical techniques.

$$I_{sp} = (K_a)_1 \cdot (K_b)_2 + (K_a)_2 \cdot (K_b)_1 - (K_a)_1 \cdot (K_a)_2 - (K_b)_1 \cdot (K_b)_2 \quad \text{Equation 5.29}$$

To ensure that a true representation of acid-base nature is acquired, one must ensure:-

1) The test probes selected (acidic, basic and amphoteric) should all have minimal self-association properties.
2) The probes must be used in sufficiently minute quantities such that the adsorption occurs at infinite dilution.
3) A large number of probes of varying acid-base character should be used to improve reliability.

Table 5.1 Probe liquid physical data table required for IGC analysis.

Probe	AN* (kcal.mol^{-1}) *2	DN (kcal.mol^{-1}) *	Molecular area - a ($10^{-20}m^2$)*	γ_L^D (mJ.m^{-2}) *	Boiling point (°C)	ΔH_d^{vap} (kJ.mol^{-1}) *1
Acetone	2.5	17.0	42.5	16.5	56.5	22.4
Ethyl acetate	1.6	17.1	48	19.6	77	29.3
Diethyl ether	1.4	19.2	47	15	34.6	25.8
THF	0.5	20.0	45	22.5	66	23.3
Chloroform	5.4	0	44	25.9	60.9	30.4
Benzene	0.17	0.1	46	26.7	80	31.3
CCl_4	0.7	0	46	26.8	76.5	31.9
Hexane	0	0	51.5	18.4	69	31.5
Heptane	0	0	57.0	20.3	98	36.5
Octane	0	0	62.8	21.3	126	41.5

* - Schultz et al., 1987 *1 - Fowkes, 1990 *2 - Riddle and Fowkes, 1990

It should be noted that three of the polar probes were not used in the acid-base analysis:-

a) Diethyl ether has the lowest boiling point of all the probes used (34.6°C), which causes it to evaporate very easily at ambient temperature. Therefore the concentration of diethyl ether vapour inside the syringe prior to injection was never small enough for infinite dilution adsorption to occur. In effect, too much diethyl ether in the column (finite dilution) lead to artificially low retention times, since the excess vapour passed relatively unhindered through the powder column, resulting in the probe being consistently plotted well below the straight line for each powder.

b) Benzene and carbon tetrachloride (both slightly acidic) were not used in the acid-base analysis because chloroform is much more acidic in nature and has no basic character at all.

5.2 Method

5.2.1 Silanisation method

Each glass column was silanated in order that the glass surface would be made hydrophobic and non-interactive with any gaseous probe. To achieve this, the glass loops were washed sequentially with distilled water, methanol and finally with toluene. They were then soaked for 12 hours in a solution of 5% dichloromethyl silane (DCMS) in toluene, after which they were rinsed with toluene, then methanol to remove any unreacted DCMS and finally water before being dried in an oven overnight (Mohammad and Fell, 1982).

5.2.2 Packing of glass loop

Before packing the dry mass of the column was recorded. The powder was packed using a small funnel and rubber tubing attached to one end of the column, into which the powder was fed. It was then moved into and around the column with a mixture of

tapping and controlled vibrating using a whirlimixer. The powder bed was packed sufficiently so that there were no air pockets seen, with about 3cm of empty tube at either end. The column was reweighed, silanated glass wool packed into either end to prevent any of the powder form escaping during use and the column weighed again. The powder bed was then completely dried by inserting the column onto the gas chromatography apparatus and passing dry nitrogen (20 $kN.m^{-2}$) over the powder at an oven temperature of 100°C for 24 hours. The column was then reweighed and the dry mass of the powder calculated using Equation 5.30.

Dry mass of powder = (Mass of column, glass wool and dry powder)
-[(Mass of column, glass wool and undried powder
- mass of column and undried powder) + (mass of dry column)]

Equation 5.30

5.2.3 Powder analysis protocol

The powder bed was allowed to settle for 24 hours at an oven temperature of 35°C and a nitrogen flow of 20 $kN.m^{-2}$. The oven temperature was monitored with a max./min. thermometer, ensuring that the temperature of the column was constant throughout the experiment. A reference probe consisting mainly of methane (gas tap) was firstly injected into the column, since it would have no interaction with the column whatsoever, giving a minimum retention time (t_0). This reference was repeated at several times throughout the experiment to ensure that the retention times were constant and therefore none of the conditions had altered.

For each probe, 1µl was pulled up into a clean 10µl Hamilton syringe several times before being emptied. The syringe was then used to inject 1µl of air (containing minute concentrations of gaseous probe) into the column. This was repeated at least three times for each probe. The chart recorder allowed the retention times of each probe to be measured, from the time of injection to the maximum peak height.

5.3 Results and discussion

5.3.1 Caffeine, Theophylline, Salicylic acid, Ethacrynic acid and Ibuprofen

5.3.1.1 Effect of temperature

The temperature of the Caffeine powder bed was held at four elevated temperatures, so as to determine any effect that temperature may have on the adsorption of the probes.

Figure 5.4 Passage of n-alkane probes through a caffeine powder column at four elevated temperatures.

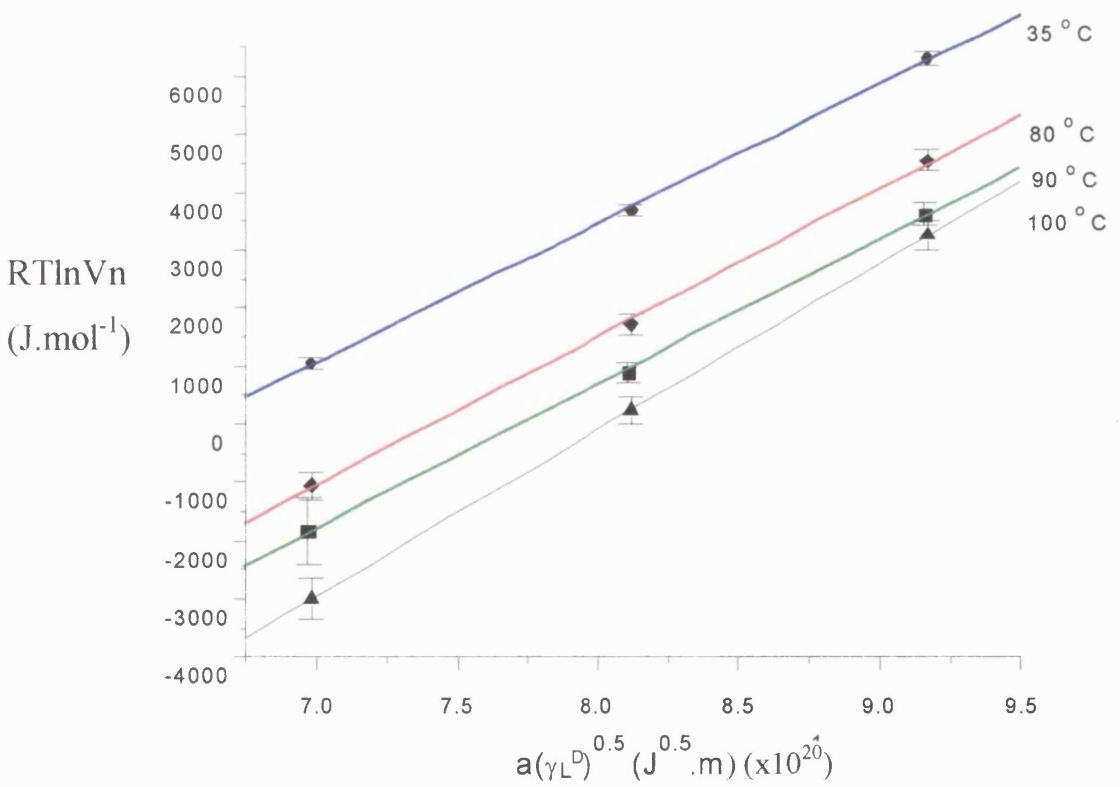

Figure 5.4 illustrates how increasing temperature causes an increase in thermal motion and decreases the ability for the alkanes to bind to the powder surface, consequentially reducing their retention time within the powder column. Although it

is interesting to note that the gradient of each alkane plot does not alter significantly over the temperature range (Table 5.2).

Table 5.2 Non-polar surface energy of Caffeine over a range of temperatures.

Temperature (°C)	γ_S^D (mJ.m^{-2})	SD_{n-1}
35	39.9	1.5
80	40.3	3.5
90	37.9	8.0
100	47.4	6.5

It is also evident that the reproducibility was greatly increased at the lowest temperature, since the retention times were greater with a smaller percentage error, therefore all further IGC analysis was carried out at 35°C.

5.3.1.2 Analysis using $a(\gamma_L^D)^{0.5}$

For this analysis the free energy values (ΔG) were calculated from the plot using molecular areas (a) of each polar probe (Section 5.1.2).

Figure 5.5 Acid / base plot for acidic model powders using $a(\gamma_L^D)^{0.5}$.

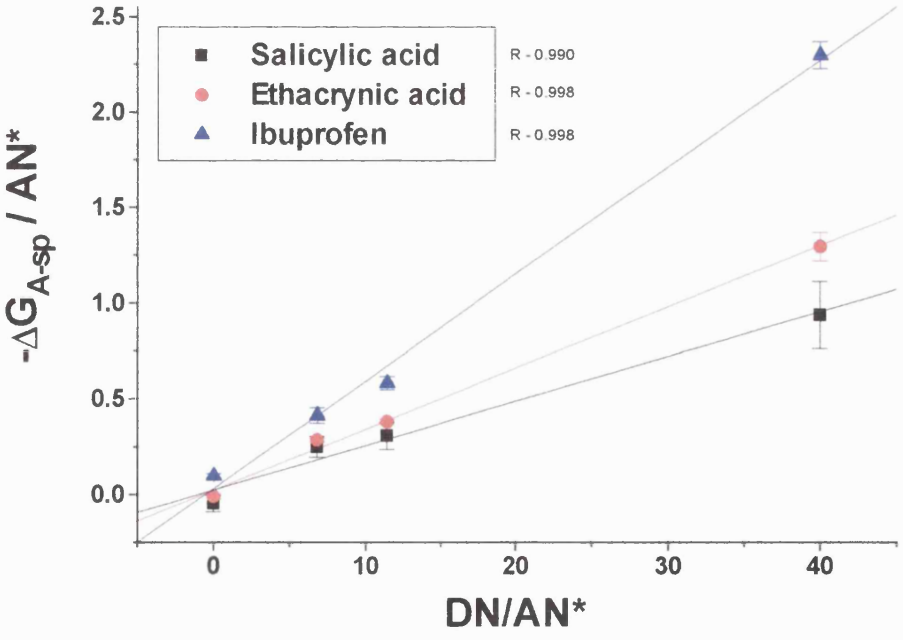

Figure 5.5 highlights how the IGC is able to readily distinguish between three powders, merely by a visual assessment of gradients. Table 5.3 lists the gradients and y-intercepts, giving a quantitative acid-base profile of the three test powders.

Table 5.3 Acid / base character for the model powders using $a(\gamma_L^D)^{0.5}$.

	K_A (Acidic character)	SD	K_B (Basic character)	SD
Salicylic Acid	0.0233	0.0024	0.0229	0.0498
Ethacrynic acid	0.0320	0.0013	0.0221	0.0280
Ibuprofen	0.0560	0.0026	0.0328	0.0548

Figure 5.6 Acid character for the model powders using $a(\gamma_L^D)^{0.5}$.

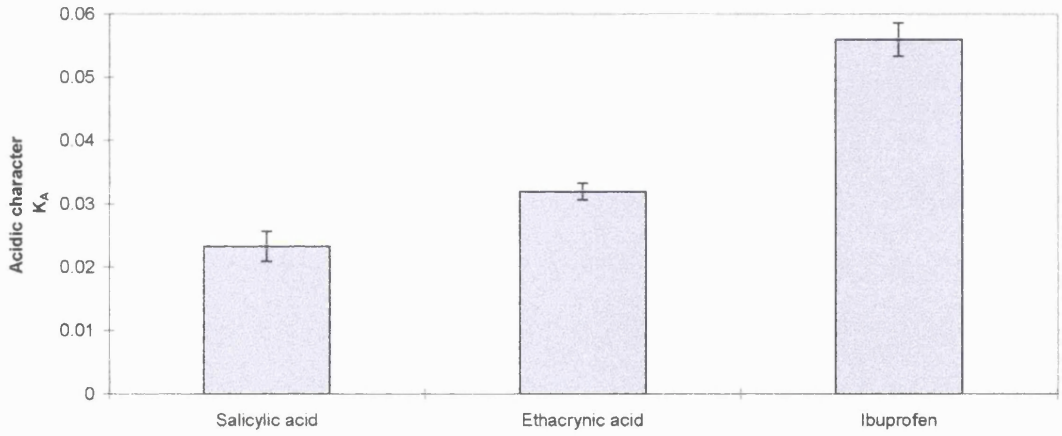

Figure 5.7 Basic character for the model powders using $a(\gamma_L^D)^{0.5}$.

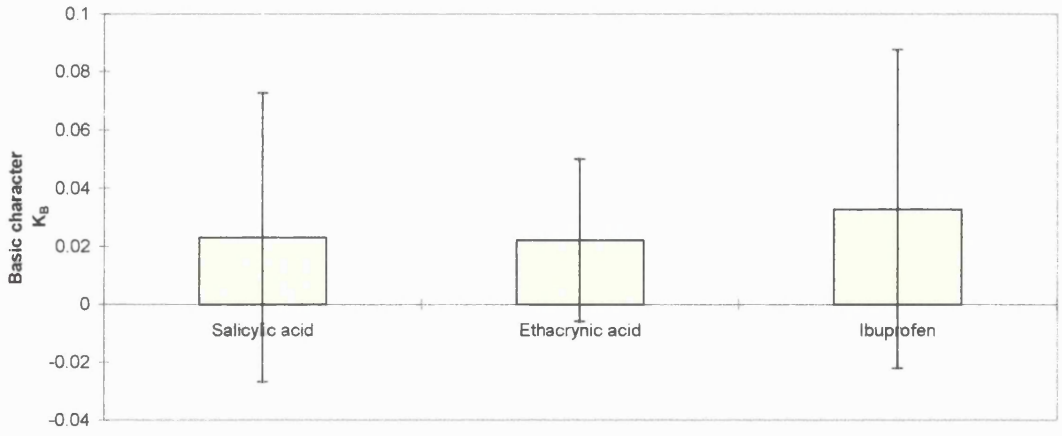

Figure 5.6 clearly shows that the three powders have very different acidic properties, Ibuprofen being the most acidic and Salicylic acid the least. Figure 5.7 illustrates that the basic characters of each powder are indistinguishable from one another due to the large error bars. This could be a result of each of the three acidic powders only having a very small basic ability, therefore any differences are beyond the sensitivity of the IGC.

Figure 5.8 Acid / base plot for basic model powders using $a(\gamma_L^D)^{0.5}$.

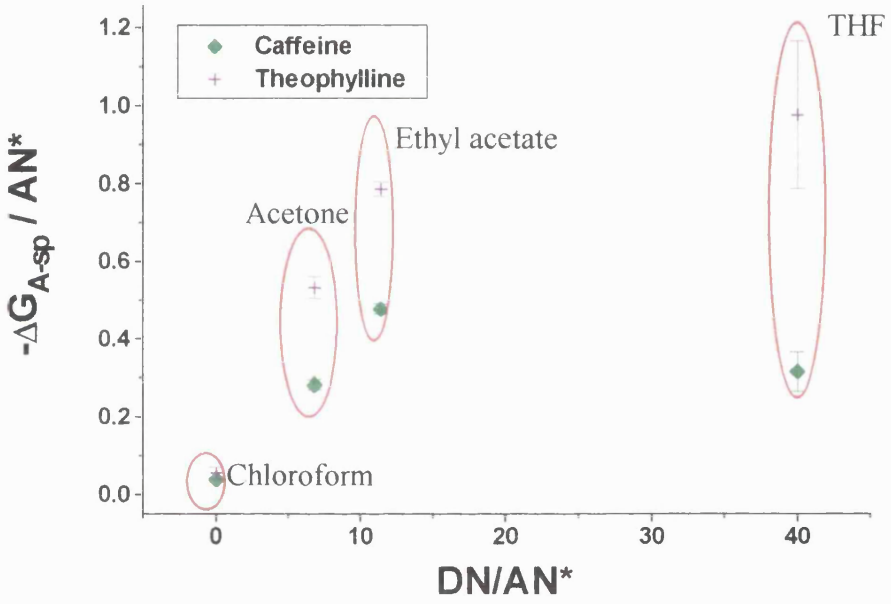

Unfortunately Figure 5.8 shows that this method appears not to be suitable for the two basic powders, Caffeine and Theophylline, since a straight line cannot be drawn between the probe points. It is clear that without the THF probe a straight line could be achieved for both basic powders. THF (27%), ethyl acetate (18%) and acetone (31%) all have relatively large percentages of self-association compared to chloroform (1.6%). Thus a significant amount of the three self-associated probes will pass through the IGC column unhindered by any interaction with the powder surface. In the calculation of the free energy of adsorption due to polar interaction, the probe molecular areas used, allow the theory to assume that each probe has a negligible percentage self-association since they are being compared to alkane probes that have none. Therefore the retention time for these polar probes with large percentages of

self-association will be less than for a theoretical probe with zero self-association with the same molecular area and acid-base character. Since the two powders in this case are basic, the THF probe (mainly basic) will not interact a great deal with these powders anyway. The self-association error will reduce this interaction even further, resulting in a probe that is plotted very close to the alkane straight line. This results in an artificially small free energy value, which in combination with a multiplication factor of 2 (DN/AN*, where AN* = 0.5), yields a THF probe point in Figure 5.8 that is lower in magnitude than it should be. Conversely, acetone and ethyl acetate are mainly acidic in character and were able to interact more with the two basic powders, resulting in far larger free energy values. In addition, these values are then divided by 2.5 for acetone (AN* = 2.5) and 1.6 for ethyl acetate (AN* = 1.5) to achieve more accurate and precise points in Figure 5.8.

Table 5.4 Non-polar component of surface energy for the model powders using $a(\gamma_L^D)^{0.5}$.

Powder	γ_S^D (mJ.m^{-2})	$SD_{(n-1)}$
Salicylic acid	53.0	3.3
Ethacrynic acid	34.9	2.3
Ibuprofen	39.5	4.8
Caffeine	39.9	1.5
Theophylline	50.8	4.2

Table 5.4 shows that the non-polar (dispersive) component of surface energy for each powder can be easily calculated giving a value that is directly comparable with other methods of surface energy analysis. In all five cases, the non-polar values with IGC are significantly greater than those achieved using the Wilhelmy plate glass slide method (Figure 5.9). The reason for this is discussed in Section 9.1. Within this method, the mean data was analysed to determine any statistical differences using the Student T-test assuming unequal variances (Table 5.5).

Table 5.5 Statistical differences between the non-polar component of surface energy for the model powders.

No difference	Highly significant (<1%)	Very highly significant (<0.1%)
Ibuprofen / Ethacrynic acid	Theophylline / Caffeine	Theophylline / Ethacrynic acid
Ibuprofen / Caffeine	Theophylline / Ibuprofen	
Theophylline / Salicylic acid	Caffeine / Ethacrynic acid	
	Salicylic acid / Caffeine	
	Salicylic acid / Ibuprofen	
	Salicylic acid / Ethacrynic acid	

Statistically the IGC is shown to have a good differentiation ability with the non-polar surface energy values alone, showing highly significant differences between most powder samples.

Figure 5.9 Comparison between IGC and glass slide Wilhelmy plate using $a(\gamma_L^D)^{0.5}$ for the model powders.

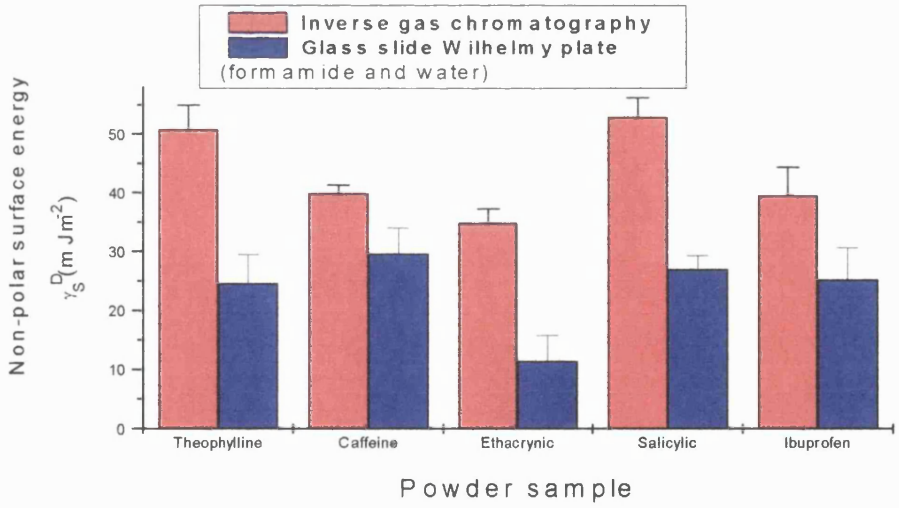

5.3.1.3 Using delta Heat of vaporisation (ΔH_d^{vap})

This second method of analysis was attempted to improve the acid-base analysis of the basic powders. Instead of using molecular areas, it requires values for the delta Heat of vaporisation (ΔH_d^{vap}) for the test probes, which takes into account the probes differing percentages of self-association.

Figure 5.10 Acid / base plot for model acidic powders using ΔH_d^{vap}.

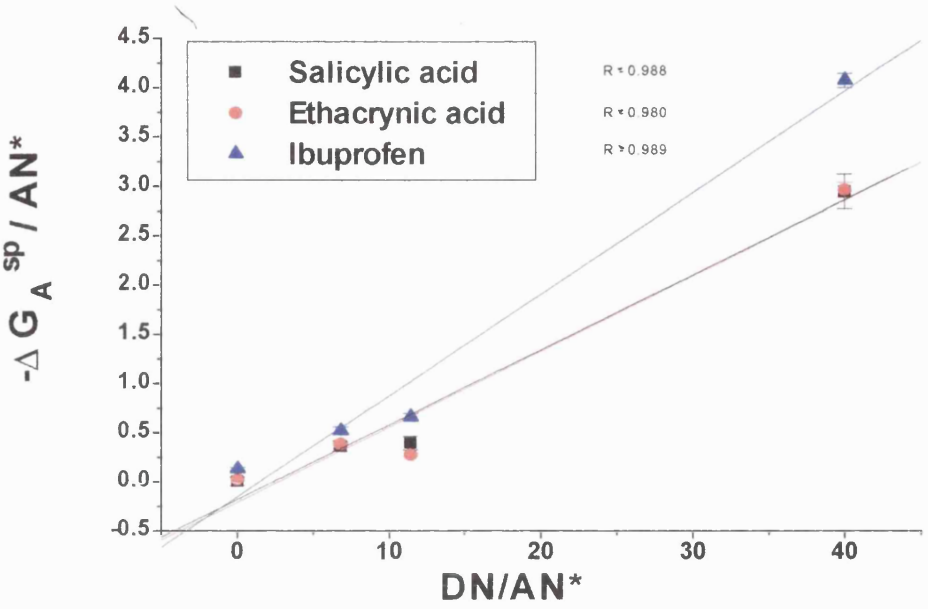

The gradients for the acidic powders have a close correlation with the probe points, although not as close as the previous method (Section 5.3.1.2) which used molecular areas to calculate the free energy of adsorption, ΔG_a^{sp}.

Figure 5.11 Acid / base plot for basic model powders using ΔH_d^{vap}.

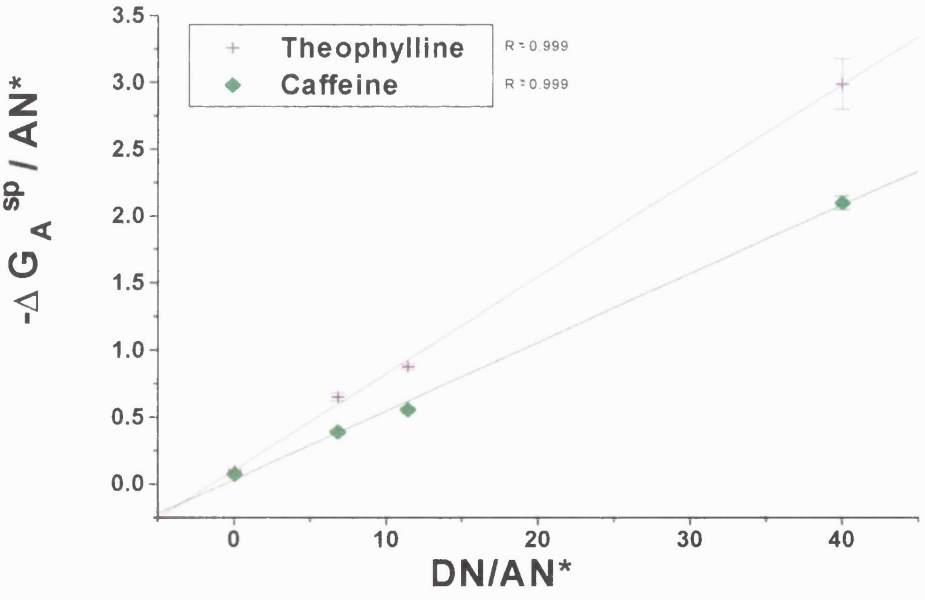

Figure 5.11 shows that this method of analysis has produced a much better straight line correlation when using the two basic powders, than the previous method using $a(\gamma_L^D)^{0.5}$.

Table 5.6 Acid / base character for the model powders using ΔH_d^{vap}.

	K_A (Acidic character)	SD	K_B (Basic character)	SD
Theophylline	0.0719	0.0018	0.1052	0.0371
Caffeine	0.0512	0.0018	0.0344	0.0371
Salicylic acid	0.0762	0.0083	-0.1828	0.1752
Ethacrynic acid	0.0767	0.0109	-0.2058	0.2304
Ibuprofen	0.1029	0.0109	-0.1513	0.2304

Figure 5.12 Acid character for the model powders using ΔH_d^{vap}.

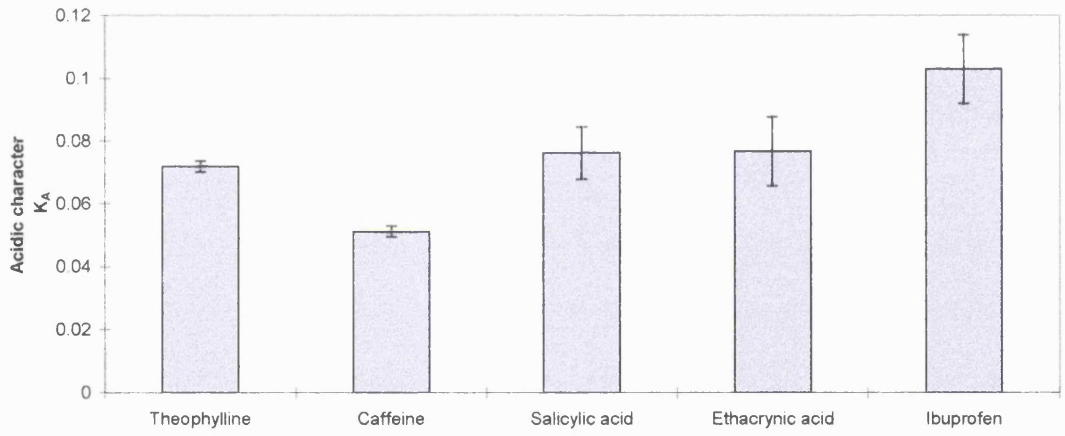

In Figure 5.12, Ibuprofen is the most acidic (as with the previous method), although it was not possible to distinguish between Salicylic acid, Ethacrynic acid and Theophylline. Caffeine, as expected, is the least acidic. The use of ΔH_d^{vap} plots results in small error bars for a wide range of powders proving that this method is more generally applicable than the previous method using probe surface areas.

Figure 5.13 Basic character for the model powders using ΔH_d^{vap}.

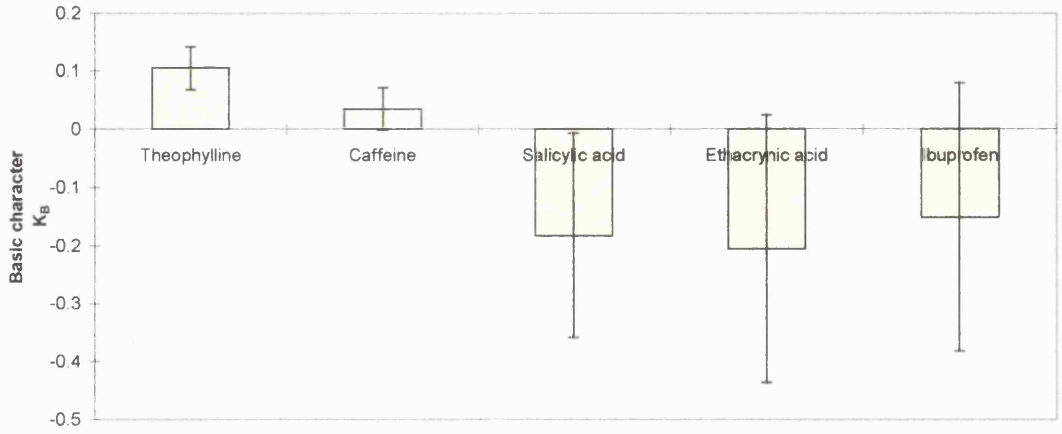

Figure 5.13 indicates that Theophylline is more basic than Caffeine with a high degree of both acid and base character (amphoteric). Salicylic acid is far less basic than Caffeine and Theophylline, having a negative value with this method of analysis. All the three acidic powders have mean values below the baseline, suggesting they have a very limited basic character.

5.3.1.4 Using boiling points

The third method of analysis proposed in the literature is to plot the data as a function of the boiling point of the liquid probes used. The main advantage being that the boiling points of various test liquids are well known and documented, making the calculation quick and easy to perform.

Figure 5.14 Acid / base plot for acidic model powders using boiling point data.

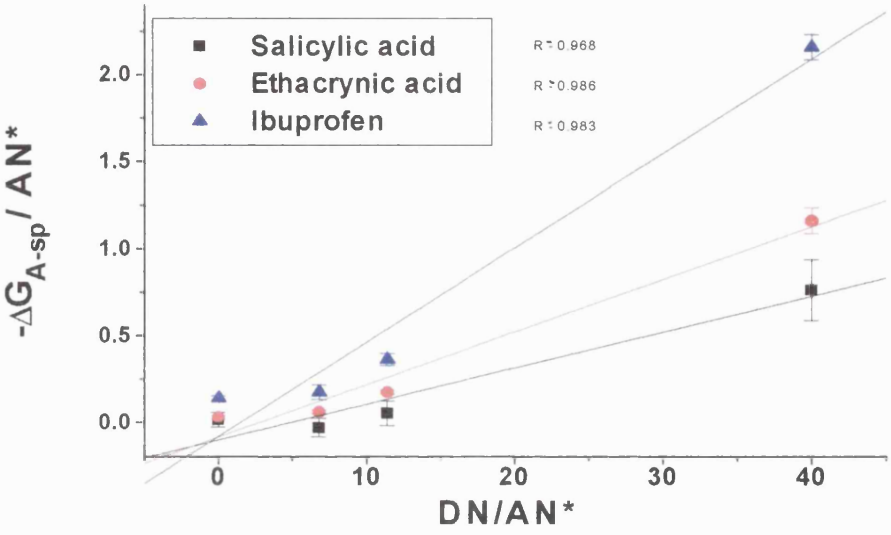

The probe values are only able to give an indication of acid-base character.

Figure 5.15 Acid / base plot for basic model powders using boiling point data.

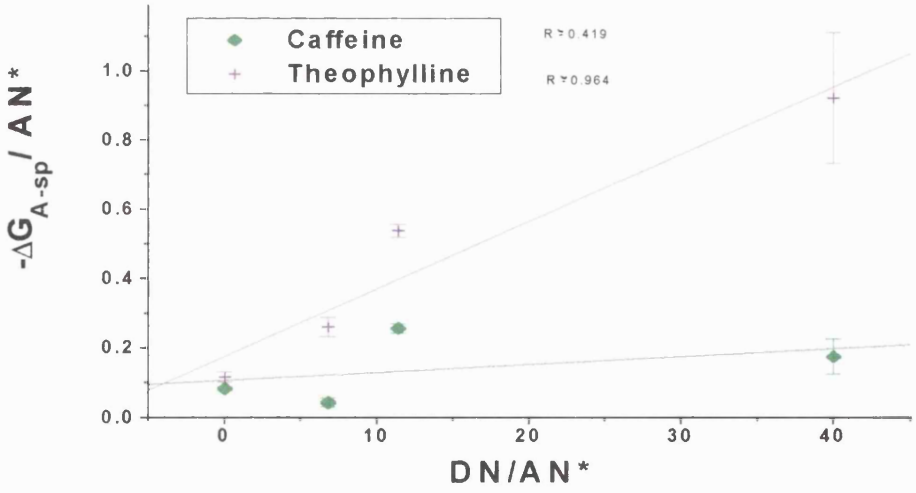

The basic powders are not well characterised using this method, as was the case when using probe surface area data (Section 5.3.1.2).

Table 5.7 Acid / base character for the model powders using boiling point data.

	K_A (Acidic character)	SD	K_B (Basic character)	SD
Theophylline	0.0195	0.0038	0.1753	0.0797
Caffeine	0.0023	0.0035	0.1057	0.0736
Salicylic acid	0.0207	0.0038	-0.1021	0.0798
Ethacrynic acid	0.0303	0.0037	-0.0845	0.0775
Ibuprofen	0.0543	0.0072	-0.0805	0.1519

Figure 5.16 Acid character for the model powders using boiling point data.

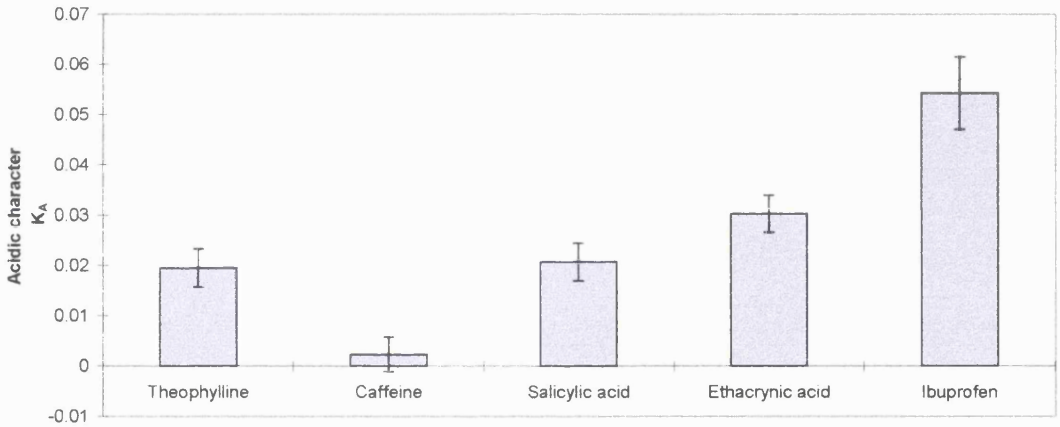

This method has successfully differentiated between Caffeine (least acidic), Ibuprofen (most acidic) and Ethacrynic acid (second most acidic). Salicylic acid and Theophylline appear to have similar acidic characters, below that of Ethacrynic acid, all of which is in general agreement with the previous two methods.

Figure 5.17 Base character for the model powders using boiling point data.

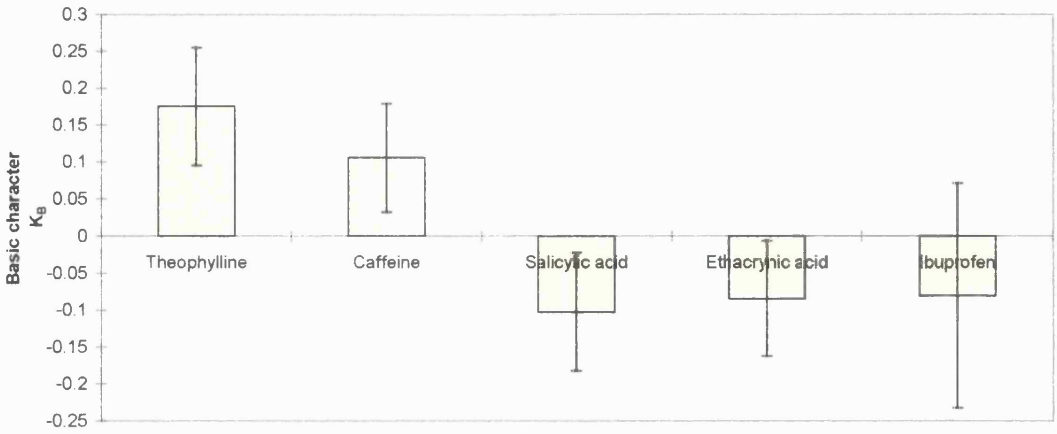

Figure 5.17 has been able to distinguish between two of the acidic powders (Ethacrynic acid and Salicylic acid) and the two basic powders (Caffeine and Theophylline), with Ibuprofen unfortunately having too large error bars. Although this method appears to be one that provides a less accurate characterisation, it has given each powder a similar acid-base character to those achieved with the other two, more complicated methods of analyses. Therefore, it is a useful method if one needs a quick appraisal of a powder's acid-base character.

5.3.1.5 Summary of three methods of analyses

⇒ The method of analysis using $[a(\gamma_L^D)^{0.5}]$ can be used to calculate the non-polar component of surface energy which is directly comparable with contact angle methods of surface analysis. The acid-base characterisation is more accurate with powders that have a predominantly acidic nature, due to the high degree of self-association of the basic probe THF affecting the interaction with basic powders described in Section 5.3.1.2.

⇒ The method of analysis using $[\Delta H_d^{vap}]$ yields a more precise acid-base determination of basic powders, in addition to the acidic powders. This may be due to the fact that only this method takes into account the self-association character of the polar probes. THF, acetone and ethyl acetate all have relatively large percentage self-association which could otherwise affect (decrease) the

distance above the non-polar alkane straight line, in turn altering the calculated acid-base character. Unlike the first method it is unable to give non-polar surface energy components.

⇒ The method of analysis using boiling points gives acid-base profiles that are in general agreement with the other two methods, and since the boiling point data of every probe liquid is easily available, this method is more easily applied in practice. Unlike the first method it is unable to give non-polar surface energy components.

⇒ The acid-base analysis for all three methods appears to be overly reliant on one probe (THF) that is plotted to the far right on the x-axis (x = 40), with the next closest probe (ethyl acetate) at x = 11.4. THF is the most basic of all the probes used and whilst ethyl acetate has only a slightly smaller basic nature, it also has a much greater acidic one, resulting in a far smaller x-axis value. A basic probe that would be plotted in between these two probes is required to achieve a greater confidence in the straight line used to determine the acid-base character.

5.3.2 Saquinavir

Since all three methods of analysis have proved useful with the five model powders, they were all used to analyse the different Saquinavir batches.

Figure 5.18 Raw data graph of Saquinavir (Ro8959-003) original sample using $a(\gamma_L^D)^{0.5}$.

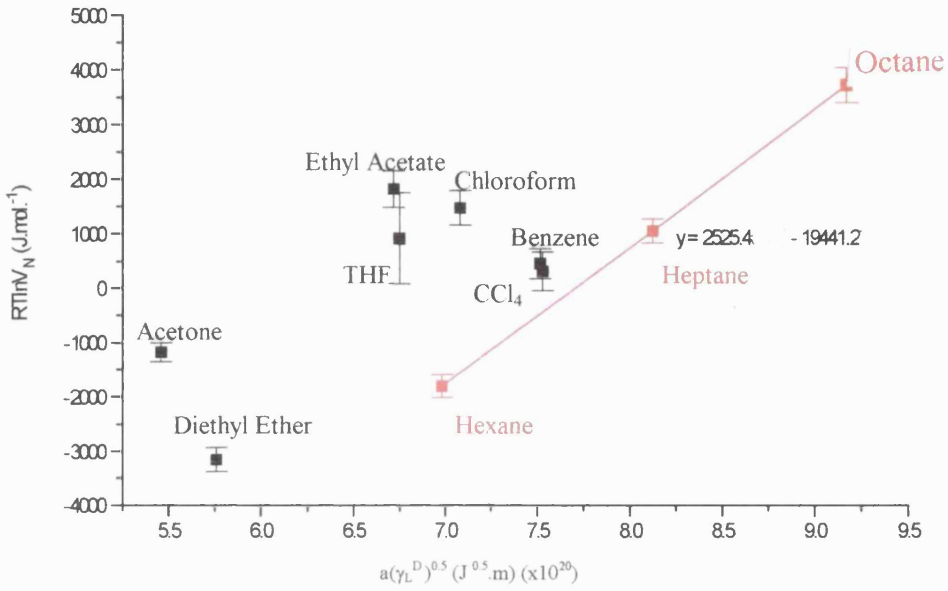

Figure 5.19 Raw data graph of Saquinavir (Ro8959-003) original sample using ΔH_d^{vap}.

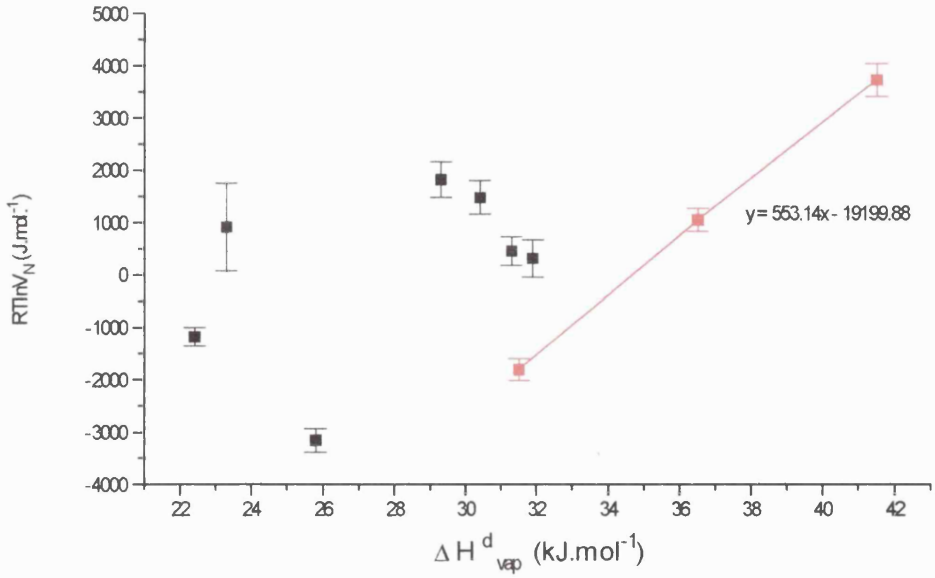

Figure 5.20 Raw data graph of Saquinavir (Ro8959-003) original sample using boiling point data.

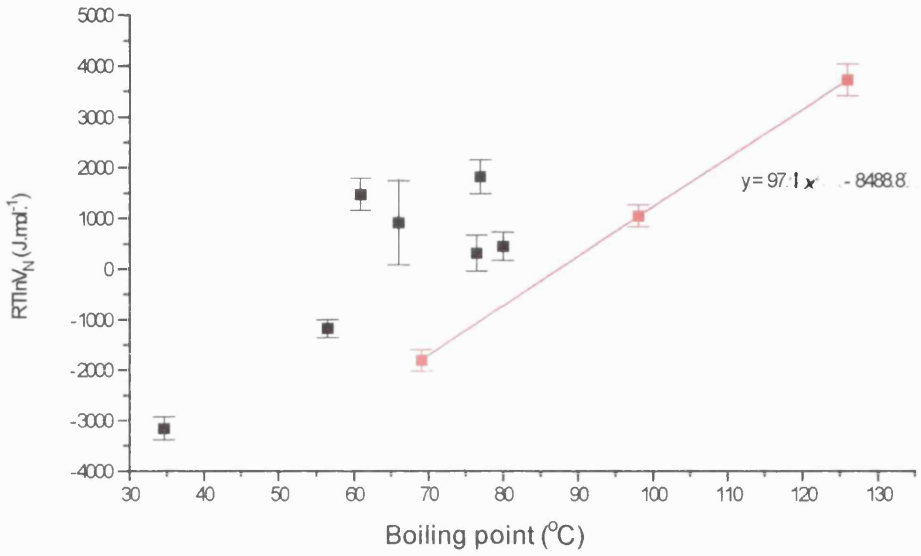

In the three Figures 5.18-5.20, using the three methods of analysis, in each case, the polar probes are plotted above the n-alkane straight line, showing that the theory is valid. A polar probe adsorbing onto a powder has both a polar and non-polar interaction. The total interaction time is due to the sum of both of these. The polar (acid-base) interaction can be separately quantified by comparing the retention time with that of a non-polar probe (alkane) of the same dimensions. By plotting the polar probe along the same axes as the non-polar probes, the polar probe must come above the alkane straight line, since it should have the same non-polar interaction as the straight line plus the polar interaction taking it above the line. For the further figures, only those graphs using $[a(\gamma_L^D)^{0.5}]$ have been included, since only these graphs gave gradients that can be used to calculate non-polar surface energies.

Figure 5.21 Raw data graph of tray dried Saquinavir (batch 001) using $a(\gamma_L^D)^{0.5}$.

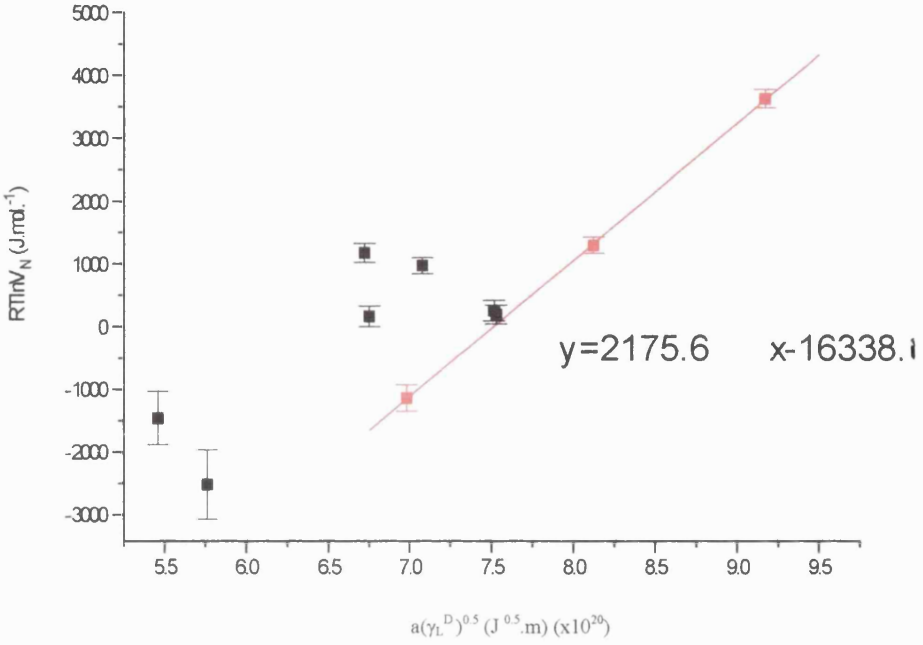

Figure 5.22 Raw data graph of spin dried Saquinavir (batch 002) using $a(\gamma_L^D)^{0.5}$.

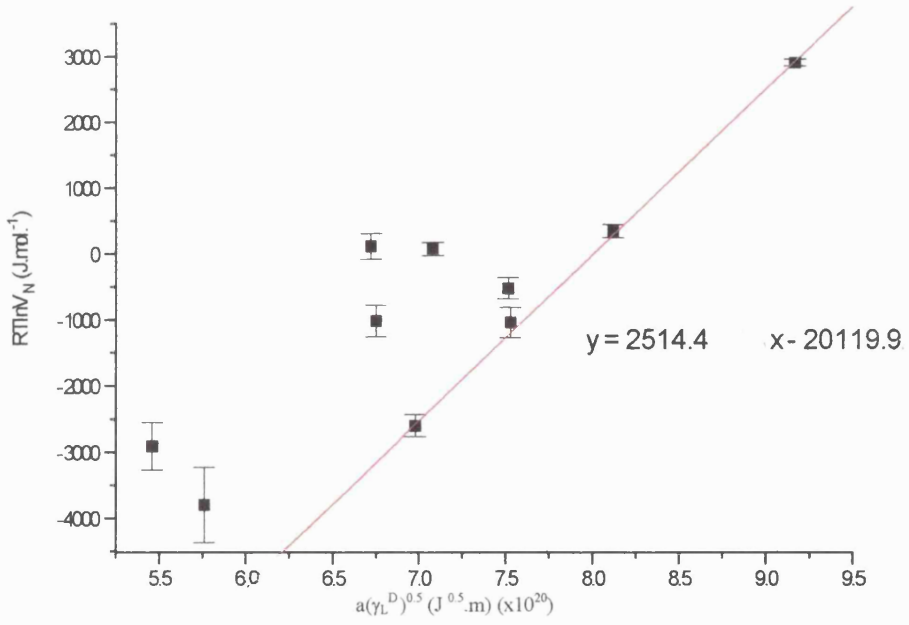

Figure 5.23 Raw data graph of tray dried Saquinavir (batch 010) using $a(\gamma_L^D)^{0.5}$.

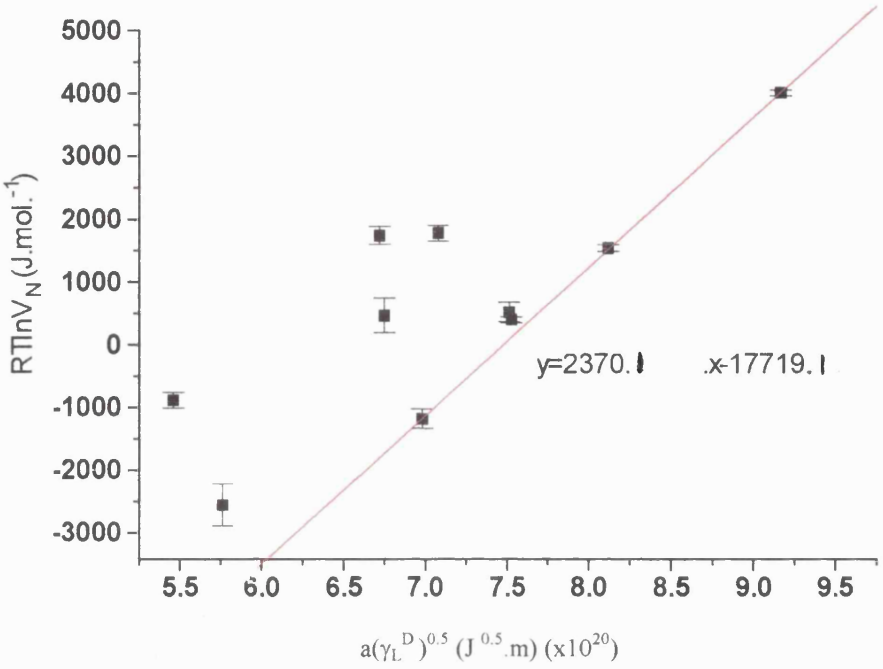

Figure 5.24 Raw data graph of vacuum dried Saquinavir (batch 020) using $a(\gamma_L^D)^{0.5}$.

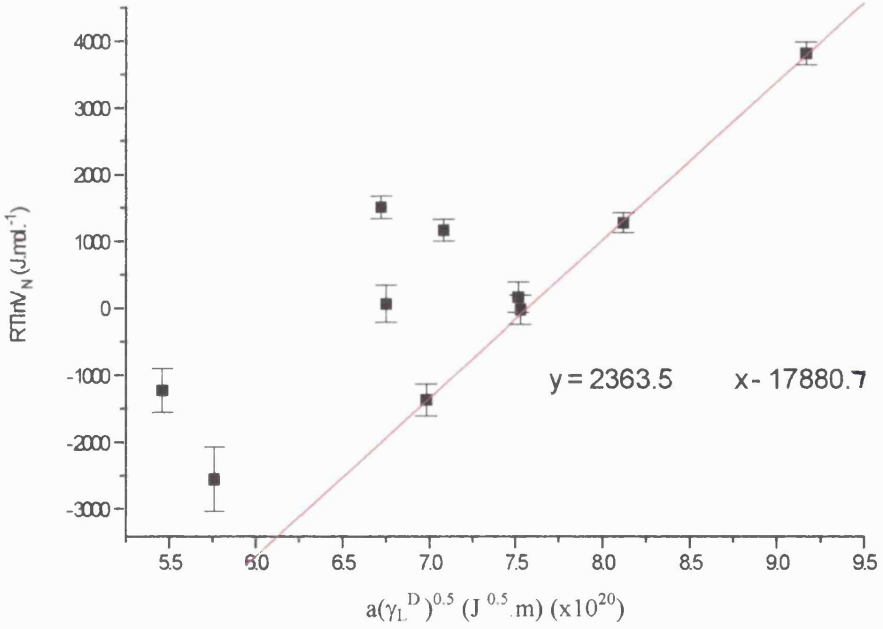

Figure 5.25 Raw data graph of heated Saquinavir (batch 030) using $a(\gamma_L^D)^{0.5}$.

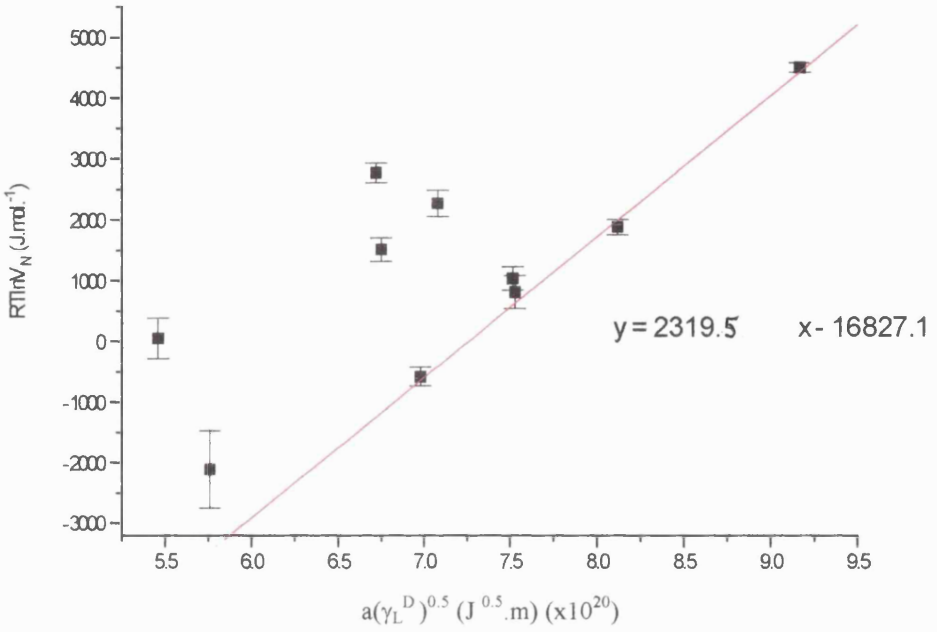

5.3.2.1 Surface energy analysis using $a(\gamma_L^D)^{0.5}$

Since the Saquinavir batches (Figures 5.21-5.25) did not show any dramatic change in surface character evident in the graphs, further acid-base analysis was carried out to detect any small variations, as yet unseen.

5.3.2.1.1 Non-polar surface energy component using $a(\gamma_L^D)^{0.5}$

Table 5.8 Non-polar component of surface energy for all Saquinavir batches using $a(\gamma_L^D)^{0.5}$.

Powder	γ_S^D (mJ.m^{-2})	SD_{n-1}
Ro8959-003	44.0	3.0
Batch 001 (tray dried)	32.6	1.6
Batch 002 (spin dried)	43.6	2.8
Batch 010 (tray dried)	38.7	2.2
Batch 020 (vacuum dried)	38.5	2.7
Batch 030 (heated only)	37.1	1.6

Table 5.9 Statistical differences between the non-polar component of surface energy for the Saquinavir batches.

No difference	Significant (<5%)	Highly significant (<1%)	Very highly significant (<0.1%)
Original / b002	Original / b010	Original / b030	Original / b001
b010 / b020	b002 / b010	b001 / b020	b001 / b002
b010 / b030	b002 / b020	b002 / b030	b001 / b030
b020 / b030			

The gradients of Figures 5.18, 5.21-25 show that the non-polar surface energy components are quite similar for all the Saquinavir batches, but are not exactly the same. Using the Student T-test (assuming unequal variances), all the batches were found to be significantly different to the original Saquinavir sample except for the spin dried batch (b002), showing the good differentiating ability between batches of the same powder with this method. The tray dried (b001) had a very reduced non-polar surface energy value of only 75% of the original. The other three batches (b010,020,030) all had similar but not statistically different non-polar surface energy values form one another but were all significantly lower than the original. Additionally, all the powders tested produced non-polar surface energy values that were far greater than those achieved with the glass slide Wilhelmy plate method.

5.3.2.1.2 Acid-base characterisation using $a(\gamma_L^D)^{0.5}$

Figure 5.26 Acid / base plot for original, b001 and b002 Saquinavir batches using $a(\gamma_L^D)^{0.5}$.

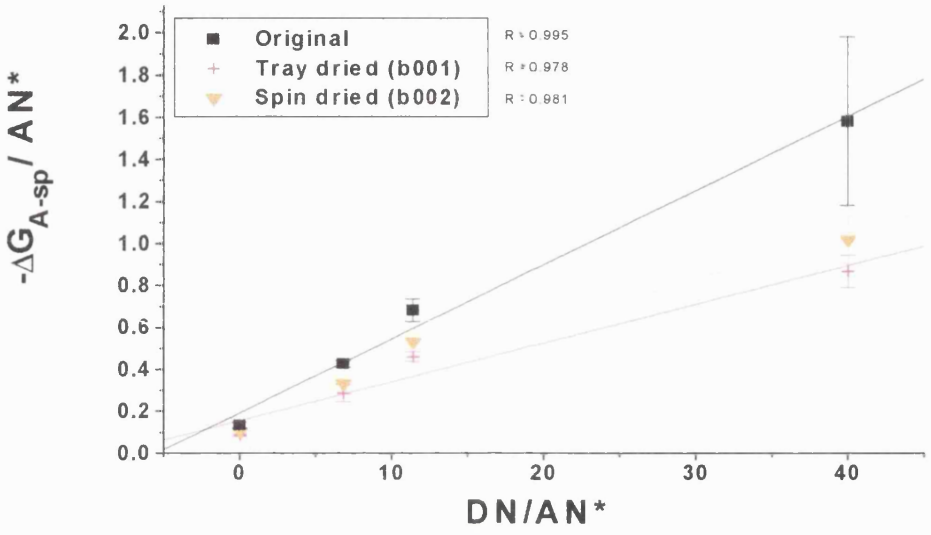

Figure 5.26 clearly shows the two treated batches are significantly different to the original Saquinavir.

Figure 5.27 Acid / base plot for original, b010, b020 and b030 Saquinavir batches using $a(\gamma_L^D)^{0.5}$.

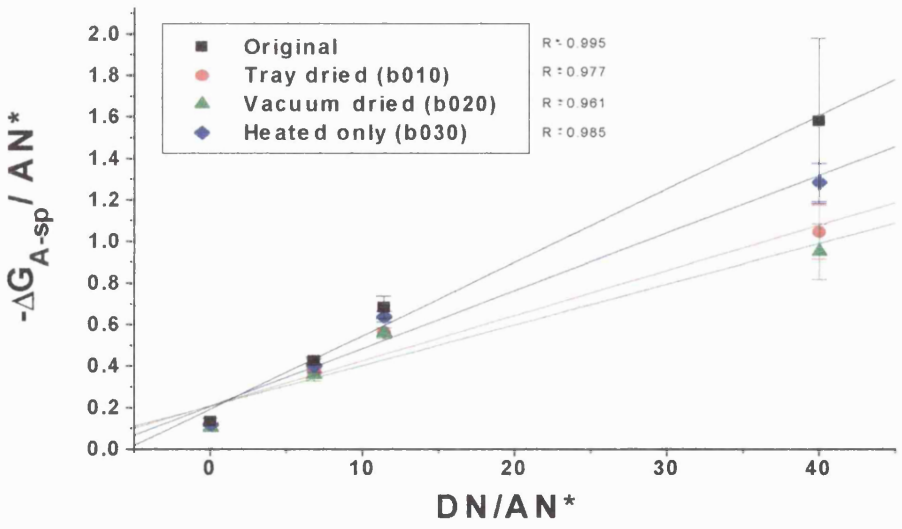

The vacuum dried (b020) and tray dried (b010) were similar to each other but dissimilar in nature to the original Saquinavir and heated batch (b030) (Figure 5.27). Unfortunately, due to the large error bars for the THF probe with the original Saquinavir, their is no definite distinction between the original and heated (b030) batches. The reason for large error bars with THF and basic powders has been previously discussed in Section 5.3.1.2.

Table 5.10 Acid / base character for Saquinavir batches using $a(\gamma_L^D)^{0.5}$.

	K_A (Acidic character)	SD	K_B (Basic character)	SD
Ro8959-003	0.0353	0.0025	0.193	0.0531
Batch 001 (tray dried)	0.0185	0.0028	0.156	0.0594
Batch 002 (spin dried)	0.0217	0.0031	0.182	0.0643
Batch 010 (tray dried)	0.0217	0.0033	0.209	0.0701
Batch 020 (vacuum dried)	0.0196	0.0040	0.208	0.0836
Batch 030 (heated only)	0.0278	0.0035	0.207	0.0732

Figure 5.28 Acid character for all Saquinavir batches using $a(\gamma_L^D)^{0.5}$.

Table 5.10 gives a more quantitative representation of the Saquinavir batches. Figure 5.28 shows that the original Saquinavir has the largest acidic character, equivalent to that of Ethacrynic acid. The heated only batch (b030) has a significantly reduced acidic character to the original, whilst all the batches that came into contact with water in their treatment (b010, 020, 001 and 002) have even smaller acidic characters, indistinguishable from one another. The vacuum dried (b020) and tray dried (b001) have a lower acidic character than the heated only batch.

Figure 5.29 Base character for all Saquinavir batches using $a(\gamma_L^D)^{0.5}$.

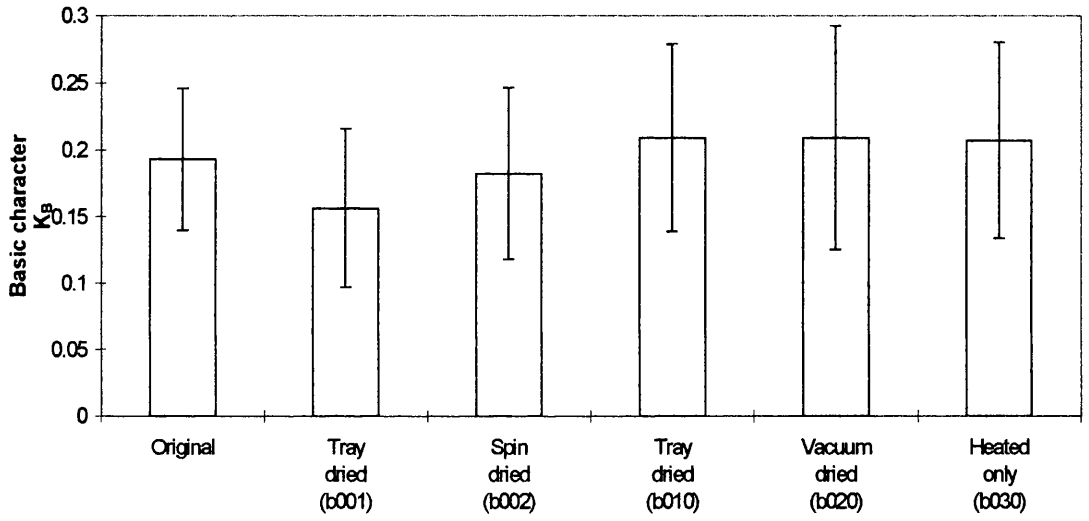

The basic character for all the batches does not appear to alter significantly, suggesting that there has been no change in the basic nature of Saquinavir with processing.

5.3.2.2 Acid-base characterisation using enthalpy of vaporisation

Since this method of analysis has been shown to be more effective with basic powders it was used with Saquinavir, since the first method showed that Saquinavir had a large basic activity.

Figure 5.30 Acid / base plot for original, b001 and b002 Saquinavir batches using ΔH_d^{vap}.

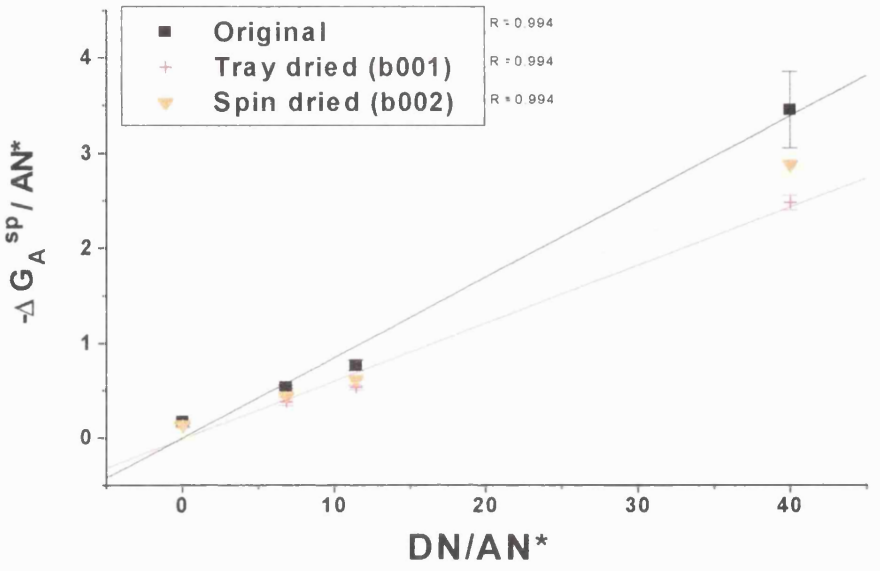

Figure 5.30 clearly shows the difference between three Saquinavir batches with a good correlation between the probe values and their respective straight lines.

Figure 5.31 Acid / base plot for original, b010, b020 and b030 Saquinavir batches using ΔH_d^{vap}.

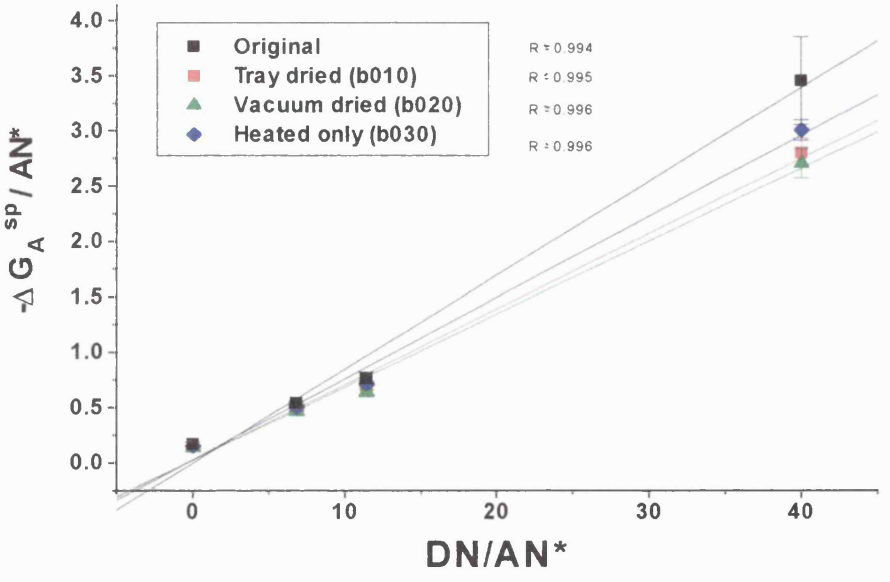

Figure 5.31 highlights that the original and heated only Saquinavir batches are very similar in acid-base nature. The tray and vacuum dried batches are similar to each other but are significantly different to the original and heated only batches.

Table 5.11 Acid / base character for Saquinavir batches using ΔH_d^{vap}.

	K_A (Acidic character)	SD	K_B (Basic character)	SD
Ro8959-003	0.0848	0.0063	-0.0018	0.1333
Batch 001 (tray dried)	0.0611	0.0048	-0.0117	0.1004
Batch 002 (spin dried)	0.0709	0.0057	-0.0113	0.1205
Batch 010 (tray dried)	0.0681	0.0049	0.0267	0.1038
Batch 020 (vacuum dried)	0.0659	0.0043	0.0260	0.0899
Batch 030 (heated only)	0.0733	0.0046	0.0285	0.0972

It can be seen from Table 5.11 that the original Saquinavir is more acidic than the other Saquinavir batches, followed by the heated only batch (b030). Since the basic values are close to zero, one could be excused for assuming that Saquinavir is not basic. On the contrary, when compared to Ethacrynic acid (basic value of -0.2058), all of the batches are more basic, although not as basic as Theophylline (basic value of -0.1052). There are differences in basicity between the Saquinavir batches but since the whole range from Theophylline to Ethacrynic acid is large, the Saquinavir variation is small enough as to be insignificant.

Figure 5.32 Acid character for the Saquinavir batches using ΔH_d^{vap}.

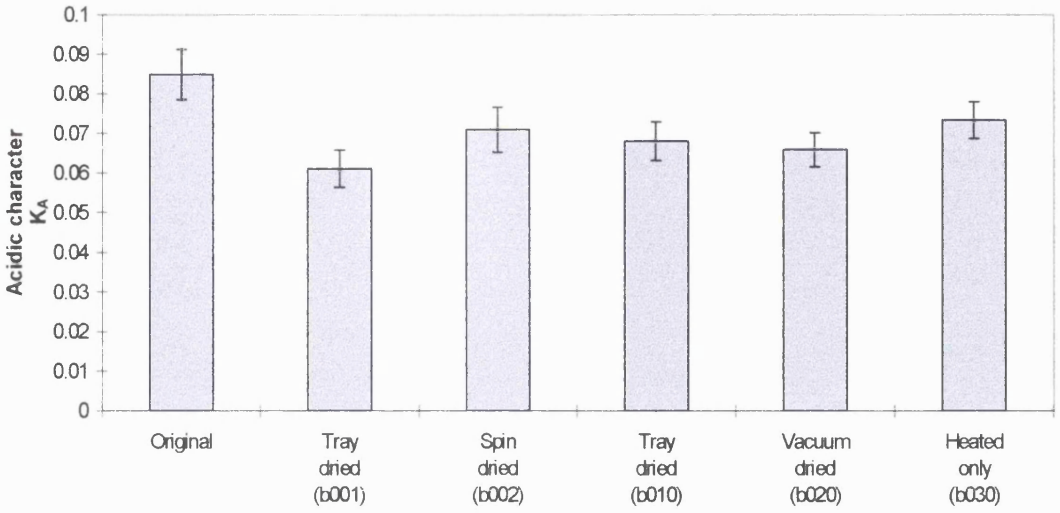

Figure 5.32 shows that the original Saquinavir is most acidic, as with the previous method. The heated only batch (b030) is less acidic compared to the original, whilst all the batches that came into contact with water in their treatment (b010, 020, 001 and 002) are even less acidic and are indistinguishable from one another. The tray dried (b001) is the least acidic.

Figure 5.33 Base character for the Saquinavir batches using ΔH_d^{vap}.

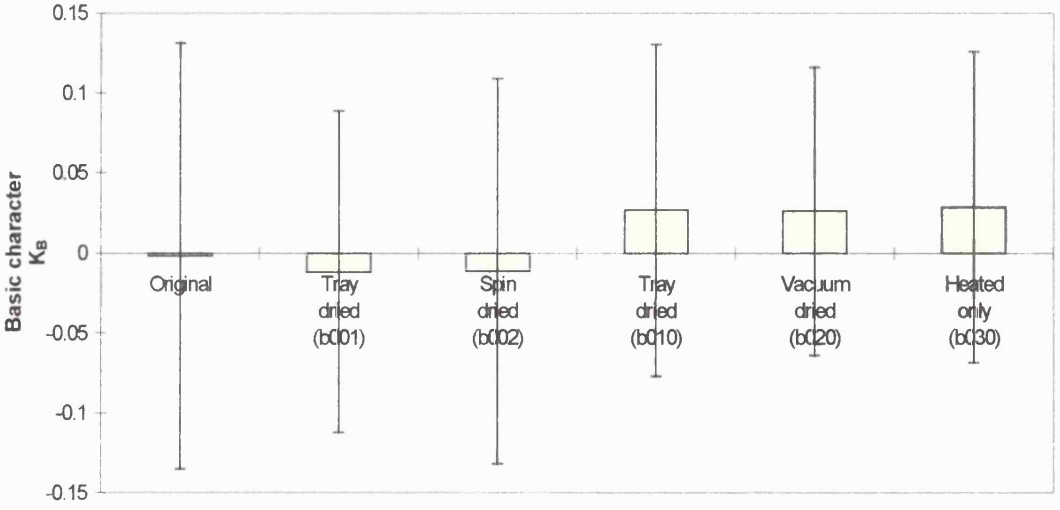

The basic character for all the batches are very small and do not appear to alter significantly, suggesting that there has been no change in the basic nature of Saquinavir with processing.

5.3.2.3 Acid-base characterisation using boiling points.

This method has been shown to provide a true indication of acid-base nature, so it has been used to back up any conclusions made with the Saquinavir batches using the previous two methods of analysis.

Figure 5.34 Acid / base plot for original, b001 and b002 Saquinavir batches using boiling point data.

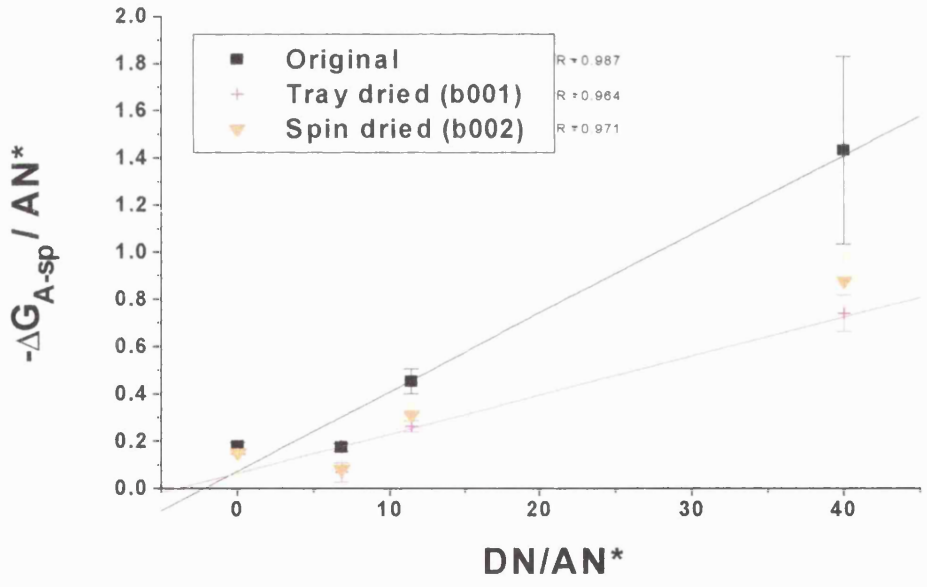

Figure 5.35 Acid / base plot for original, b010, b020 and b030 Saquinavir batches using boiling point data.

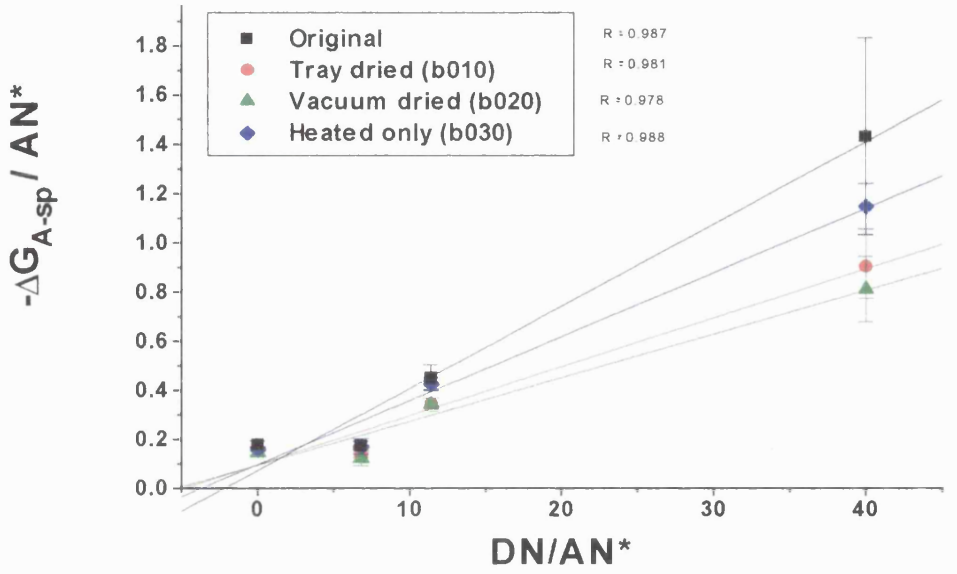

As with the other two methods, using boiling point data can show clear differences between similar but not identical powders.

Table 5.12 Acid / base character for Saquinavir batches using boiling point data.

	K_A (Acidic character)	SD	K_B (Basic character)	SD
Ro8959-003	0.0334	0.0039	0.0730	0.0813
Batch 001 (tray dried)	0.0165	0.0032	0.0650	0.0677
Batch 002 (spin dried)	0.0199	0.0034	0.0663	0.0725
Batch 010 (tray dried)	0.0200	0.0028	0.0968	0.0588
Batch 020 (vacuum dried)	0.0178	0.0027	0.0960	0.0563
Batch 030 (heated only)	0.0261	0.0029	0.0971	0.0616

Plotting the data as a function of boiling points resulted in Ibuprofen having the largest acidic value of 0.0543 and Caffeine the least of 0.0023 whilst Theophylline had the largest basic value of 0.1753 and Salicylic acid the least of -0.1021. In comparison, the original Saquinavir in Table 5.12 has a significantly greater acidic

character than the other batches, followed by the heated only batch (b030). The basic values do not alter to a large extent in comparison with the ten fold difference between Theophylline and Salicylic acid. So this method has been able to increase the confidence with the acid-base data profiling, in that a dramatic change has occurred with the acidic nature of the Saquinavir upon treatment, in comparison with the original untreated Saquinavir.

Figure 5.36 Acid character for Saquinavir batches using boiling point data.

Figure 5.37 Base character for Saquinavir batches using boiling point data.

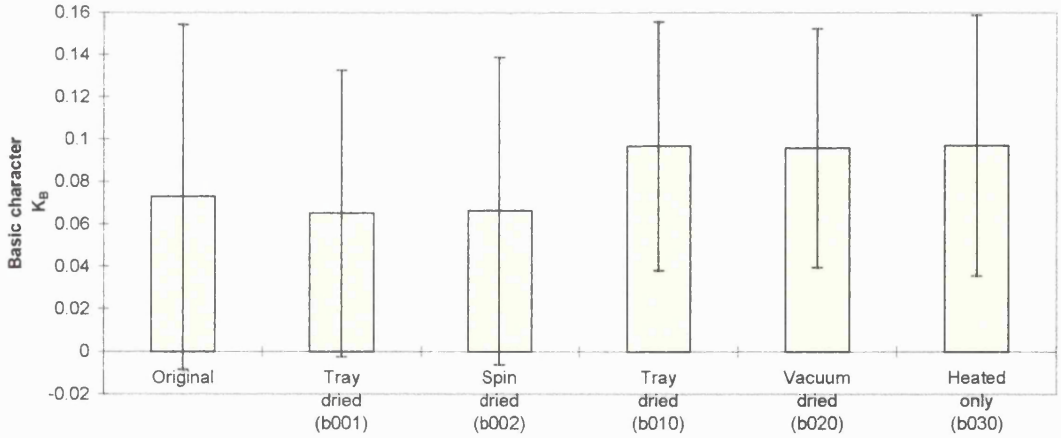

5.3.2.4 Overall conclusions with the batches of Saquinavir from the IGC results

⇒ The basic behaviour of each batch is similar in magnitude.

⇒ The acidic behaviour has changed with processing.

⇒ The non-polar surface energy components are quite similar for all the Saquinavir batches, but are not exactly the same.

To achieve this detailed analysis of the Saquinavir batches all three methods of analysis were employed to obtain the most information, but perhaps only the methods using $a(\gamma_L^D)^{0.5}$ and ΔH_d^{vap} for the graphical analysis are required, the former giving non-polar surface energy data and the latter giving an acid-base (polar) nature.

5.4 Conclusions

5.4.1 High non-polar surface energy values

All the powders analysed with IGC yielded non-polar surface energy values that were consistently and significantly larger than those obtained for the same powders using the Wilhelmy plate glass slide technique which gave contact angle data most representative of the true powder sample (see Chapter 3). IGC involves injecting minute amounts of gaseous test probes over a powder surface. The concentration of probe is so small that it is at infinite dilution; this is necessary to ensure that the adsorption of probe molecules onto the powder surface is the dominant process. At infinite dilution, the probe molecules interact with approximately 1-3% of the total surface (Ticehurst, 1995), thus IGC is very sensitive to the higher energy sites on the surface. Possible causes for batch variations could be due to minor differences in surface crystallinity leading to a minority of high energy hot spots readily detectable with IGC. If these higher energy sites are only present at the surface and are not spread throughout the bulk of the powder, then techniques focusing on the bulk properties (e.g. X-ray powder crystallography) will not be able to detect any change. A powder does not consist of identical crystals which all have the same energy at their surface. Vapours used in IGC interact with the surface at a molecular level (Fafard et al., 1994) showing that there is an indication of surface heterogeneity among non-polar binding sites. Whereas the large volumes of liquids required for contact angle measurement cover a macroscopic surface region and are unable to detect surface heterogeneity. An additional factor that may influence batch to batch variation could be due to various levels of high energy impurities within each batch, although all Saquinavir batches originated from the same source batch, and they would consequentially contain equal amounts of impurities, if any.

5.4.2 Acid-base analysis

The three different methods of determining acid-base character were used to rank the six powders in Tables 5.13 and 5.14 below:-

Table 5.13 Acid character of all six powders using three methods of analysis.

	$a(\gamma_L^D)^{0.5}$	ΔH_d^{vap}	B.p.
Least acidic		Caffeine	Caffeine
↓		Theophylline	Theophylline
	Salicylic Acid	Salicylic Acid	Salicylic Acid
	Ethacrynic Acid	Ethacrynic Acid	Ethacrynic Acid
	Original Saquinavir	Original Saquinavir	Original Saquinavir
Most acidic	Ibuprofen	Ibuprofen	Ibuprofen

Table 5.14 Base character of all six powders using three methods of analysis.

	$a(\gamma_L^D)^{0.5}$	ΔH_d^{vap}	B.p.
Least basic	Ethacrynic Acid	Ethacrynic Acid	Salicylic Acid
↓	Salicylic Acid	Salicylic Acid	Ethacrynic Acid
	Ibuprofen	Ibuprofen	Ibuprofen
	Original Saquinavir	Original Saquinavir	Original Saquinavir
		Caffeine	Caffeine
Most basic		Theophylline	Theophylline

The three methods each rank the six powders in the same order of magnitude for both acid and basic values. The only exception is the basic character of Ethacrynic acid and Salicylic acid, since they both have small and very similar basic characters. This suggests that all the three methods give reliable data able to accurately compare the acid-base nature of a range of different powders.

5.4.3 Accuracy

For accurate non-polar surface energy characterisation with the IGC, good linearity and accurate slope determination are essential with the plot of $RT\ln V_N$ against $a(\gamma_{LV}^{D})^{0.5}$. Since the slope values are multiplied by a constant that is three orders of magnitude greater than the gradients and is then raised to the second power, any small inaccuracy in the gradient will be magnified greatly. A change of 10% in the gradient would produce a 20% change in the surface energy. In addition, the molecular probe areas (a) are affected by both the surface of the powder and the temperature of the experiment (Panzer and Schreiber, 1992), whereby any temperature variation may result in significant surface energy alterations, and should be taken into account when analysing IGC data. This could partly explain any difference in surface energy values between IGC and more traditional techniques.

Three methods of analysing IGC data using boiling point, molecular area and the dispersive component of the heat of vaporisation have resulted in similar enthalpy values for each powder suggesting that no single method is better than another.

5.4.3.1 Y-axis errors

For all three methods of analysis, T and V_N come directly from experimental results, whereby the temperature (T) can be kept within narrow limits (±0.25 °C) and the retention times are within 5% error margins. One must also realise that the logarithmic function of V_N significantly reduces the experimental uncertainty (Garnier and Glasser, 1993). Therefore the overall error is minimal.

5.4.3.2 X-axis errors

The molecular area of the adsorbate (a) does present a problem in it's definition. The size of the adsorbed molecule is not constant but actually varies depending on the nature of the solid adsorbent (McClellan and Harnsberger, 1967), with temperature and even with the reference carrier used (i.e. Nitrogen, helium or krypton). To overcome the effect of the solid surface on the probe molecule's diameter, Schultz and

Lavielle determined the surface area of various n-alkane and polar molecules on neutral reference solids (PTFE and PE), and adopted these values for calculating γ_S^D of unknown surfaces. For consistency, literature values (Schultz et al., 1987) for the probe molecular areas have also been used in this case.

The method using delta heat of vaporisation takes into account the different amount of self-association of the probe vapours, therefore reducing the errors caused by the inaccurate plotting of highly self-associated probes. In addition, due to the heat of vaporisation being calculated using calorimetric measurements at 25°C, this method can be assumed to be most accurate when the IGC is used at temperatures close to ambient.

The final method utilising boiling point data is the least precise of the three methods of analysis, although does provide a fast approximate analysis if so required.

5.4.4 Advantages of IGC

a) Very sensitive method, able to detect changes on the powder surface that may not necessarily be evident in the bulk of the powder.
b) Able to analyse powders through a range of temperatures.
c) Simple and easy to use.
d) Powder sample is physically unaltered by process (i.e. no compacting necessary).
e) Small quantity required for analysis when compared with contact angle analysis.

5.4.5 Disadvantages of IGC

a) Relies on measurement of adsorption characteristics in the region of infinite dilution along the adsorption isotherm. Since most solid surfaces are energetically heterogeneous, such analysis assesses only the high energy sites and therefore this may not be wholly representative of the majority of the population. In addition, where a probe binds very strongly to a binding site, it may not always be possible to obtain concentration independent adsorption within the detectors sensitivity

range.

b) The probe molecular areas are not well known and their determination varies with each method used. They do play a vital role in quantifying the acid-base interaction.

Chapter 6

Isothermal Microcalorimetry

6 Isothermal Microcalorimetry

Isothermal heat conduction microcalorimetry measures the heat flow as a function of time during an ongoing reaction. By integrating the heat flow peak over a timed interval, one can calculate the heat change that has occurred throughout a reaction process.

6.1 Introduction

All chemical and physical processes are accompanied by changes in heat. Microcalorimetry provides a highly controlled environment in which any minute heat change can be identified and accurately measured using thermopiles. The voltage from these are recorded and relative to a control cell, the heat changes can be evaluated. Many pharmaceuticals with an amorphous aspect are sensitive to moisture changes, since the amorphous material is able to absorb water vapour as it crystallises. This is readily detectable as an enthalpic event with the isothermal microcalorimetry. When no amorphous drug is present within a sample, the water vapour is adsorbed onto the powder surface and no absorption occurs. This process is most commonly described as a type II adsorption isotherm illustrated in Figure 6.1.

Figure 6.1 Type II adsorption isotherm

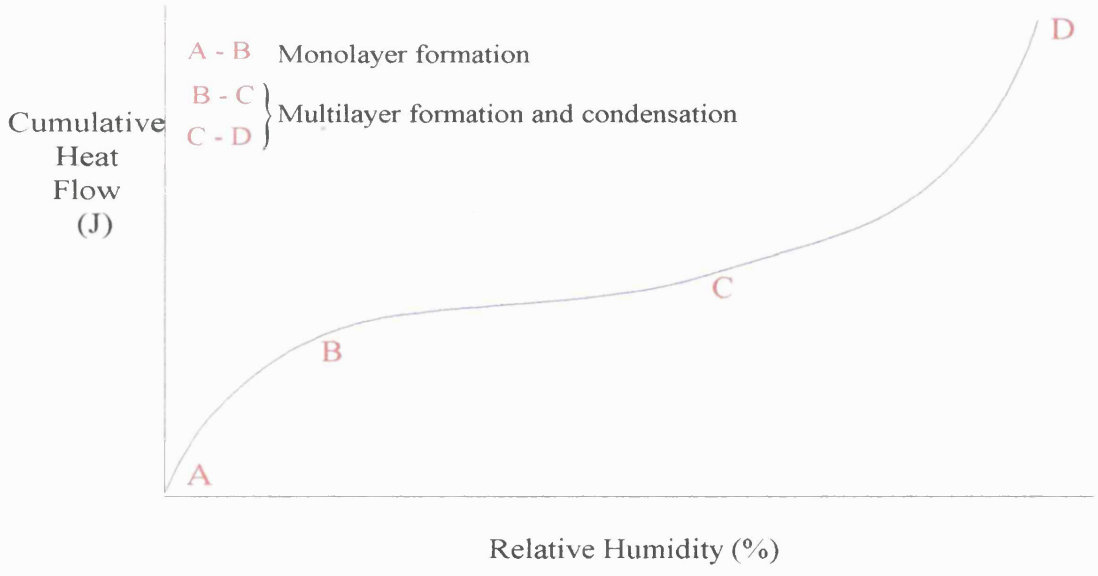

The process of water molecules forming a monolayer (A-B) at the surface is important when considering how a powder interacts with either vapour or liquid during wetting, even though most of the adsorption occurs after that (between C and D).

6.2 Method

Small heat changes down to 1×10^{-6} J are able to be measured by the 2277 Thermal Activity Monitor (TAM), Thermometric, Sweden. Four calorimeters are housed within a 25 litre water bath which is able to keep the temperature constant over a range of 5 to 80°C ($\pm 2 \times 10^{-4}$). The TAM sensitivity can be adjusted for a maximum reading of 3, 10, 30, 100, 300 or 3000μW, the latter being the sensitivity in this case. The apparatus is stored in a temperature controlled room (18°C ± 1), to ensure that the water bath is able to control its core temperature within strict limits.

Figure 6.2 Schematic diagram of a single microcalorimetric unit of the TAM.

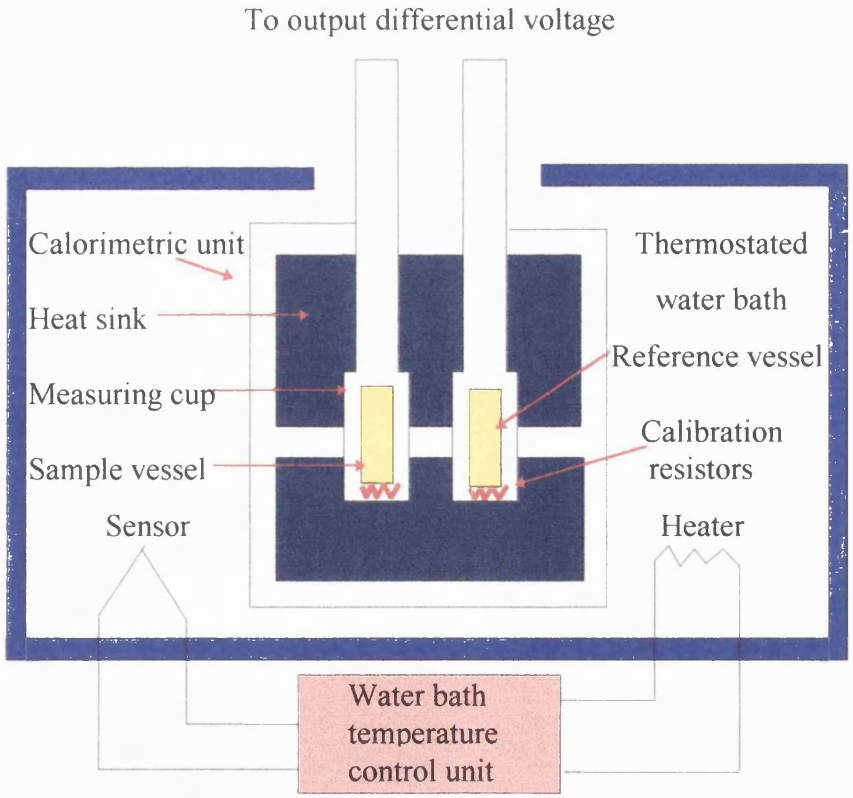

At the measurement position in the middle of the water bath, the sample cell and the reference cell (both 4ml stainless steel cylinders) are each sited between a pair of thermopiles, through which heat is transported. Any temperature difference between the metal sink and the sample or reference cells creates a voltage that is proportional to the heat flow. The voltage - time integral is proportional to the heat quantity evolved (exothermic) or absorbed (endothermic), that is to say, the area under the peak of a voltage versus time plot. The two pairs of thermopiles are electrically connected in such a way that the voltage output consists only of the difference in voltage between the two sources (sample and reference cells). This ensures that any system change affecting both cells, will not have any affect on the differential voltage. This voltage is interpreted using Digitam™ software which is able to plot power output versus time, and consequently integrate the peaks or troughs giving the total energy output for each process be it endothermic or exothermic.

6.2.1 Calibration

Calibration is carried out on each individual cell every month. It involves heating calibration resistors which are present in both the test and reference channels within the calorimeter with a set amount of power. The heat output is calibrated to the expected value for the power input into the system.

The reference cell contains an empty stainless steel cell of exactly the same proportions as the test cell to prevent any baseline shift that might have occurred due to environmental changes. Each cell is cleaned thoroughly with water and then ethanol to remove any foreign particles that could affect the heat exchange. Both cells are lowered halfway into each channel and allowed to reach an equilibrium temperature with the water bath for at least 30 minutes. Once lowered completely into the measurement position, the sensitivity required for the experiment is selected (3 to 3000μW) and the baseline allowed to settle to a constant value. If the baseline is not at zero, it is adjusted to zero. The calibration program heats up the electrical resistors with the correct amount of power to generate a full scale deflection which is detected by the thermopiles. When the value detected by the thermopiles remains constant, the

amplifiers are adjusted to read the correct full scale deflection.

Figure 6.3 Schematic diagram of a single flow cell.

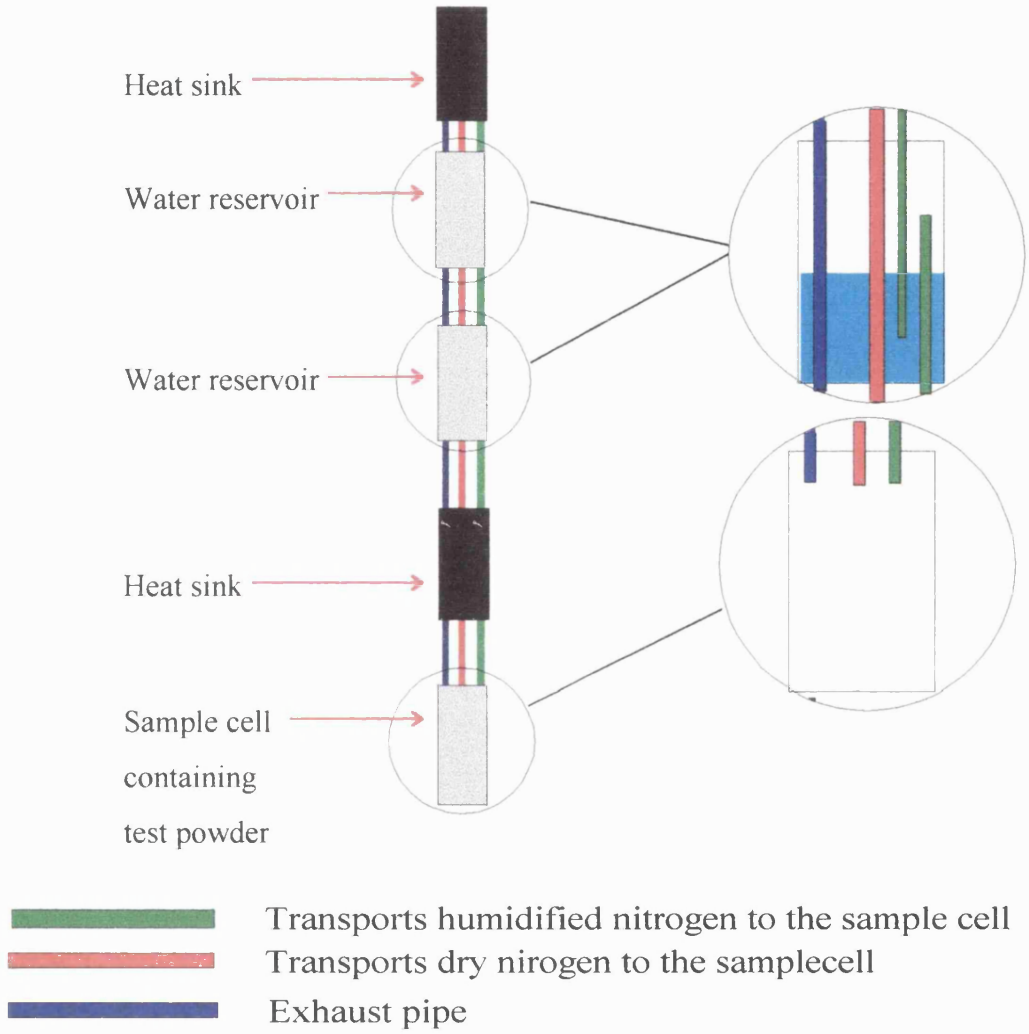

50mg of the test powder was placed into the bottom of the cell, and then the cell was reconnected to the flow controller and inserted halfway into the water bath (25°C) and left to equilibrate for 30 minutes. The flow cell was connected to a nitrogen cylinder with stainless steel piping incorporating a flow controller to achieve a constant flow of 3mls per minute. This flow rate was chosen since it allowed rapid humidity control whilst having no adverse effect on the baseline reading. This new set-up allowed a consistent flow of dry nitrogen which could be easily monitored and controlled. The room temperature is controlled at 18°C, below that of the water bath,

to enable the water bath temperature to be controlled within very tight limits, less than 0.0001 °C change in 24 hours. The flow cell is then slowly lowered to the base of the water bath and again allowed to equilibrate for up to 30 minutes.

The microcalorimeter is controlled by an interfaced computer with TAM software, able to record power signals at programmed intervals for the length of time required. The baseline was recorded for approximately 10 hours at 0% RH prior to the increase in humidity so that there was sufficient time for any moisture to fully desorb from the powder sample and the flow cell to reach equilibrium conditions. Only when the baseline is constant and remains within strict limits can the computer begin raising the humidity. The experiment involved a 15% stepwise increase in relative humidity flowing through the cell starting at 0% and ending at 90% and then repeated for two more cycles. Three separate samples from each powder were used.

6.2.2 Surface area analysis

6.2.2.1 Method

The apparatus was the Quantasorb B.E.T. Surface Area Analyser with the triple point Brunauer, Emmett and Teller (BET) nitrogen adsorption analysis. The condensation of gaseous nitrogen onto an unknown powder surface can be used to calculate a solid powder's surface area. Gaseous nitrogen is passed over the sample and when the sample is immersed externally in liquid nitrogen, the gaseous nitrogen condenses onto the powder surface. When the sample is warmed to room temperature, the condensed nitrogen adsorbed to the powder evaporates off and this excess nitrogen is accurately measured. Further calibration injections of nitrogen are used in conjunction with the experimental values to enable the surface area to be calculated using Equation 6.1 overleaf:-

$$\frac{V}{V_{mon}} = \frac{c.z}{(1-z).\{1-(z(1-c))\}}$$

Equation 6.1

c - constant

z = P / P_o

v - volume of gas adsorbed at any time

v_{mon} - volume of gas for a complete monolayer

For greater accuracy, three or more different combinations of nitrogen and helium concentration ratios were used in a multipoint analysis. The results from each were then used by the Quant2PC computer program to calculate the surface area.

6.3 Results and discussion

The microcalorimetric method of passing water vapour over a powder sample was first developed and evaluated using Caffeine, Ethacrynic acid, Ibuprofen, Theophylline and Salicylic acid.

6.3.1 Cumulative adsorption isotherms of the five model powders

The cumulative adsorption isotherms of each of the five model powders were able to show clear differences, with Salicylic acid, Ethacrynic acid and Theophylline all having very individual isotherms. Unfortunately, both Ibuprofen and Caffeine have very similar isotherms, requiring further analysis to differentiate between them (Section 7.5.1). Each isotherm was corrected to incorporate surface area variations between powders.

Table 6.1 Surface areas of five model powders using BET analysis (Section 6.2.2).

Model powder	Surface Area (m^2/g)	±
Caffeine	0.876	0.139
Theophylline	0.551	0.016
Salicylic acid	0.205	0.018
Ibuprofen	0.418	0.134
Ethacrynic acid	0.629	0.124

Figure 6.4 Cumulative adsorption of model powders with corrected surface areas.

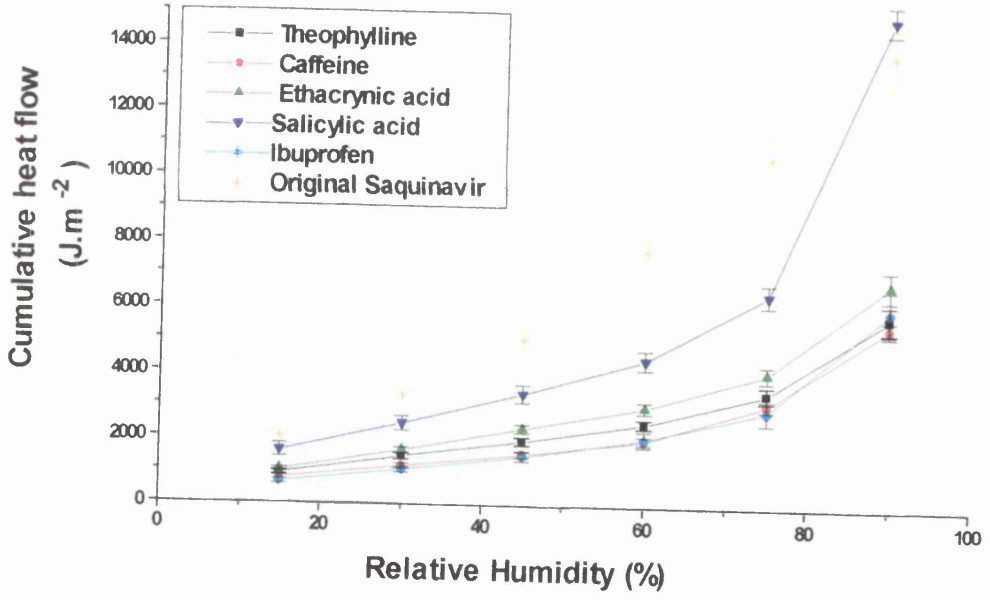

6.3.2 Cumulative adsorption isotherms of the Saquinavir batches

The microcalorimetry was used to show how four different batches of Saquinavir can be differentiated using a stepwise increasing humidity above the powder cell. For each batch, three separate samples were used and each sample was tested on a three cycled run. The cumulative isotherm data for the different Saquinavir batches appeared to clearly distinguish between all batches (Figure 6.5).

Figure 6.5 Cumulative adsorption isotherm of all Saquinavir batches.

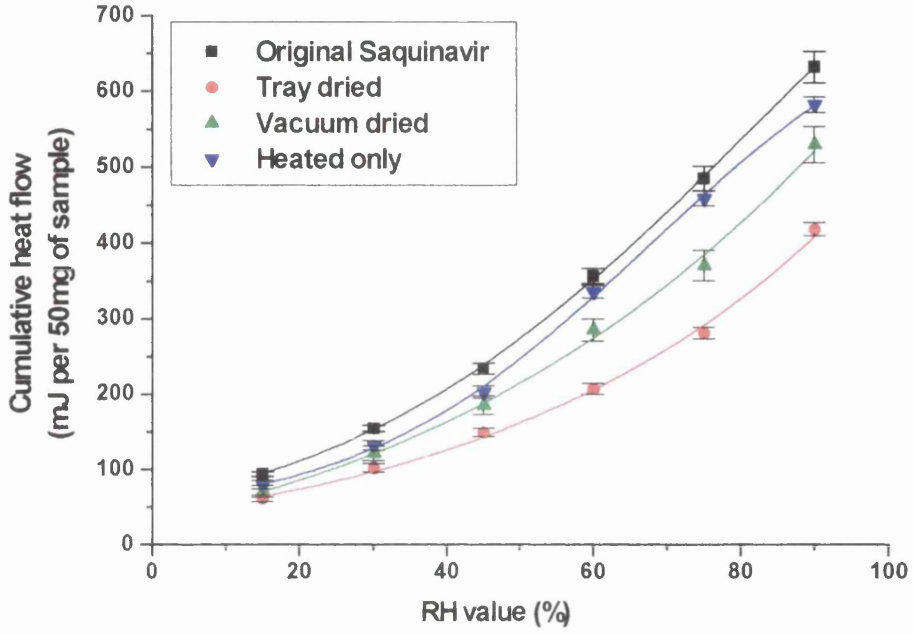

Although this was not the complete picture, since any alteration in surface area had to be taken into account. Table 6.2 indicates that the surface areas of the Saquinavir batches are not exactly identical, with the two batches that were exposed to water having a similarly lower value than the original and heated only samples.

Table 6.2 Surface areas of Saquinavir batches using BET analysis (Section 6.2.2).

Batch	Surface Area (m^2/g)	±
Original	0.914	0.109
Tray dried (b010)	0.697	0.002
Vacuum dried (b020)	0.712	0.018
Heated only (b030)	0.841	0.086

Figure 6.6 Cumulative adsorption isotherm of all Saquinavir batches (corrected for surface area variation).

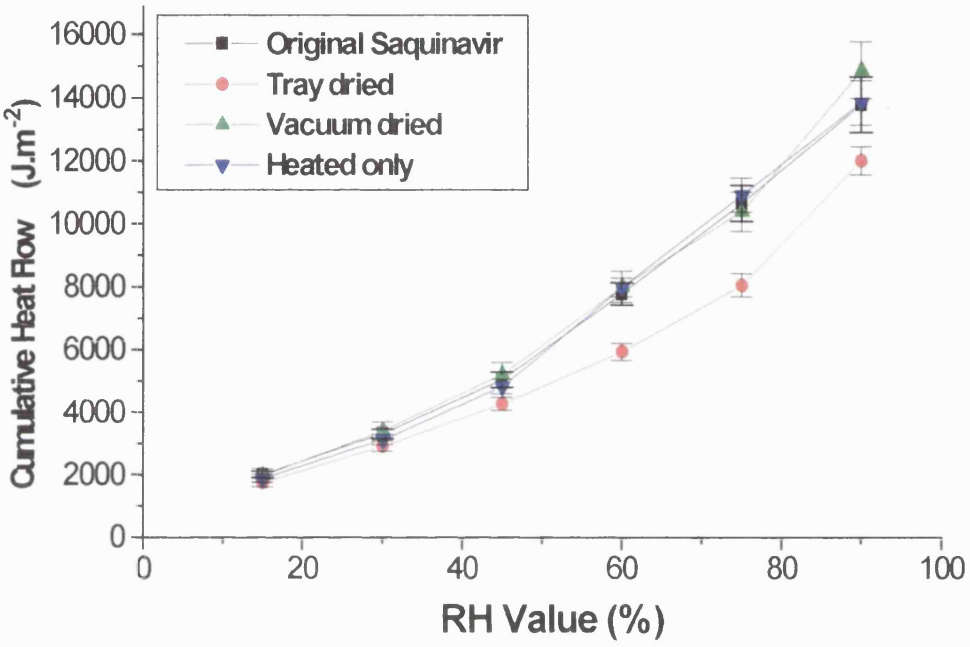

It is evident from Figure 6.6 that the tray dried Saquinavir remains greatly different to the original Saquinavir, although this method of analysis is unable to find any further differences between the other Saquinavir batches.

6.3.3 Non-cumulative adsorption isotherms of Saquinavir

The data was re-analysed plotting non-cumulative (individual points) adsorption isotherms.

Figure 6.7 Adsorption isotherm of tray dried batches (b0-10,11,12) compared to the original Saquinavir.

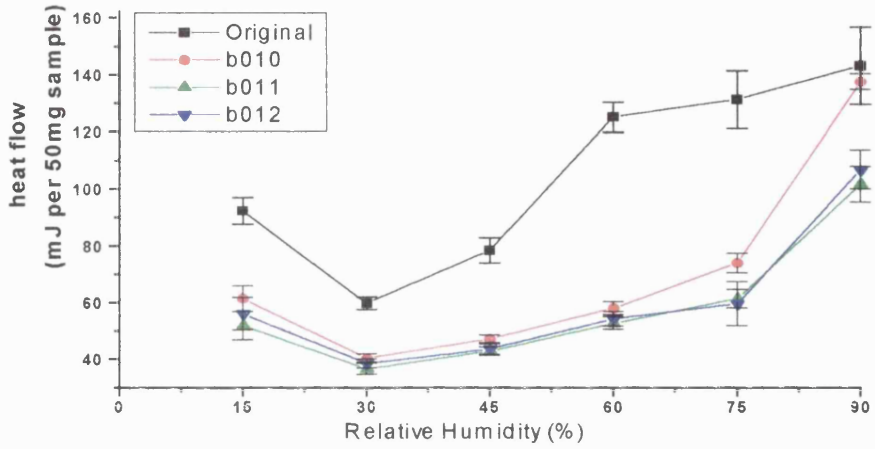

The three tray dried batches in Figure 6.7 have very similar isotherms, which are all quite separate from the original in shape, evolving far less energy than the original Saquinavir at each relative humidity. The process that they have undergone, although a very simple one involving a single wetting and drying cycle, has irreversibly changed the surface nature of the powder.

Figure 6.8 Adsorption isotherm of vacuum dried batches (b0-20,21,22) compared to the original Saquinavir.

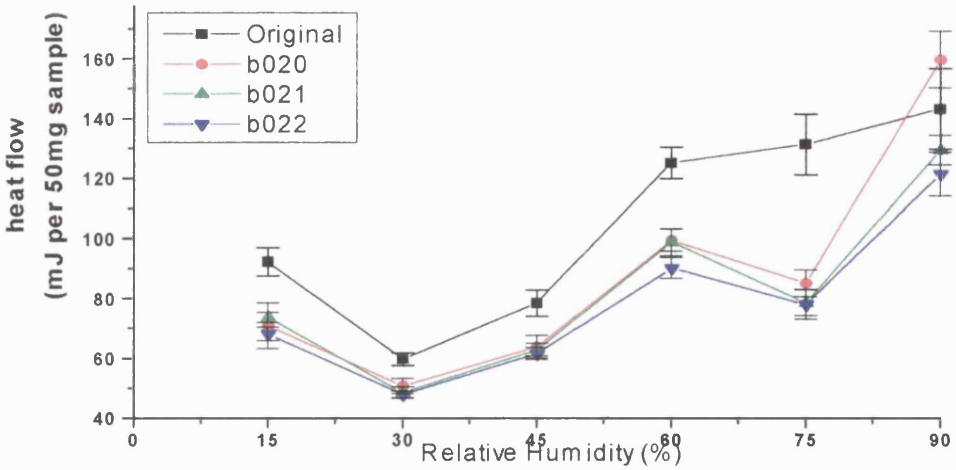

Figure 6.8 shows the three vacuum dried batches have very similar isotherms to each other, proving that the wetting and drying process produces reproducible transformations in the nature of the powder. They are also quite distinct from the original Saquinavir isotherm at each relative humidity apart from 90%.

Figure 6.9 Adsorption isotherm of heated batches (b0-30,31,32) compared to the original Saquinavir.

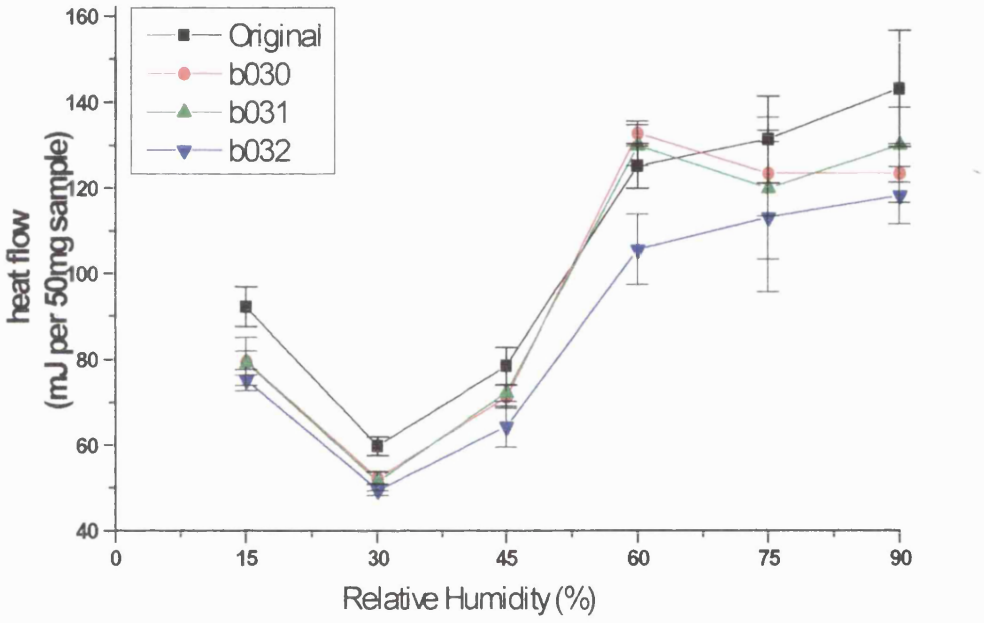

Figure 6.9 shows the three heated batches to be similar in nature to each other and the original Saquinavir, suggesting that the heating process alone was not enough in itself to induce a change in the powders' character.

Figure 6.10 Adsorption isotherm of original, tray dried (b001) and spin dried (b002) Saquinavir batches.

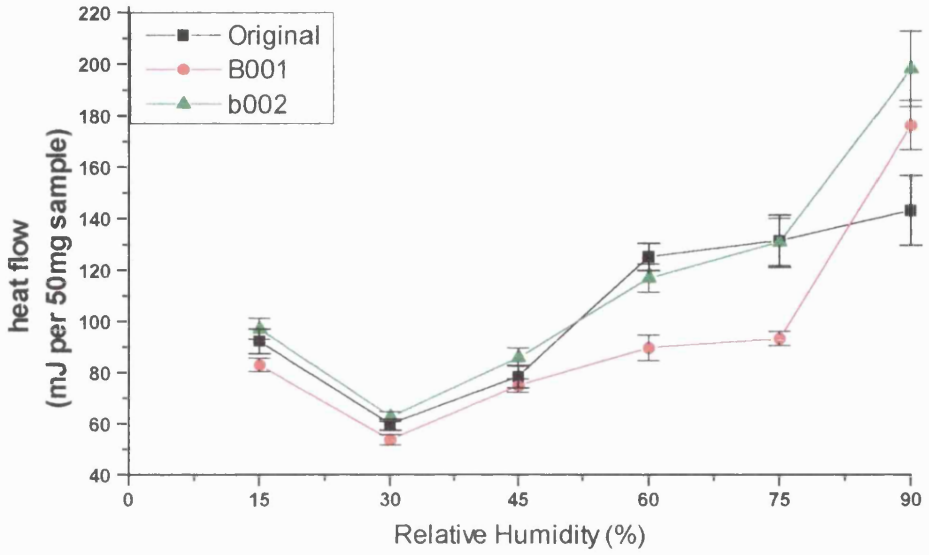

In Figure 6.10, the spin dried batch appears to be similar to the original apart from the 90% relative humidity, whereas the tray dried batch behaves in a very similar manner to the three main tray dried batches described earlier.

6.3.4 Summary of isotherm data

The three samples for each drying method were combined to give a simpler representation of their adsorption isotherms in Figure 6.11. It shows clearly that whilst the heated and original samples have a similar isotherm shape, although not overlapping at all points, both the vacuum dried and the tray dried batches yield isotherms that are quite different to each other and to the original. The tray dried isotherm is the most different.

Figure 6.11 Mean adsorption isotherm of Saquinavir batches.

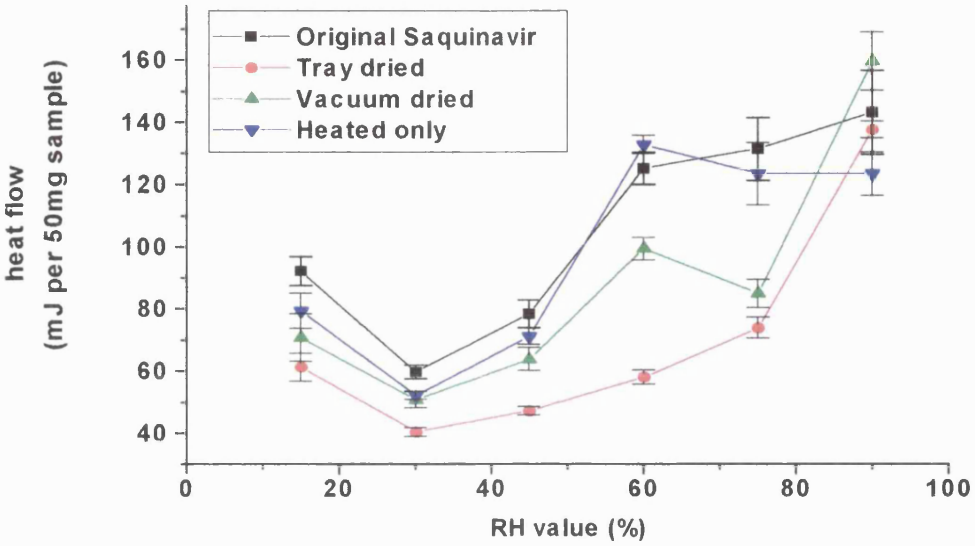

For a more quantitative evaluation of adsorption data, surface area measurements can be incorporated into the isotherms. Therefore it is possible to re-plot Figure 6.11 with the y-axis corrected for any change in surface areas between the batches.

Figure 6.12 Mean adsorption of Saquinavir batches (corrected for surface area variation).

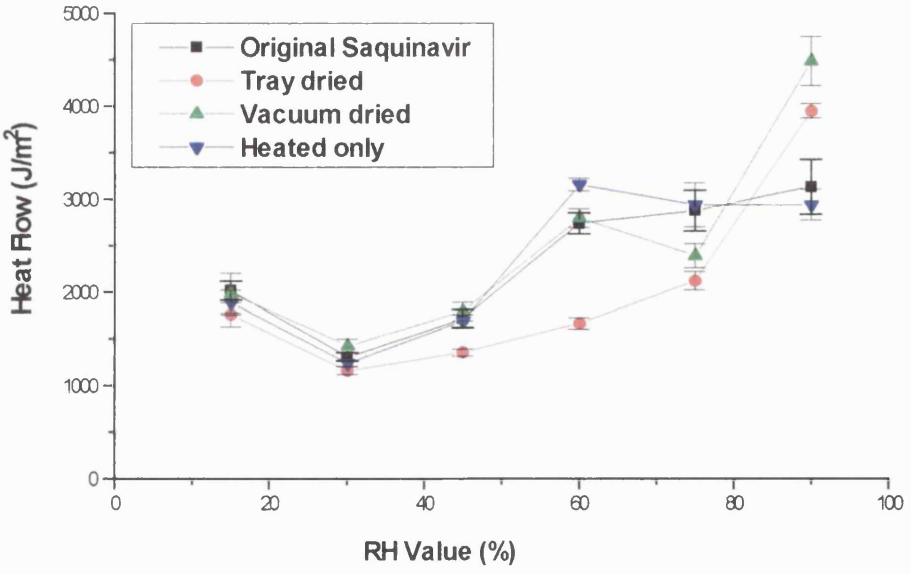

Figure 6.12 clearly shows that even with surface area alterations being taken into account, there is still a marked difference between the tray dried sample and the original. This difference is apparent from 45% humidity and above. The vacuum dried sample also differs from the original at the 75% and 90% humidity values, where the isotherm becomes more like the tray dried isotherm in character. The heated only isotherm is almost exactly identical to that of the original sample, except for a slightly differing value at 60% humidity.

This method of analysis was able to identify differences between the original, tray dried and vacuum dried Saquinavir batches. The vacuum dried Saquinavir difference would have been overlooked if only cumulative plots were studied.

6.3.5 Alterations in adsorption isotherms of Saquinavir with repeating cycles

Since each experiment involved three cycles of relative humidity change from 0% to 90%, a plot of the three individual isotherms can be made, which gives a precise indication of any change in the physical nature of the sample during the humidity stress process. It was found that in some cases there was a change in the amount of adsorption at a relative humidity of 75% and 90%, with no apparent change below that range. It is evident that as the original Saquinavir sample 'ages', the adsorption enthalpy at the 75% relative humidity range falls significantly over the three identical cycles (Figure 6.13). There is no significant alteration in adsorption enthalpy at any of the other humidity points during the experiment.

Figure 6.13 Individual adsorption isotherm of original Saquinavir.

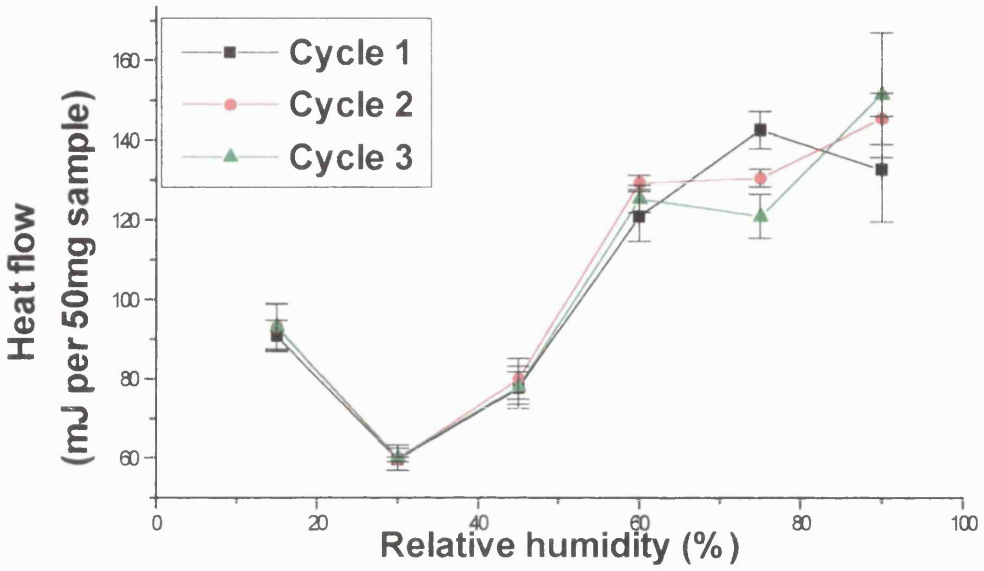

Figure 6.14 Individual adsorption isotherm of tray dried Saquinavir (b010).

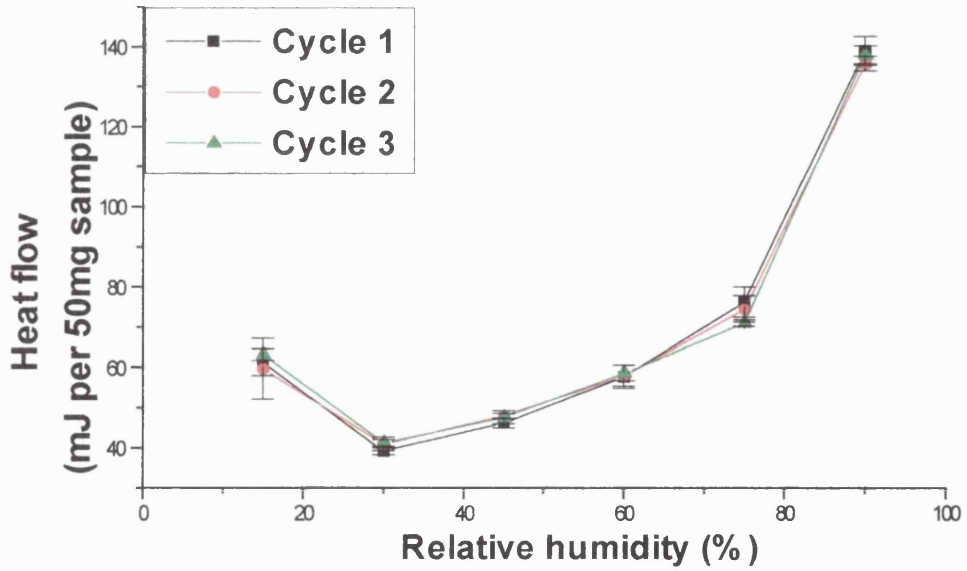

The tray dried sample (b010) does not appear to be affected at all by the three humidity cycles, which suggests that it the powder is in a much more stable form than the original Saquinavir batch (Figure 6.14).

Figure 6.15 Individual adsorption isotherm of vacuum dried Saquinavir (b020).

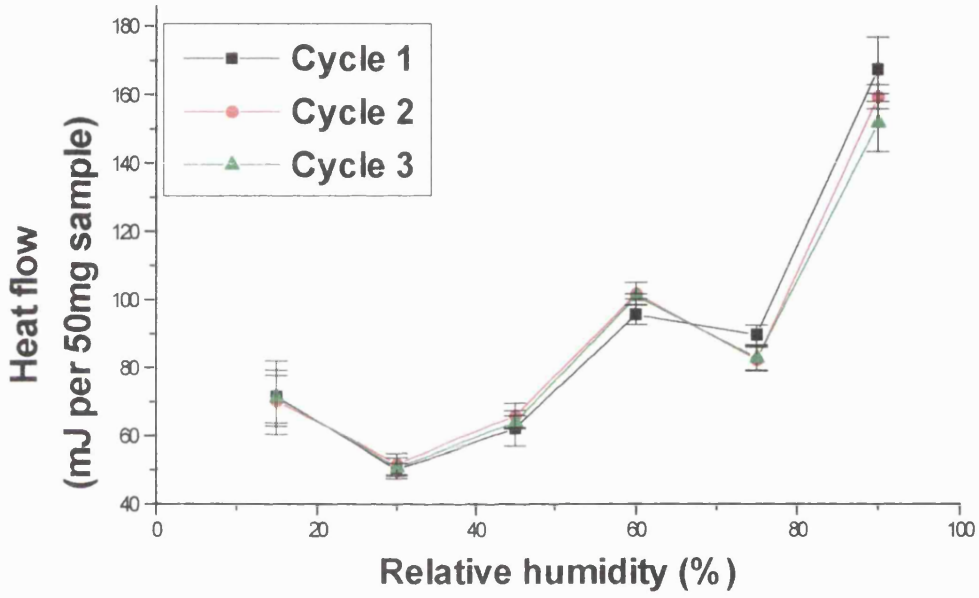

The vacuum dried Saquinavir (b020) is affected by the cycling process to a small degree, where there was a lower adsorption enthalpy at 60% and a higher adsorption enthalpy at 75% in the first cycle compared to the others (Figure 6.17). In both cases, the change was small but significant.

Figure 6.16 Individual adsorption isotherm of heated Saquinavir (b030).

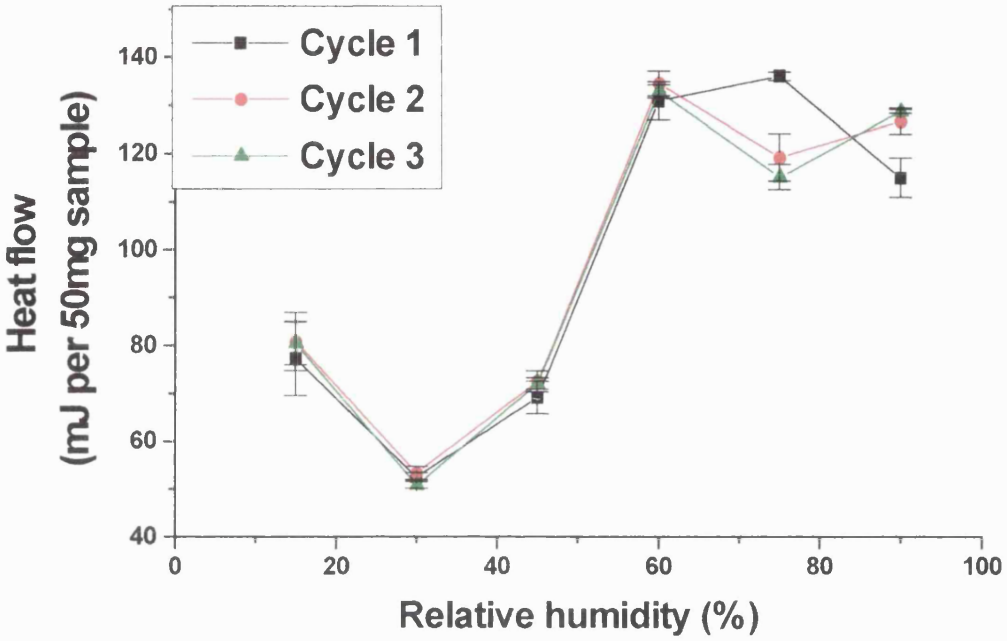

The heated Saquinavir (b030) has a very similar isotherm to the original Saquinavir, where at 75% RH there is a marked fall in adsorption enthalpy after the first cycle (Figure 6.16). In addition, there was an increase in adsorption enthalpy at 90%.

6.3.5.1 Reproducibility

All the graphs from Section 6.3.4 were reproduced with two more samples from each method of preparation, those being (tray dried) b011, b012, (vacuum dried) b021, b022 and (heated only) b031, b032. They all gave the same degree of changes in adsorption enthalpy as the batches described previously, giving a good indication of the method's and the microcalorimeter's excellent reproducibility.

6.4 Conclusions

The adsorption isotherms of the model powders showed that it is important to include any variations in surface area when comparing different powders, and whilst this should be also be taken into account with different batches of the same powder, the Saquinavir batches' isotherms were not altered to such a degree that the original conclusions were made invalid. Those being the tray dried and vacuum dried batches were significantly different to each other and to the original Saquinavir, whilst the heated only batch had not altered from the original state (section 9.2). In addition, the tray dried Saquinavir batch isotherm was similar in shape to all the model powders' type II adsorption isotherms. The original and heated Saquinavir had similar isotherms to each other, whilst the vacuum dried Saquinavir presented an isotherm that had the original character from 0% to 60% humidity and the tray dried character from 75% to 90% humidity. The vacuum dried Saquinavir may have been partly altered from the original state towards that of the tray dried Saquinavir (section 9.2). The presence of water would appear to be necessary to achieve this conversion, since the heated only Saquinavir behaved exactly like the original sample. An elevated temperature may quicken the process, since the vacuum dried Saquinavir was only partially changed after being dried at 80°C instead of 160°C as in the case of the tray dried Saquinavir.

Further analysis was achieved by plotting separate isotherms during the three cycles from 0 to 90 % humidity of the Saquinavir powders. It should be noted that the other five model powders did not alter in any way with cycling and the results were not included in this chapter. Tray dried Saquinavir yielded a similar isotherm to the model powders with repeated cycles. It was found that the original and heated Saquinavir isotherms increased slightly at 60%, fell significantly at 75% and increased at 90 % with cycling. This ageing process with cycling appears to be moving their isotherms towards the tray dried Saquinavir isotherm shape. The vacuum dried Saquinavir isotherms decreased significantly at 75% and at 90 % humidity with cycling, again moving the isotherm towards the tray dried isotherm shape. The 60 % value does not appear to change a great deal, possibly because the Saquinavir requires a higher temperature in the presence of 60 % humidity for a change to occur.

Isothermal microcalorimetry has shown great sensitivity with a high degree of accuracy, able to distinguish between different powders and small batch to batch variation of the same powder.

Chapter 7

Dynamic Vapour Sorption

7 Dynamic Vapour Sorption

7.1 Introduction

The Dynamic Vapour Sorption (DVS) apparatus was situated inside a thermal incubator which maintained the apparatus at a constant temperature of 25°C throughout the experiment, and the whole apparatus is situated in a temperature controlled room (18°C ±1), below that of the incubator enabling it to keep within a very narrow temperature range. The dry nitrogen flow was controlled by a needle valve keeping the gas pressure between 140-210 $kN.m^{-2}$, while the computer program controlled the flow more accurately, dividing it up into dry nitrogen and water saturated nitrogen (passed through a water reservoir), the ratio of dry to wet flow depending on what relative humidity was specified by the computer program (0% to 98% ± 0.4). There is also a constant flow of dry nitrogen through the balance head, the purge gas, that prevents water vapour entering the balance head, preventing any mass drift that would otherwise occur. Inside the DVS there is a Cahn microbalance able to weigh masses varying between 1 and 1500mg (±0.001).

The DVS apparatus allows the water sorption (absorption, adsorption and desorption) kinetics to be studied in detail producing sorption isotherms over a range of relative humidities. Adsorption will usually result in a less than 1% mass change whilst water absorption will be a far greater at around 20%. The free energy of adsorption, ΔG_{dvs}, of water vapour to a solid powder can be derived from the two equations below.

$$K_{ad} = \frac{b}{P_o}$$ Equation 7.1

b - No. of water molecules sorbed per gram

P_0 - Saturated water vapour pressure at 25°C

$$\Delta G_{dvs} = -RT\ln K_{ad}$$ Equation 7.2

Figure 7.1 Schematic diagram of the DVS apparatus.

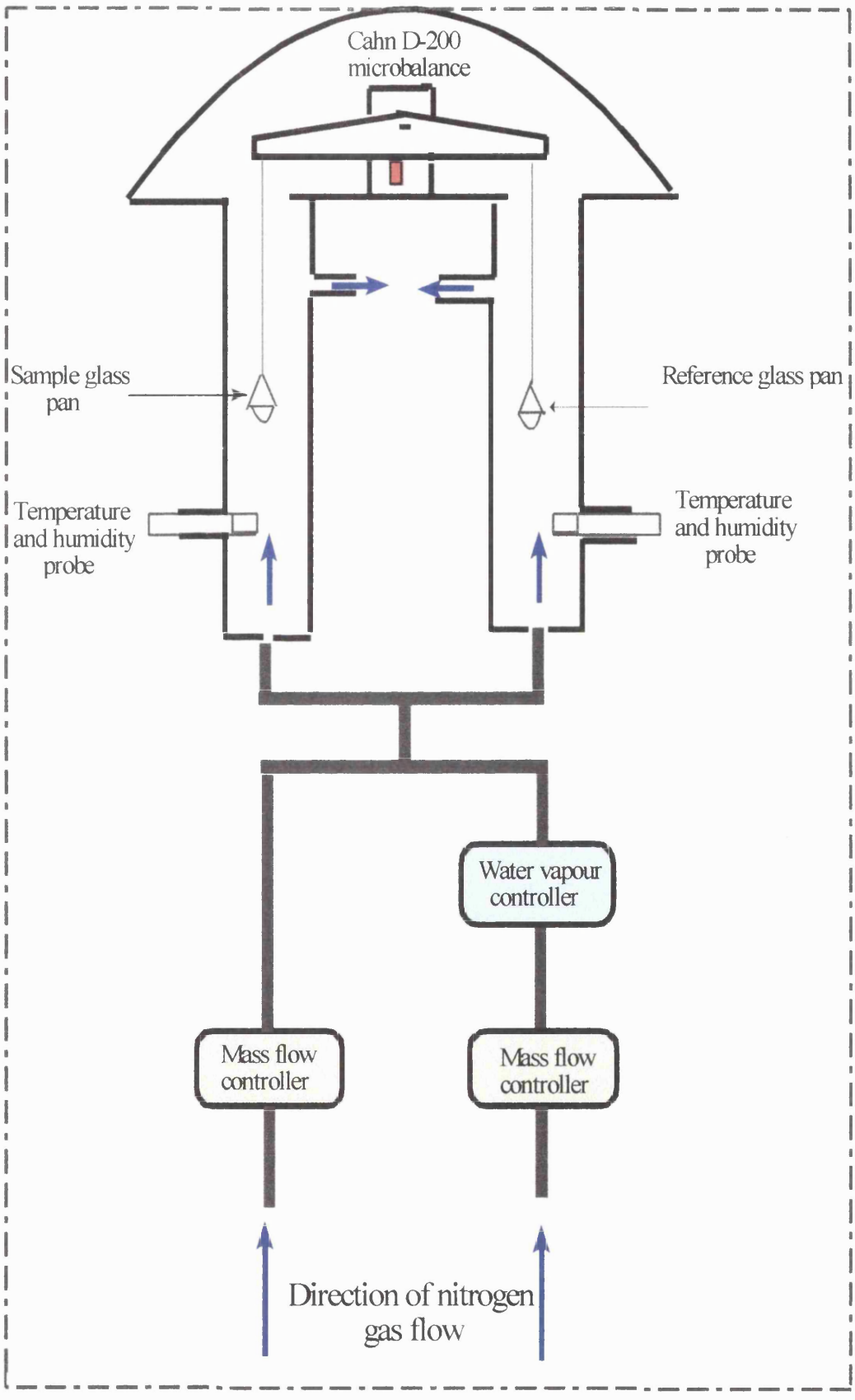

7.2 Method

The DVS 2 Automated Water Sorption Analyser is designed to be able to characterise the water sorption properties of materials, in this case pharmaceutical powders, ranging from 5 to 1500 mg, with a resolution of 0.1 μg.

Figure 7.2 Diagrammatic representation of DVS set-up.

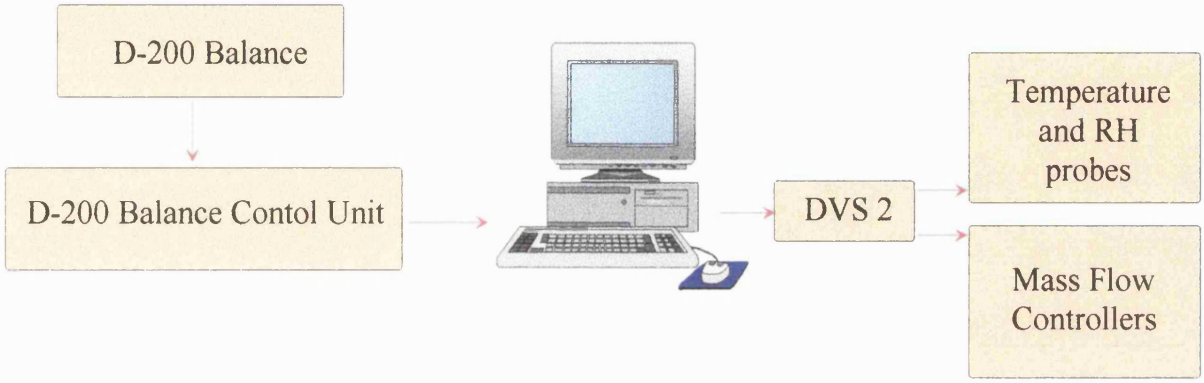

7.2.1 Validation of relative humidity

It is necessary that the relative humidity within the DVS is equivalent to that which the computer specifies. The partial vapour pressure of water above a saturated salt solution in equilibrium with its surroundings is constant at a particular temperature. The method developed uses a selection of saturated salt samples to quickly and easily evaluate the accuracy of the relative humidity produced, which should be carried out on a regular basis to ensure the correct humidity control of the DVS.

7.2.2 Calibration

The DVS was calibrated monthly with a 100mg calibration weight. The Cahn microbalance employs a magnet suspended in an electromagnetic coil. As the mass suspended changes, the current passing through the coil has to change to maintain the neutral positioning of the balance arm. The amount of current required to achieve this is directly proportional to the force on the balance arm.

7.2.3 Cleaning

The glass pans, both sample and reference, are cleaned prior to use with distilled water, then rinsed with ethanol and left on the DVS to dry by evaporation for 15 minutes. The DVS must be left open to the environment until all the ethanol has evaporated off, since the humidity probes within the DVS are easily damaged with volatile vapours such as ethanol.

7.2.4 Static

Before the test powder is loaded onto the sample pan, the DVS is closed and the relative humidity within is increased to 95% for at least 10 minutes, to ensure that any static on the glassware is dissipated before the experiment. If the powder being tested has its own static build up, this can be eradicated using a commercial static gun (e.g. Zerostat 3). Static build up on either the glassware or the powder itself will result in a slow but continuous mass drift in one direction either above or below the baseline, which can interfere with certain hydrophobic powders that tend to adsorb minimal amounts of water.

7.2.5 Loading sample

Approximately 70 mg of the test powder was carefully placed onto the sample pan and the DVS closed to the outside atmosphere. After a few minutes equilibrating, the true mass can be noted from the computer display. The experiment involved a stepwise increase and decrease in relative humidity over the sample and control pans of 15% from 0% to 90% and back to 0% again and then repeated twice more.

Figure 7.3 Graphical representation of experimental protocol.

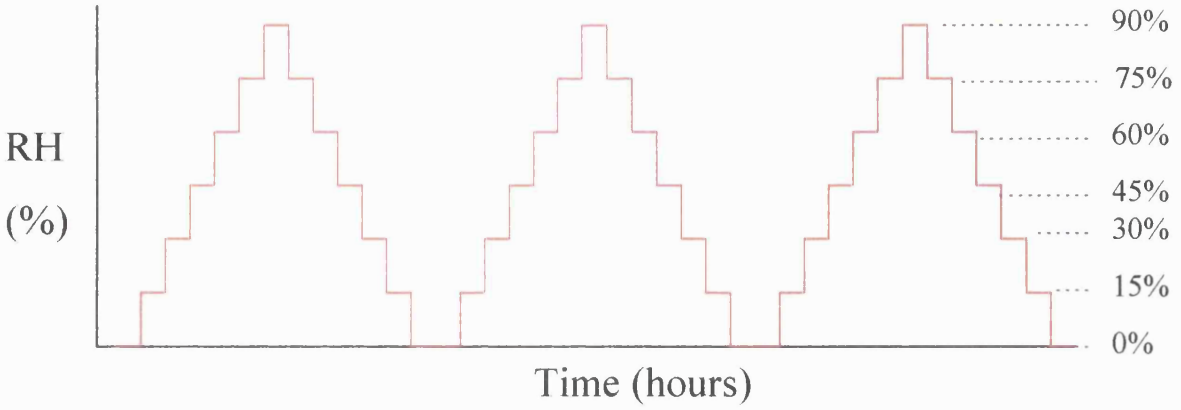

7.3 Results and discussion

7.3.1 Humidity validation

The DVS was validated using seven salts, presented both as saturated salt solutions and solid crystals.

Table 7.1 Deliquescent relative humidities of a range of crystalline salts.

RH Value	KOH	LiCl	$MgCl_2$	K_2CO_3	NaCl 98%+	KCl	K_2SO_3
Solid	9.2	11.6	31.9	43.0	74.1	82	96.5
$SD_{n-1\ (n=3)}$	0.2	0.1	0.1	0.0	0.1	0.0	0.1
Sat. Soln.	9.4	12.0	31.3	43.0	74.2	82	96.4
Nyqvist, 1983	8-9	11.3	32.8	43.8	75.3	84.3	97.3

The dry crystals produced consistent critical relative humidities with small standard deviations that were very similar to those of the saturated solutions for each salt used. In addition, the critical relative humidity values for both solid crystals and saturated solutions were closely comparable with literature values (Nyqvist, 1983).

It can be concluded that the use of saturated salt solutions and dry salt crystals allows the validation of experimental data and by extrapolation the measurement of the critical RH for an unknown material can be undertaken with ease and accuracy using this technique.

7.3.2 Adsorption isotherms of five model powders

The experimental protocol was first developed and evaluated using Salicylic acid, Ethacrynic acid, Ibuprofen, Caffeine and Theophylline.

Figure 7.4 Adsorption isotherm of Caffeine.

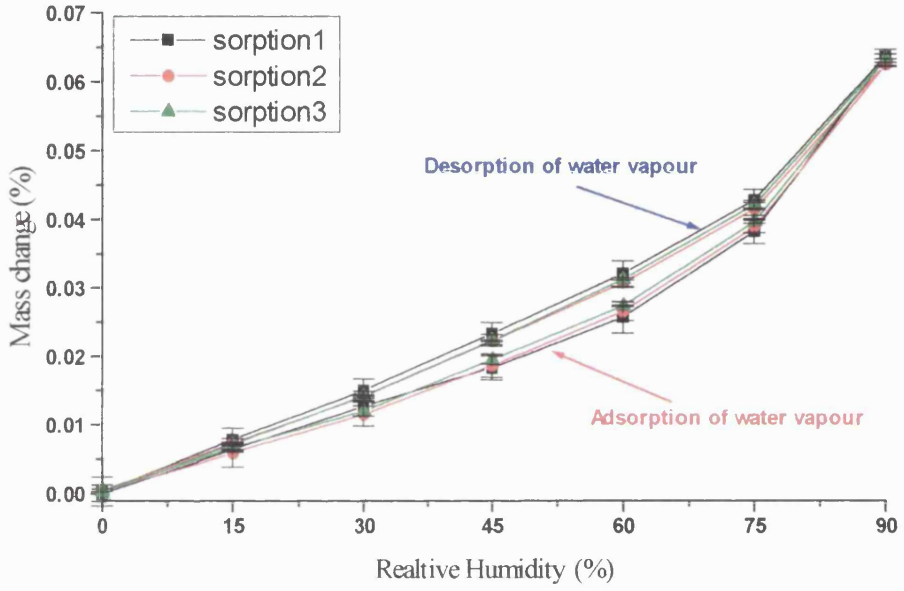

The cumulative adsorption isotherm of Caffeine (Figure 7.4) enables the following deductions to be made:-

a) No water vapour is absorbed by Caffeine over the whole humidity range.

b) The amount of water adsorption does not vary with repeated cycles, therefore the sample remains unchanged throughout the experiment and no change in the surface nature has occurred.

Figure 7.5 Adsorption isotherm of Theophylline.

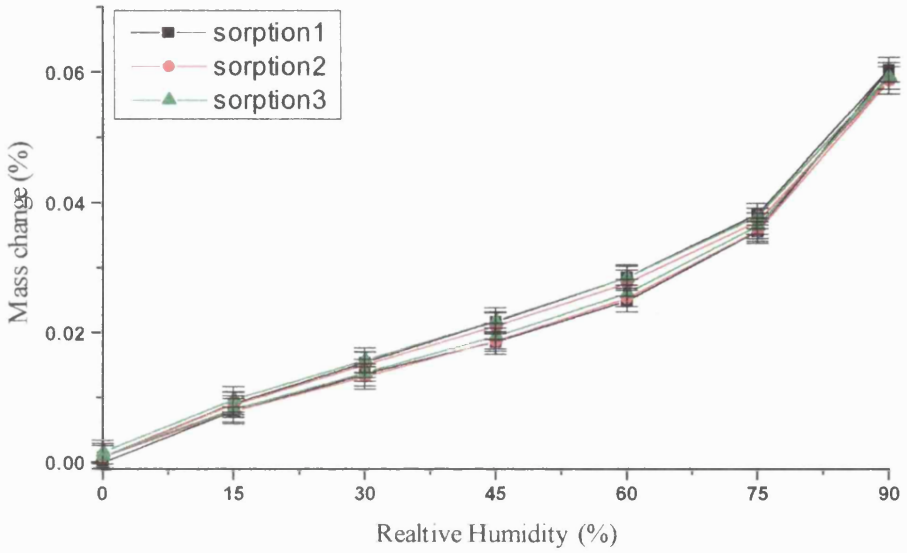

The adsorption isotherm of Theophylline (Figure 7.5) is very similar to that of Caffeine, and the same conclusions can be taken from it, in addition to the fact that the difference between the adsorption and desorption (hysteresis) is much smaller in this case.

Figure 7.6 Adsorption isotherm of Ethacrynic acid.

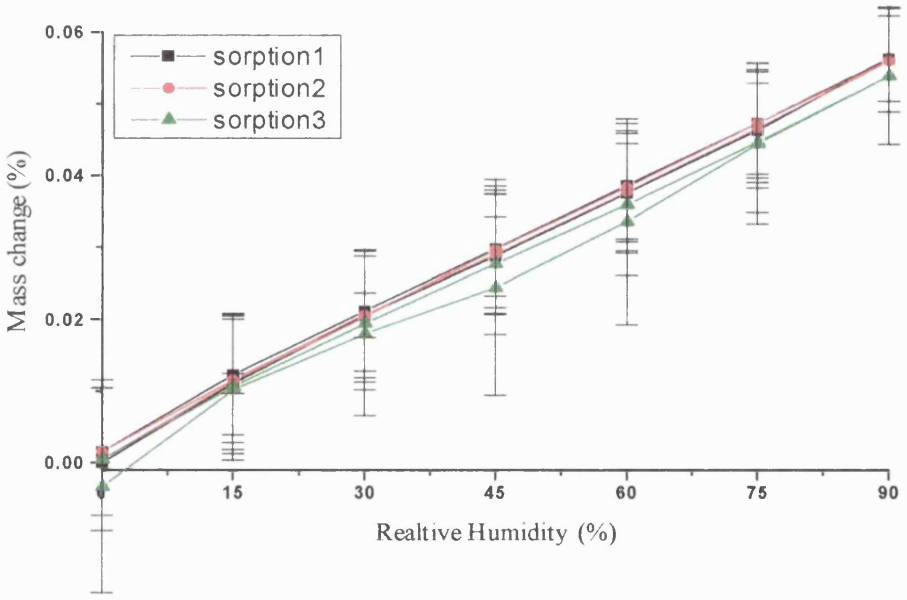

The adsorption isotherm for Ethacrynic acid (Figure 7.6) is more linear in shape than the previous two powders. The error margin appears to be large, although it must be borne in mind that the total mass change was only 0.06% of the total mass, therefore with a mass of 100mg, the mass increase is only 60μg with an error margin of ±10μg.

Figure 7.7 Adsorption isotherm of Ibuprofen.

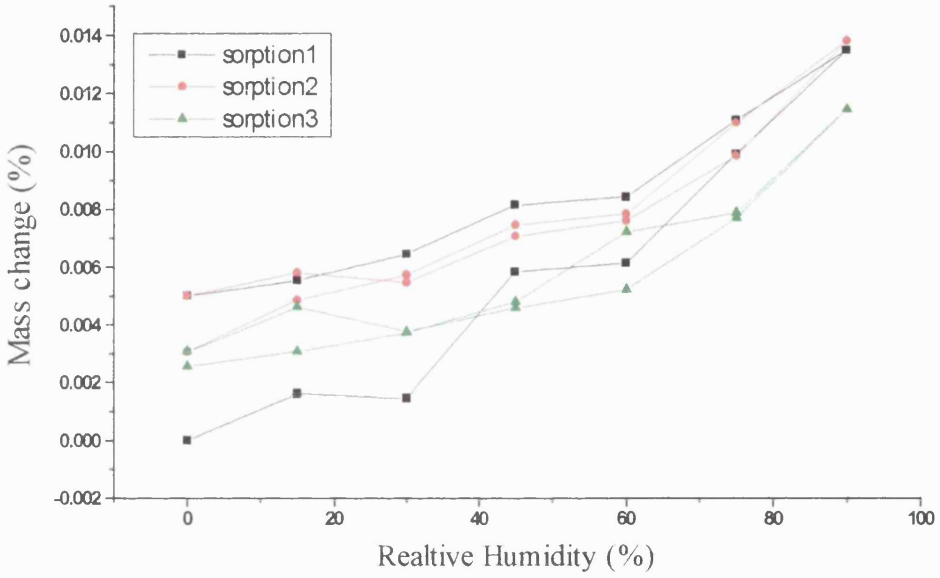

Ibuprofen only adsorbed a very minute amount of water, 0.0012% at 90% relative humidity. Salicylic acid did not adsorb any water vapour at all due to its small surface area and very high hydrophobic nature. Both powders were successfully differentiated from each other and the other three model powders, but due to their isotherms being so small they were not analysed further in Section 7.5.

Figure 7.8 Adsorption isotherms of model powders (corrected for surface area variation).

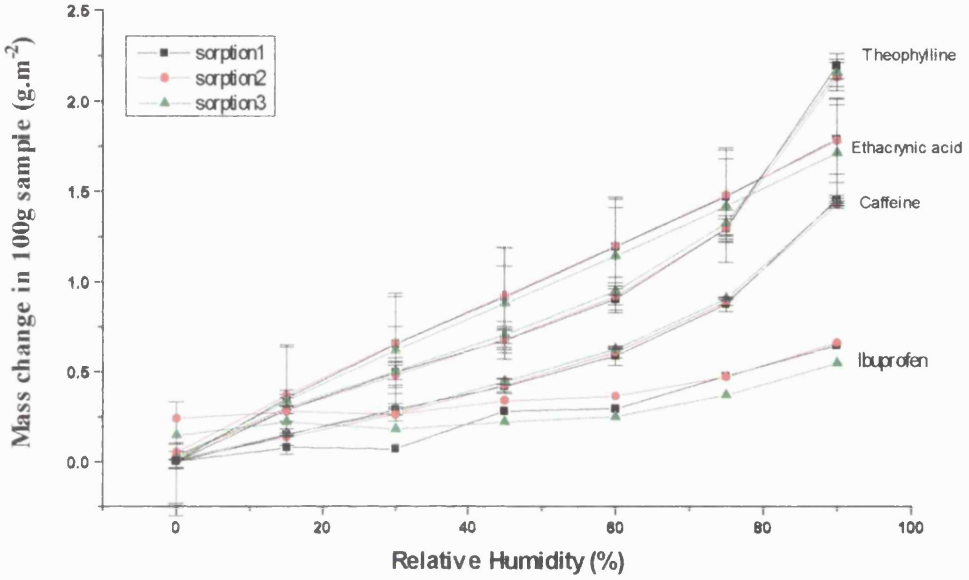

Figure 7.8 shows that the four model powders all have different isotherms even after their specific surface areas have been taken into account. It is interesting to note that whilst Caffeine and Ibuprofen have very similar adsorption isotherms with the microcalorimetry, the DVS shows a distinct difference in the mass of water uptake.

7.3.3 Adsorption isotherms of Saquinavir batches

Each Saquinavir batch had three different samples analysed within the DVS, each sample being subjected to three cycles of 0% to 90% relative humidity.

Figure 7.9 Adsorption isotherm of Saquinavir (original sample).

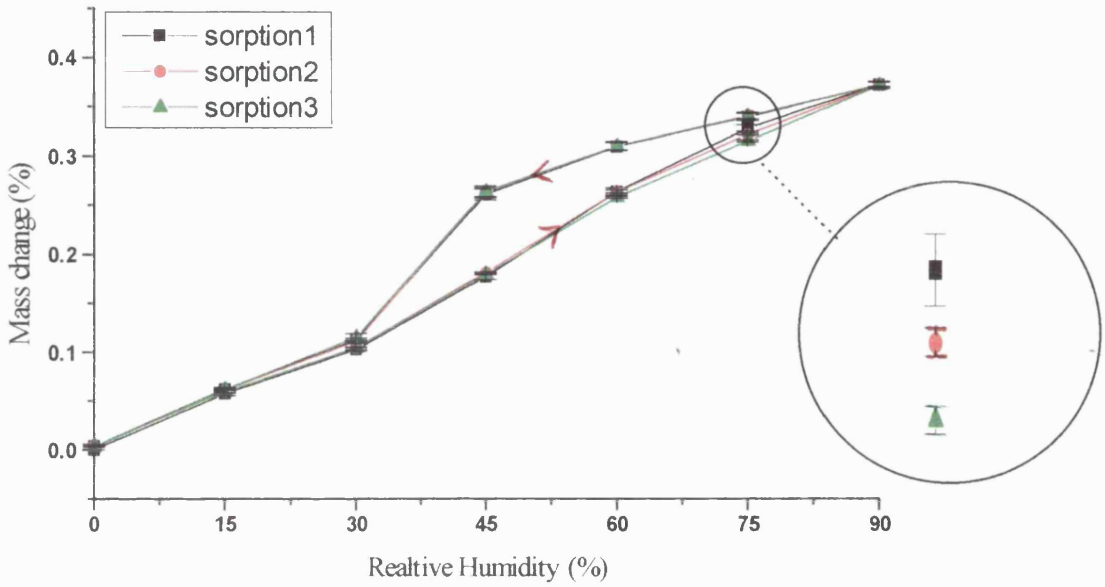

The original Saquinavir sample exhibits a significant decrease in water vapour uptake at the 75% RH upon repeated cycling (Figure 7.9).

Figure 7.10 Adsorption isotherm of tray dried Saquinavir (b010).

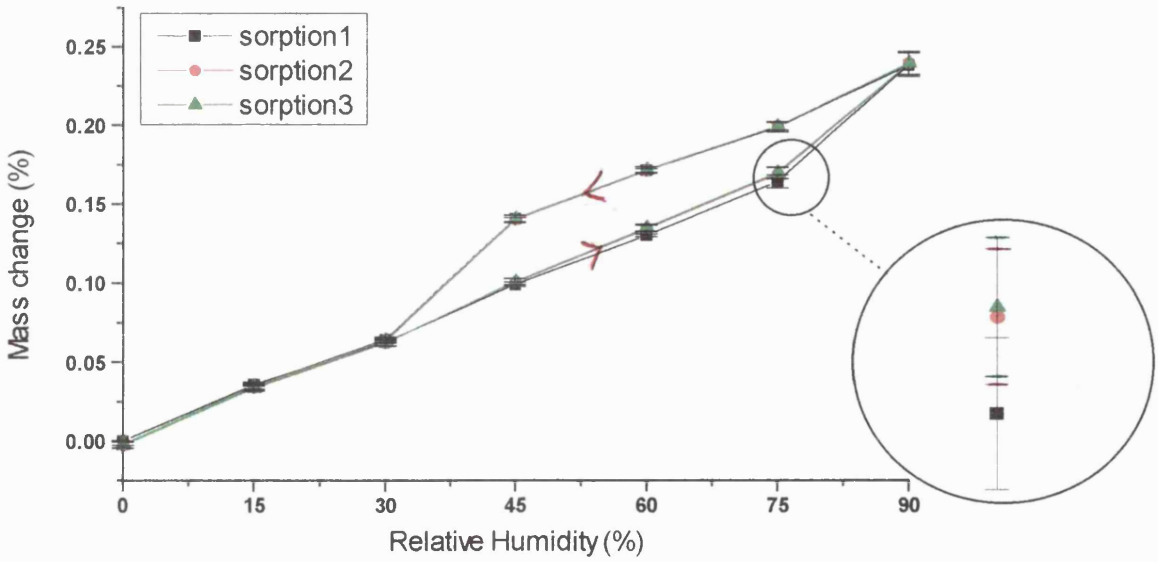

The tray dried sample (Figure 7.10) does not seem to have a significant alteration in its adsorption behaviour with repeated cycles, although at 75% RH the first cycle appears to tend to take up slightly less water vapour than the further cycles. It is however very different to the original Saquinavir in both the amount of mass increase being smaller and the overall shape of the isotherm.

Figure 7.11 Adsorption isotherm of vacuum dried Saquinavir (b020).

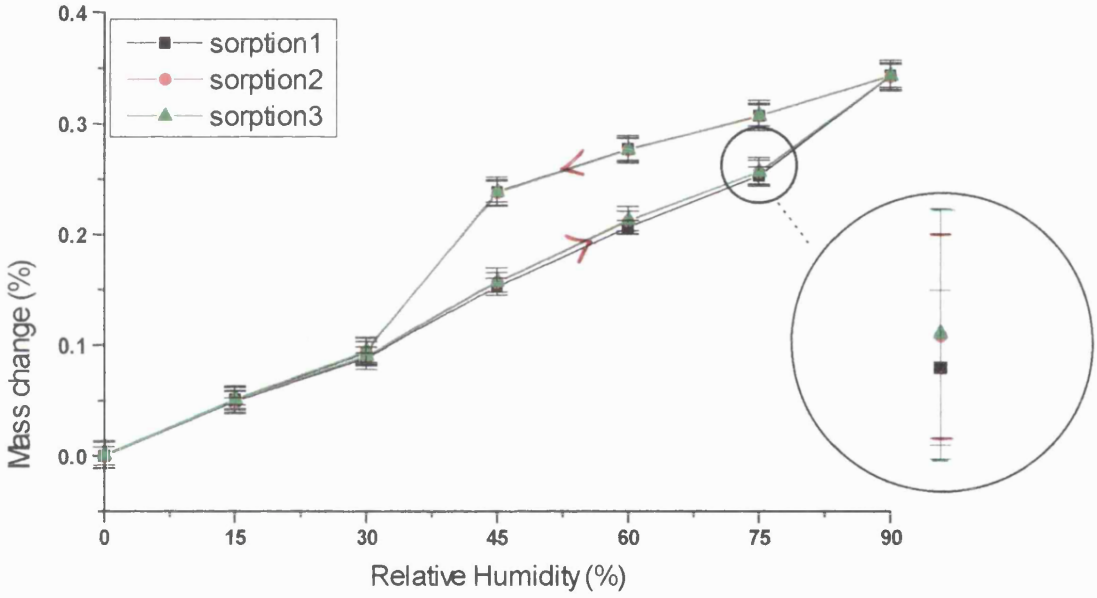

The vacuum dried isotherm (Figure 7.11) is similar in shape to the tray dried isotherm, and the vapour uptake at 75% RH does not change over the three cycles. The isotherm is similar to the tray dried batch in that it has a smaller total mass increase and an altered isotherm shape to the original Saquinavir. The decreased mass adsorption is consistent with the reduced surface area of the tray and vacuum dried batches compared to the original Saquinavir.

Figure 7.12 Adsorption isotherm of heated Saquinavir (b030).

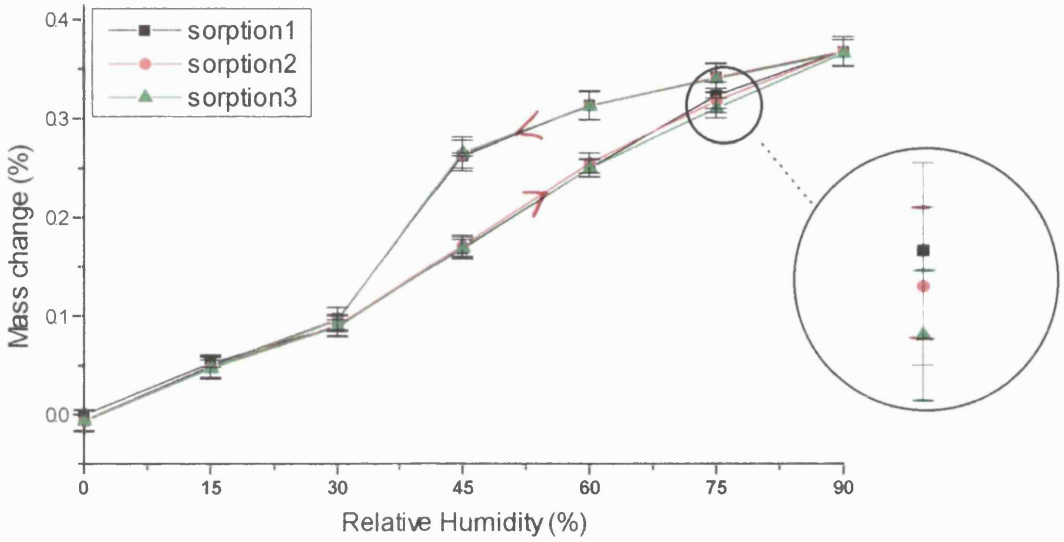

The heated Saquinavir has an isotherm that is very similar in shape and magnitude to the original Saquinavir (Figure 7.12). Although there is no significant decrease in vapour uptake at 75% RH with cycling, there does appear to be a trend in that direction, similar to the original Saquinavir.

Figure 7.13 Adsorption isotherm of tray dried Saquinavir (b001).

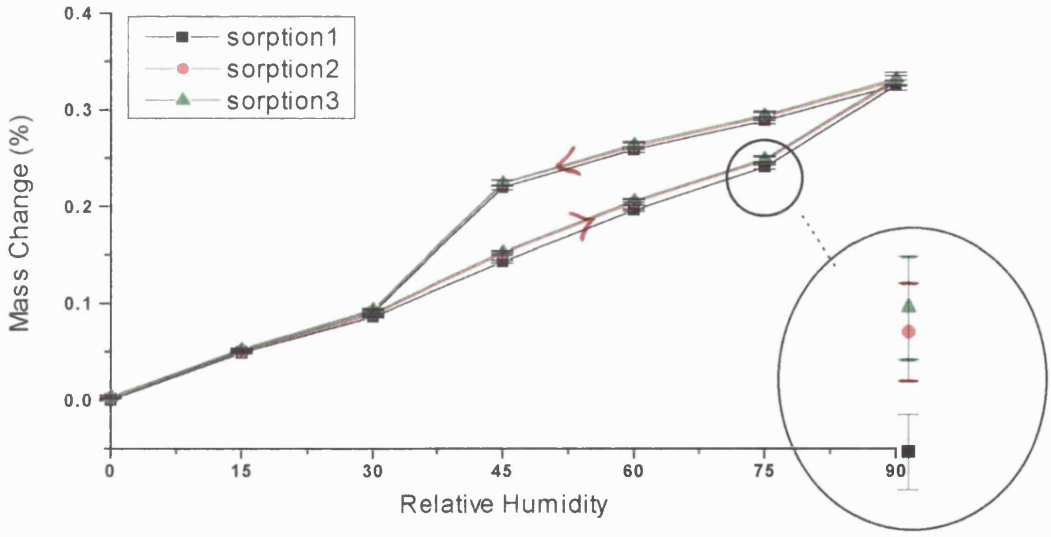

The tray dried sample in Figure 7.13, as with batch 010, does not seem to have a significant alteration in its adsorption behaviour with repeated cycles, although at 75% RH the first cycle appears to tend to take up slightly less water vapour than the further cycles. It is very different to the original Saquinavir in both the amount of mass increase being smaller and the overall shape of the isotherm.

Figure 7.14 Adsorption isotherm of spin dried Saquinavir (b002).

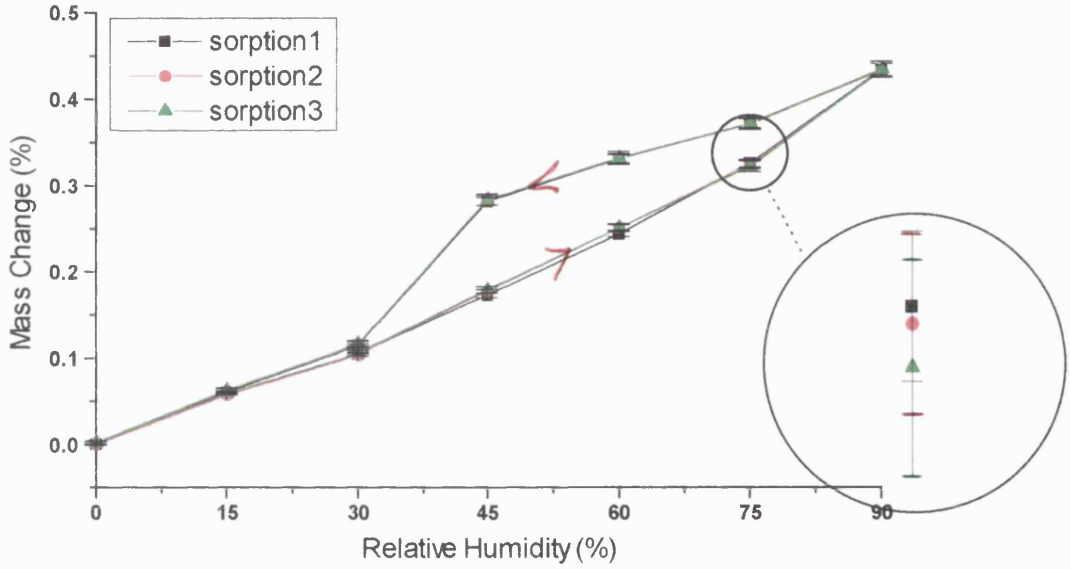

The spin dried Saquinavir shows no significant changes over the three cycles. It is similar in shape to the tray dried isotherm, and the vapour uptake at 75% RH does not change with time.

The following Figures (7.15 and 7.16) are the adsorption and desorption isotherms of the Saquinavir batches after their different surface areas have been taken into account. Both figures show that the tray dried batch (b010) is very different in its adsorption isotherm profile even with the incorporation of surface area correction.

Figure 7.15 Adsorption isotherm of Saquinavir batches (corrected for surface area variation).

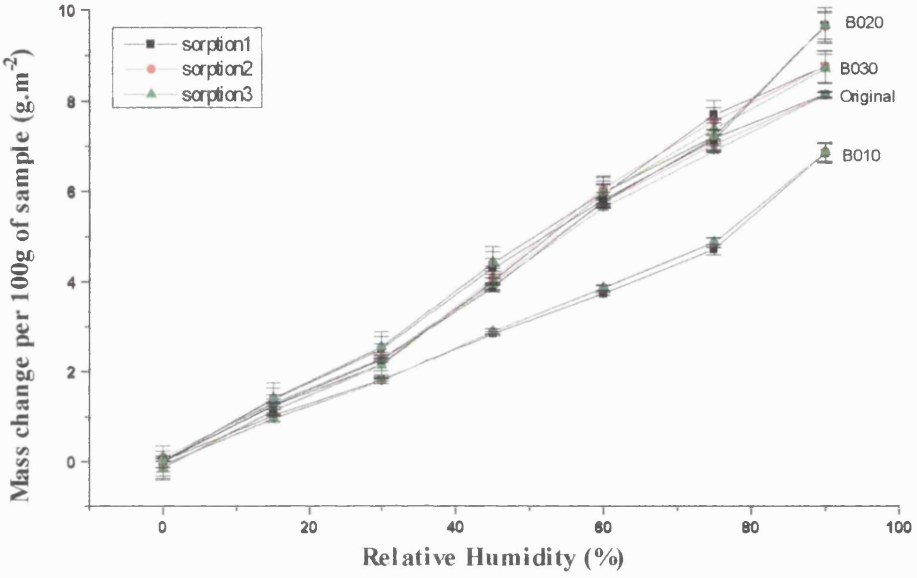

Figure 7.16 Desorption isotherm of Saquinavir batches (corrected for surface area variation).

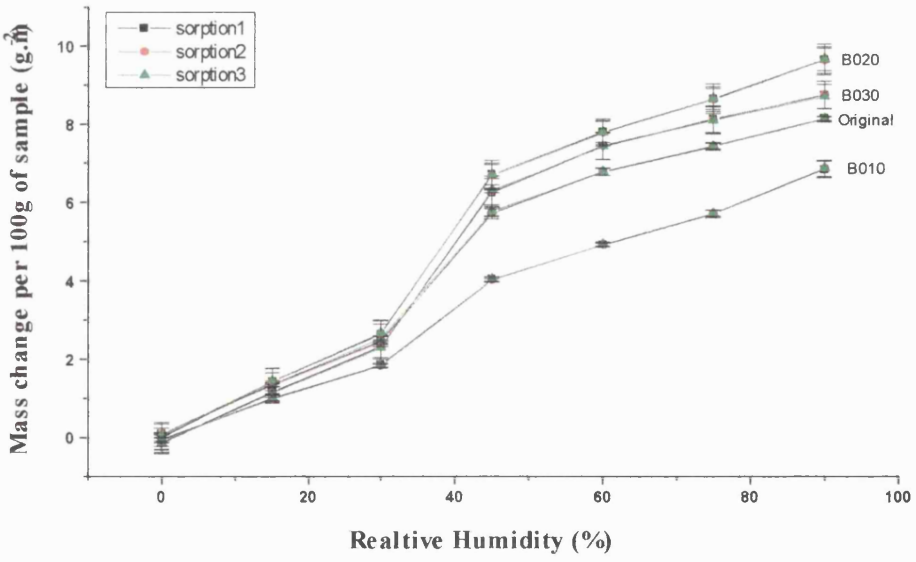

In addition, the vacuum dried batch may only differ from the original Saquinavir at 90% RH but the desorption isotherm is significantly different between 40% and 90% RH. This method of presenting data has been able to distinguish between the water treated batches of Saquinavir and the original.

7.3.4 Hysteresis measurements

The graphical analysis of sorption hysteresis was able to more clearly indicate any differences between batches of the same material.

Figure 7.17 Sorption hysteresis of original Saquinavir.

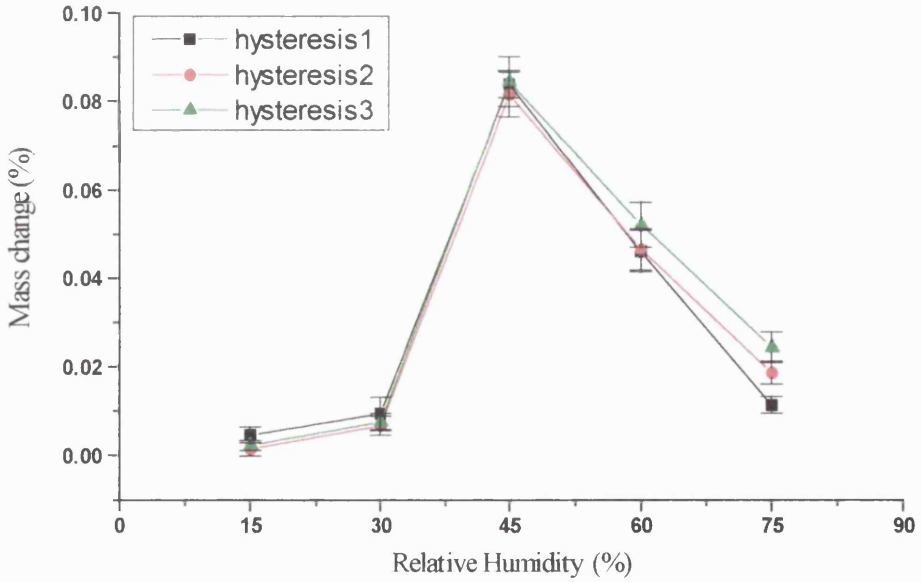

Figure 7.17 indicates there is a significant increase in hysteresis at 75% RH, as the water vapour uptake is reduced, with repeated cycles.

Figure 7.18 Sorption hysteresis of tray dried Saquinavir (b010).

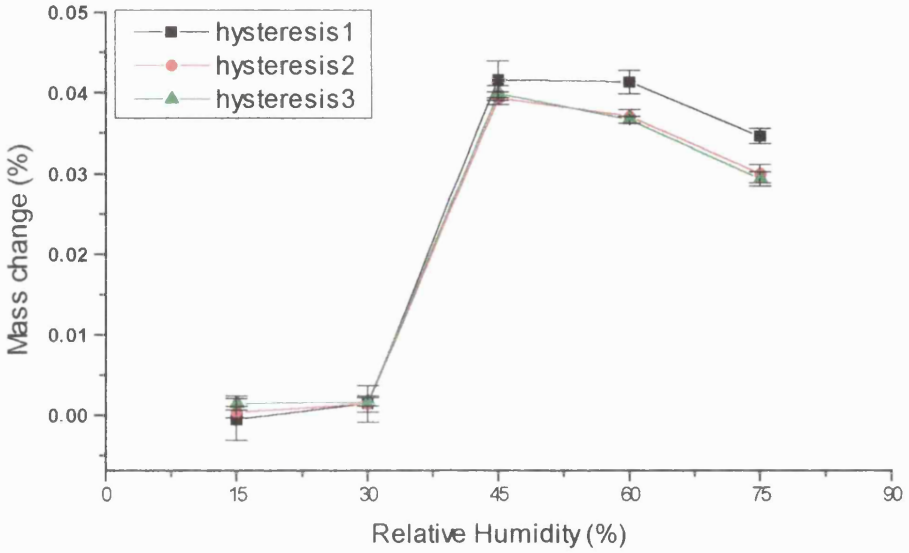

The tray dried Saquinavir (Figure 7.18) has a small but significant increase in water vapour uptake at both the 60% and 75% RH level after the first cycle, in addition to having a differently shaped hysteresis to the original Saquinavir.

Figure 7.19 Sorption hysteresis of vacuum dried Saquinavir (b020).

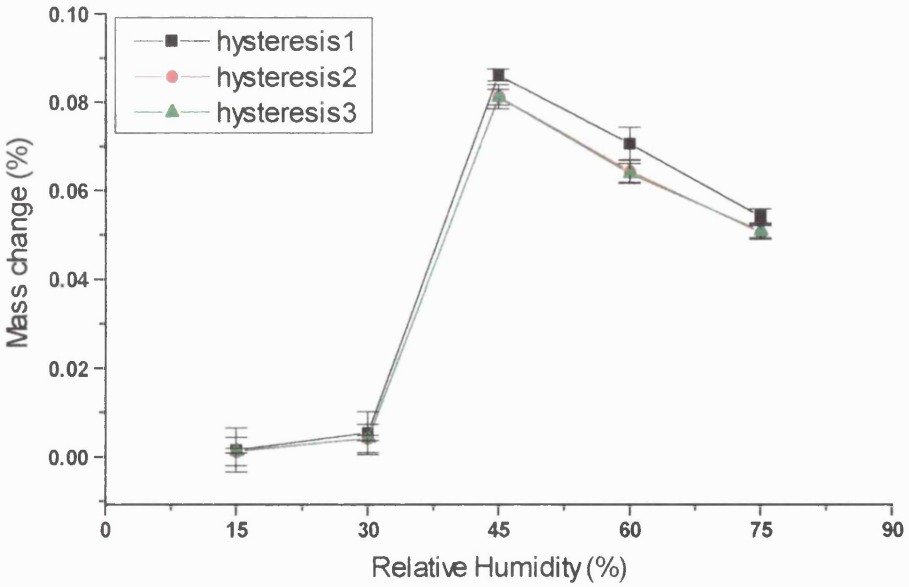

The vacuum dried Saquinavir (Figure 7.19) is almost identical in shape to the tray dried sample, again with a small increase in water vapour uptake at the 60% and 75% RH levels.

Figure 7.20 Sorption hysteresis of heated Saquinavir (b030).

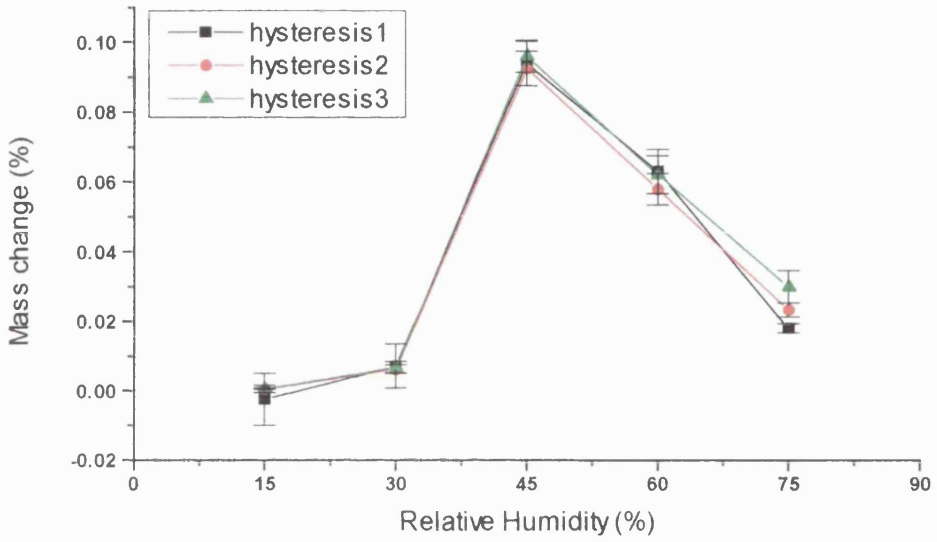

Figure 7.21 Sorption hysteresis of spin dried Saquinavir (b002).

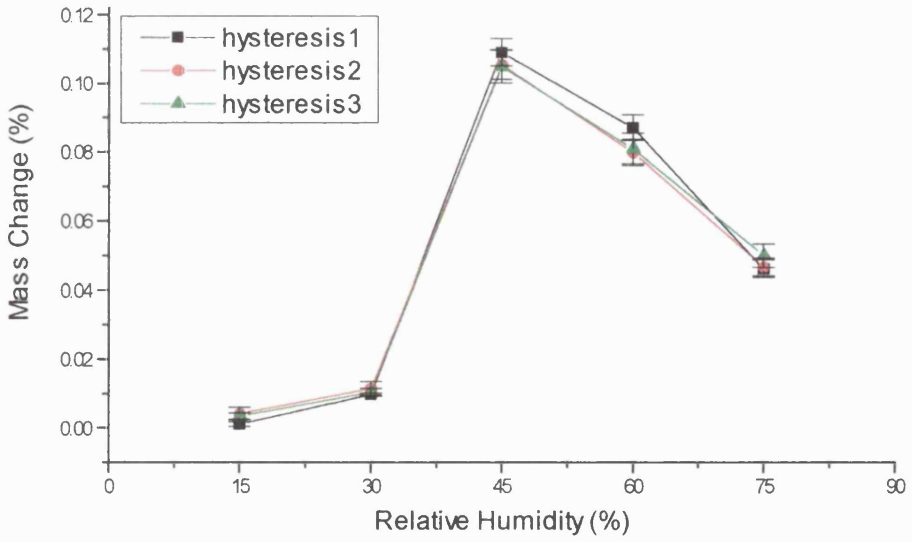

The heated Saquinavir (Figure 7.20) exhibits a significant decrease in water uptake at 75% RH, the overall shape being identical to the original Saquinavir.

Figure 7.21 shows the spin dried batch has a hysteresis similar to the original Saquinavir in shape, although there was a resemblance to the vacuum dried batch at 60% RH.

Figure 7.22 Sorption hysteresis of tray dried Saquinavir (b001).

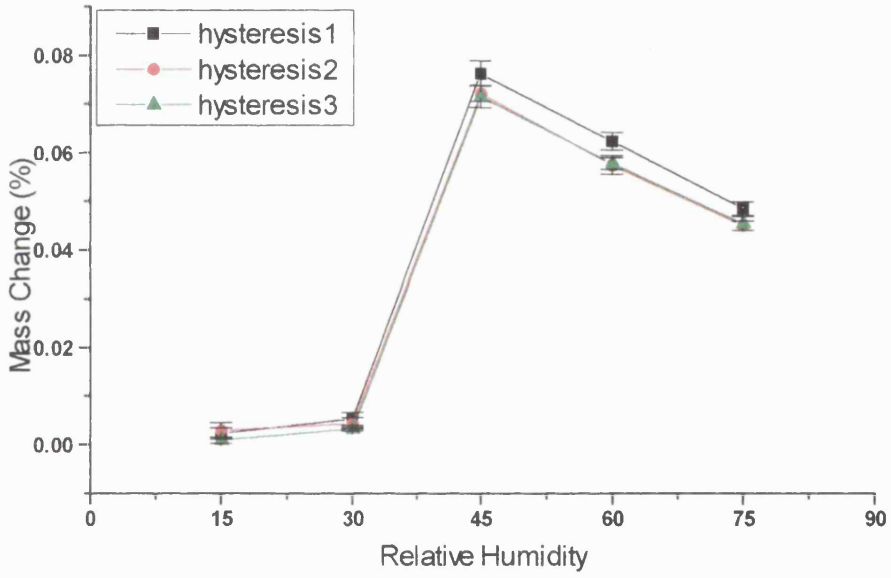

The tray dried sample (b001) was identical in nature to the other tray dried sample (b010).

7.4 Conclusions

- All five model powders adsorbed and desorbed differing amounts of water vapour, therefore they were easily distinguishable using the DVS. Unfortunately, Salicylic acid adsorbed no water vapour at all and Ibuprofen only a minute amount, which does hinder any detailed analysis of their surface character beyond recognition.

- The original Saquinavir had an adsorption isotherm that was very similar in shape and magnitude (with surface area correction) to the heated only Saquinavir (b030), which did not come into contact with water during processing.

- The tray dried Saquinavir batches (b001, b010) had adsorption isotherms that were similar in shape to the vacuum dried (b020) and the spin dried (b002) Saquinavir. These four batches were readily distinguishable from the original Saquinavir using the DVS.

- By subjecting each sample to three cycles of the humidity range, each cycle's individual isotherm was investigated. The original Saquinavir gradually changes with cycling, and this presents itself as a gradual fall in the amount of water vapour adsorbed onto the powder surface at the 75% relative humidity point of the adsorption segment of the isotherm. This phenomenon was not apparent with any of the other batches although the heated only (b030) Saquinavir did appear to be following a similar pattern.

- By studying the hysteresis between the adsorption and desorption isotherm segments, the differences between batches could be more readily discovered. With this method, again the same observations as above are seen, except that it is apparent that the tray dried Saquinavir batches are the most altered from the original, with the vacuum dried batches still significantly different. The spin dried batch yielded a hysteresis plot that was a mixture of the vacuum dried and the original Saquinavir batches' characteristics.

- The hysteresis plots of the original and heated (b030) Saquinavir batches also very clearly identify significant mass gain alterations at 75% humidity with repeated cycles. This method is able to show that the heated only Saquinavir was exactly the same in character as the original sample, which had not been fully proven by studying the adsorption isotherms alone.

7.5 Combining DVS and Microcalorimetry data

The data from the DVS and the microcalorimeter can be combined (Section 1.7.5) to realise meaningful thermodynamic data describing the process of water sorption to the powders over the complete humidity range. The value of Gibbs free energy (ΔG) has been obtained from the sorption isotherm using the DVS, the enthalpy value (ΔH) from sorption isotherms using the microcalorimeter and the entropy value (ΔS) is derived from the previous two data sets.

7.5.1 Thermodynamic consideration of three model powders

The water sorption properties of Salicylic acid and Ibuprofen could not be treated in this way, since they only adsorbed minute amounts of water vapour in the DVS.

Figure 7.23 Gibbs free energy of adsorption for three model powders.

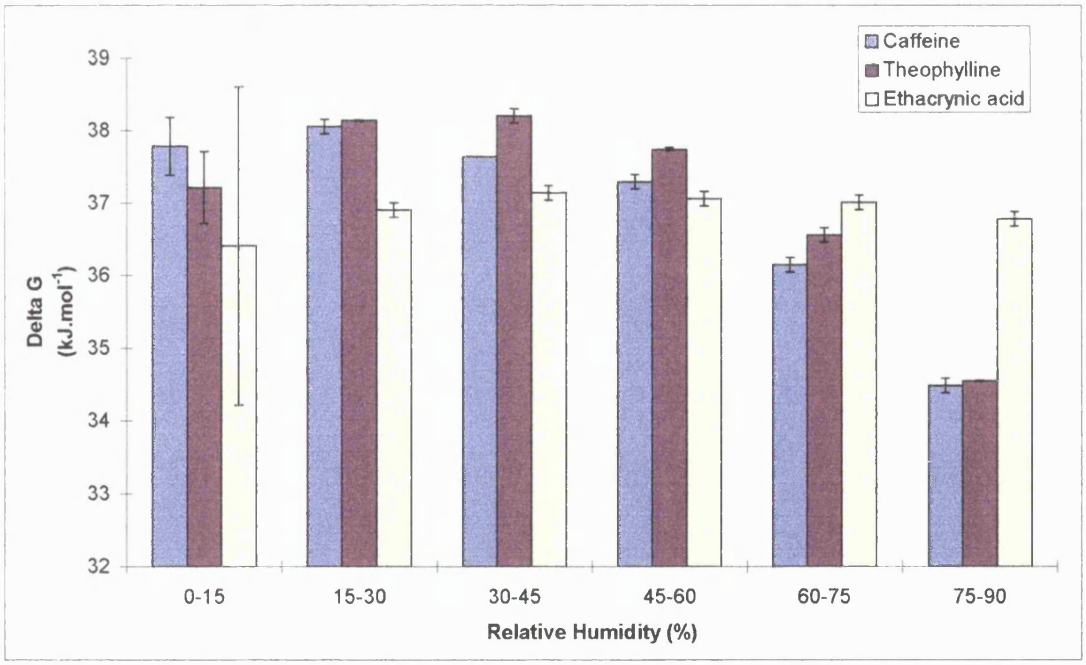

The Gibbs free energy plot (Figure 7.23) shows that Caffeine and Theophylline have similar ΔG values over the RH range. This is due to the fact that both powders adsorbed almost identical amounts of water vapour onto a standard weight of each

powder at each relative humidity. The positive ΔG values indicate that wetting is not favoured.

It must be noted that in the calculation of ΔG and consequentially ΔS, the derivation of the equilibrium constant (K_{ad}) requires units to be chosen which define a standard state. In this instance these have been selected to be the number of moles of water divided by the percentage relative humidity change. Any change in the definition of standard state will result in the thermodynamic data values being altered in magnitude. Therefore the values for ΔG and ΔS are not absolute and are only able to give a relative indication of variation between powder samples.

Figure 7.24 Enthalpy of adsorption for three model powders.

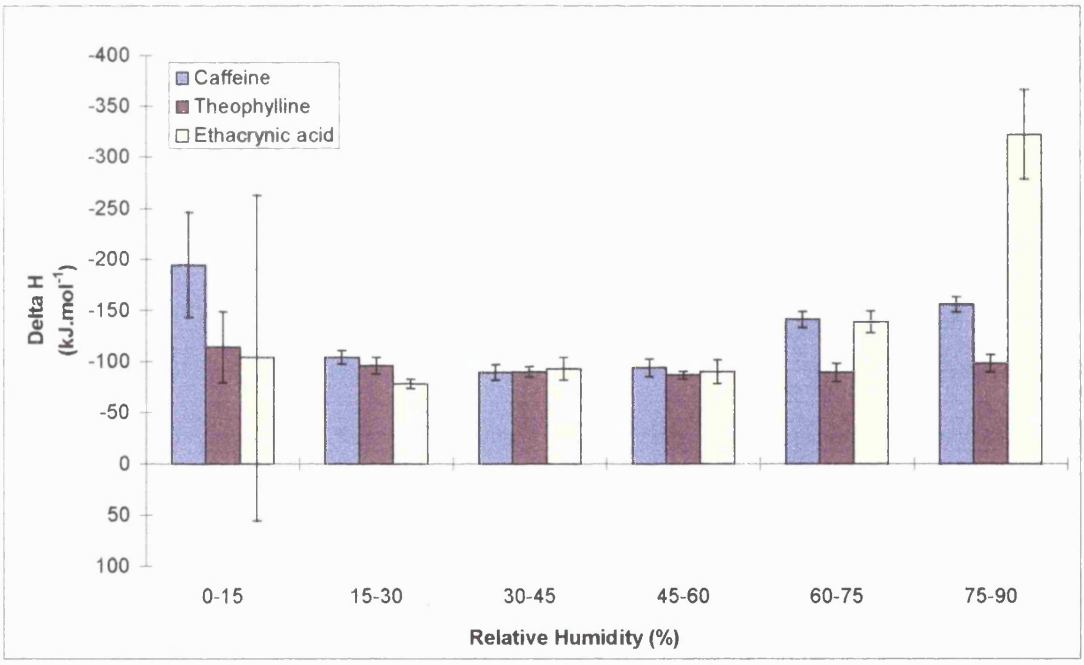

At 15% RH there is a larger enthalpic driving force for the adsorption of water to Caffeine than to Theophylline, causing it to adsorb water vapour more readily, releasing more heat. Between 30% and 60% all three powders have similar enthalpy values, forming a plateau. At 90% RH Ethacrynic acid has a very large enthalpy value that is too great for hydrogen bonding alone, suggesting that at such a high RH some dissolution may be occurring at the powder surface.

Figure 7.25 Entropy of adsorption for three model powders.

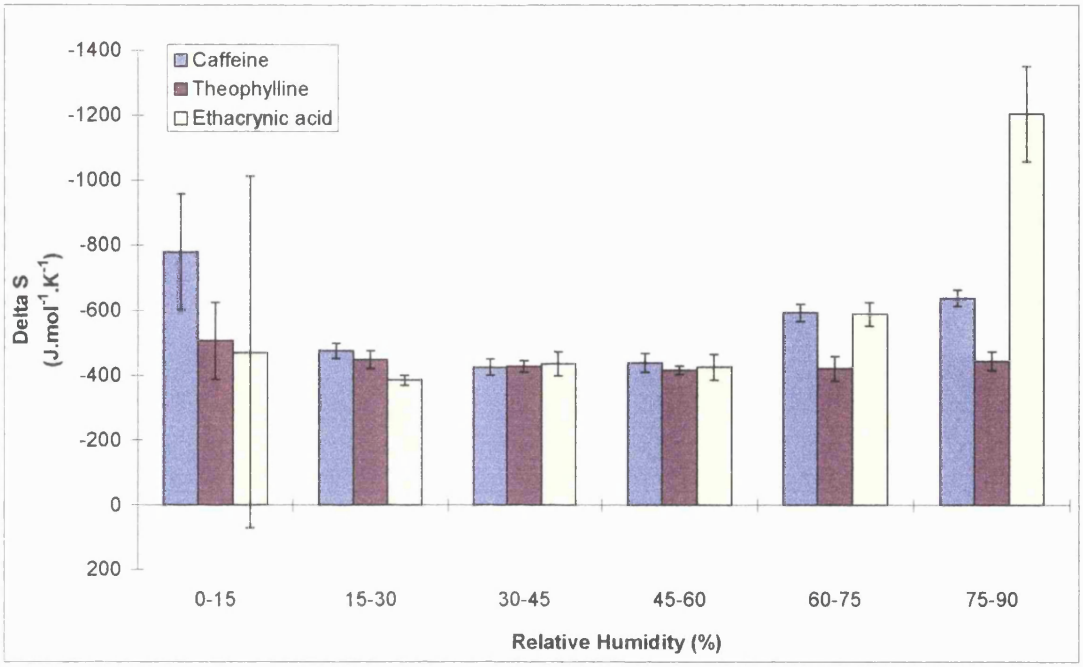

The degree of disorder between the three powders is most different at 90% RH, with Ethacrynic acid having the most negative value, suggesting that the adsorption process, plus any related process e.g. dissolution, is least favourable. The most likely reason for the large ΔH and ΔS values at 90% RH are due to the DVS data where the total mass uptake for each of the three powders was very small (0.06%) and any error would have a greater effect. An error of 0.003% (3μg in a 100mg Ethacrynic acid sample) would cause a change in ΔH and ΔS of 146.8 $kJ.mol^{-1}$ and 495.8 $J.\ mol^{-1}.K^{-1}$, respectively.

7.5.2 Thermodynamic consideration of the Saquinavir batches

The free energy changes in Figure 7.26 indicate that the original and heated only Saquinavir are very similar in their overall process of adsorption since the DVS measured similar mass gains over the whole humidity range. The positive value for all the Saquinavir batches shows that wetting is not favoured as with most hydrophobic powders. The tray and vacuum dried Saquinavir behaved differently from the original and each other. For a spontaneous process to occur, such as water adsorption, the free energy value should decrease in magnitude with increasing

humidity. It is clear that this is not the case for the Saquinavir batches, although it is apparent that the original and heated only batches have similar ΔG values, whilst the tray dried and vacuum dried mirror each other's rise and fall across the RH range.

Figure 7.26 The Gibbs free energy of sorption for Saquinavir batches.

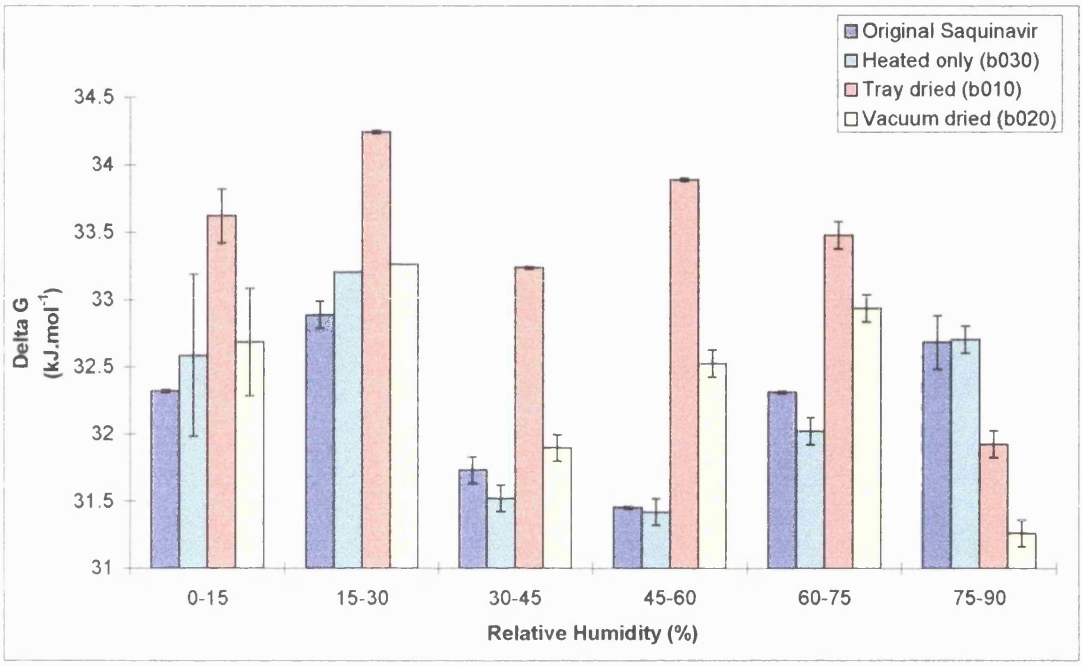

Figure 7.27 Enthalpy of sorption for Saquinavir batches.

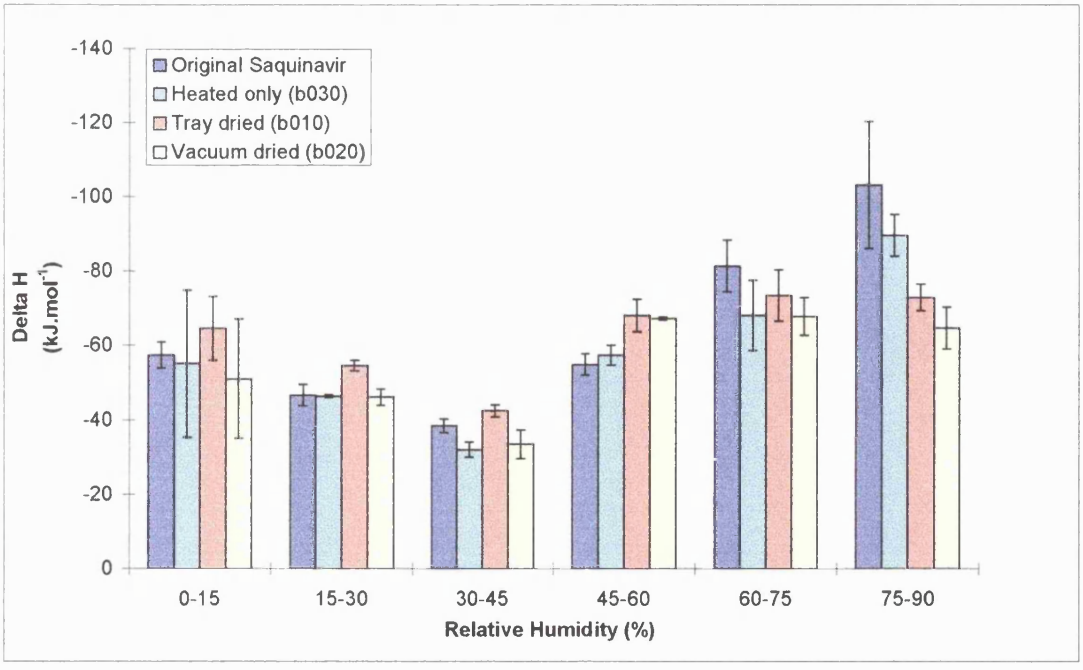

From 0% to 45% RH, all the powders have enthalpy values that are steadily decreasing towards zero, indicating that the process is becoming less enthalpically favoured and less heat is being released in the exothermic reaction. Beyond 45% RH, the enthalpy becomes more negative again as the reaction becomes increasingly enthalpically favourable and more heat is released. The behaviour of the heated only and original Saquinavir batches are similar to each other, in that from 45% RH onwards, the enthalpy of sorption becomes more negative at a constant rate, whilst the tray and vacuum dried Saquinavir batches have similar isotherms to each other but very different isotherms compared to the first two samples. At 60% RH, both the tray and vacuum dried samples have a significantly more negative enthalpy which remains close to this level with increasing humidity.

Figure 7.28 Entropy of sorption for Saquinavir batches.

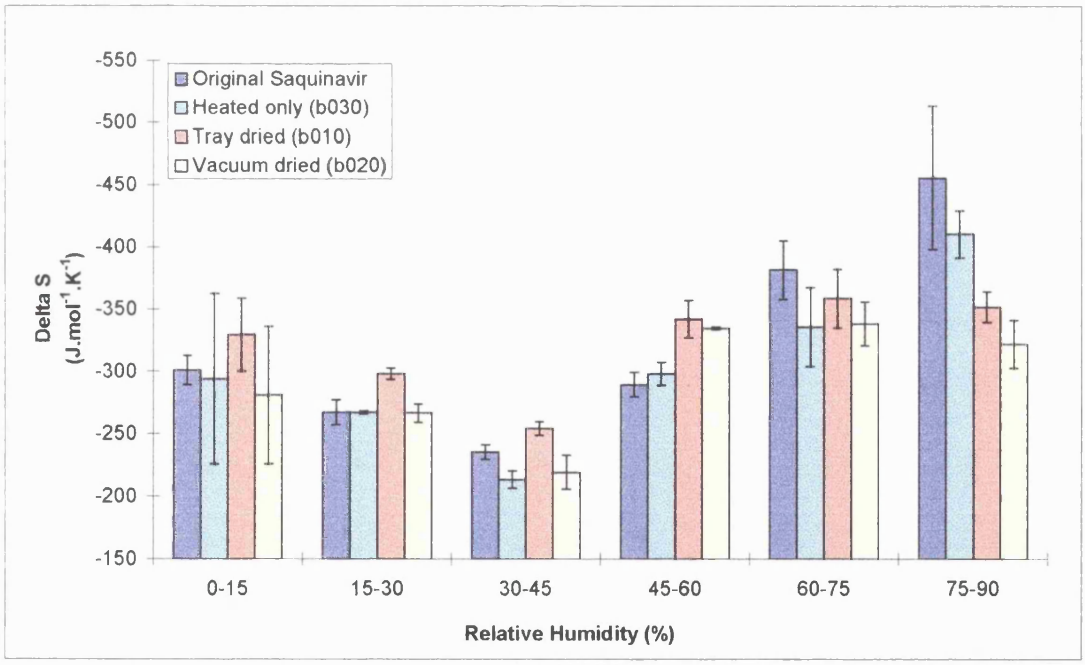

The entropy of the sorption process in Figure 7.28 mirrors the enthalpy changes, in that the degree of disorder for all the batches appears to decrease steadily from 0% to 45% RH, indicating an increase in order of the system and a slight decrease in ability of the process to occur. Beyond 45% RH, the change in degree of disorder increases at a steady rate for the original and heated only Saquinavir, whilst the tray and vacuum dried Saquinavir reach a plateau from 60% RH.

The wetting process of all the Saquinavir batches is strongly favoured enthalpically although this is easily outweighed by the entropic hindrance of this hydrophobic powder, resulting in an adsorption process that is entropically controlled.

7.5.3 The monolayer capacity of the powder samples

The monolayer capacity is the amount of water required to form a monolayer over the powder surface, calculated theoretically from Equation 7.3. This value can then be used in combination with the DVS adsorption isotherms to find the relative humidity at which a monolayer is formed with each powder.

$$c_m = \frac{A_s}{a_m N}$$ Equation 7.3

c_m = monolayer capacity ($mol.g^{-1}$)
A_s = specific surface area of the adsorbent (m^2g^{-1})
a_m = area occupied by each molecule of the adsorbate (m^2)
(11.4×10^{-20} m^2)
N = Avogadro's number

It must be noted that the specific surface area is calculated using nitrogen, whereas the DVS uses water vapour. Nitrogen is non-specific in binding whilst water, being a polar molecule, binds to specific polar sites on the powder surface. In addition, the nitrogen molecules are larger (16.2×10^{-20} m^2) than the water molecules (11.4×10^{-20} m^2), with the result that water molecules are able to access the internal surface area of the powder more easily. Therefore the calculated surface area using nitrogen and the corresponding monolayer capacity may not be accurate for each powder (Djordjevic et al., 1992).

Table 7.2 Relative humidities required for monolayer formation in the DVS.

	c_m (mol.g^{-1})	Mass of monolayer (μg) on 50mg powder sample	Mass increase (%)	RH required for monolayer (%)
Original Saquinavir	1.33×10^{-5}	11.98	0.024	<15
Tray dried	1.02×10^{-5}	9.14	0.018	<15
Vacuum dried	1.04×10^{-5}	9.33	0.019	<15
Heated only	1.23×10^{-5}	11.03	0.022	<15
Caffeine	1.28×10^{-5}	11.48	0.023	54-58
Theophylline	8.03×10^{-6}	7.22	0.014	32-35
Salicylic acid	2.99×10^{-6}	2.69	0.005	n/a
Ibuprofen	6.09×10^{-6}	5.48	0.011	75-90
Ethacrynic acid	9.16×10^{-6}	8.25	0.016	22-27

Table 7.2 shows that for all the Saquinavir batches, the monolayer formation is achieved at very low relative humidities (below 15% RH), which concurs with their lower entropy values at 15% RH compared to the other model powders, showing a slightly more ordered system since water molecules have condensed from a gaseous state onto the powder surface forming a complete monolayer.

7.5.4 Discussion

The DVS and microcalorimetry can be primarily used to obtain the enthalpy of adsorption (ΔH_{ads}) outlined in section 1.7.3.2. This value is the sum of the initial monolayer formation (ΔH_{mon}) and the following multilayer adsorption (ΔH_{cond}). It is assumed from the BET equation (Brunauer et al., 1938) that only the monolayer adsorption gives information of the powder surface. This is due to the monolayer being directly in contact with powder surface whilst further water layers are only interacting with each other in the process of condensation or evaporation. ΔH_{cond} can be easily calculated from the difference between the enthalpies of formation of water (-286 kJ.mol^{-1}) and of water vapour (-242 kJ.mol^{-1}), equalling -44 kJ.mol^{-1} (data from Stark and Wallis, 1978). In the same way, the entropy of adsorption (ΔS_{ads}) can also be divided into ΔS_{mon}, due to the ordered formation of a monolayer and ΔS_{cond}, due to

multlayer formation involving water molecules alone. ΔS_{cond} can be calculated giving a value of -119.1 $J.mol^{-1}.K^{-1}$. Using the above data, the thermodynamic values for monolayer formation can be calculated with Equations 7.3, 7.4 and 7.5.

$$\Delta H_{mon} = \Delta H_{ads} - \Delta H_{cond} \qquad \text{Equation 7.3}$$

$$\Delta S_{mon} = \Delta S_{ads} - \Delta S_{cond} \qquad \text{Equation 7.4}$$

$$\Delta G_{mon} = \Delta H_{mon} - T\Delta S_{mon} \qquad \text{Equation 7.5}$$

Table 7.3 Thermodynamic analysis of Caffeine, Theophylline, Ethacrynic Acid and Saquinavir batches.

	ΔG_{ads} $kJ.mol^{-1}$	ΔH_{ads} $kJ.mol^{-1}$	ΔS_{ads} $J.mol^{-1}.K^{-1}$	ΔG_{mon} $kJ.mol^{-1}$	ΔH_{mon} $kJ.mol^{-1}$	ΔS_{mon} $J.mol^{-1}.K^{-1}$
Caffeine	36.5	-137.3	-583.4	45.1	-93.3	-464.3
Theophylline	36.7	-96.3	-446.4	45.2	-52.3	-327.3
Ethacrynic acid	36.9	-139.0	-590.3	45.4	-95.0	-471.2
Original Saquinavir	32.2	-61.7	-314.9	40.9	-17.4	-195.8
Tray dried b010	33.3	-63.9	-326.0	41.8	-19.9	-206.9
Vacuum dried b020	32.3	-55.2	-293.6	40.8	-11.2	-174.5
Heated only b030	32.2	-56.6	-297.7	40.6	-12.6	-178.6

To explain Table 7.3, ΔG_{ads} gives an indication of the favourability of adsorption of water onto each powder surface. It ranks Ethacrynic acid with the greatest ΔG value, having the least favourable adsorption process whilst the Saquinavir has the smallest ΔG value and the most favourable adsorption process of the four powders.

A model of the possible adsorption mechanism must be hypothesised (Buckton and Beezer, 1987). The wetting of a powder is assumed to be governed by the number of appropriate binding sites and their ability to be accessed. Figure 7.29 describes the two adsorption extremes that could occur.

Figure 7.29 Two possible methods of adsorption.

Figure 7.29 shows that the total adsorption (ΔG_{ads}) could be very similar in 1b) and 2b), in addition to the total enthalpy (ΔH_{ads}) involved in the powder/water and water/water interactions. Although it is also apparent that the droplet layer in 2b) is a more ordered system than 1b), with a correspondingly lower entropy value (ΔS_{ads}). Of the three model powders, contact angle studies (Chapter 3) showed that Ethacrynic acid was the most hydrophobic. The hypothesis is that the greater the hydrophobicity of a powder, the less binding sites there are available for water molecules to attach to (as described in part 2 of Figure 7.29). Table 7.3 indicates that for water molecules to bind with all available sites, Ethacrynic acid has the largest negative entropy value, the most ordered and also the least favoured process. As more water molecules attach themselves to other water molecules to form multilayers, the system becomes increasingly ordered for all the powders. Thus Ethacrynic acid's hydrophobic nature is due to any difficulty in water molecules initially accessing and attaching themselves to the binding sites, making the wetting process entropically unfavourable. Caffeine, Theophylline and Saquinavir are less hydrophobic, having their mechanisms of water adsorption involve a greater quantity of binding sites as in part 1) of Figure 7.29, leading to a less ordered multilayer that is not so entropically hindered.

The Saquinavir batches have ΔH_{mon} values (11.2-19.9 $kJ.mol^{-1}$) that are in keeping with those found for physical adsorption and hydrogen bonding (5-20 $kJ.mol^{-1}$) from 0% to 45% RH, suggesting that the adsorption process is more likely to be a physical

process than a chemical one. Beyond this humidity, the enthalpy values increase which may be due to an additional process taking place.

Since there is a marked difference in adsorption behaviour seen between the Saquinavir batches between 60% and 90%RH, Table 7.4 outlines the thermodynamic data involved.

Table 7.4 Thermodynamic analysis of Saquinavir batches between 60% and 90% RH.

	ΔG_{ads} kJ.mol^{-1}	ΔH_{ads} kJ.mol^{-1}	ΔS_{ads} J.mol^{-1}.K^{-1}
Original Saquinavir	32.5	-91.4	-415.7
Tray dried (b010)	32.6	-73.0	-354.4
Vacuum dried (b020)	32.0	-65.7	-327.7
Heated only (b030)	32.3	-77.3	-367.9

It is evident from Table 7.4 that the total adsorption does not change between batches, but both the changes in entropy and enthalpy are more negative with the original and heated only batches than the tray and vacuum dried Saquinavir. The large negative enthalpy value for the original Saquinavir and to some extent the heated only Saquinavir would suggest that the process is not purely hydrogen bonding. In each case T.ΔS is greater than ΔH, which means the process is an unfavourable entropy-controlled one. Therefore the original and heated only batches are more entropically hindered than the other two batches between 60% and 90% RH as the system becomes more ordered. The mechanism proposed is that when the original and heated only Saquinavir are subjected to 60%-90% RH, certain amorphous areas (not present on the crystalline surfaces of the tray and vacuum dried batches) absorb enough water at high humidities to be able to slowly crystallise yielding enthalpy values above 60 kJ.mol^{-1}. The absorbed water has a marked effect on the overall entropy causing the system as a whole to be more ordered. ΔS_{ads} is more negative than for the tray and vacuum dried batches which have fewer, if any, amorphous binding sites and therefore has less absorbed water.

7.5.5 Thermodynamic changes on repeated cycling of Saquinavir batches

There is also evidence that the thermodynamic properties of the Saquinavir batches alter during cycling of the same sample.

Figure 7.30 The Gibbs free energy of sorption for the original Saquinavir over 3 cycles.

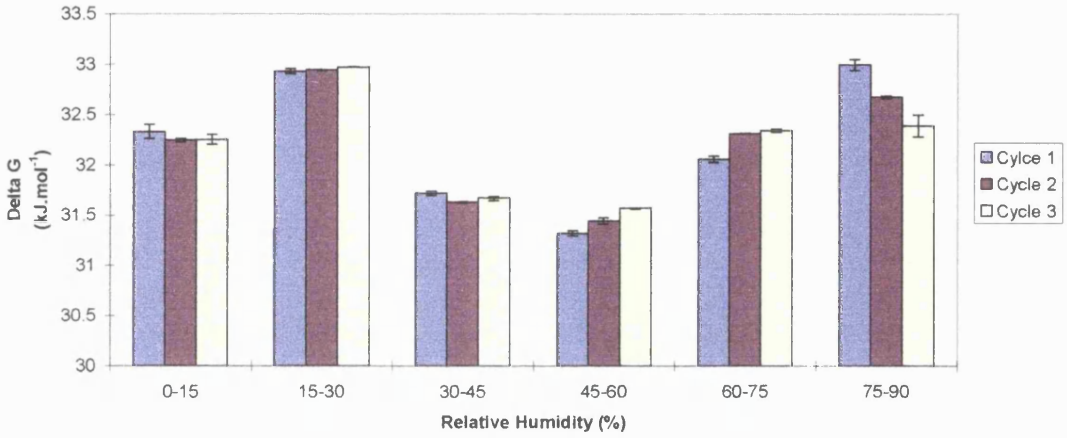

Figure 7.31 The Gibbs free energy of sorption for the tray dried Saquinavir over 3 cycles.

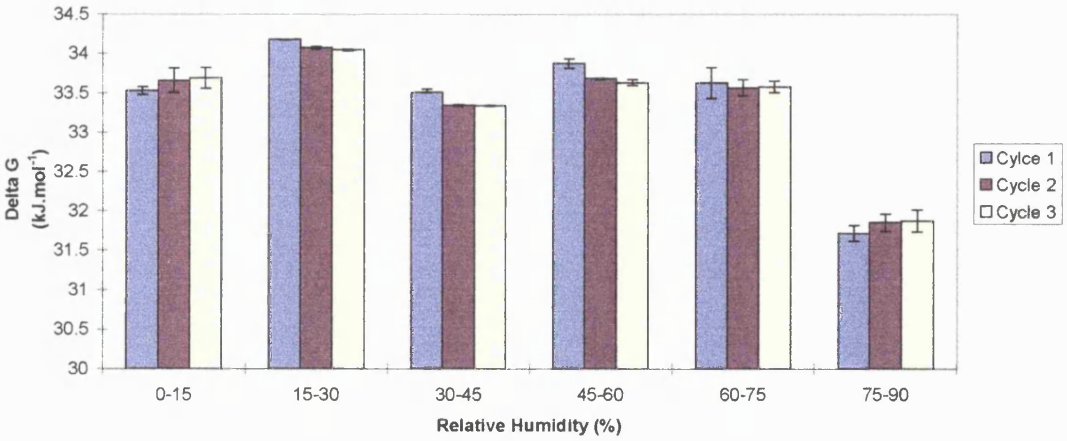

Figure 7.32 The Gibbs free energy of sorption for the vacuum dried Saquinavir over 3 cycles.

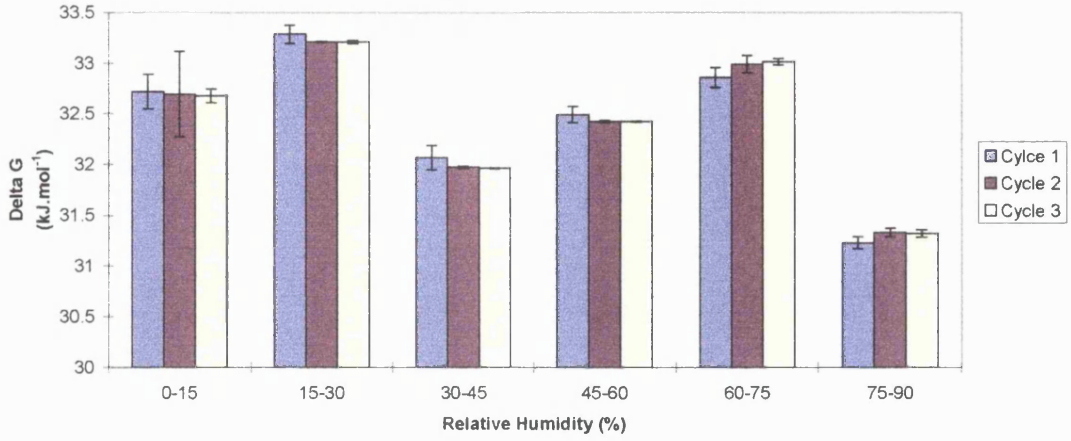

Figure 7.33 The Gibbs free energy of sorption for the heated only Saquinavir over 3 cycles.

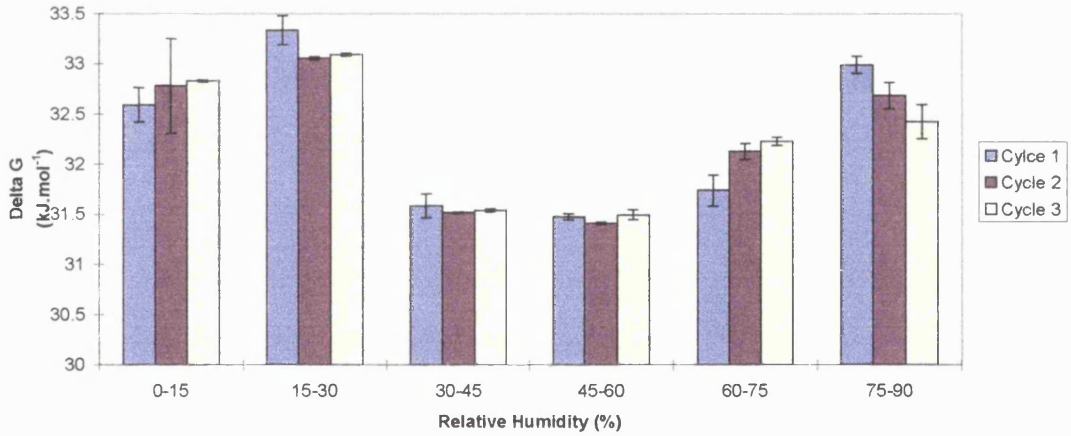

Over the three cycles, there are no major changes in ΔG at the lower relative humidities (0 - 45%) with any of the Saquinavir batches. Beyond 45% RH there are significant changes in the thermodynamic properties of each batch detailed in Figure 7.34.

Figure 7.34 Change in ΔG between 60% and 90% RH with repeated cycling.

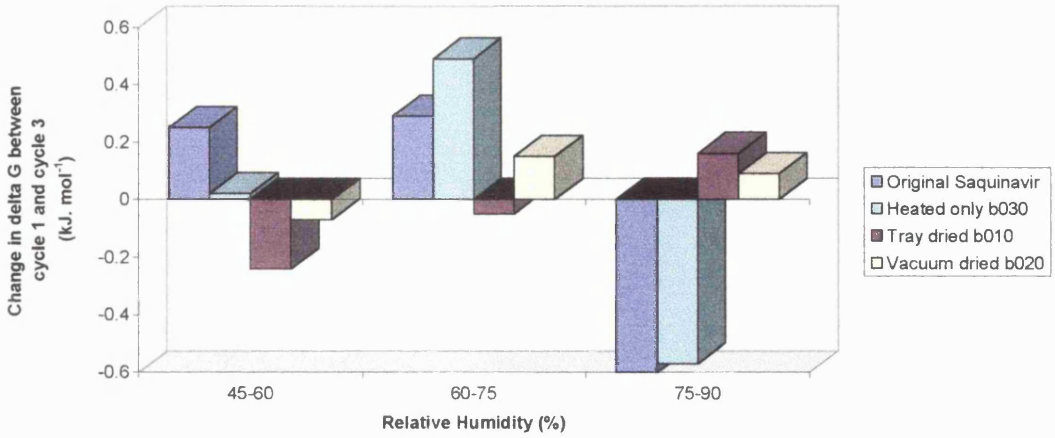

It is clear from Figure 7.34 that the original and heated only Saquinavir have similar changes in ΔG especially at 60%-75% and 75%-90% RH. At 60%-75% RH both batches have an increase in free energy, with a large drop at 75%-90% RH indicating that the process is becoming less favourable at 60%-75% and more favourable at 75%-90% RH with repeated cycles. The tray and vacuum dried batches do not follow this pattern at all, with only a slight decrease at 45%-60% and small increases in free energy between 60% and 90% RH. The exact thermodynamic nature of what is occurring at the powders' surfaces can be seen more clearly by interpreting the enthalpy and entropy data.

Figure 7.35 Enthalpy of sorption for the original Saquinavir over 3 cycles.

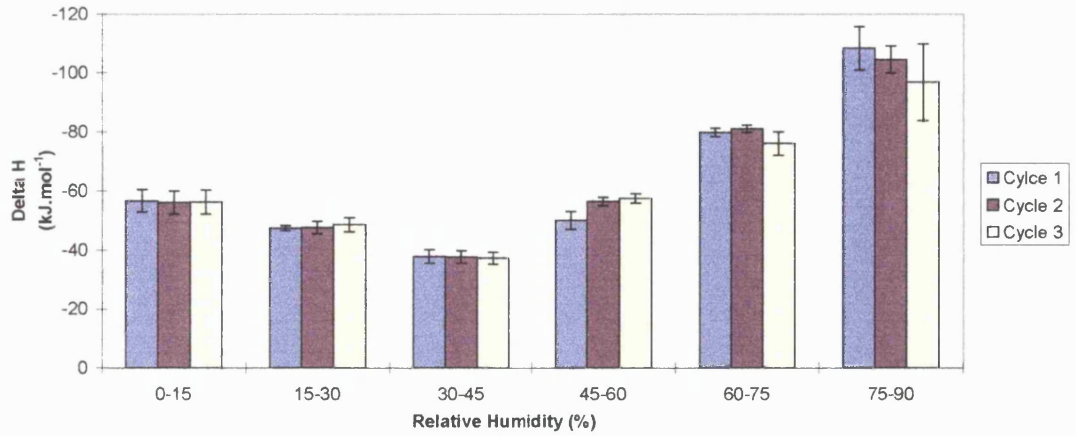

Figure 7.36 Enthalpy of sorption for the tray dried Saquinavir over 3 cycles.

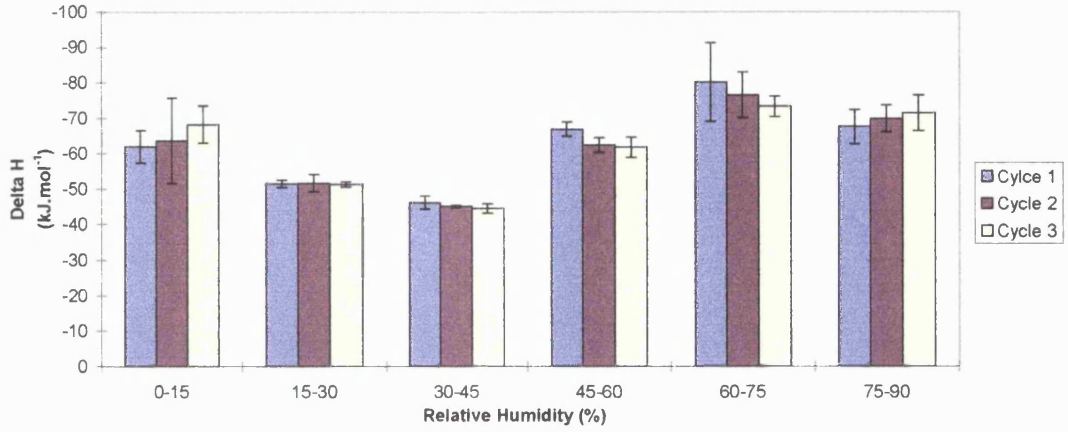

Figure 7.37 Enthalpy of sorption for the vacuum dried Saquinavir over 3 cycles.

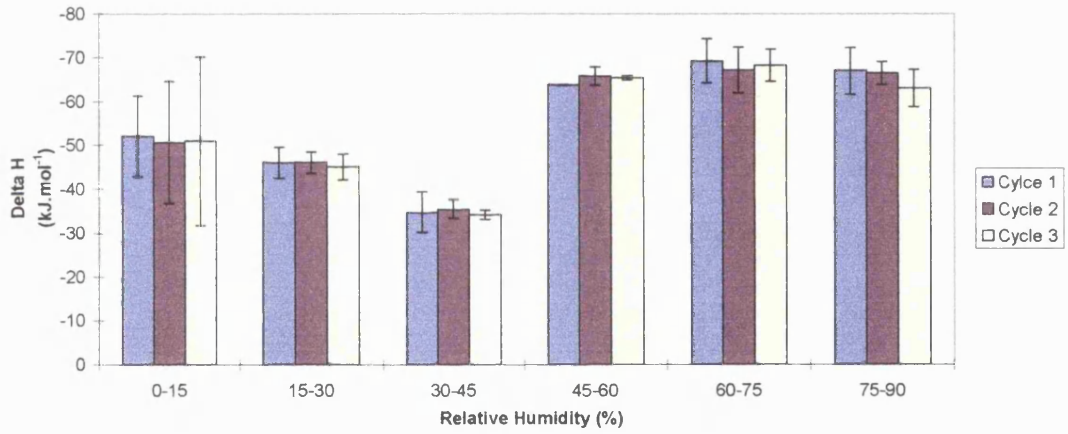

Figure 7.38 Enthalpy of sorption for the heated only Saquinavir over 3 cycles.

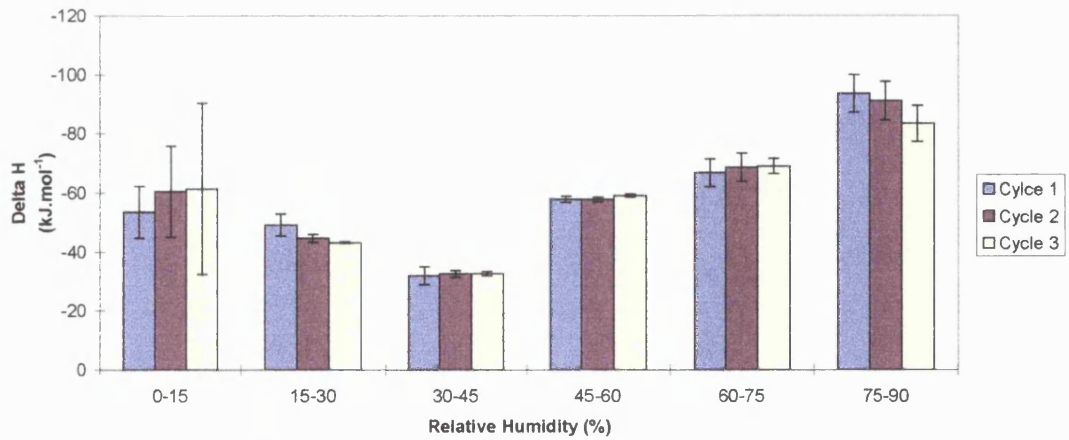

Figure 7.39 Change in ΔH between 60% and 90% RH with repeated cycling.

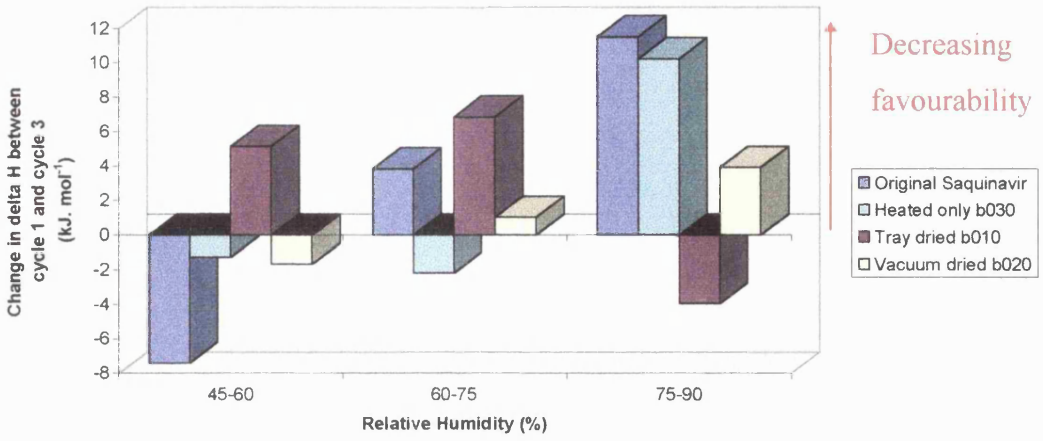

The original and heated only Saquinavir batches have a large positive enthalpy change at 75%-90% RH. This is because the number of amorphous areas on the surface decreases each time the humidity is sufficiently great to enable the crystallisation process to occur. The tray and vacuum dried batches do not have any large changes in enthalpy since their surfaces are much more stable over the whole RH range, with limited crystallisation of amorphous areas, if any, and enthalpy values indicative of water adsorption only (hydrogen bond formation).

Figure 7.40 Entropy of sorption for the original Saquinavir over 3 cycles.

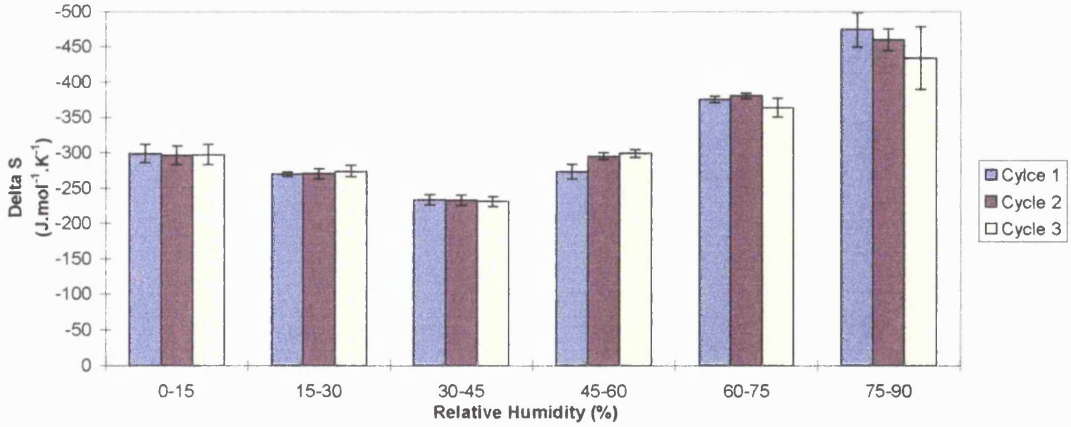

Figure 7.41 Entropy of sorption for the tray dried Saquinavir over 3 cycles.

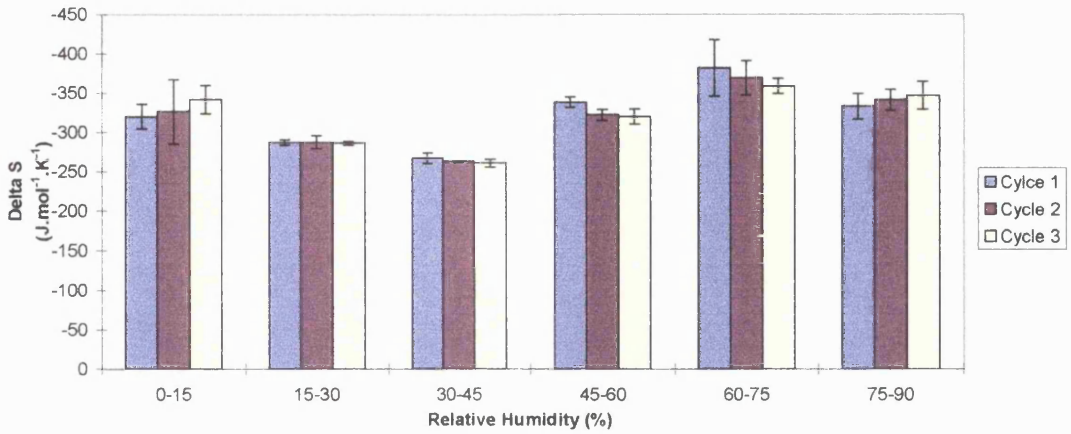

Figure 7.42 Entropy of sorption for the vacuum dried Saquinavir over 3 cycles.

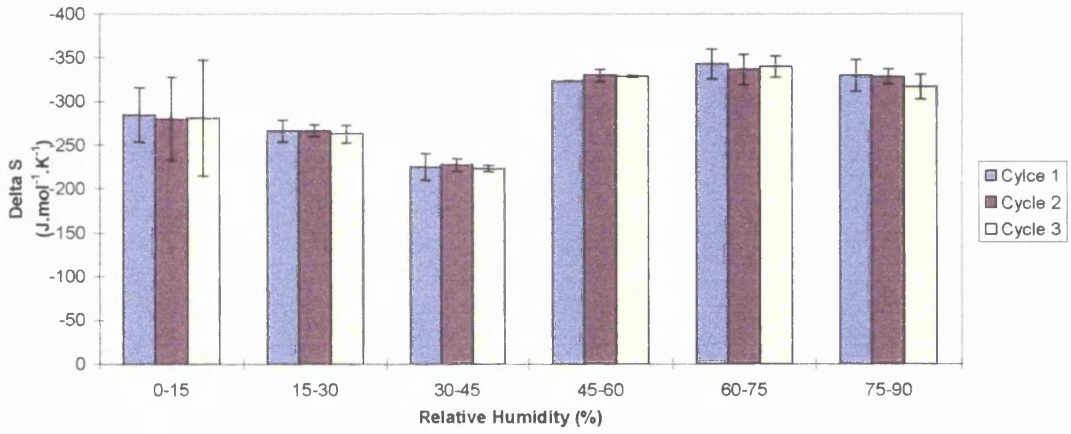

Figure 7.43 Entropy of sorption for the heated only Saquinavir over 3 cycles.

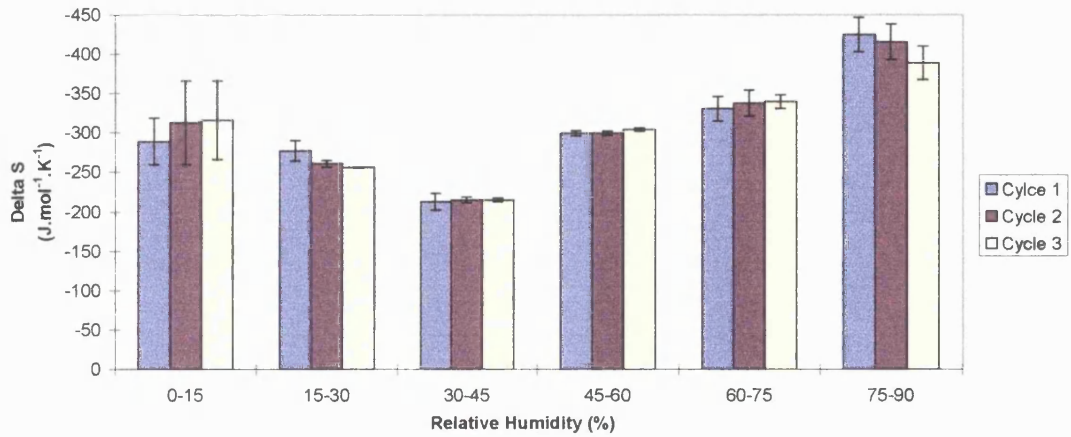

Figure 7.44 Change in ΔS between 60% and 90% RH with repeated cycling.

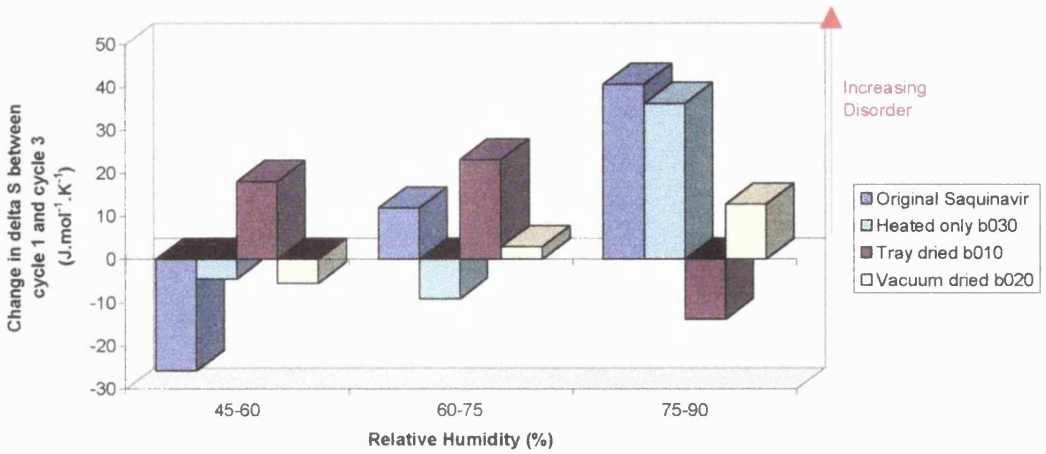

The entropy change for the original and heated only batches is most significant at 90% RH. The large increase indicates an increasing favourability of the process which is also indicated in the change in free energy (Figure 7.34) proving that this process is entropically controlled. This reflects an increase in disorder, which can be explained by the reducing number of amorphous binding sites as they gradually crystallise at these high humidities and in doing so releases the water molecules that were absorbed there. After each cycle, less and less absorbed water molecules are present resulting in less order. The change in entropy is towards that of the tray and vacuum dried batches which have values only indicative of multilayer formation which do not vary greatly with repeated cycles. This process also occurs to a smaller extent with the vacuum dried Saquinavir as it also has a small proportion of amorphous binding sites at the outset.

7.5.6 Conclusions

A clear difference between the sorption process was detected between the Saquinavir batches, depending on their pre-treatment conditions, whilst the degree of wettability was accurately predicted for all the powders used in this section.

The combination of DVS and microcalorimetric data allows a comprehensive thermodynamic analysis of the water sorption mechanism that gives more information on wetting behaviour than any single technique alone.

Chapter 8

Further Analysis

8 Introduction

8.1 Mixer Torque Rheometer

Wet granulation is an important step in determining the processability and final quality of many pharmaceutical products. Any alterations in the surface energy of the powder may affect the granulation process leading to possible batch failure. The Mixer Torque Rheometer (MTR) is a small scale mixer that is able to directly measure the cohesiveness of a granulation mixture during preparation. The MTR consists of a 250ml capacity mixer fitted with a variable speed d.c. motor. There are two mixing blades, one rotating at twice the speed of the other to ensure efficient mixing. A computer linked to the rheometer via a calibrated dynamometer is able to give a torque with time reading that quantifies and characterises the rheological behaviour and consistency of a wet granulation.

Figure 8.1 Diagrammatic representation of the dynamometer output.

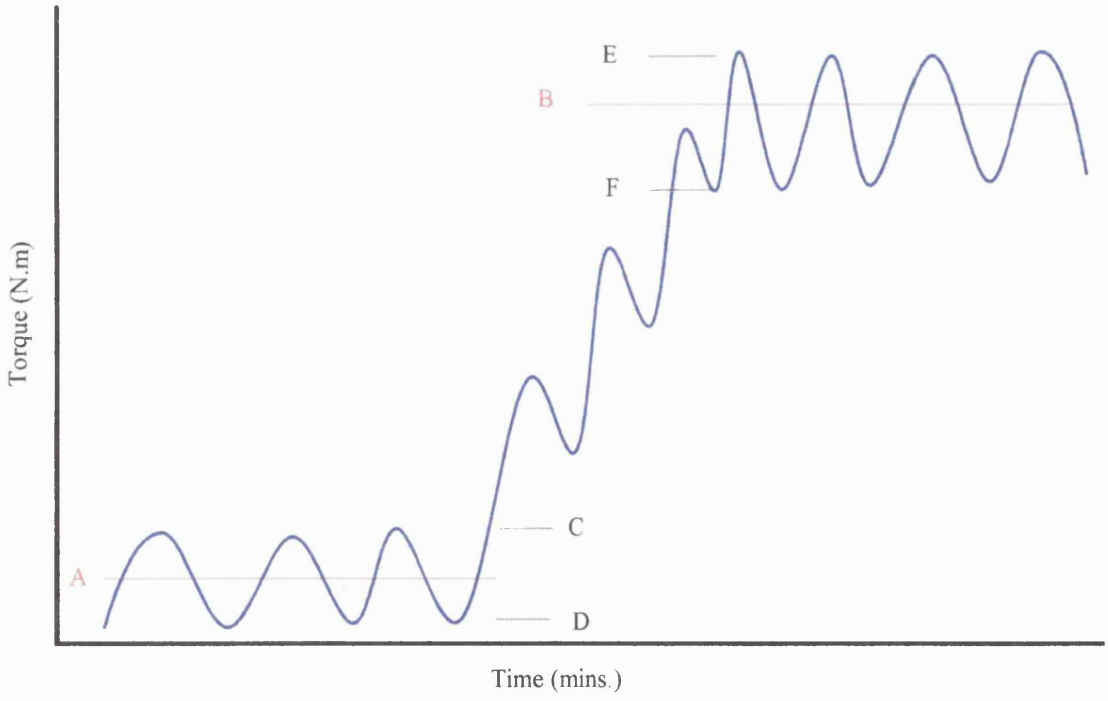

There are two possible measurements that can be analysed:-

a) The difference between mean torque values A and B.

b) The difference in amplitudes of C-D and E-F.

8.1.1 Investigation of the granulation process

As the amount of liquid binder (usually water) is increased, there is usually a corresponding increase in the measured torque values up to a maximum, after which the formulation turns into a wet, loose slurry and the torque values fall rapidly. This phenomenon is due to the different saturation stages of the powder particles. Primarily, when the liquid concentration is low, lens-shaped rings of liquid are formed at the point of contact with the particles (pendular state). As more liquid is introduced, it forms a continuous liquid network interspersed with air spaces (the funicular state). Both the pendular and funicular state allow the particles to become more cohesive, which is a desirable feature in wet granulation, and thus the measured torque values increase in the MTR. A crucial point is reached when the air spaces become filled with liquid (the capillary state), which corresponds to the maximum torque value, and as more liquid enters the system the solid particles become totally dispersed within the liquid and a slurry is formed. The MTR measures the whole wetting process in granulation, although in a real wet granulation, liquid addition is halted when the particles are in the funicular state to achieve large consistent granules.

Figure 8.2 Wetting process.

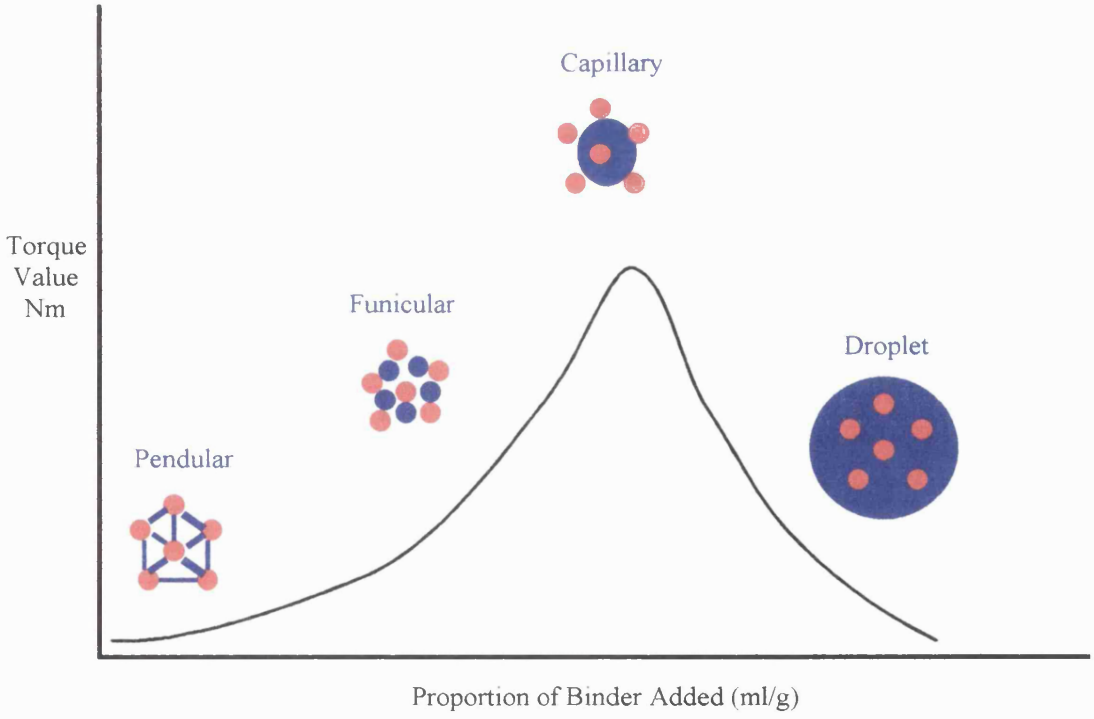

those being the surface characteristics of the formulation, where a small change in batches can achieve a different granulation profile (Parker et al., 1990).

8.2 Methods

For every experiment, the following formulation was used:

Lactose MED/200	3.26g
Avicel pH102	3g
Kollidon K30	0.6g
Ac-Di-Sol	0.3g
Water	As required
Saquinavir	7.5g

Two methods were used to examine the granulation properties of the Saquinavir batches. The first experiment required the addition of 1ml of water beginning a minute after the mixer had been turned on, and every minute thereafter for 15 minutes. The mean torque was measured for each minute interval. The second experiment involved adding 6mls of water to the formulation, again one minute after the mixer had been turned on, and allowing it to measure mean torque values.

8.3 Results

Figure 8.3 shows that the MTR was unable to differentiate between the four batches of Saquinavir, when having multiple additions of binder. Whilst Figure 8.4 shows that this MTR method of adding an initial amount of binder and mixing continuously was also unable to distinguish between the four Saquinavir batches.

Figure 8.3 Rheometer analysis of granulation properties of Saquinavir batches by sequential addition of liquid binder.

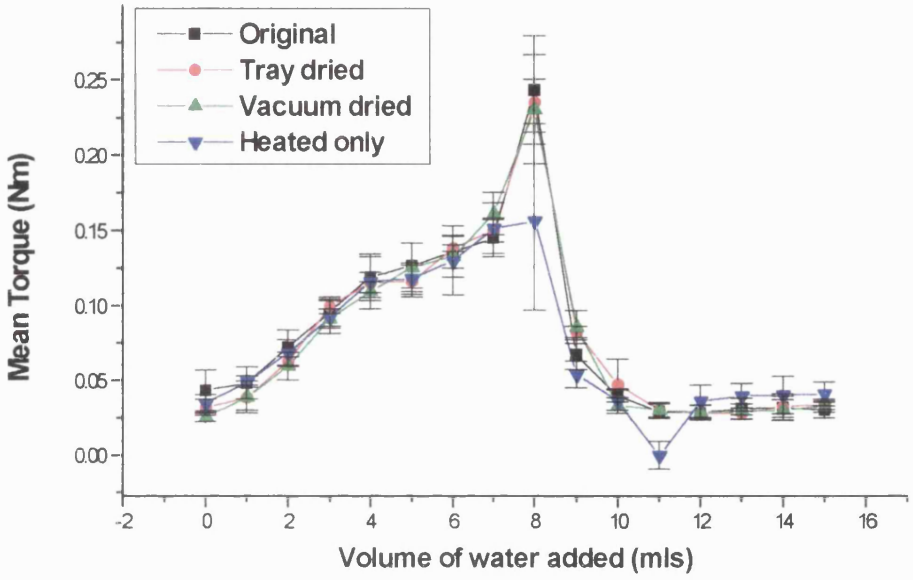

Figure 8.4 Rheometer analysis of granulation properties of Saquinavir batches over time (with addition of liquid binder at time zero).

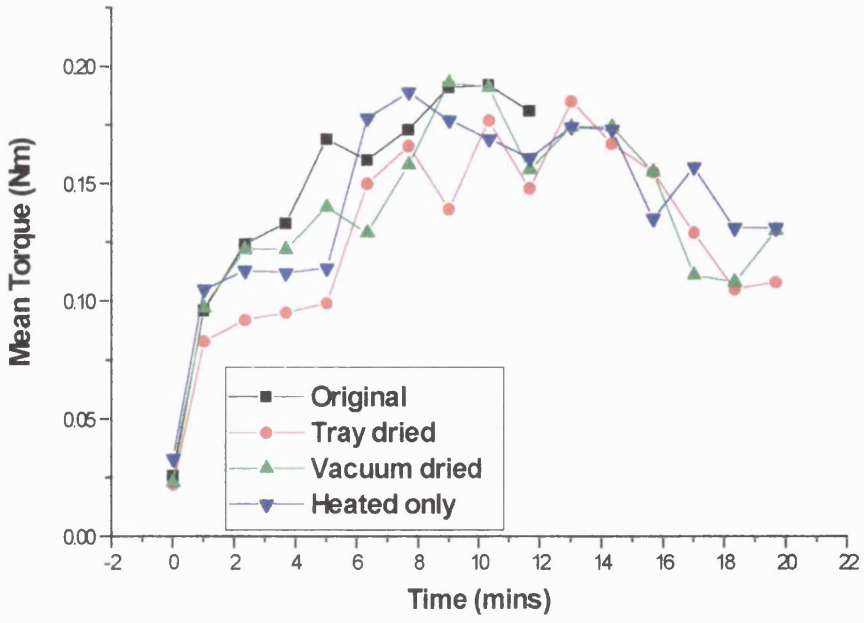

8.4 Microscopy

Figure 8.5 Caffeine

Figure 8.6 Theophylline

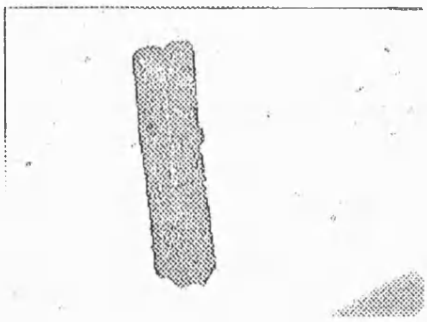

Figure 8.7 Salicylic acid

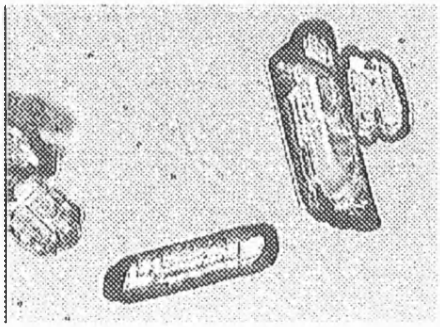

Figure 8.8 Ibuprofen

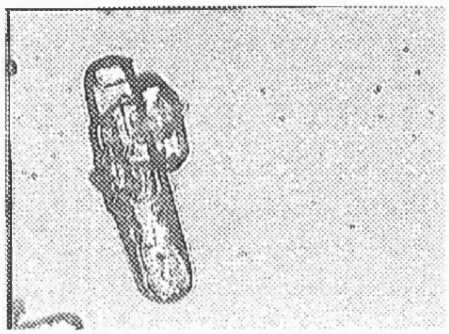

Figure 8.9 Ethacrynic acid

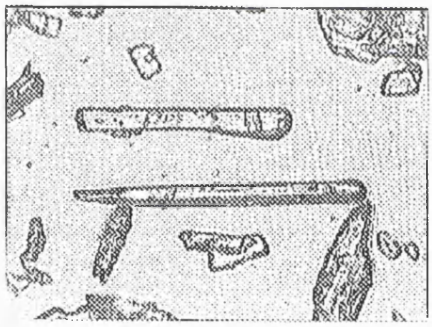

10μm

The Saquinavir batches all had crystals of similar size and shape.

Figure 8.10 Original Saquinavir

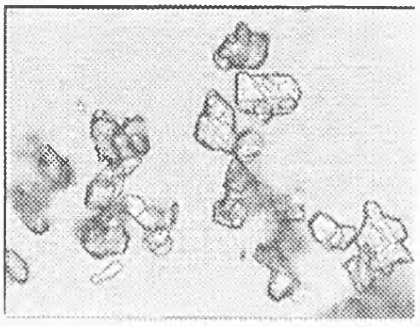

Figure 8.11 Tray dried Saquinavir (b010)

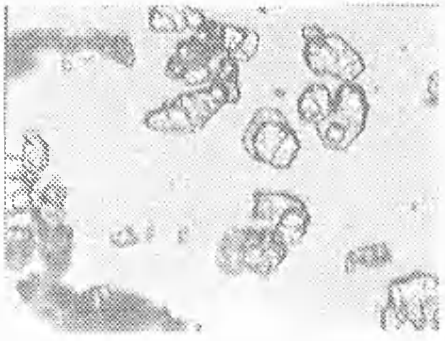

Figure 8.12 Tray dried Saquinavir (b001)

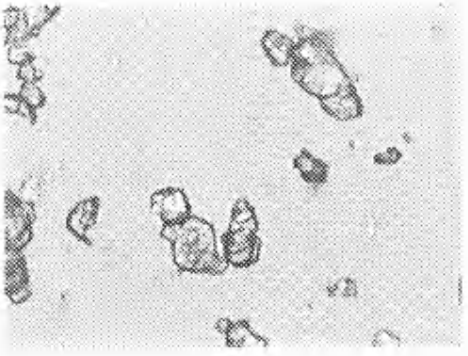

Figure 8.13 Vacuum dried Saquinavir (b020)

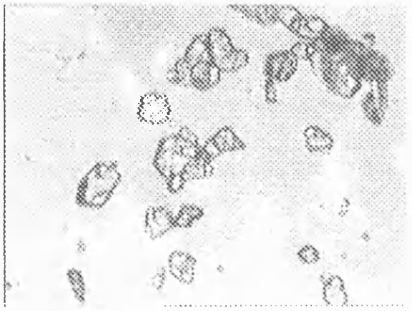

Figure 8.14 Heated only Saquinavir (b030)

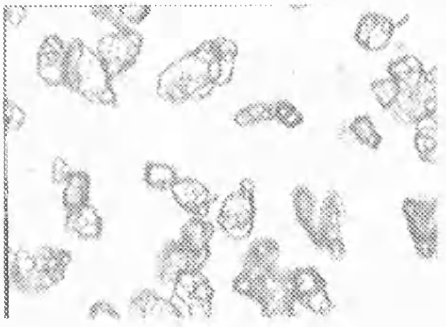

Figure 8.15 Spin dried Saquinavir (b002)

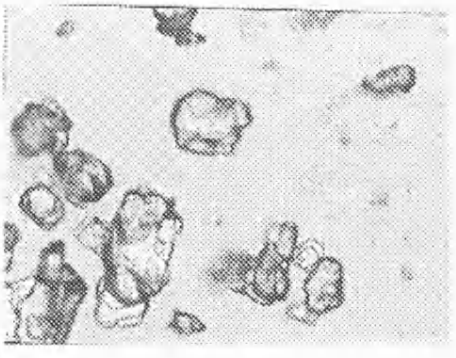

8.5 Thermogravimetric analysis (TGA) and differential scanning calorimetry (DSC)

Both methods of analysis required placing the sample in conditions of gradually increasing temperature, until the sample melted. The TGA measures any mass change whilst the DSC measures any heat energy taken in or evolved over the whole temperature range.

Table 8.1 Tabulated results from DSC and TGA analysis of Saquinavir batches.

	TGA		DSC	
Batch sample	No. of peaks	Temperature of onset of peak (°C)	No. of peaks	Temperature of onset of peak (°C)
Original	1	≈250	1	248.8
Tray dried b010	1	≈250	1	248.2
Vacuum dried b020	1	≈250	1	248.2
Heated only b030	1	≈250	1	248.5
Tray dried b001	1	≈250	1	248.6
Spin dried b002	1	≈250	1	247.8

Both the TGA and the DSC were able to detect the melting point of the Saquinavir, which did not change with any of the batches. No other peaks were observed along the temperature ramp. Both methods were unsuccessful in pinpointing any differences between the Saquinavir batches, due to the fact that they are only able to analyse changes in the bulk and are not sensitive enough to detect smaller alterations present only on the surface of the Saquinavir.

8.6 Conclusions

All four techniques employed in this chapter were unsuccessful in detecting any batch to batch variation with the Saquinavir batches. The microscopy showed no change in crystal habit, the mixer torque rheometer detected no alterations during granulation and the DSC and TGA found no differences when heated gradually to Saquinavir's melting point. It can be assumed that these techniques are only sensitive enough to detect

changes within the bulk of the material, of which there were none. Other more sensitive surface analytical techniques used in previous chapters have been able to find surface variation, which only represents a small fraction of a powder.

Chapter 9

Discussion

9 Discussion

9.1 Comparison of techniques

9.1.1 Contact Angle methods

The choice of liquids used along with the theory applied to the data analysis can greatly effect the overall surface characterisation as has been shown in Chapter 3 and 4.

9.1.1.1 Compressed powder Wilhelmy plate

This method has been widely used and in this case it was able to distinguish between the five model powders, giving reproducible surface energy data, although not being wholly representative of the powders in their original non-compacted form. With all the powders analysed, this method consistently over estimated the non-polar surface energy values in comparison to other techniques, most probably due to the Wilhelmy plate preparation process involving compaction before contact angle measurement. This method is unable to determine realistic surface energy data, although it is able to compare and distinguish between very different powders.

9.1.1.2 Powder covered glass slide

This novel Wilhelmy plate method was successfully able to characterise the five model powders, finding realistic differences in their surface energy makeup. It was not sensitive enough to show any significant alterations with the Saquinavir batches, and is not suitable to distinguish small variations between batches. This method has shown that the procedure involved in preparing a powdered slide is reproducible in that consistent surface coverage can be achieved with each glass slide leading to reproducible surface energy data. The main advantages of this technique are that:-

a) The sample is not altered in any way by the preparation process.

b) Only a very small quantity of sample is required for complete analysis.

c) Procedure is very rapid and simple to perform.

9.1.1.3 Liquid penetration

Liquid penetration has proved to be of limited use. All too often, the powder bed would either be highly soluble or repellent to the test liquids available for use, leaving too few contact angles for a realistic analysis. In addition, the measurement of these contact angles relies on the operator choosing the points through which to calculate a gradient, resulting in greater error margins. This method did produce limited surface energy data that were realistic, although it is not an adequate method to use quickly and reliably on a large number of powders for which the surface energies are unknown.

9.1.1.4 Procedure for contact angle measurement

By calculating surface energy data with two separate theories and with different combinations of test liquids, it has been possible to propose the optimum procedure using the most reliable test liquids. This is outlined in Figure 9.1.

Figure 9.1 Preferred technique for contact angle measurement on powdered samples.

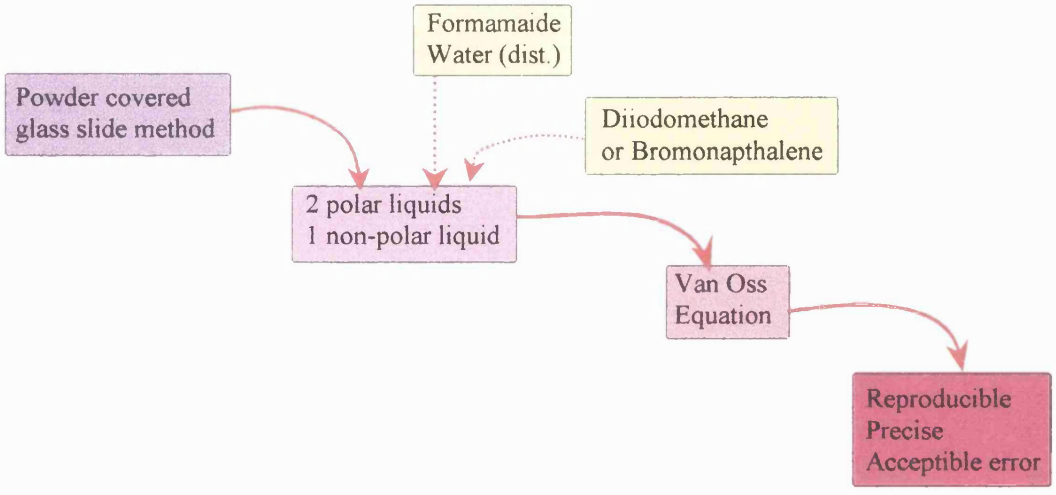

9.1.2 Inverse Gas Chromatography

By the use of IGC, significant physicochemical differences could be readily distinguished in the surfaces of the five model powders, giving reproducible surface energy data. The non-polar surface energy dataaredirectly comparable (same units) to non-polar surface energies obtained with the more traditional contact angle methods. The IGC has shown to consistently produce non-polar surface energy values of slightly greater magnitude than the most reliable contact angle method (powder covered glass slide). This is due to the experimental procedure being carried out at infinite dilution, whereby the minute amounts of test vapours injected preferentially interact with the higher energy binding sites, therefore making the overall value biased towards those sites. With the combination of the polar and non-polar nature of each powder, IGC was able to differentiate between the five model powders, as did all the contact angle methods, but was also sensitive enough to be able to differentiate between the small changes in surface nature of the Saquinavir batches. Therefore it can be deduced that IGC is an extremely sensitive method able to detect minor changes in the surface character of different batches of the same drug.

9.1.3 Flow cell Microcalorimetry

Both the five model powders and the Saquinavir batches were easily distinguished between with the use of flow cell microcalorimetry. It is an extremely accurate and reproducible technique that is ideally suited to detecting minute changes in the adsorption behaviour between powders (even with Salicylic acid which is hydrophobic and which had a small surface area) or different batches of the same powder. This method was even able to show significant changes in water adsorption with repeated cycling of the same sample due to the high accuracy of its measurements. Although the method was time consuming, the results were highly encouraging, and show the suitability of this method to a wide range of powders.

9.1.4 Dynamic Vapour Sorption

The five model powders and the different Saquinavir batches were again easily distinguished between using the DVS, although the changes with repeated cycling were not as clearly defined when using microcalorimetry. Two of the model powders, Salicylic acid and Ibuprofen were not suitable candidates for using the DVS, due to their inability to adsorb water vapour, although in practice most powders readily adsorb water vapour. This method was less time consuming than microcalorimetry and easily set up.

9.1.5 Differences between methods

The main advantage of using IGC, DVS and microcalorimetry when compared to the contact angle methods is that the powder does not have to be pre-treated in order to obtain surface energy data. IGC uses probes at infinite dilution (not enough for monolayer formation), resulting in a bias towards analysing the binding sites that are most reactive (highest energy) and yielding data that is not a representation of the average of the whole spectrum of binding sites. Although this may be the case, IGC was still able to differentiate between the different powders and the batches of Saquinavir. DVS and microcalorimetry use water vapour at higher concentrations (0% to 90% RH), resulting in many more binding sites being accessed. The water molecule has both a polar and non-polar interaction with a powder surface. Both DVS and microcalorimetry were able to distinguish between the different powders and batches of Saquinavir by analysing both monalayer and multilayer formation.

9.1.6 Combining DVS with Microcalorimetry

Thermodynamic adsorption processes were examined with the combined data from the DVS and microcalorimetry, allowing a more detailed analysis of any surface differences. The results were able to reconfirm the differences between three of the five model powders and the Saquinavir batches.

9.2 Effect of processing on Saquinavir

Within a crystalline structure there may be areas of local disorder (amorphous) which are able to take up more water than any totally crystalline area. If the amount taken up is enough to plastisize the amorphous powder to a point where the glass transition state is lowered to that of the ambient temperature, the molecular mobility will then be great enough to support enhanced dissolution rates (Fukuoka et al., 1986). If this is the case with the original untreated Saquinavir, the amorphous areas could be able to recrystallise in the presence of high humidity within the DVS or microcalorimeter, resulting in the observed fall in water adsorption with repeated humidity cycling. If this process were allowed to continue, the amount of adsorption at high relative humidities would fall to a level similar to the tray dried Saquinavir sample. The tray dried sample will have crystallised all the amorphous areas during the preparation process in the presence of water at an elevated temperature. The results from the DVS and microcalorimetry indicate that the vacuum dried Saquinavir may have only partially converted its amorphous aspect during preparation. This is due to the lower drying temperature in the oven causing the rate of conversion to be that much slower. The DVS and microcalorimetry are highly sensitive and are able to detect this conversion process at room temperature and high humidities.

In the presence of water, the amorphous particles present are able to go into solution first since the solubility of Saquinavir in water is 0.22g in 100mls. Therefore with 90mls of water used to wet the Saquinavir, the mass able to go into solution was 198mg, representing 0.66% of each batch of 30g. When the wetted powder was dried in a tray oven, the dissolved Saquinavir probably crystallises onto larger crystals, thereby reducing the total surface area of the powder batch (76.3% and 77.9% of the original surface area for the tray dried and vacuum dried batches respectively). There may be a granulation effect occurring whereby the particles join together so reducing the samples overall surface area.

9.3 Conclusions

This detailed study of several completely different techniques of surface characterisation has been able to address the advantages and disadvantages of each in detail. This knowledge will be a useful guide to obtaining the most reliable and realistic surface energy data for each individual unknown powder. Table 9.1 and 9.2 illustrate which methods of analysis are suitable for different criteria being studied in addition to a summary of the results obtained within this thesis. The choice of surface characterisation method depends on many factors, for example, sensitivity required, powder quantity available and whether the surface energy is being evaluated or compared for batch to batch variation. It is evident that batch to batch variation is not readily detectable with contact angle techniques, which should therefore be reserved for a fast and easy indication of the magnitude of a powder's surface energy. Whereas DVS, microcalorimetry and IGC are able to provide straightforward and highly sensitive methods of analysing surface properties and the degree of variation between batches of the same drug.

Table 9.1 Checklist for choosing surface characterisation technique.

Method	Provides Polar	Provides Acid-base	Provides Non-polar	Sensitivity (5 - most)	Detects batch to batch variation	Quantity of powder required	Ease of use (5 - easiest)	Time for one powder	Incorporate organic vapours	Temperature range*
Compressed powder Wilhelmy plate	✓	✓	✓	2	✗	HIGH ≈5g	5	≈1 day n=15	✓ (liquids)	✗
Coated slide Wilhelmy plate	✓	✓	✓	2	✗	MEDIUM ≈1g	5	≈1 day n=15	✓ (liquids)	✗
Liquid penetration	✓	✓	✓	1	✗	HIGH ≈5g	4	≈2 days n=15	✓ (liquids)	✗
IGC	✗	✓	✓	4	✓	MEDIUM ≈2g	1	≈5 days n=1	✓ (vapours)	✓ 30°-200°
Microcalorimetry	✗	✗	✗	5	✓	LOW ≈150mg	4	≈7 days n=3	✓ (vapours)	✓ 25°-80°
DVS	✗	✗	✗	3	✓	LOW ≈300mg	5	≈3 days n=3	✓ (vapours)	✓ 25°-80°

* Temperature of the test liquids can be easily varied in the range of 10°-50° although the powder will remain at ambient temperature within the Cahn apparatus.

Table 9.2 Overview of powder surface characteristics.

	Compressed powder Wilhelmy plate		Coated slide Wilhelmy plate		IGC			ΔG_{mon} DVS / Microcalorimetry
	Using van Oss theory with diiodomethane, formamide and water.							
	γ_S^{LW} $mJ.m^{-2}$	γ_S^{AB} $mJ.m^{-2}$	γ_S^{LW} $mJ.m^{-2}$	γ_S^{AB} $mJ.m^{-2}$	γ_S^{LW} $mJ.m^{-2}$	K_A $x10^3$	K_B $x10^3$	$kJ.mol^{-1}$
Salicylic acid			28.8	2.6	53.0	76.2	-182.8	
Ethacrynic acid	31.8	0	20.0	0	34.9	76.7	-205.8	45.4
Ibuprofen	30.7	4.9	23.6	3.1	39.5	103	-151.3	
Theophylline			38.3	2.8	50.8	71.9	-105.2	45.2
Caffeine			25.4	10.7	39.9	51.2	-34.4	45.1
Original Saquinavir	42.8	4.9	24.3	0	44.0	84.8	-1.8	40.9
Tray dried Saquinavir	43.2	7.6	24.1	0	38.7	68.1	26.7	41.8
Vacuum dried Saquinavir	43.7	4.9	26.0	0	38.5	65.9	26.0	40.8
Heated only Saquinavir	41.1	8.2	26.1	0	37.1	73.3	28.5	40.6

9.4 Future Work

There are several opportunities within this thesis for further research to be carried out:-

Inverse gas chromatography

For a more complete analysis using IGC, the experiment can be performed over a range of temperatures and with a more extensive range of probe liquids. This would enable the enthalpy (ΔH) and entropy (ΔS) of adsorption to be calculated. It would also allow the acid-base analysis to be calculated without any possible errors due to temperature effects being incorporated into the calculation.

Another useful technique involves the probes being injected in greater concentrations (finite dilution), which allows the probes to interact with all available binding sites irrespective of their energy status. This would yield surface energy data that may be more similar to other techniques due to the similar range of binding sites being accessed.

Dynamic vapour sorption

The DVS is able to calculate the surface energy of a powder by measuring the adsorption isotherms of a several different organic vapours rather than water vapour. An isotherm using a totally non-polar organic vapour (e.g. decane) will give the equilibrium spreading pressure (π_e) using Equation 9.1.

$$W_{SL} = \gamma_{LV}(1+\text{Cos}\theta) + \pi_e \qquad \text{Equation 9.1}$$

An isotherm using a polar organic vapour (e.g. methanol) can then be used to calculate both the polar and non-polar surface energy of the powder.

Isothermal microcalorimetry

The microcalorimeter can be used over a range of temperatures (25°C to 80°C), allowing a more complete adsorption picture, possibly pin-pointing small changes in surface properties with temperature.

Another avenue would be the use of organic rather than water vapours to obtain various adsorption isotherms, possibly utilising these in the evaluation of non-polar and acid-base chemistry.

References

Ahlneck, C. and Zografi, G. The molecular basis of moisture effects on the physical and chemical stability of drugs in the solid state. *International Journal of Pharmaceutics*, **1990**, 62, 87-95.

Anberg, M., Nystrom, C. and Castensson, S. Evaluation of heat conduction microcalorimetry in pharmaceutical stability studies. I. Precision and accuracy for static experiments in glass vials. *Acta Pharm. Suec.* **1988**, 25, 307-320.

Anberg, M., Nystrom, C. and Castensson, S. Evaluation of heat conduction microcalorimetry in pharmaceutical stability studies. II. Methods to evaluate the microcalorimetric response. *International Journal of Pharmaceutics,* **1990**, 61, 67-77.

Anberg, M., Nystrom, C. and Castensson, S. Evaluation of heat conduction microcalorimetry in pharmaceutical stability studies. III. Crystallographic changes due to water vapour uptake in anhydrous lactose powder. *International Journal of Pharmaceutics,* **1991**, 73, 209-220.

Anberg, M., Nystrom, C. and Castensson, S. Evaluation of heat conduction microcalorimetry in pharmaceutical stability studies. IV. The influence of microcrystalline cellulose on the hydration rate of anhydrous lactose. *International Journal of Pharmaceutics,* **1991**, 77, 269-277.

Anberg, M., Nystrom, C. and Castensson, S. Evaluation of heat conduction microcalorimetry in pharmaceutical stability studies. V. A new approach for continuous measurements in abundant water vapour. *International Journal of Pharmaceutics,* **1992**, 81, 153-167.

Anberg, M., Nystrom, C. and Castensson, S. Evaluation of heat conduction microcalorimetry in pharmaceutical stability studies. VI. Continuous monitoring of the interaction of water vapour with powders and powder mixtures at various relative humidities. *International Journal of Pharmaceutics,* **1992**, 83, 11-23.

Anhang, J. and Gray, D.G. *J. Appl. Polym. Sci*, **1982**, 27, 71-78.

Bandosz, T.J., Jagiello, J. and Schwarz, J.A. Changes in the acidic properties of pillared taeniolites on heat treatment or alkene decomposition. *Journal of the Chemical Society, Faraday Transactions,* **1996**, 92(22), 4631-4635.

Becker, H. and Gnauck, R. Determination of dead times for inverse gas chromatography: measurements by use of methane. *J. Chromatography*, **1986**, 366, 378-381.

Blair, T., Buckton, B., Beezer, A.E. and Bloomfield, S.F. The interaction of various types of microcrystalline cellulose and starch with water. *International Journal of Pharmaceutics,* **1990**, 63, 251-257.

Bonifaci, L. and Ravanetti, G.P. Thermodynamic study of polystyrene-n-alkane systems by inverse gas chromatography. *Journal of Chromatography*, **1993**, 641, 301-307.

Briegleb, G. Elecktronen-Donator-Acceptor-Komplexe. Springer Verlag, Berlin, **1961**.

Briggner, L.E., Buckton, G., Bystrom, K. and Darcy, P. The use of isothermal microcalorimetry in the study of changes in crystallinity induced during the processing of powders. *International Journal of Pharmaceutics,* **1994**, 105, 125-135.

Brunauer, S., Emmett, P.H. and Teller, E. Adsorption of gases in multimolecular layers. *Journal of the American Chemical Society*, **1938**, 60, 309-319.

Buckton, G. and Beezer, A.E. A microcalorimetic study of powder surface energetics. *International Journal of Pharmaceutics*, **1988**, 41, 139-145.

Buckton, G. and Beezer, A.E. The applications of microcalorimetry in the field of physical pharmacy. *International Journal of Pharmaceutics*, **1991**, 72, 181-191.

Buckton, G. and Newton, J.M. Assessment of the wettability and surface energy of a pharmaceutical powder by liquid penetration. *J. Pharm. Pharmacol.*, **1985**, 37, 605-609.

Buckton, G. and Newton, J.M. Liquid penetration as a method of assessing the wettability and surface energy of pharmaceutical powders. *J. Pharm. Pharmacol.*, **1986**, 38, 329-334.

Buckton, G. and Newton, J.M. Assessment and wettability of powders by use of compressed powder discs. *Powder Technology*, **1986**, 46, 201-208.

Buckton, G. Surfactants. In: Florence, A.T. *Interfacial phenomena in drug delivery and targeting*, **1995**, 136-164, Harwood Academic Publishers.

Buckton, G., Beezer, A.E and Newton, J.M. A vacuum microbalance technique for studies on the wettability of powders. *Journal of Pharmacy and Pharmacology*, **1986**, 38, 713-720.

Buckton, G., Darcy, P. and McCarthy, D. The extent of errors associated with contact angles 3. The influence of surface roughness effects on angles measured using a Wilhelmy plate technique for powders. *Colloids and surfaces A : Physicochemical and engineering aspects*, **1995**, 95, 27-35.

Carthew, D.L., Physico-chemical properties of poloxamer surfactants related to their adsorption. *Ph D. Thesis*, **1996**, University of London.

Cassie, A.B.D., *Discussions Faraday Society,* **1948**, 3, 11-16.

Chemimi, M.M. and Pigois-Landureau, E. Determination of acid-base properties of solid materials by inverse gas chromatography at infinite dilution. *Journal of Material chemistry,* **1994**, 4(5), 741-745.

Conder, J.R. and Young, C.L. in *Physiochemical Measurements by Gas Chromatography*, **1979**, Wiley-Interscience, New York.

Coulson, C.A. and Longuet-Higgins, H.C. *Proc. R. Soc. (London) Ser. A*, **1947**, 191, 39.

DeBoer, J.H. The dynamic character of adsorption. Oxford, Clarendon Press, 1953.

Dettre, R.H. and Johnson, R.E. Contact angle hysteresis III. Study of an idealised heterogenous surface., *The Journal of Physical Chemistry,* **1964**, 68, 7, 1744-1750.

Dettre, R.H. and Johnson, R.E. Contact angle hysteresis IV. Contact angle measurements on heterogenous surfaces., *The Journal of Physical Chemistry,* **1965**, 69, 5, 1507-1515.

Djordjevic, N.M., Rohr, G., Hinterleitner, M. and Schreiber, B. Adsorption of water on cyclosporin A, from zero to finite surface coverage. *International Journal of Pharmaceutics*, **1992**, 81, 21-29.

Dorris, G.M. and Gray, D.G. Adsorption of n-alkanes at zero surface coverage on cellulose paper and wood fibres. *Journal of Colloid and Interface Science*, **1980**, 77, 2, 353-362.

Dorris, G.M. and Gray, D.G. Adsorption, spreading pressure and london force interactions of hydrocarbons on cellulose and wood fibre surfaces. *Journal of Colloid and Interface Science,* **1979**, 71, 1, 93-106.

Drago, R.S. and Wayland, B.B. A double scale equation for correlating enthalpies of lewis acid-base interactions. *Journal of the American Chemical Society,* **1965**, 87, 3571.

Dyer, A.M., Khan, K.A. and Aulton, M.E. Effect of the drying method on the mechanical and drug release properties of pellets prepared by extrusion-spheronization. *Drug Development and Industrial Pharmacy*, **1994**, 20 (20), 3045-3068.

Etxeberria, A., Alfageme, J., Uriarte, C. and Iruin, J.J. Inverse gas chromatography in the characterisation of polymeric materials. *Journal of Chromatography,* **1992**, 607, 227-237.

Fafard, M., El-kindi, M., Schreiber, H.P., Dipaola-baranyi, G. and Hor, A.M. Estimating surface energy variations of solids by inverse gas chromatography. *Journal of Adhesion Science Technology,* **1994**, 8, 12, 1383-1394.

Fowkes, F.M. Attractive forces at interfaces. *Ind. Eng. Chem.* **1964**, 56 (12), 40-52.

Fowkes, F.M. Quantitative characterisation of the acid-base properties of solvents, polymers and inorganic surfaces. *Journal of Adhesion Science Technology*, **1990**, 4, 8, 669-691.

Fox, H.W. and Zisman, W.A. The spreading of liquids on low energy surfaces. I. Polytetrafluoroethylene. *Journal of Colloid Science*, **1950**, 5, 514-531.

Fukuoka, E., Makita, M. and Yamamura, S. Some physio-chemical properties of glassy indomethacin. *Chem. Pharm. Bull.*, **1986**, 34, 4314-4321.

Fukuoka, E., Makita, M. and Yamamura, S. Evaluation of crystallite orientation in tablets by X-ray diffraction methods. *Chemical Pharmaceutical Bulletin*, **1987**, 35(4), 1564-1570.

Garnier, G and Glasser, W.G. Measurement of the surface energy of amorphous cellulose by alkane adsorption: A critical evaluation of inverse gas chromatography. *Journal of Adhesion,* **1994**, 46, 165-180.

Garnier, G. and Glasser, W.G. Measuring the surface energies of spherical cellulose beads by inverse gas chromatography. *Polymer Engineering and Science*, **1996**, 36, 6, 885-894.

Good, R.J. A thermodynamic derivation of Wenzel's modification of Young's equation for contact angles; together with a theory of hysteresis. *Journal of the American Chemical Society*, **1953**, 5041-5046.

Good, R.J. Contact angle, wetting and Adhesion: A critical review. *Contact angle, Wettability and Adhesion,* Ed. K.L. Mittal, **1993**.

Good, W.R. A comparison of contact angle interpretations. *Journal of Colloid and Interface Science,* **1973**, 44, 63-71.

Gutmann, V. The donor-acceptor approach to molecular interactions. New York, Plenum, 1978.

Gutmann, V, Steininger, A and Wychera, E. *Montash. Chem.*, **1966**, 97, 460.

Hadjar, H., Balard, H. and Papirer, E. An inverse gas chromatography study of crystalline and amorphous silicas. *Colloids and Surfaces A: Physicochemical and Engineering Aspects,* **1995**, 99, 45-51.

Hansford, D.T., Grant, D.J.W. and Newton, J.M. Surface energetics of the wetting of a hydrophobic powder. *Journal of the Chemical Society, Faraday I,* **1980**, 76, 2417-2431.

Hegedus, C.R. and Kamel, I.L. A review of inverse gas chromatography theory used in the thermodynamic analysis of pigment and polymer surfaces. *Journal of Coatings Technology*, **1993**, 65, 820, 23-30.

Hendriksen, B.A. Characterisation of calcium fenoprofen 1. Powder dissolution rate and degree of crystallinity. *International Journal of Pharmaceutics,* **1990**, 60, 243-252.

Ingold, C.K. Significance of tautomerism and of the reactions of aromatic compounds in the electronic theory of organic reactions. *Journal of the Chemical Society*, **1933**, 1120-1127.

Jacob, P.N. and Berg, J.C. Acid-base surface energy characterisation of microcrystalline cellulose and two wood pulp fibre types using inverse gas chromatography, *Langmuir* **1994**, 10, 3086-3093.

Johnson, R.E. and Dettre, R.H. Wettability and contact angles. *Surface and Colloid Science*, **1969**, 2, 85-153.

Katz, S. and Gray, D.G. The adsorption of hydrocarbons on cellophane 1. Zero coverage limit. *Journal of Colloid and Interface Science,* **1981**, 82 , 2, 318-325.

Kiesvaara, J. and Yliruusi, J. The effect of compression times on the surface energy of tablets. *Acta Pharm. Nord.*, **1991**, 3, 171-177.

Kiesvaara, J. and Yliruusi, J. The use of the Washburn method in determining the contact angles of lactose powder. *Int. J. Pharm.*, **1993**, 92, 81-88.

Kiesvaara, J., Yliruusi, J. and Ahomaki, E. Contact angles and surface free energies of theophylline and salicylic acid powders determined by the Washburn method. *Int. J. Pharm.*, **1993**, 97, 101-109.

Kloubek, J. and Schreiber, H.P. *Journal of Coatings Technology*, **1993**, 42, 87.

Landin, M., Martinez-Pacheco, R., Gomez-Amoza, J.L., Souto, C., Concheiro, A. and Rowe, R.C. Effect of country of origin on the properties of microcrystalline cellulose. *International Journal of Pharmaceutics,* **1993**, 91, 123-131.

Lara, J.A. and Schreiber, H.P. *Journal of Coatings Technology,* **1991**, 63, 81.

Lechner, H. Characterisation of wetting behaviour of pharmaceutical powders by contact angle measurement using capillary rise technology, *Proceedings APGI/APV*, **1995**, 137-138.

Lerk, C.F., Schoonen, J.M. and Fell, J.T. Contact angles and wetting of pharmaceutical powders. *J. Pharm. Sci.*, **1976**, 65, 6, 843-847.

Lewis, G.N. Valence and the structure of atoms and molecules. The Chemical Catalogue Co., New York, **1923**, 141-142.

Lloyd, T.B. Experimental procedures to characterise acid-base and dispersion force contributions to solid wettability. *Colloids and Surfaces A: Physicochemical and Engineering Aspects,* **1994**, 93, 25-37.

Martin, R.L. *Analytical Chemistry*, **1961**, 33, 347.

McClellan, A.L. and Harnsberger, H.F. Cross-sectional areas of molecules adsorbed on solid surfaces. *Journal of Colloid Interface Science*, **1967**, 23, 577-599.

Mohammad, H.A.H. and Fell, J.T. Contact angles of powder mixtures consisting of spherical particles. *International Journal of Pharmaceutics,* **1982**, 11, 149-154.

Mukhopadhyay, P. and Schreiber, H.P. Aspects of acid-base interactions and use of inverse gas chromatography. *Colloids and surfaces A: Physicochemical and engineering aspects,* **1995,** 100, 47-71.

Nyqvist, H. Saturated salt solutions for maintaining specified relative humidities. *International Journal of Pharmaceutics,* **1983**, 4, 47-48.

Nardin, M. and Papirer, E. Relationship between vapour pressure and surface energy of liquids: Application to inverse gas chromatography. *Journal of Colloid and Interface Science*, **1990**, 137, 2, 534-545.

Odidi, I.O., Newton, J.M. and Buckton, G. The effect of surface treatment on the values of contact angles measured on a compressed powder surface. *Int. J. Pharm.*, **1991**, 72, 43-49.

Otsuka, M. and Kaneniwa, N. Effect of grinding on the crystallinity and chemical stability in the solid state of cephalothin sodium. *International Journal of Pharmaceutics,* **1990**, 62, 65-73.

Panzer, U. and Schreiber, H.P. On the evaluation of surface interactions by inverse gas chromatography. *Macromolecules*, **1992**, 25, 3633-3637.

Papirer, E., Perrin, J.M., Siffert, B., Philipponneau, G. and Lamerant, J.M. The influence of grinding on the surface properties of α-aluminas. *Journal of Colloid and Interface Science,* **1993**, 156, 104-108.

Parker, M.D., Rowe, R.C. and Upjohn, N.G. Mixer Torque Rheometry: A method for quantifying the consistency of wet granulations. *Pharm. Tech. Int.*, **1990**, 2, 50-64.

Parfitt, G.D. Dispersion of powders in liquids. Elsevier, Amsterdam, 1969.

Parsons, G.E., Buckton, G. and Chatham, S.M. The extent of the errors associated with contact angles obtained using liquid penetration experiments. *International Journal of Pharmaceutics*, **1992**, 82, 145-150.

Pearson, R.G. Hard and sorft acids and bases. *Journal of the American Chemical Society,* **1963**, 85, 3533.

Pepin, X., Blanchon, S. and Couarraze, G. A new approach for determination of powder wettability. *International Journal of Pharmaceutics*, **1997**, 152, 1-5.

Phadke, D.S., Keeney, M.P. and Norris, D.A. Evaluation of batch to batch and manufacturer to manufacturer variability in the physical properties of talc and stearic acid. *Drug Development and Industrial Pharmacy,* **1994**, 20(5), 859-871.

Pimentel, G.C. and McClellan, A.L. The hydrogen bond. W.H. Freeman, San Francisco, **1960**.

Riddle, F.L. and Fowkes, F.M. Spectral shifts in acid-base chemistry. 1. Van der waals contributions to acceptor numbers. *Journal of the American Chemical Society*, **1990**, 112, 9, 3259-3264.

Sa, M.M. and Sereno, A.M. Effect of column material on sorption isotherms obtained by inverse gas chromatography. *Journal of Chromatography*, **1992**, 600, 341-343.

Schultz, J., Lavielle, L. and Martin, C. The role of the interface in carbon fibre-epoxy composites. *Journal of Adhesion*, **1987**, 23, 45-60.

Sebhatu, T., Angberg, M. and Ahlneck, C. Assessment of the degree of disorder in crystalline solids by isothermal microlcalorimetry. *International Journal of Pharmaceutics,* **1994**, 104, 135-144.

Sedgwick, N.V. The electronic theory of valency. Clarendon Press, Oxford, **1927**.

Shanker, R.M., Baltusis, P.J. and Hruska, R.M. Development of a new technique for the assessment of wettability of powders. *Pharmaceutical Research,* **1994**, 11, 10, S-243.

Sheridan, P.L., Buckton, G. and Storey, D.E. Comparison of two techniques for the assessment of the wettability of pharmaceutical powders. *Journal of Pharmacy and Pharmacology*, **1993**, 45, 1097.

Sheridan, P.L. Assessment of the surface properties of pharmaceutical powders. *Ph.D. Thesis*, **1994**, University of London.

Stark, J.G. (1978) Chemical Data Book, Murray, 33-49.

Ticehurst, M.D. Characterisation of the surface energetics of pharmaceutical powders by inverse gas chromatography. *Ph.D. Thesis*, **1995**, University of Bradford.

Ticehurst, M.D., Rowe, R.C. and York, P. Determination of the surface properties of two batches of salbutamol sulphate by inverse gas chromatography. *International Journal of Pharmaceutics*, **1994**, 111, 241-249.

Ticehurst, M.D., York, P., Rowe, R.C. and Dwivedi, S.K. Characterisation of the surface properties of α-lactose monohydrate with inverse gas chromatography, used to detect batch variation. *International Journal of Pharmaceutics*, **1996**, 141, 93-99.

Van Krevelen, D.W. Properties of polymers. Their estimation and correlation with chemical structure. Elsevier, Amsterdam, **1976**, 2nd edition.

Van Oss, C.J., Chaudhury, M.K. and Good, R.J. Interfacial lifshitz van der waals and polar interactions in macroscopic systems. *Chemical Reviews*, **1988**, 88, 927-941.

Van Oss, C.J. and Costanzo, P.M. Adhesion of anionic surfactants to polymer surfaces and low-energy materials. *J. Adhesion Sci. Technol.*, **1992**, 6, 4, 477-487.

Van Oss, C.J., Giese, R.F., Li, Z., Murphy, K., Norris, J., Chaudhury, M.K. and Good, R.J. Determination of contact angles and pore sizes of porous media by column and thin layer wickering. *J. Adhesion Sci. Technol.*, **1992**, 6, 4, 413-428.

Van Oss, C.J., Giese, R.F., Wentzek, R., Norris, J. and Chuvilin, E.M. Surface tension parameters of ice obtained from contact angle data and from positive and negative particle adhesion to advancing freezing points. *J. Adhesion Sci. Technol.*, **1992**, 6, 4, 503-516.

Van Oss, C.J., Good, R.J. and Chaudhury, M.K. *Langmuir,* **1988**, 4, 884-891.

Vidal, A. and Papirer, E. Surface chemistry and surface energy of silicas. *Advancing in Chemistry Series,* **1994**, 234, 245-255.

Voelkel, A. and Janus, J. Elimination of adsorption effects of polarity parameters determined by inverse gas chromatography. *Journal of Chromatography A*, **1995**, 693, 315-323.

Voelkel, A., Andrzejewska, E., Maga, R. and Andrzejewski, M. Examination of surfaces of solid polymers by inverse gas chromatography. 1. Dispersive properties. *Polymer*, **1996**, 37, 3, 455-462.

Volpe, C.D. Contact angle measurements on samples with dissimilar faces by Wilhelmy microbalance. *J. Adhesion Sci. Technol.*, **1994**, 10, 12, 1453-1458.

Washburn, E.W. *Phys. Rev.* **1921**, 17, 273-283.

Wasiak, W., Voelkel, A. and Rykowska, I. Physico-chemical characterisation of chemically bonded stationary phases including metal complexes by inverse gas chromatography. *Journal of Chromatography A*, **1995**, 690, 83-91.

Williams, D. Inverse gas chromatography of solid surfaces. *Chromatography and Analysis*, **1991**, 9-11.

Willson, R.J., Beezer, A.E., Mitchell, J.C. and Loh, W. Determination of thermodynamic and kinetic parameters from isothermal heat conduction microcalorimetry: Applications to long term studies. *Journal of Physical Chemistry*, **1995**, 99, 7108-7113.

Wu, S. Calculation of interfacial tension in polymer systems. *Journal of Polymer Science Part C*, **1971**, 34, 19-30.

Young, T. *Phil. Trans. R. Soc.*,**1805**, 95, 65.

Young, S.A. and Buckton, G. Particle growth in aqueous suspensions: the influence of surface energy and polarity. *International Journal of Pharmaceutics*, **1990**, 60, 235-241.

Zografi, G. and Tam, S.S. Wettability of pharmaceutical solids: Estimates of solid surface polarity. *J. Pharm. Sci.*, **1976**, 65, 8, 1145-1149.